ARTIFICIAL TRANSMEMBRANE SIGANLLING

Yudi Ding PhD 2019

UNIVERSITY OF CAMBRIDGE

Deposit & Copying of Dissertation Declaration

UNIVERSITY OF CAMBRIDGE

Board of Graduate Studies

Please note that you will also need to bind a copy of this Declaration into your final, hardbound copy of thesis - this has to be the very first page of the hardbound thesis.

1 Surname (Family Name)	Forenames(s)	Title
Ding	Yudi	PhD

2 Title of Dissertation as approved by the Degree Committee
Artificial Transmembrane Signalling

In accordance with the University Regulations in *Statutes and Ordinances* for the PhD, MSc and MLitt Degrees, I agree to deposit one print copy of my dissertation entitled above and one print copy of the summary with the Secretary of the Board of Graduate Studies who shall deposit the dissertation and summary in the University Library under the following terms and conditions:

1. Dissertation Author Declaration

I am the author of this dissertation and hereby give the University the right to make my dissertation available in print form as described in 2. below.

My dissertation is my original work and a product of my own research endeavours and includes nothing which is the outcome of work done in collaboration with others except as declared in the Preface and specified in the text. I hereby assert my moral right to be identified as the author of the dissertation.

The deposit and dissemination of my dissertation by the University does not constitute a breach of any other agreement, publishing or otherwise, including any confidentiality or publication restriction provisions in sponsorship or collaboration agreements governing my research or work at the University or elsewhere.

2. Access to Dissertation

I understand that one print copy of my dissertation will be deposited in the University Library for archival and preservation purposes, and that, unless upon my application restricted access to my dissertation for a specified period of time has been granted by the Board of Graduate Studies prior to this deposit, the dissertation will be made available by the University Library for consultation by readers in accordance with University Library Regulations and copies of my dissertation may be provided to readers in accordance with applicable legislation.

3 Signature	Date
	17 November 2019

Corresponding Regulation

Before being admitted to a degree, a student shall deposit with the Secretary of the Board one copy of his or her hard-bound dissertation and one copy of the summary (bearing student's name and thesis title), both the dissertation and the summary in a form approved by the Board. The Secretary shall deposit the copy of the dissertation together with the copy of the summary in the University Library where, subject to restricted access to the dissertation for a specified period of time having been granted by the Board of Graduate Studies, they shall be made available for consultation by readers in accordance with University Library Regulations and copies of the dissertation provided to readers in accordance with applicable legislation.

UNIVERSITY OF CAMBRIDGE

Artificial Transmembrane Signalling

This dissertation is submitted for the degree of Doctor of Philosophy

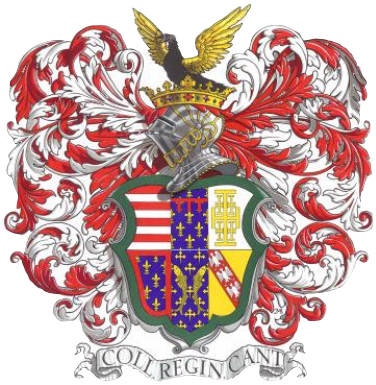

Yudi Ding
The Queen's College of St Margaret and St Bernard

Prof. Christopher A. Hunter FRS *Supervisor*
Faculty of Physics & Chemistry

University of Cambridge
2019

to those who are
fighting against prejudice

Artificial Transmembrane Signalling

Yudi Ding

Signalisation Artificielle Transmembranaire

Yudí Ding

人工跨膜信号传导

丁宇迪

Declaration

This dissertation is the result of my own work and includes nothing which is the outcome of work done in collaboration except as declared in the Preface and specified in the text.

It is not substantially the same as any that I have submitted, or, is being concurrently submitted for a degree or diploma or other qualification at the University of Cambridge or any other University or similar institution except as declared in the Preface and specified in the text. I further state that no substantial part of my dissertation has already been submitted, or, is being concurrently submitted for any such degree, diploma or other qualification at the University of Cambridge or any other University or similar institution except as declared in the Preface and specified in the text.

It does not exceed the prescribed word limit for the Degree Committee for the Faculty of Physics & Chemistry.

This page is intentionally left blank

Contents

This page is intentionally left blank

Preface

It has been exciting and at the same time intimidating to be the first doctoral student who works on this topic in the group. Reflecting on my decision of choosing the project at the start of the PhD, I realised that being the first or only one doing something has intrigued and motivated me. Like every self-congratulatory graduate student who just received an offer from Cambridge, I had a peacockish ambition that I would be changing the world with my great scientific discovery during my PhD – curing cancer, solving global warming and such. Now that I am writing up what I have done for the past three years, only do I hope that I could have contributed to a tiny little barely-to-be-seen push at the boundary of human knowledge, as depicted by Matt Might in his *Illustrated guide to a PhD*.[1]

However, even this tiny little barely-to-be-seen push would not be made possible without all the support I received. I would like to thank Professor Christopher A. Hunter, the best supervisor that I could wish for, for his British humour (essential talent), for his guidance and mentorship both in science and personal development, as well as his full understanding and support. I remembered well that there was a time when, after several months of synthesis, I became very discouraged about my research because a key experiment did not work as designed. I presented Prof. Hunter the data with a sad face and, out of my surprise, he showed no disappointment at all. "There must be something much more interesting going on", he said, "and we will figure that out". He was right. Walking back to the lab I saw the sun shined through heavy clouds and it cheered me up, just like his encouragements that made I felt I was still doing a good job.

Before I joined the group, Dr Maria Ciaccia, Dr Flore Keymeulen and Dr Matthew J. Langton have done an enormous work in the project and provided the foundation of this thesis. I especially thank Dr Langton for his day-to-day hands-on supervision in the laboratory during my first year. Apart from technical skills and scientific knowledge, his calmness and the ability to stay composed in all situations are what I found most valuable to learn. Except for one time when Dr Langton went furious as *Yorkshire tea*, i.e. proper British tea, got mixed up in the kitchen and I quote that he has "now discovered that lemon, ginger and milk is not a popular combination for a good reason, and for an English person this is as high on the disaster scale as pineapple on pizza and chorizo in paella!"

Gossip tends to get more pervasive when people work in an open-plan office and up to 90% of conversations could qualify as gossip.[2] This is especially the case in our office as for example,

almost everyone was asked by Mr Peter Bolgar about Dr Istvan Kocsis' dating preferences after his interview with the group, and even with Dr Francesco Fasano's excellent online stalking skills we could not figure it out. Only once I started working with him did I clear up the mystery. Dr Kocsis is an extraordinary colleague and an awesome friend to spend time with. He is also a keen advocate for collaboration and a potent idea generator who makes the *Transduction* team strong and productive. I also thank Ms Lucia Trevisan for her contribution to the team. For details of our collaboration, please see Chapter 5.

Three years of research would have been monotonous without Professor Steven V. Ley being my mentor, whose guidance and encouragement led my way to business schools (both HBS and Judge). The economic knowledge I gained completely changed my perspective of this constantly evolving world, and suddenly current political affairs that used to puzzle me started to make sense. Until then, I realised how Xu Zhimo, the eminent poet from King's College whose name brings Chinese tourists flooding into Cambridge throughout the year, felt when one century ago he wrote the following sentences in a prose[3]:

> "
>
> *… I dare not say how knowledgeable I have become through my education in Cambridge, I dare not say one can be regenerated and deified through the baptism of Cambridge. What I dare say is that it was Cambridge that opened my eyes, it was Cambridge that aroused my curiosity in knowledge, it was Cambridge that generated the awareness of 'I' in me."*

I am not at King's. I chose Queens' College because of its colour – a lush, emerald green. It seems random to most, but this was probably one of the best decisions I have made. I was lucky enough to have been involved in the college Governing Body and which allowed me to peer into the eight-hundred-year formality of this University from a unique angle. It was fun.

And time flies.

One take-home message for those who cannot be bothered to read the rest of the thesis: bring flowers next time when you meet Her Majesty the Queen, she will come and say hi.[4]

Cambridge, Oct 2019 *Yudi Ding*

References

(1) Might, M. The Illustrated Guide to a Ph.D. http://matt.might.net/articles/phd-school-in-pictures/ (accessed Oct 14, 2019).

(2) Bassuk, A.; Lew, C. The Antidote to Office Gossip. *Harvard Business Review*. November 11, 2016.

(3) Xu Z. On Smoking and Culture; 1915.

(4) The Patroness returns to Queens' https://www.queens.cam.ac.uk/life-at-queens/news-and-events/the-patroness-returns-to-queens (accessed Oct 16, 2019).

This page is intentionally left blank

This page is intentionally left blank

Abstract

Cell membranes coordinate a large variety of biological processes by selectively recognising and responding to different external stimuli, and membrane-spanning proteins play a vital role in these signalling pathways. A large number of examples of synthetic membrane channels and transporters have been reported in the past four decades. However, signal transduction without mass transfer is considerably more challenging. In this dissertation, an indirect artificial transmembrane signalling mechanism which operates by controlled translocation of a synthetic transducer across the lipid bilayer was investigated. The fundamental concept of the translocation mechanism is the switching of membrane-permeability of the two head groups of the transducers. The recognition head group of the transducer becomes membrane-permeable in response to an external chemical stimulus, which leads to membrane translocation, exposing a catalytic head group to the interior of the vesicle. Catalytic hydrolysis of an internal substrate generates an amplified output signal.

Previously reported examples showed that the transducer could respond to different external stimuli, such as pH (hydroxide ions) or metal ions. Herein, we present efforts towards generalising the concept and extending the scope of this mechanism into more biological systems. Firstly, a maleimide transducer was designed as a "stem transducer" to which a wide range of recognition groups could be attached *in situ* by using maleimide-thiol conjugation chemistry. Secondly, a carboxylic acid transducer was studied in an attempt to achieve controlled cargo-release in response to an acid input. Thirdly, a vesicle-to-vesicle communication system was assembled with a desthiobiotin transducer by leveraging the desthiobiotin-avidin-biotin system. This example represents a key step towards designing artificial cell-like compartments that communicate in a similar way to cells. Furthermore, we explored an analogue of the β-galactose transducer and the viability of using enzymatic cleavage as an input on the membrane surface. Finally, ^{19}F NMR studies were conducted to provide insight into the positioning of the catalytic head groups of transducers in the membrane, and a fluorescence quenching assay was used to determine the ion transport ability of transducers.

This work provides further understanding of the proposed membrane translocation mechanism and extends the scope of artificial transmembrane signal transduction from purely synthetic assemblies into more sophisticated biological systems. This opens up the potential for the future development of responsive vesicles in bionanotechnology.

This page is intentionally left blank

Résumé de Thèse

Les membranes cellulaires coordonnent une grande variété de processus biologiques en reconnaissant et en répondant sélectivement à différents stimuli externes. Les protéines transmembranaires jouent un rôle vital dans ces voies de signalisation. Un grand nombre d'exemples de canaux membranaires synthétiques et de transporteurs ont été rapportés au cours de ces quarante dernières années. Cependant, la transduction de signal sans transfert de masse est considérablement plus difficile. Le mécanisme de translocation induit par la translocation contrôlée d'un transducteur synthétique à travers la bicouche lipidique a été étudié au cours de ce travail. Ce mécanisme repose sur la commutation de la perméabilité membranaire d'un groupe de reconnaissance et d'un groupe catalytique d'un transducteur. En réponse à un stimulus chimique externe, le groupe de reconnaissance du transducteur devient perméable à la membrane ce qui conduit à une translocation, exposant le groupe catalytique à l'intérieur de la vésicule. L'hydrolyse catalytique d'un substrat interne génère ainsi un signal de sortie amplifié.

Les exemples précédemment rapportés ont montré qu'un transducteur peut répondre à différents stimuli externes, tels qu'une modification de pH par ajout de base ou la présence d'ions métalliques. Nous présentons ici les efforts déployés pour généraliser ce concept et étendre la portée de ce mécanisme à davantage de systèmes biologiques. Tout d'abord, un transducteur possédant un groupement maléimide a été conçu comme transducteur de base auquel un large éventail de groupes de reconnaissance pourrait être attaché *in situ* en utilisant une chimie de conjugaison maléimide-thiol. Deuxièmement, un transducteur possédant un groupement acide carboxylique a été étudié dans le but d'obtenir une libération contrôlée de la cargaison en réponse à une modification de pH par ajout d'acide. Troisièmement, un système de communication de vésicule à vésicule a été construit avec un transducteur dérivé de desthiobiotine, en utilisant le système de desthiobiotine-avidine-biotine. Cet exemple représente une étape clé dans la conception de compartiments artificiels ressemblant à des cellules et communiquant comme ces dernières. De plus, nous avons exploré un analogue du transducteur β-galactose ainsi que la viabilité de l'utilisation de clivages enzymatiques comme moyens d'entrée à la surface de la membrane. Enfin, des études de RMN ^{19}F ont été conduites pour étudier le positionnement des groupes catalytiques des transducteurs dans la membrane. Un test d'extinction de fluorescence a aussi été utilisé pour déterminer la capacité de transport ionique des transducteurs.

Ces travaux permettent de mieux comprendre le mécanisme de translocation membranaire et ouvre la voie au développement de vésicules capable de communiquer entre elles en construisant des systèmes *pseudo* biologiques à partir d'assemblages synthétiques.

This page is intentionally left blank

概 述

生物细胞膜通过选择性识别和响应不同的外部刺激来协调多种复杂的生物功能。跨膜蛋白在这些信号传导途径中起着至关重要的作用。在过去的四十年中化学家们报导了许多人工跨膜通道和转运蛋白进行物质传递的例子，然而通过间接（非物质传递）方式进行跨膜信号转导仍难以实现。本论文研究了一种间接人工跨膜信号转导机制——跨膜转位机制。该机制通过控制一类合成分子（转位子）在人造囊泡双分子膜中的跨膜运动而实现信号传导。其基本原理是通过改变转位子两个官能基团的膜渗透性的来控制其整体的跨膜运动。通过响应于外部化学刺激，转运子的识别基从原本的膜不可渗透转为膜可渗透，促使转位子发生跨膜运动而将其催化基暴露于囊泡内部。经活化的催化基则加速水解囊泡中的底物，产生经过扩增的输出信号。

先前报道的研究表明，转位子可以选择性响应不同的外部刺激，如碱性物质（氢氧根离子）或金属离子。本文中，我们希望推广这一概念并将此机制的范围扩展到更广泛的生物系统中。首先，我们设计了一种**马来酰亚胺转位子**，希望通过利用马来酰亚胺与硫醇在膜表面的原位反应将不同的识别基直接连接到该转位子上。其次，我们研究了一种**羧酸转位子**以试图完成在酸性环境中的靶向可控药物释放。再者，通过利用脱硫生物素-生物亲和素-生物素系统，我们组装了一种由**脱硫生物素转位子**传导的囊泡-囊泡通信系统。作为设计人造细胞的关键步骤，该系统可以通过与细胞间通信类似的方式进行跨膜通信。此外，我们还探索了一类**β-半乳糖转位子**以及使用水解酶作为在膜表面输入信号的可行性。最后，我们通过氟原子核磁共振技术为转位子催化基在膜中的位置提供信息，并通过使用一种荧光素的猝灭实验测定了转位子换的跨膜离子转运能力。

这项工作有助于我们进一步理解之前所提出的跨膜转位机制，并将人工跨膜信号转导的范围从纯实验合成系统扩展到了更为复杂的生物系统中，为未来人工智能响应囊泡的设计与发展提供潜力。

This page is intentionally left blank

Abbreviations

Aib	α-Aminoisobutyric Acid
AmB	Amphotericin B
ATP	Adenosine Triphosphate
Boc	*tert*-Butyloxycarbonyl Group
cAMP	Cyclic Adenosine Monophosphate
DCM	Dichloromethane
DMAP	4-Dimethylaminopyridine
DMF	*N,N*-Dimethylformamide
DMSO	Dimethyl Sulfoxide
DNA	Deoxyribonucleic Acid
DNPC	Dinervonoylphosphocholine
DOPC	1,2-Dioleoyl-*sn*-glycero-3-phosphocholine
DOPE	1,2-Dioleoyl-*sn*-glycero-3-phosphoethanolamine
DXR	Doxorubicin
EA	Ethyl Acetate
EDC	1-Ethyl-3-(3-dimethylaminopropyl)carbodiimide
EDTA	Ethylenediaminetetraacetic Acid
EGF	Epidermal Growth Factor
FRET	Förster Resonance Energy Transfer
FT-IR	Fourier-Transform Infrared Spectroscopy
gA	Gramicidin
GDP	Guanosine Diphosphate
GPCR	G-Protein Coupled Receptor
GTP	Guanosine Triphosphate
GUV	Giant Unilamellar Vesicle
H-bond	Hydrogen-Bond
HABA	4-Hydroxyazobenzene-2-carboxylic Acid
HEPES	4-(2-Hydroxyethyl)-1-piperazineethanesulfonic Acid
HPLC	High-performance Liquid Chromatography
HPTS	8-Hydroxypyrene-1,3,6-trisulfonic Acid
HR-MS	High Resolution Mass Spectrometry

K_a	Association Constant
K_d	Dissociation Constant
LC-MS	Liquid Chromatography–Mass Spectrometry
LDH	Lactate Dehydrogenase
LMV	Large Multilamellar Vesicle
LUV	Large Unilamellar Vesicle
m.p.	Melting Point
MES	2-(*N*-morpholino)ethanesulfonic Acid
MVV	Multivesicular Vesicle
NAv	NeutrAvidin
NBD	Nitrobenzoxadiazole
NHS	*N*-Hydroxysulfosuccinimide
NMR	Nuclear Magnetic Resonance
PAMAM	Polyamidoamine
PDB	Protein Data Bank
PEG	Polyethylene Glycol
POPC	1-Palmitoyl-2-oleoyl-*sn*-glycero-3-phosphocholine
r.t.	Room Temperature
RTK	Receptor Tyrosine Kinase
SEC	Size Exclusion Chromatography
SUV	Small Unilamellar Vesicles
TFA	Trifluoroacetic Acid
THF	Tetrahydrofuran
UPLC	Ultra-Performance Liquid Chromatography
UV-vis	Ultraviolet–Visible Spectroscopy

Real knowledge is to know the extent of one's ignorance.

Confucius

1 Introduction

1.1 Transmembrane Signal Transduction in Nature

Lipid bilayer membranes in biological systems form compartments to separate the interior of cells from their extracellular microenvironments. This compartmentalisation protects the cell from its surroundings and allows chemical processes to be physically decoupled on both sides of the membrane. Cell membranes coordinate a large variety of biological processes by selectively recognising and responding to different stimuli. This is of great significance for many processes, such as development, proliferation, differentiation, homeostasis and immunity.

In nature, membrane-spanning proteins play a key role in signalling processes for transmission of chemical or electrochemical signals across membranes.[1] Cells use a wide variety of specifically defined signalling pathways to regulate their activities. Whilst some of the systems respond to internal signals, which are commonly seen as metabolism messengers, the majority of them are activated by external signals. All signalling pathways can be divided into two main forms depending on whether the process involves a direct or indirect mass transfer. Common examples of direct mass transfer across the membrane are ions channels[2], aquaporin[3], and carrier proteins[4], which are responsible for mediating the selective passage of ions, water and small molecules, respectively. In 2003, the Nobel Prize in Chemistry was awarded jointly to Roderick MacKinnon for his studies on potassium channels and Peter Agre for the discovery of aquaporins.[5]

1.1.1 Ion Channels

Ion channels are one of the most widely distributed membrane proteins that allow the rapid and selective flow of ions across the cell membrane. Among many functions they perform, they play a pivotal role in regulating membrane potentials and conducting nerve impulse in higher organisms.[2] There are more than 300 types of ion channels in any given cell and they are usually classified by gating mechanisms. For example, voltage-gated ion channels are activated by changes in the electrical membrane potential[6], whilst ligand-gated ion channels are activated in response to the binding of a specific ligand[7], such as a neurotransmitter.

Figure 1.1 shows a ligand-gated potassium ion channel which consists of a selectivity filter, shown at the top of the protein, and a gating domain with a Ca^{2+} binding site, shown at the bottom.[8] The gating domains open and close the channel depending on the local concentration of Ca^{2+}. At a high Ca^{2+} concentration the channel opens the gating ring and allows potassium ion flux.

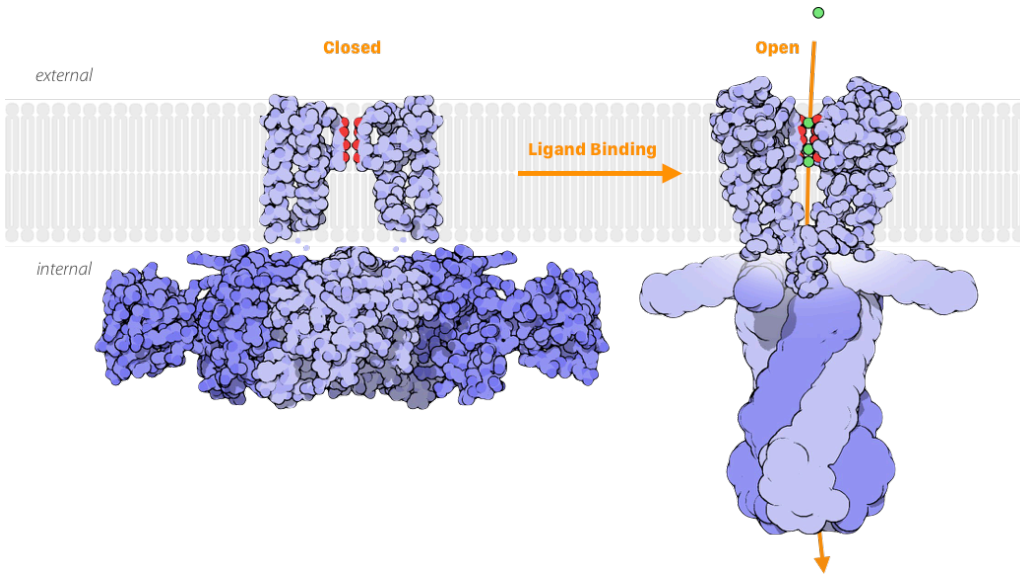

Figure 1.1 Illustration of a ligand-gated potassium ion channel in the lipid bilayer. The gating domain (in the membrane) opens upon calcium ion binding and allows K^+ influx. PDB entry: 1LNQ (left), 1K4C (right), ©copyright S. Dutta and D. S. Goodsell. This figure has been re-illustrated from the original representation under CC-BY-4.0 license.

1.1.2 Aquaporin

Aquaporins, also called water channels, are membrane proteins that selectively conduct water molecules while preventing the passage of ions and other solutes. They are extremely abundant not only in bacteria and plants but also in mammals. At least seven aquaporins are expressed in the kidney to facilitate essential functions such as formation of urine and regulation of osmolality.[9] The signalling function of aquaporin is less obvious than other membrane-expanding proteins mentioned previously and therefore is not reviewed in this section.

1.1.3 Carrier Proteins

Small molecules such as glucose, urea, and ammonia can be transported across the membrane with the help of relevant solute carrier proteins.[10–12] An important property of solute carrier proteins is that they are very specific for only one or a few structurally related molecules. For example, the glucose transport protein family, a common protein family that is found in most mammalian cells, facilitates the movement of glucose into erythrocytes. It recognises only glucose and a few similar monosaccharides, such as galactose and mannose. Moreover, the transport is stereospecific, i.e. only D- but not L-isomers of these monosaccharides can be transported across the membrane. A human genome encoded glucose transporter is shown in Figure 1.2.[13] Initially, the glucose transporter is in the conformation that exposes the binding site to the outside of the cell, which favours the binding of a D-glucose from the outside of the membrane (left). The binding event causes the transport protein to undergo a conformational change, which opens the binding site to the inside of the cell (right). The glucose can then be released in the cell and the transporter protein is free to revert to its original conformation, ready for the next cycle.

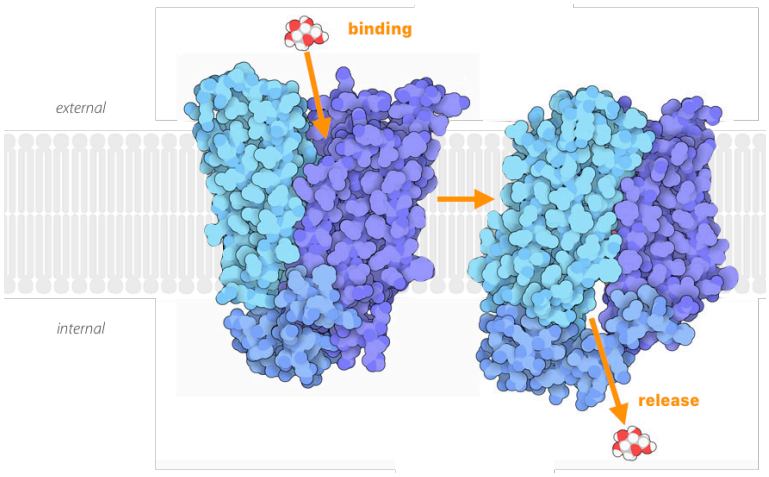

Figure 1.2 A glucose transport mechanism in the lipid bilayer. The glucose transporter is in the conformation that exposes the binding site to the outside of the cell, which favours the binding of a D-glucose from the outside of the membrane (left). The binding event causes the transport protein to undergo a conformational change, which opens the binding site to the inside of the cell and release the glucose (right). PDB entry: 4ZWC (left), 4PYP (right), ©copyright D. S. Goodsell. This figure has been re-illustrated from the original representation under CC-BY-4.0 license.

Signalling pathways that do not have direct mass transfer, i.e. where input and output signal are separated by the membrane, have more complex mechanism profiles. To date, up to 18 indirect transmembrane signalling pathways have been identified. Regardless of how different these mechanisms are, the first step of signalling is always a binding event of ligand on the outside of the membrane, which triggers a conformational change of the protein. Subsequently, information is conveyed either through protein-protein interactions (for example dimerization

or oligomerization of proteins, as observed in receptor tyrosine kinase (RTK)[14] or tumour necrosis factor receptors[15], respectively), or it is transmitted by generating diffusible yet membrane-impermeable molecules inside the cells, which are usually referred to as secondary messengers, as observed in G protein-coupled receptors (GPCRs). In 2012, the Nobel Prize in Chemistry was shared jointly to Robert J. Lefkowitz and Brian K. Kobilka for their studies of GPCRs.[16]

1.1.4 Receptor Tyrosine Kinases (RTKs)

In the human genome there are 58 receptor tyrosine kinase proteins (RTK) encoded and their principal functions involve the regulation of cell growth, differentiation, adhesion, motility and death.[17] RTK proteins have also been reported to have significant roles in the development of diseases, including diabetes and cancer.

Figure 1.3 shows an epidermal growth factor (EGF) receptor[18], a typical RTK located at the surface of cell membrane which gives cells permission to grow and divide. It consists of a large extracellular recognition domain, a membrane anchor section, a kinase domain and a long flexible tail. The recognition domain faces outwards from the cell and can bind EGF. When there is no EGF present, this extracellular domain folds back on itself, as shown on the left. Once an EGF binding (input) event happens, the recognition domain undergoes a conformational change to unfold itself. Subsequently, it binds to another copy of the EGF-bound receptor, forming a dimeric complex as shown on the right. The extracellular dimerization triggers intracellular dimerization of the kinase domain (shown at the bottom right), which then produces a cascade reaction (output) adding phosphate groups to the tyrosine on the flexible tail of the receptor. The phosphorylated tails stimulate further downstream signalling proteins in the cell.

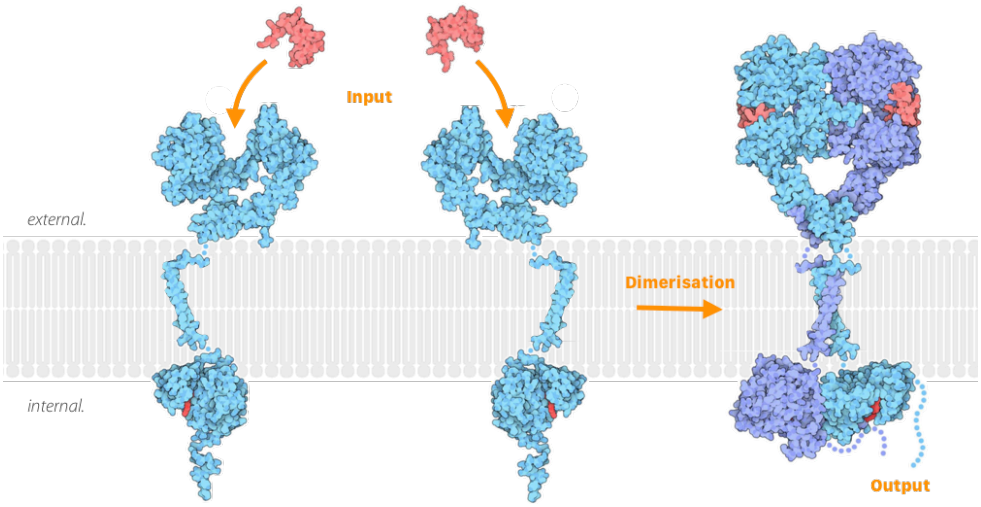

Figure 1.3 Transmembrane signalling of epidermal growth factor receptors. The receptor (blue) selectively binds EGF (input, red) and triggers a conformational change that favours dimerisation of two identical

receptors. Internal kinase domain is activated upon dimerization and produces a cascade reaction in the cell (output). PDB entry: 1EGF (EGF), 1NQL, 1IVO, 2JWA, 1M17, 2GS6 (receptor). ©copyright D. S. Goodsell. This figure has been re-illustrated from the original representation under CC-BY-4.0 license.

1.1.5 G Protein-Coupled Receptors (GPCRs)

Guanine nucleotide-binding proteins (G proteins) are a family of proteins that regulate a wide range of cell activities including metabolism, transcription, contractility, and secretion. There are two classes of G proteins depending on whether they are membrane-associated: monomeric small GTPases (not membrane-associated) and heterotrimeric G proteins (membrane-associated). The latter are receptor-mediated and are composed of α-, β-, and γ-subunits ($G_{\alpha\beta\gamma}$) on the inner membrane surface of the cell, see Figure 1.4.[19]

When the G protein is inactive, it is attached to the GPCR and there is a guanosine diphosphate (GDP) bound to G_α subunit. When a ligand, for instance a hormone, neurotransmitter, or glycoprotein, binds with a GPCR from the outside of the membrane (input), this ligand either stabilises or induces a conformational change in the receptor that releases the coupled G protein and activates it. Then the GDP dissociates from the G_α subunit and picks up a guanosine triphosphate (GTP) from the inside of the cell, and subsequently the G protein disassembles itself into G_α-GTP and $G_{\beta\gamma}$ subunits. Both subunits can activate downstream effectors.[20] For example, cyclic adenosine monophosphate(cAMP)-dependent signalling pathways, adenylyl cyclase is activated by G_α-GTP.[21] In turn, the activated adenylyl converts adenosine triphosphate (ATP) to cAMP, a typical secondary messenger. Multiple secondary messengers can be generated by one stimulus through this enzymatic reaction inside the cell to achieve amplification. An increase in concentration of the cAMP can further activate multiple signalling events, for example activation of a cyclic nucleotide-gated ion channel.[22]

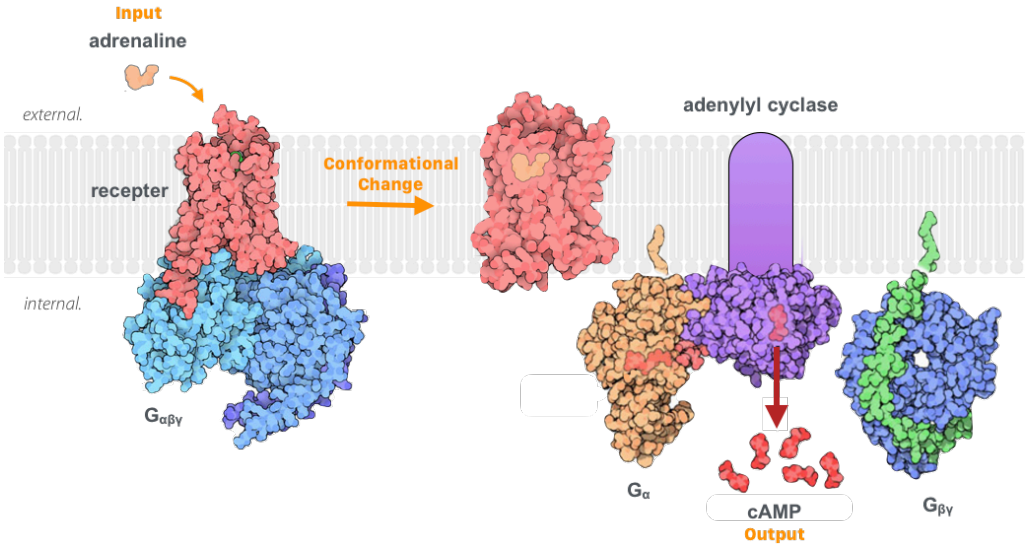

Figure 1.4 Transmembrane signalling of G protein-coupled receptor. In the initial state, the receptor (pink) is bound to the G-protein (blue). Binding with an adrenaline molecule (input) triggers a conformational change

of the receptor and release the G-protein at the inner side of the membrane. Further conformational change dissociates G_α subunit (orange) and subsequently binds and activates adenylyl cyclase (purple) and generates multiple cAMP molecules (output, red) in the cell. PDB entry: 2RH1, 1GOT, 1CUL, 1TBG (from left to right),

1.2 Vesicles and Applications

Lipid bilayer membranes not only separate cells from the surroundings, they also provide compartmentalisation for sub-cellular structures, such as the nucleus, mitochondrion, Golgi apparatus, and vesicles. In cell biology, a vesicle is a spherical structure that consists of liquid or cytoplasm encapsulated by a lipid bilayer membrane. This structure is a tool used by cells for organising cellular substances within or outside the cell and is involved in many essential cell functions such as metabolism and transport. Cell-derived extracellular vesicles also have a myriad of potential clinical applications, ranging from biomarkers to anticancer therapy.[23] The 2013 Nobel Prize in Physiology or Medicine was awarded to James E. Rothman, Randy W. Schekman and Thomas C. Südhof "for their discoveries of machinery regulating vesicle traffic, a major transport system in our cells."[24]

Artificial vesicles, commonly referred to as liposomes, have been utilised in the pharmaceutical industry due to their flexible structures and practical function since their discovery in mid-60s.[25] In fact, liposomes are the first drug delivery nanotechnology that have been successfully translated from research to clinical trials. Research on liposomal formulation has progressed from conventional liposomes (1st generation liposome) to 2nd, 3rd,and 4th generation liposome.[26] The 1st generation liposomes were simple formulations of liposome-containing drugs such as amphotericin B, *Ambisome* (Nexstar, USA), and doxorubicin, *Myocet* (Elan Pharma Int., USA). All further generations are surface, lipid composition, and charge modified variations for different therapeutic purposes. To date, there are more than 15 clinically used liposome-based products on the market that are used to treat fungal infections, inflammation, cancer, and in gene therapy.[27]

Synthetic vesicles have become a highly valued model for scientists to study and understand diverse biophysical processes in the membranes.[28–30] Apart from targeted delivery and controlled cargo release, artificial vesicles have also been actively pursued to engineer more complex functions such as recognition and signalling[31–42], membrane fusion[43–46], and construction of artificial minimal cells.[47,48]

1.2.1. Classification of Vesicles

Vesicle size can range from small (20 nm – 100 nm), large (100 nm – 400 nm), to giant (1 μm and larger), or they can be unilamellar (one lipid bilayer), multilamellar, and multivesicular (refer to multiple vesicles encapsulated in one bigger vesicle). Mixing and matching these two parameters (size and number of lamellar) creates the following terms that are widely used in the field: small unilamellar vesicles (SUVs), large unilamellar vesicles (LUVs), giant unilamellar

vesicles (GUVs), large multilamellar vesicles (LMVs), and multivesicular vesicles (MVVs).[49] A schematic illustration of the classification of vesicles is shown in Figure 1.5.

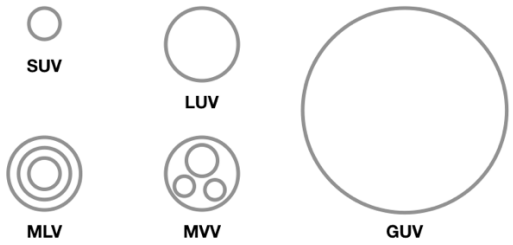

Figure 1.5 Vesicle classification based on size and number of lamellae.[49]

1.2.2 General Methods for Vesicle Preparation

Depending on the desired structure of the vesicles, various techniques can be used to prepare them.[49] Conventional methods of preparation at laboratory scale involve the following basic stages: a) drying down lipids from organic solvent; b) rehydration of lipids in aqueous media; c) mechanical dispersion such as freeze-thaw, extrusion, or sonication; d) vesicle purification. Most of the techniques start with preparing dried lipid films on a surface by evaporation under reduced pressure or blow-drying with a nitrogen or argon stream. Next, the films are rehydrated using an aqueous solution (usually a buffer) with swelling and MLVs are formed.[50] To modify the structure and size of these MLVs, various methods can be used.[51]

Rapid freezing and slow thawing cycles of MLVs create unilamellar vesicles as a result of the fusion of vesicles throughout the process.[52] It can also improve the encapsulation efficiency of solutes in the vesicles.[53,54] Extrusion of MLV suspensions using porous polycarbonate membranes is a standard method for preparing LUVs.[55,56] It is a convenient and efficient method for small scale vesicle preparation. Extrusion of vesicles through small pores (approx. 100 nm in diameter) results in relatively uniform-sized vesicles, while for larger LUVs, the extrusion technique tends to result in a more heterogeneous population of vesicles. Large pore dialysis may be used to improve dispersity.[57] One drawback of this method is that, for lipids with transition temperatures higher than room temperature, it is challenging to maintain the whole apparatus at a constant high temperature, resulting in difficult extrusion. Probe or bath sonication is the most extensively used method for the preparation of SUVs. For probe sonication, the tip of a sonicator is directly submerged into the MLVs suspension. Due to high energy input at the tip, external cooling with a water/ice bath is usually required. Disadvantages of this method include noticeable lipid degradation: for a sonication up to 1 h, 5% of the lipids may be de-esterified. Note that only a few of these methods are capable of encapsulating large quantities of water-soluble agents. To entrap bioactive agents, methods such as the reverse-phase evaporation technique[58], or ether/inject technique[59,60] can be used to yield higher efficiency. A schematic illustration of vesicles preparation is shown in Figure 1.6.[50]

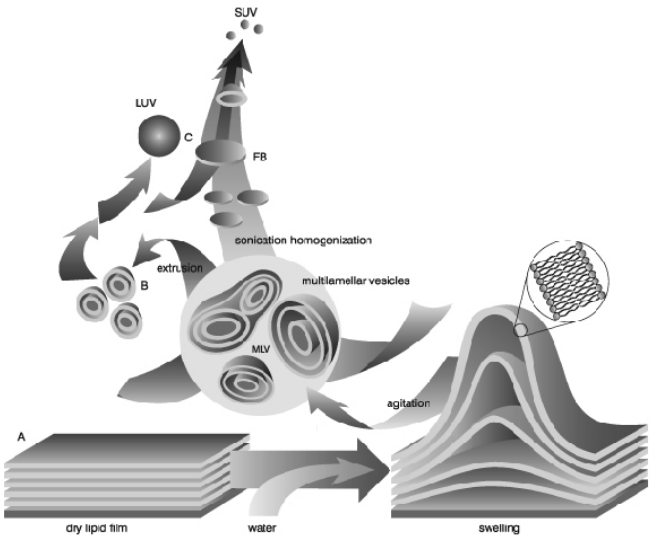

Figure 1.6 A schematic illustration showing pathways for vesicle formation. ©copyright(1988) Portland Press, reprinted under CC-BY-4.0 license.[50]

Size exclusion chromatography (SEC) is a well-established method to separate small solutes from vesicles or to narrow the size distribution.[61–63] Vesicle retention on the polymeric gel depends on the pore size, material, and mobile aqueous phase. It is a dynamic and reversible process and extra attention needs to be given when choosing the column to minimize lipid loss and sample contamination during the chromatography.[64]

1.3 Direct Mass Transfer: Artificial Transporters and Channels

Taking inspiration from nature, supramolecular chemists have designed and constructed simple molecular structures or systems to reproduce many of the fundamental functions of natural signalling proteins. A large number of synthetic systems that can physically transport ions or small molecules across lipid membranes via pores or transporters have been developed throughout the past three decades. Although it is considered to be more challenging, recent advances and new concepts in supramolecular chemistry have made it possible for the development of signalling systems that are capable of transmitting a molecular signal without physical transport of the messenger across the membranes.

There are hundreds of examples of a wide range of mechanisms and building blocks capable of conducting ion transport across the membrane. In this section, we briefly summarize some of the most important designs with a focus on the architecture of these channels or transporters. Figure 1.7 illustrates four major categories of artificial transporters and channels and their variations: carrier, barrel, ring, and helix. The carrier category represents systems with the specific ion-binding site(s) and can achieve ion transport through either a ferry-like movement or a binding relay mechanism. The other three categories represent systems with channel structures. For the barrel category, the channels are formed by vertical components that

assemble horizontally in the membrane. For the ring category, the channels are formed by horizontal ring components that assemble vertically in the membrane. The helix category is formed by helical structures, where the molecules elongate both horizontally and vertically. Due to the complex nature of different examples reported in the literature, these four categories are unlikely to be completely mutually exclusive and collectively exhaustive. However, it can form the basis of our understanding.

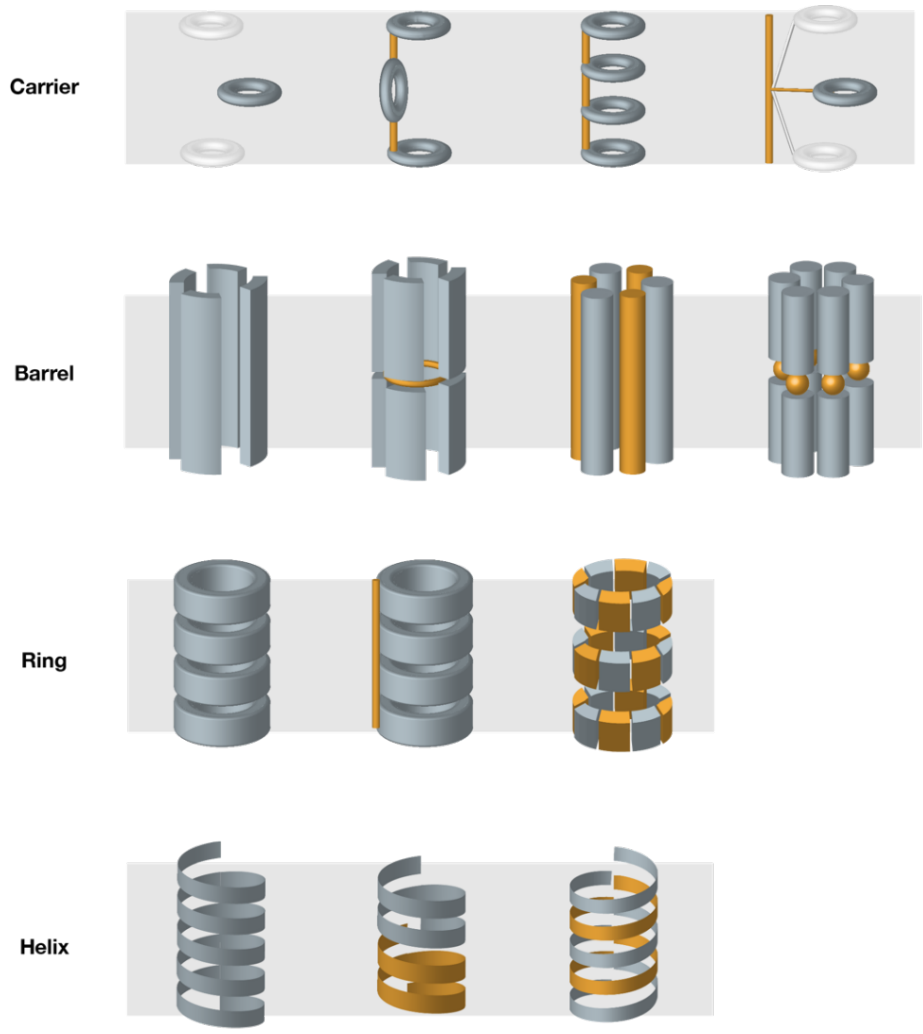

Figure 1.7 Four major categories (carrier, barrel, ring, and helix channel) of artificial transporters and channels in the lipid bilayer membrane. Carrier: (from left to right) ferry-like transporter, central relay, multiple relay, swing; Barrel: barrel-stave molecules, linked (linkage in gold) barrel-stave, aggregates (gold represents another molecule), dimer aggregates (linkage in gold); Ring: stacked rings, linked (linkage in gold) rings, rosette (monomer grey or gold); Helix channels: monomeric, dimeric, and oligomeric helix channels (monomer in grey or gold).

There are several techniques to study the ion transport mechanism. The "U-tube" transport experiment is useful for identifying synthetic carriers. In this experiment, an organic solvent (for example chloroform) where carriers are dissolved is place at the bottom of a U-shaped tube, and two aqueous buffers are deposited on both sides of the tube. If solutes that are loaded from

one side of the buffer can be detected on the other side, one can unambiguously report the presence of a carrier as the channel mechanism is not possible.[65] One well-established method is 8-hydroxypyrene-1,3,6-trisulfonic acid (HPTS) assay. HPTS is a pH-sensitive dye whose fluorescence emission can be used to monitor ion-transport-induced changes in internal pH of vesicles. However, the HPTS assay only confirms the transport of ions but does not detect the transport mechanism. Single-channel conductance experiments in planar bilayers can be used to identify the channel mechanism, as this experiment can detect the opening and closing of single ion channels. The lifetime of single channels also reveals their kinetic stability.[65]

1.3.1 Carriers

The difference between a carrier and a channel is that the former acts as a ferry and physically moves to perform metal transport, whilst the latter remain still in the lipid bilayer. In addition, carriers also recognise and bind non-covalently to one or a few specific solutes, and then release them when the complex reaches the other side the membrane. In this regard, several examples in this carrier category have structures that consist of multiple carrier monomers that form a "relay" across the membrane – the ions can be passed on from one side to another via multiple binding sites in a sequential manner. Although the carriers themselves in these particular examples might not be moving a great distance in the membrane, the mechanism is still a bind/unbind process that transports ions.

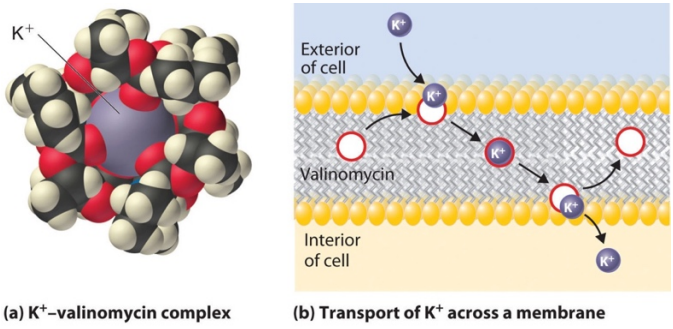

Figure 1.8 Valinomycin K^+ transporter mechanism. (a) 3D model of K^+–valinomycin complex determined by x-ray diffraction. (b) Valinomycin facilitates the transport of K^+ ions across the cell membrane. At the surface of the membrane, valinomycin binds a K^+ ion. Because the hydrophobic exterior shields the positive charge of the metal ion, the K^+–valinomycin complex is soluble in the nonpolar lipid bilayer. The complex translocates to the other side of the membrane and releases the K^+. Then the valinomycin is free to diffuse back to the other side of the membrane to repeat the cycle. ©copyright (2012) Saylor Academy[66], reprinted under CC BY-NC-SA 3.0 license.

Early emphasis on carrier systems focused on mimicking valinomycin, gramicidin, or amphotericin. Valinomycin is a naturally occurring lipid-soluble macrocyclic polypeptide that can carry K^+ across the lipid bilayer.[67] The transport mechanism consists of interfacial binding of K^+ from one side of the membrane, translocation of the cationic complex through the lipid bilayer, release of K^+ at the other side of the membrane, see Figure 1.8.[66] This transport is

electrogenic (i.e., it modifies a membrane potential) because there is a net transfer of charge across the lipid bilayer. Depending on the charge transferred, ionophores can be further classified into cationophores (including protonophores) and anionophores.

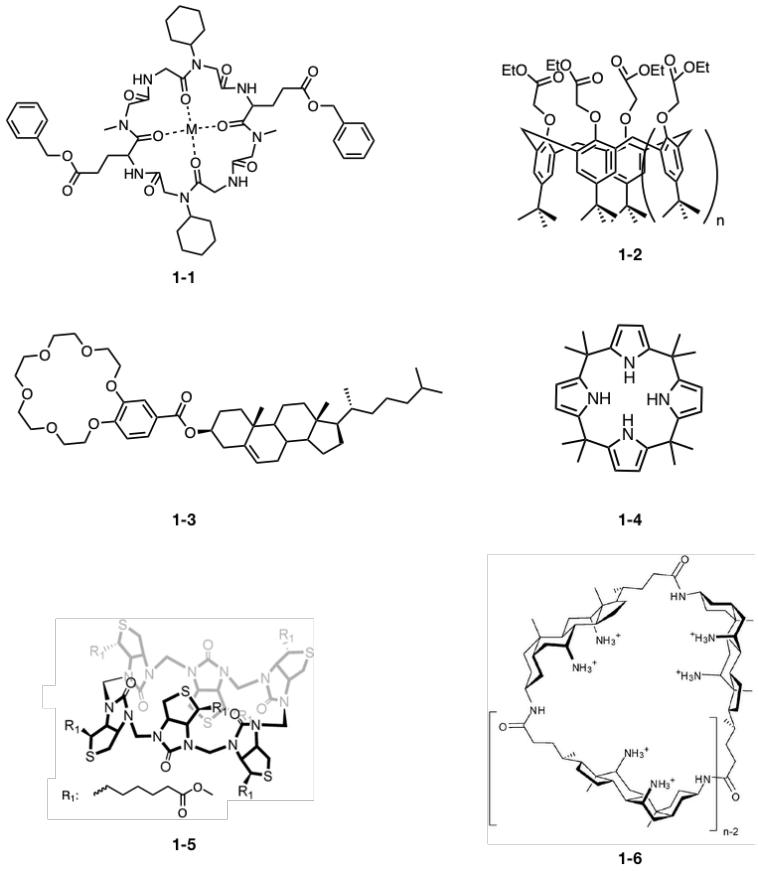

Figure 1.9 Examples of synthetic ionophores that functions as carriers.

Synthetic cationophores have been proven to conduct similar transport activity as valinomycin using structures such as cyclic peptides[68,69], calixarene esters[70], and armed crown ethers[71] (Figure 1.9). They all have a cyclic structure with an electron-rich cavity that can bind, sometimes selectively, cations and transport them across lipid bilayer membranes. Different sizes of cavity favour different cations. For example, compound **1-1** is a calcium-specific transporter that transports Ca^{2+} 10 times faster than Mg^{2+}. For the calix[n]arene esters **1-2**, each family member has a specific alkali-metal ion transport preference: Na^+ (n = 3), K^+ (n = 4), Rb^+ (n = 5), Cs^+ (n = 6). Note that there is a possibility that dimeric calix[n]arene esters form a channel-like structure, but for simple calix[n]arene esters, this claim lacks evidence.[70] Crown ether **1-3** is the classic example for host-guest interactions, and its lipophilic arm acts as an anchor in the lipid bilayer. Calix[4]pyrrole derivatives **1-4** have been studied for anion binding. Calix[4]pyrrole promotes ion pair transport such as CsCl[72]. As for anionophores, biotin[6]uril ester **1-5** favours the transport of less hydrophilic anions such as Cl^- and NO_3^- over hard, strongly hydrated anions such as HCO_3^- and SO_4^{2-}.[73] Cyclocholamides **1-6** have a

hydrophobic exterior and a strongly hydrophilic interior due to multiple NH_3^+ groups. These positive charges at the inner side of the ring make the carrier anion-selective.[74]

Supramolecular chemists have studied a wide range of mimics of prodigiosin (**1-5**), a well-known non-cyclic natural anionophore which recognises and transports anions such as Cl^- and NO_3^-, examples see Figure 1.10. Functionalised prodigiosin derivatives[75] and similar molecules with imidazole or isophthalamide moieties have been reported to conduct anion transport.[76] Dinuclear zinc complexes **1-6** is able to transport anionic molecules including phospholipids.[77] Cholapods (steroid-based anionophores, **1-7**) consist of cholate scaffolds with anion binding sites that show remarkable Cl^--selective transport. [78] Its transport activity is determined by the hydrogen-bond donors offered in the preorganized binding site. Positively charged ceragenins such as **1-8** showed the ability to mediate the efflux of anionic fluorophores or cationic quenchers.[79] Molecular umbrellas, for example **1-9**, are active in transporting protons and both Na^+ and Cl^-. They were initially studied to determine the position in the lipid bilayer membrane and the results suggested that higher total charge leads to better membrane incorporation.[80]

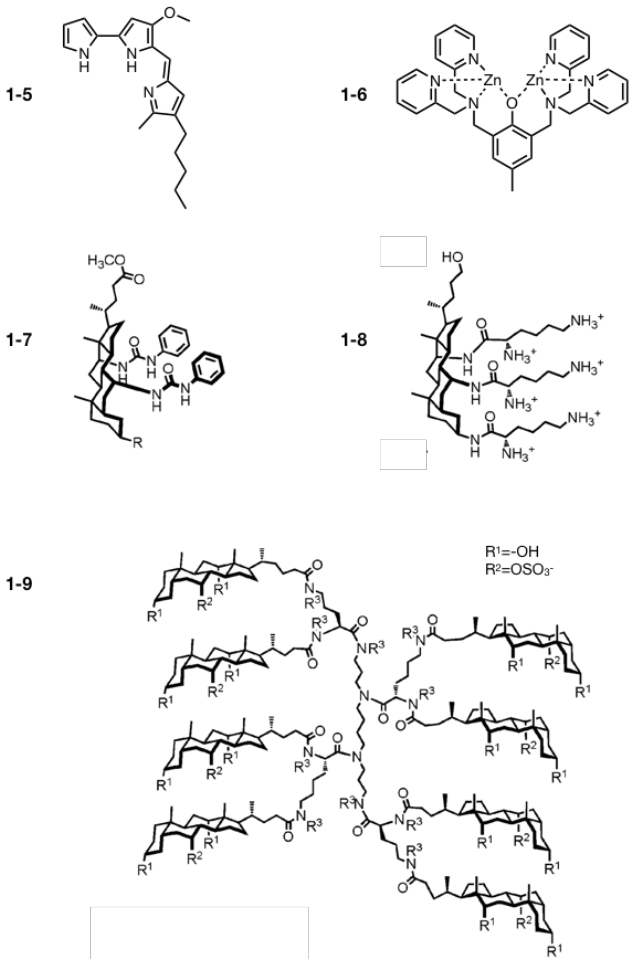

Figure 1.10 Prodogiosin (**1-5**) and examples of synthetic ionophores (**1-6** to **1-9**).

Attaching the carrier to a membrane anchor creates a molecular swing, as recently reported by Huaqiang Zeng (Figure 1.11).[81] Molecule **1-10** consists of three elements: a long rod with two membrane anchors to allow the swing to be embedded into the hydrophobic membrane regions, a 15-C-5 or 18-C-6 crown as the swing seat for binding and transporting metal ions such as K^+, and a flexible polyethylene glycol chain which acts as the swing. The swing mechanism is supported by both HPTS H^+/M^+ transport assay as well as single-channel experiment. The system is essentially a carrier system with extra elements that facilitate and guide the movement of the carrier.

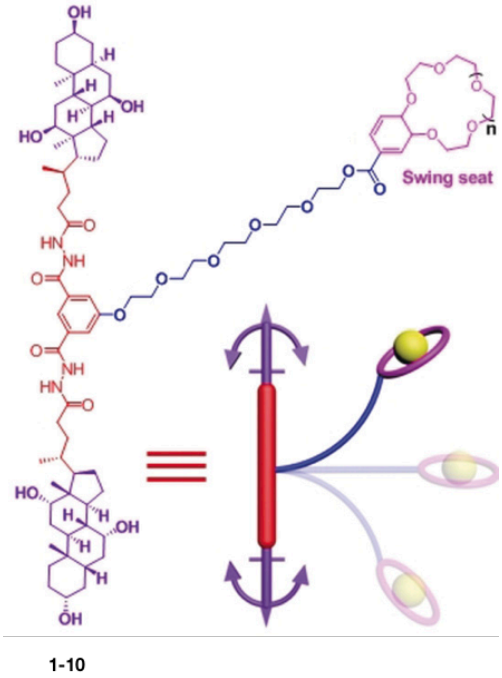

Figure 1.11 An example of a molecular swing. ©copyright 2019 Wiley-VCH, reprint with permission.[81]

The oligocrown scaffold **1-11** is a classic example of a central relay mechanism, see Figure 1.12. The two crowns at the end of the molecule are located at the membrane-aqueous interface whilst the middle one is embedded in the lipid bilayer and perpendicular to the other two crowns.[82] Cations such as Na^+ binds in a sequence of end-middle-end crowns and get released at the other side of the membrane. Longer relay has also been proven possible. Compound **1-12** contains four 18-C-6 crown binding sites with a ferrocene active centre connecting the middle two.[83] The ferrocene unit also performs redox-gating. When oxidized from Fe^{2+} to Fe^{3+}, the transport of Na^+ or K^+ across the bilayer is inhibited. Compound **1-13** is one of a series of synthetic helical peptides that are oligomers of a repeating unit with five leucine residues and 21-C-7 aligned on one side of the helix axis.[84]

Normand Voyer and coworkers have further investigated how far can an ion travel through membranes in the relay mechanism by using a series of helical peptide with crown ether binding sites.[85] These molecules have a different distance between any adjacent two crown ether

units and their Na^+ transport ability was measured by classic HPTS assay. The distance between two binding sites for which significant transport can be observed is 11 Å.

The relay does not necessarily have to be a crown ether system. Figure 1.13 demonstrates a halogen anion hopping on **1-14**, a linear oligomer of p-oligophenyls functionalised with tetrafluoroiodobenzyl groups.[86] This rigid-rod scaffold can span the lipid bilayer and effectively transport halogen anions. Figure 1.14 shows another membrane transporter that uses the relay mechanism.[87] The phosphatidylcholine derivative **1-15** is equipped with a urea group. The relay mechanism requires that the transporter must reside in both leaflets of the bilayer so that the anion can be transferred from one leaflet to another via an intermediate 1:2 complex. This hypothesis was confirmed by using two different transport loading methods: pre-incorporation and external addition. No Cl^- transport was observed when the experiment was done by external addition method, suggesting the transporter cannot flip flop from one leaflet to another.

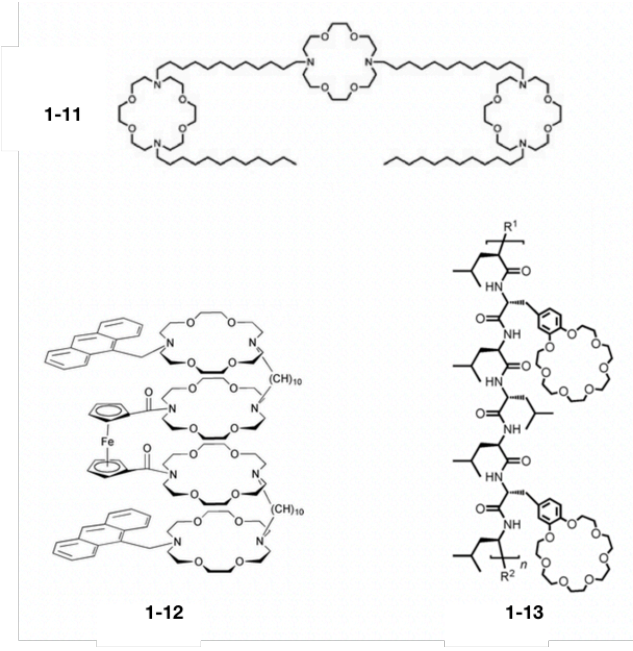

Figure 1.12 Examples of molecules that conduct ion transport by a carrier relay mechanism.

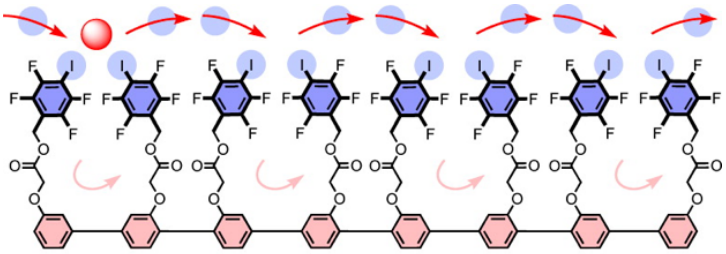

1-14

Figure 1.13 An example of halogen relay mechanism. ©copyright (2013) American Chemical Society, reprint with permission.[86]

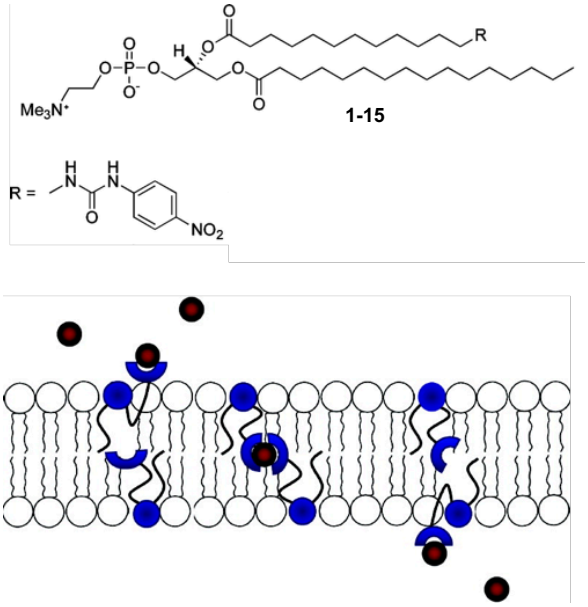

1-15

Figure 1.14 An example of dimeric relay mediated by urea-anion binding relay. ©copyright (2008) American Chemical Society, reprint with permission.[87]

1.3.2 Barrel Channels

In the literature, multiple terms are used in describing a channel system formed by an aggregation of vertical components. The use of these terms is sometimes ambiguous and overlapped. However, despite the name differences, all systems are topologically similar to each other and therefore each individual system can be regarded as a barrel. Stefan Matile elaborated the nuances between the beta-barrels, barrel-stave, bundles in a review article[88].

The term "barrel-stave" was first used in 1996 by Koji Asami and co-workers, who have synthesized template-assembled alamethicins in which three to five 18-mer alamethicin fragments were arranged to form a channel **1-16** – **1-18**, see Figure 1.15.[89] The alamethicin oligomer forms alpha helix bundles which are linked by a macrocycle. Ion transport was confirmed by single-channel conductance experiments and the largest cycle (n = 5) has various conductance states, which could be attributed to the conformational flexibility.

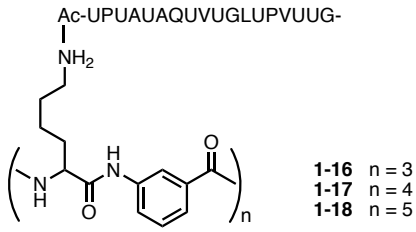

Figure 1.15 Molecular structure and schematic presentation a barrel-stave channel.

Stefan Matile and co-workers reported systematic studies on artificial rigid-rod beta-barrels (**1-19** – **1-20**) that forms pores in the membrane.[90] In these systems, short peptide strands are attached to a molecular rod. It is proposed that the amino acid residues on the peptide strands point alternatively to the barrel interior and the outer surface, see Figure 1.16, and programming these residues can achieve various functionalities such as enzyme sensing.

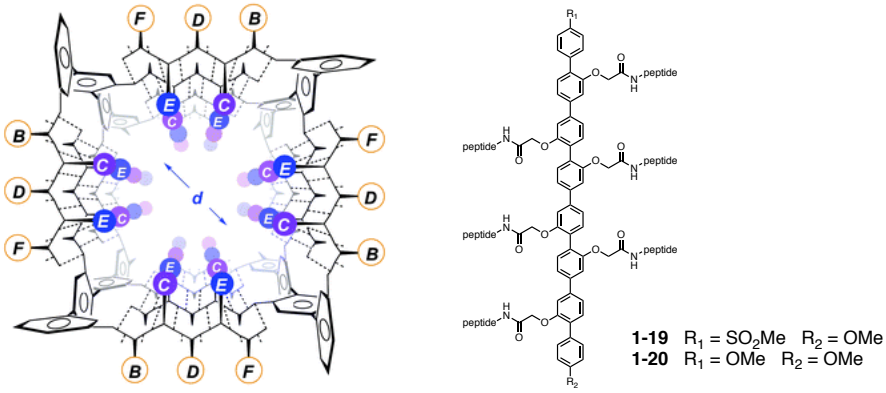

Figure 1.16 Proposed self-assembly of *p*-octiphenyls rods into rigid-rod β-barrel channel. Residue: A = G, B = L, C = K, D = L/W, E = H/D, F = L/V. ©copyright (2003) The Royal Society of Chemistry, reprint with permission.[90]

Yoshiaki Kobuke and co-workers presented the first synthetic voltage-gated ion channel system by introducing electrical asymmetry to the two ends of the scaffold molecule, namely carboxylic acid and phosphoric acid for compound **1-21**, and hydroxyl and carboxylic acid for compound **1-22**, see Figure 1.17.[91] In basic pH environments, the head groups have charges of -1/-2 and 0/-1, respectively, resulting in a charge density asymmetry of the channel. When embedded in a lipid bilayer membrane, application of positive voltage induces alignment of the more negative head groups to the same side, affording rectified single-channel currents.

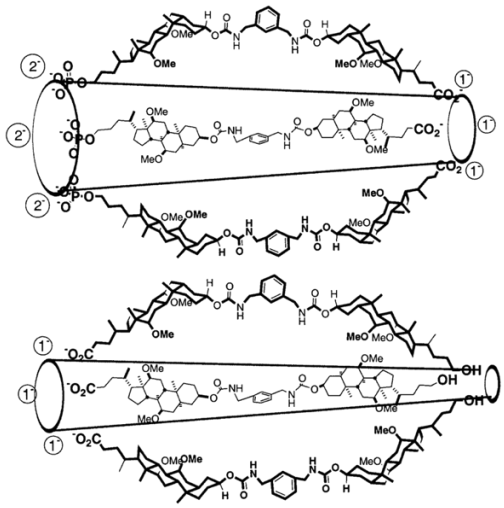

1-21

1-22

Figure 1.17 A proposed structure of voltage-gated synthetic ion channel. ©copyright (2001) American Chemical Society, reprint with permission.[91]

Amphotericin B (AmB), which has an amphiphilic macrocyclic structure (Figure 1.18a), forms membrane-spanning aggregates in the lipid bilayer, creating a hydrophilic pore. The lipophilic side is a polyene and the hydrophilic side is enriched with hydroxyl groups. The channel structure is believed to be maintained by an intermolecular hydrogen-bonding system, which is reminiscent of barrel structure in Figure 1.18b.[92] On average, approx. 75% of the hydroxyl groups form hydrogen bonds with neighbouring AmB molecules. The channel enables rapid exchange of monovalent ions such as K^+, Na^+, H^+, Cl^-, resulting in anti-fungal activity.

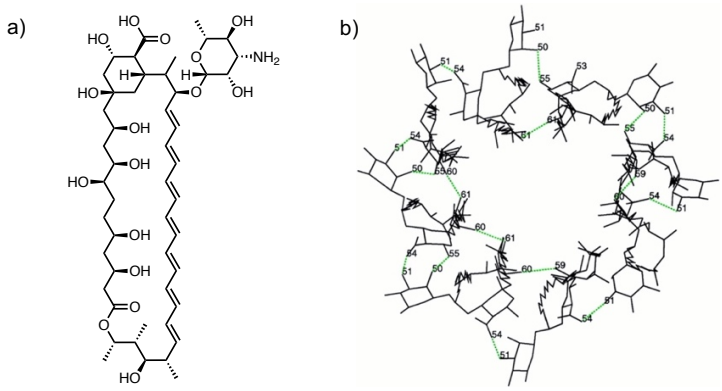

Figure 1.18 a) Molecular structure of Amphotericin B amphiphilic macrocycle. b) A simulated structure of hydrogen-bonding system in Amphotericin B channel. ©copyright (1997) ASPET, reprint with permission.[92]

Jürgen-Hinrich Fuhrhop and co-workers have reported a 38-membered tetraether macrocycle compound **1-23**, which can be converted into a two-headed amphiphile by oxidation or alkylation of the sulphur atoms, see Figure 1.19.[93] When incorporated into vesicle membranes, the addition of the oligoamine compound **1-24** triggers aggregation and pores are formed in

the lipid bilayer, leading to Li^+ and Fe^{2+} transport, as suggested by a fluorescein quenching assay. It is also possible to stop the transport by sealing these pores with "stopper" molecules such as ethylenediaminetetraacetic acid (EDTA) or taurine.

1-23

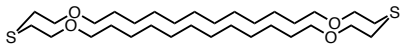

1-24

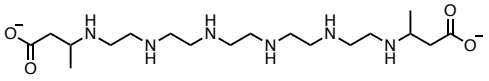

Figure 1.19 Molecular structures of a channel-forming system.

Simon J. Webb and co-workers have developed a system using palladium coordination to gate half-channel molecules **1-25**, see Figure 1.20.[94] The monomer is ineffective at transporting ions across the membrane. Incubating vesicles with $PdCl_2$ gave at least a 9-fold enhancement in the transport rate of Na^+ and a 5-fold increase of K^+ in the HPTS assay. Hexathia-18-crown-6 (18S6) can be used to switch transport off, and the addition of further $PdCl_2$ restores ion transport. This method was further developed for Pd^{2+}-mediated assembly of porphyrin channels in the membrane.[95]

1-25

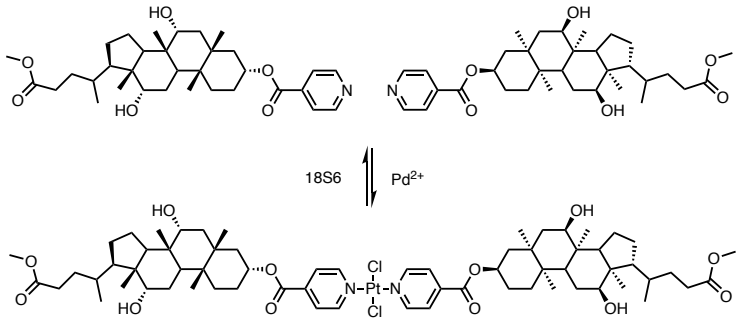

Figure 1.20 Palladium gated ion channel. When embedded into lipid bilayer, adding palladium salt dimerize the half-channel molecule and enables ion transport. Addition of hexathia-18-crown-6 removes Pd^{2+} and therefore dissociate the channel.

Foldamers are synthetic oligomers that can form well-defined and stable helical structures like protein or peptides. Jonathan Clayden, Simon J. Webb and co-workers have demonstrated that 3_{10}-helical α-aminoisobutyric acid (Aib) foldamers **1-26** have ionophoric activity in the lipid bilayer, see Figure 1.21.[96] A series of Aib oligomers have been synthesized and the strongest conductance was observed for foldamers that have end-to-end distances greater than the hydrophobic width of the bilayer. Single-channel conductance and HPTS assay confirmed alkali ion transport and suggested that the length of the scaffolding molecule is one of the essential parameters for forming a channel in the membrane.

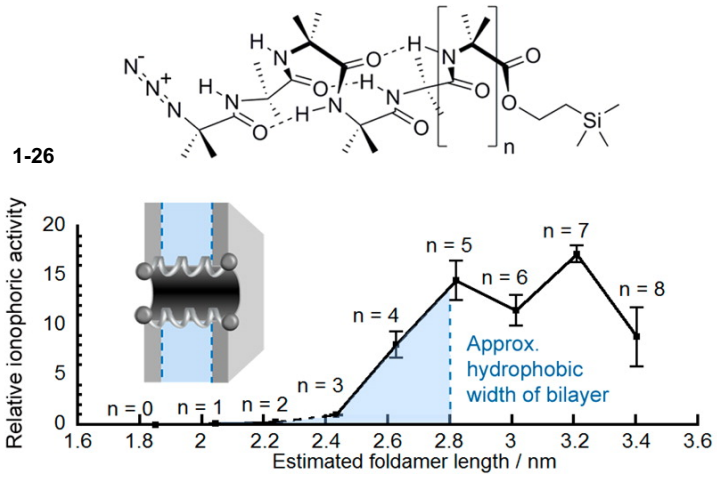

Figure 1.21 An Aib foldamer structure and relative rate constant for Na^+ transport Aib foldamers vs number of Aib residues for foldamers. ©copyright (2016) American Chemical Society, reprint with permission.[96]

With advances in deoxyribonucleic acid (DNA) nanotechnology, Hendrik Dietz, Friedrich C. Simmel and coworkers created scaffolded DNA origami that can penetrate and span a lipid bilayer, forming membrane pores, see Figure 1.22.[97] TEM image confirmed that DNA channels could bind to lipid bilayers as designed. Single-channel conductance experiments suggest that these DNA origamis can not only transport ions but also detect and discriminate between single-DNA strands as a single molecule biosensor.

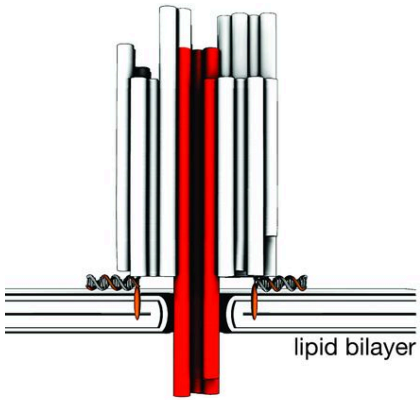

Figure 1.22 Synthetic DNA origami channel embedded in lipid bilayer membrane. Schematic illustration of the channel formed by 54 double-helical DNA domains packed on a honeycomb lattice. Cylinders indicate double-helical DNA domains. Red denotes transmembrane stem; orange strands with orange ellipsoids indicate cholesterol-modified oligonucleotides that hybridize to single-stranded DNA adaptor strands. ©copyright (2016) AAAS, reprinted under CC-BY-4.0 license.[97]

1.3.3 Ring Channels

Many channel transport systems with cyclic ring structures have been reported. Hitoshi Ishida and co-workers have prepared a series of cyclic peptides possessing an alternative natural/non-

natural amino acids sequence with a long acryl chain (compound **1-27**, Figure 1.23). Depending on ring size and side-chain length, the cyclic peptides showed different cation selectivity.[98] A similar strategy using cyclic peptides has been developed. M. Reza Ghadiri and co-workers synthesized a cyclic peptide analogue with alternating D, L- amino acids which can form β-sheet-like tubular structures.[99,100] These peptides can self-assemble using a hydrogen-bonding system that connects neighbouring layers vertically with amide groups, as confirmed by single-channel experiments. Amino acid side chains of the peptides are therefore in the equatorial positions around the macrocycle facing towards the membrane lipids. Apart from conducting Na^+ or Cl^-, one of the cyclic peptides showed high efficiency in transporting glutamic acid.

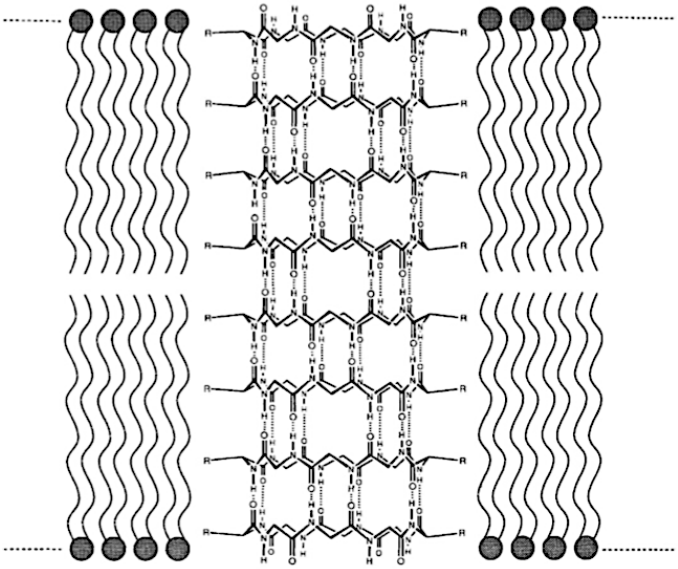

1-27

Figure 1.23 A channel-forming cyclic peptide in a self-assembled tubular configuration embedded in a lipid bilayer membrane (for clarity most side chains are omitted). ©copyright (1994) Nature Publishing Group, reprint with permission.[98]

Apart from cyclic peptides, other ring structure components have been used to form channel structures by ring stacking. Bing Gong, Zhifeng Shao and co-workers have reported a series of shape-persistent macrocycles with aromatic oligourea, sulfonamide, and oligohydrazide backbones that can form K^+ channels (supported by single-channel conductance and HPTS assay) through a ring stacking mechanism, an example is shown in Figure 1.24.[101,102] Apart from the intramolecular hydrogen-bonding system that stiffens the ring structure, intermolecular hydrogen-bonding of side chains can be introduced to enforce stacking into a self-assembling nanotube.

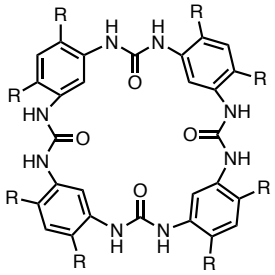

1-28

Figure 1.24 An example of shape-persistent macrocycles with aromatic oligourea.

Pengyang Xin, Changpo Chen and coworkers reported a series of hybrid pillararene-cyclodextrin molecules with different lengths that form membrane channels, see Figure 1.25. According to single-channel experiments and HPTS assay, channel **1-29** which possesses the shortest linker showed specific transport preference for K^+ over other alkali metal ions. Elongation of the linkers in the channels **1-30** and **1-31** increases the flexibility of the tubular structures and the distance between the binding sites, which might be responsible for the decreased ion transport selectivity.[103]

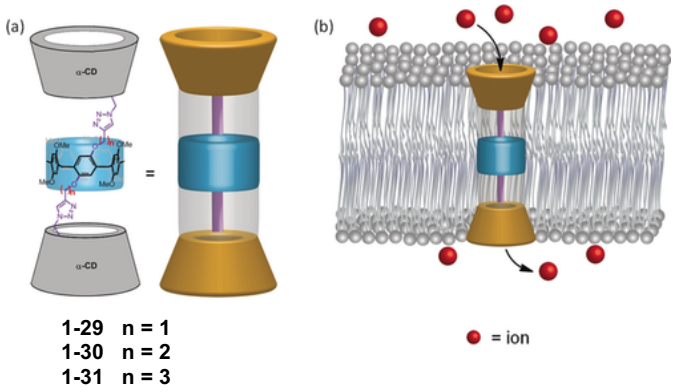

1-29 n = 1
1-30 n = 2
1-31 n = 3

Figure 1.25 Structures of pillararene-cyclodextrin molecules. a) molecular structure of channels **1-29** – **1-31.** b) Schematic illustration of the ion transport mechanism. ©copyright (2019) Wiley-VCH, reprint with permission.[103]

Another noticeable design to construct rings is metal-organic cyclic structures. Paolo Tecilla and co-workers designed a stable tetraporphyrin metallacycle with Re(I) corners and peripheral carboxylic acid residues (compound **1-32**) that is capable of forming pores in the lipid bilayer, see Figure 1.26.[104] HPTS assay confirmed alkali metal ion transport. As the corresponding methyl ester (compound **1-33**) does not transport ions, the presence of the properly oriented carboxylic acid groups is essential for the transport ability. Therefore, a dimeric structure of channel assembled with hydrogen-bonding system was proposed. This channel can also be blocked by the addition of a cystamine core polyamidoamine (PAMAM) dendrimer that occupies the metallacycle.

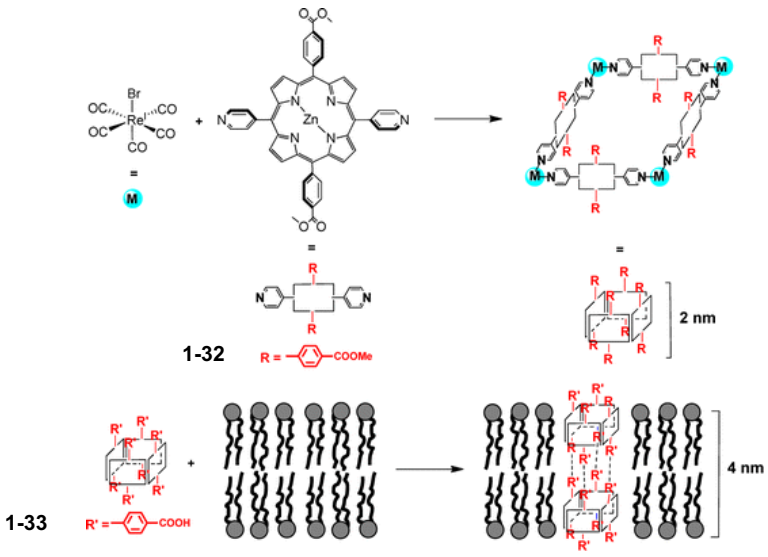

Figure 1.26 Schematic representation of the porphyrin metallacycle and formation of a transmembrane nanopore upon hydrogen-bonding driven dimerization. ©copyright (2012) American Chemical Society, reprint with permission.[104]

Julio D. Martin and co-workers proposed a transport mechanism channel that is formed by self-assembly of rosette monomers joined by hydrogen-bonding networks.[105,106] The monomer **1-34** – **1-36** has two carboxylic acid groups that can construct cyclic two-dimensional hydrogen bond arrays in crystal structure, see Figure 1.27. The bicyclic backbone provides steric demands which orientate the angle of two carboxylic acid groups in order to form the supramolecular macrocycle. When incorporated into the lipid bilayer membrane, these molecules showed transmembrane Na^+ transport activity. No further evidence of channel formation was reported. Other cyclic assemblies with various functional groups have also been reported.[107–109]

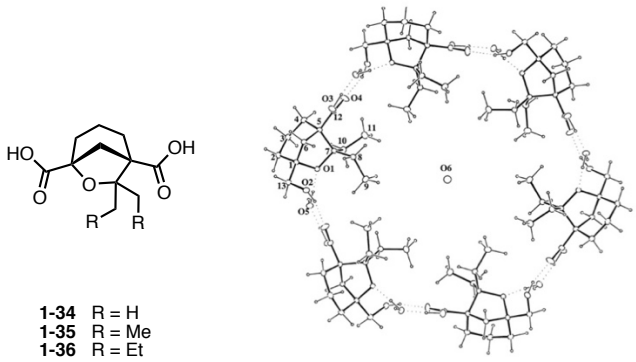

Figure 1.27 Rosette monomer and a hexametric association. ©copyright (2000) American Chemical Society, reprint with permission.[106]

1.3.4 Helix Channels

Gramicidin (gA) peptides form head-to-head helical dimers in the lipid bilayer that open a tubular channel which allows transmembrane ion exchange (e.g. Na^+). The 3D structure is shown Figure 1.28.[110] The canonical mechanism of gA channels is reversible transmembrane dimerization of two nonconducting subunits that reside in opposite bilayer leaflets, and the channel can associate and dissociate. However, this mechanism was challenged by Tyson L. Jonas and co-workers who suggested that gA channels are internally gated.[111] The two mechanisms are illustrated in Figure 1.29.[112]

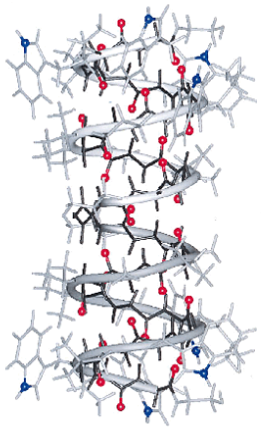

Figure 1.28 Gramicidin A channel (PDB entry: 1MAG) determined by solid state NMR spectroscopy in uniformly aligned lamellar phase lipid bilayers. ©copyright (1999) Nature Publishing Group, reprint with permission.[110]

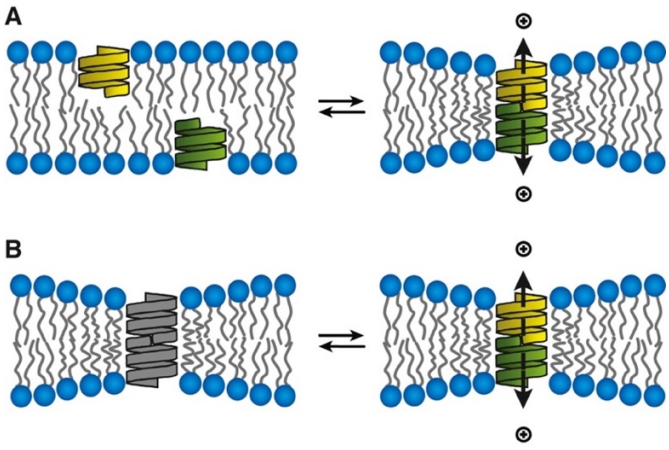

Figure 1.29 Two mechanism proposed for gramicidin channels. (A) the canonical model in which gramicidin channels are formed by reversible transmembrane dimerization of two nonconducting subunits. (B) the switching model proposed by Jones et al., in which gramicidin channels exist as dimers that can switch between conducting and nonconducting states. ©copyright (2017) Elsevier, reprint with permission.[112]

Huaqiang Zeng and co-workers have reported a helical foldamer **1-37** that could self-assemble into a helix superstructure for guest encapsulation and water transport.[113] The water transport was determined by a dynamic light scattering experiment, and the HPTS fluorescence assay suggested that the system does not transport Na^+ or K^+, providing a potential in desalination applications. The structure is stabilized by a combination of different factors such as aromatic π–π stacking, water-host or water-water binding, and intermolecular C=O···H–C type H-bonds, as shown in Figure 1.30.[113]

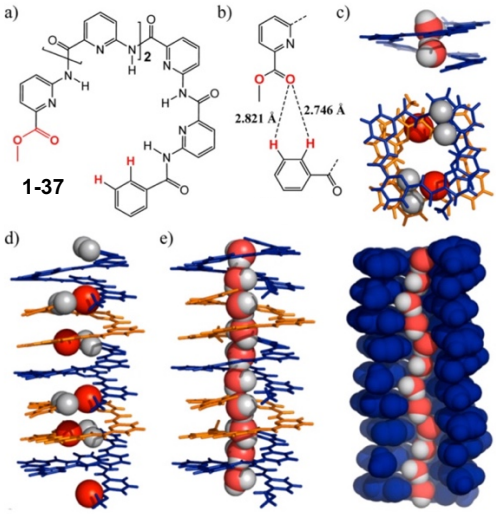

Figure 1.30 (a) Structure of a foldamer monomer. (b) H-bond in the solid state. (c)–(e) illustrate crystal structure with water chain in the cavity. ©copyright (2016) American Chemical Society, reprint with permission.[113]

1.4 Signal Transduction without Direct Mass Transfer

1.4.1 Dimerisation Mechanism

The earliest example using dimerization mechanism of synthetic molecules to achieve signal transduction was demonstrated by J. Kikuchi[31], see Figure 1.31. In this system, synthetic receptor **1-38** was embedded in the membrane and pig heart lactate dehydrogenase (LDH) was bound to the vesicle surface through electrostatic interactions. Cu^{2+} effectively inhibited the LDH activity. When an input signal 1-hydroxy-2-naphthaldehyde **1-39** was added, it formed an imine bond with the receptor **1-40**. The resulting Schiff base then scavenged and chelated Cu^{2+}, forming a 2:1 complex in the membrane due to enhanced binding affinity, as confirmed by UV-vis spectroscopy. The activated LDH increased the observed rate of pyruvic acid dehydrogenation (output). However, the input and output signal were on the same side of the membrane - transmembrane signalling was not achieved.

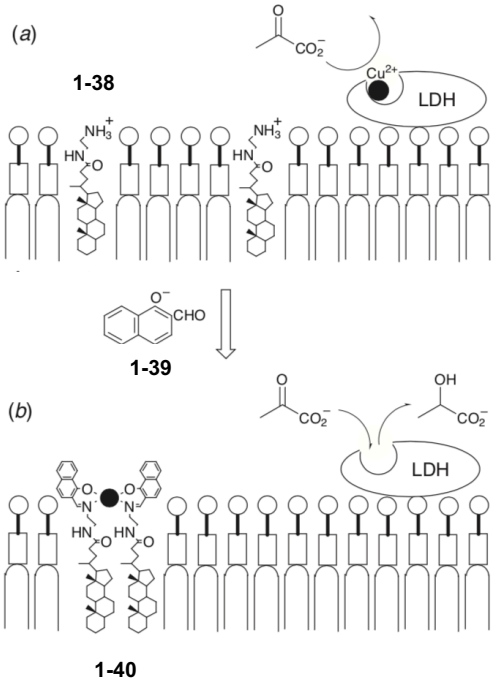

Figure 1.31 Schematic illustration of switching of LDH activity mediated by an artificial cell-surface receptor **1-38**. (a) and (b) represent the off- and on-states of LDH in the absence and presence of an external signal **1-39**, respectively. ©copyright (1999) The Royal Society of Chemistry, reprint with permission.[31]

In 2002, the Hunter group demonstrated a simple synthetic system that mimics RTK dimerisation signal transduction.[32] The system consists of two membrane-spanning molecules (**1-40** and **1-41**, Figure 1.32). Two thiol groups (orange), or a thiol (orange) and a disulfide (grey) are connected by a bis-cholenic acid derivative that enables the molecules to span the lipid membranes of vesicles. An external oxidant input dimerised the thiols by forming a disulfide bond, which accelerated nucleophilic disulfide bond formation on the inside of the vesicles to release the thiopyridine chromophore (green). This is the first example of a synthetic signalling system that enabled molecular communication across the membrane without direct contact between the species involved. Further examples based on this system have also been developed.[35,37]

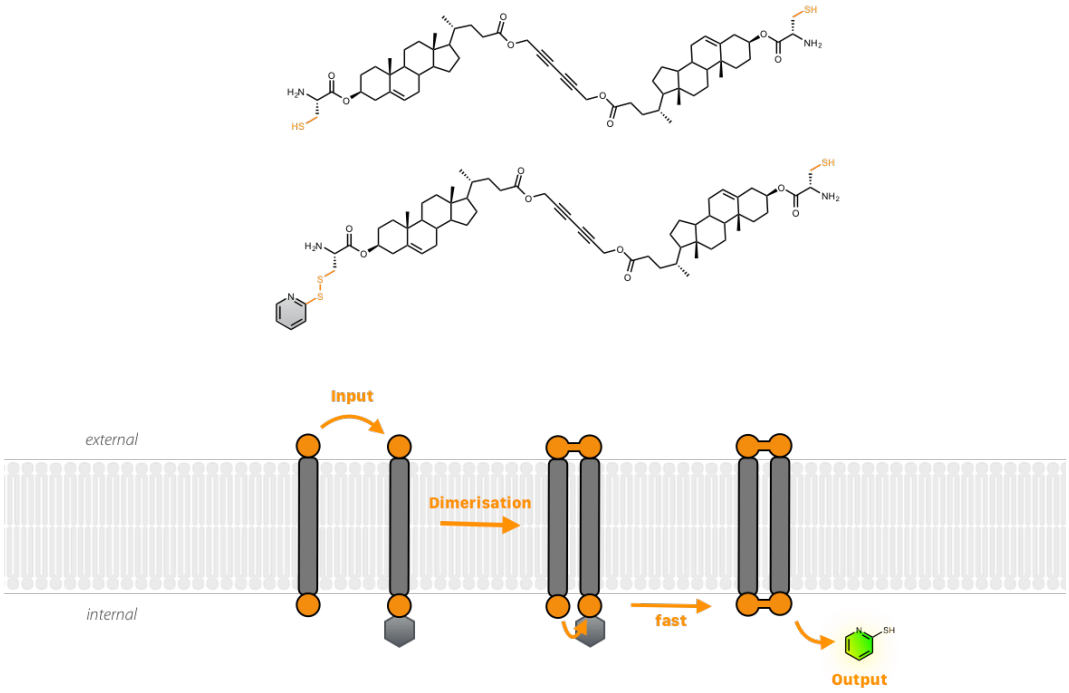

Figure 1.32 Design and function of a synthetic RTK mimic. Top: Structure of two components of the synthetic RTK mimic. Bottom: Extra-vesicle oxidation of thiols forms disulfide group (orange). Intra-vesicle intramolecular disulfide formation is subsequently triggered and a chromophore (green) is released.

1.4.2 Conformational Change Mechanism

Synthetic mimicry of GPCR has not yet been achieved. However, Jonathan Clayden, Simon Webb and co-workers have made significant progress towards it[114] and have recently reported a synthetic membrane-bound receptor **1-42** which can be modulated by a ligand-binding event. This system consists of three components: a metal-containing binding site (green), a helical peptide spacer (grey), which anchors the receptor into the membrane and relays conformational changes from the binding site to the reporter, and a fluorophore (blue) as a spectroscopic indicator of conformational change (Figure 1.33). The two helical conformations of the peptide spacer are interchangeable. Adding different chiral ligands to the vesicles changes the ratio of excimer-to-monomer emission, which corresponds to an increase in the proportion of one of the conformations.

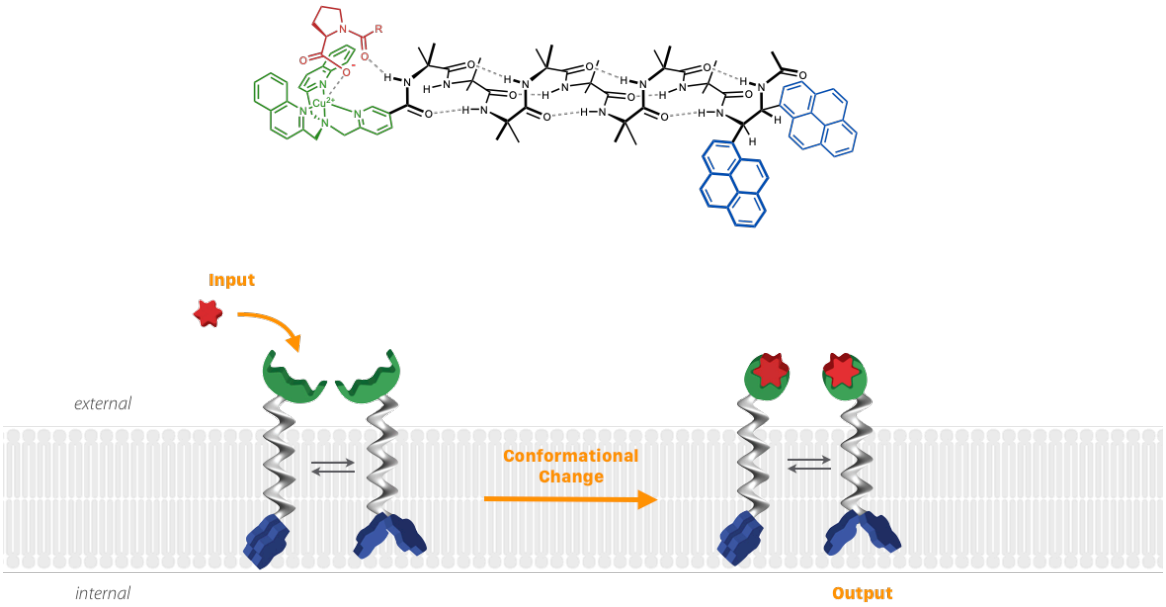

Figure 1.33 Design and function of a synthetic GPCR mimic. Top: Structure of Aib peptide with copper(II) cofactor binding a carboxylate ligand (red). Bottom: Change in equilibrium population distribution of right- and left-handed screw-sense conformers in response to reversible binding of a chiral carboxylate ligand (red). This figure has been re-illustrated from the original published version under CC-BY-4.0 license.[114]

1.4.3 Membrane Translocation Mechanism

These two previously reported systems have several limitations. The molecules are synthetically challenging. Switching between two states is not all or nothing, and the input or output signals are not useful. Biological receptors are usually conjugated with a catalytic domain that amplifies the signal, but the synthetic molecules achieve no signal amplification. Recently, the Hunter group has developed a novel membrane translocation mechanism for signal transduction and amplification, which is not observed in nature. The basic design principles of a synthetic transducer are illustrated in Figure 1.34. Two polarity switchable head groups (blue and green when polar, purple and red when apolar) are attached to a short hydrophobic spacer (grey) which cannot span the bilayer: one head group acts as an external input sensor and the other is a pro-catalyst which is able to generate the output.

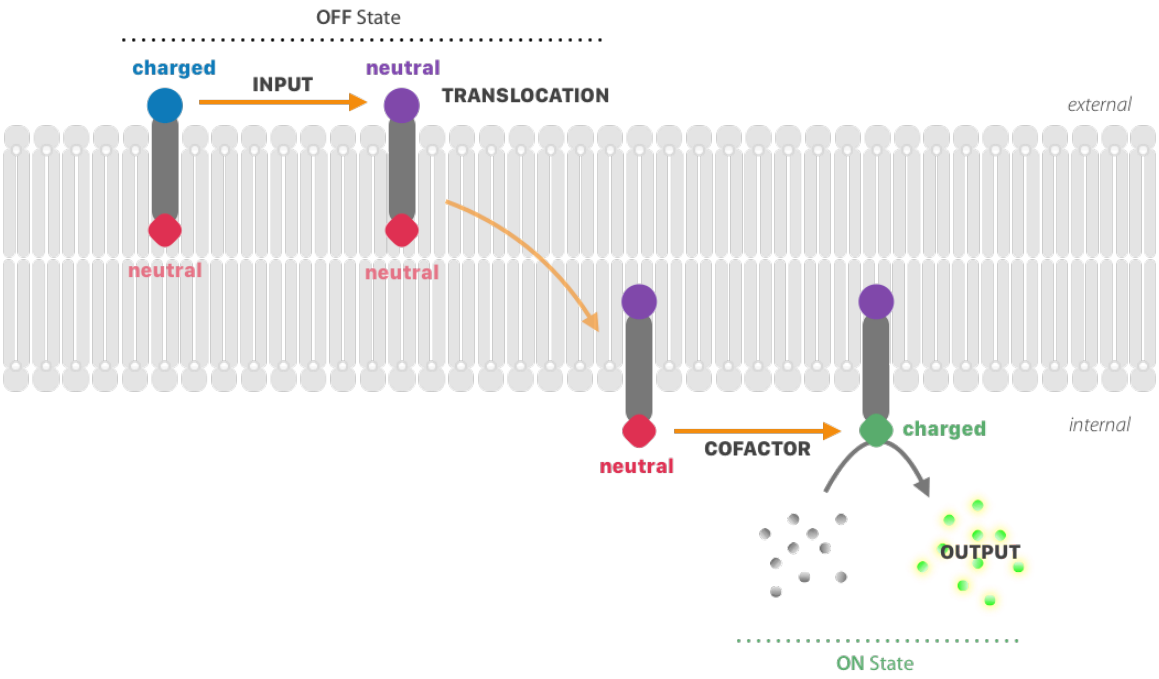

Figure 1.34 Membrane translocation mechanism. A synthetic transducer consists of two polarity switchable head groups is initially embedded in the outer leaflet of the lipid bilayer membrane. In the initial OFF state, the pro-catalyst remains inactive in the membrane (red). Switching of polar head groups (blue, green) to polar (red, purple) drives translocation of the transducer across the bilayer. Binding of a charged cofactor generates the ON state, where the activated catalyst (green) is exposed to the internal aqueous phase and turns over an encapsulated substrate (grey) to generate an amplified output signal (light green).

The polarity of head groups is essential to determine the position of the transducer as it changes the solubility of the head group: when the head groups are polar they tend to stay in the aqueous phase, and when they are apolar they can enter the membrane and are free to move. This bistable transducer therefore provides a mechanism for a controlled translocation of the molecule across a bilayer membrane. In the initial OFF state, the sensor head group is polar (blue) and sits in the external aqueous solution which anchors the transducer in the outer leaflet of the membrane. Meanwhile, the pro-catalyst head group is apolar (red) and remains inactive inside the membrane. An input signal switches the external head group from polar to apolar (blue to purple), which allows the transducer to translocate across the lipid bilayer. The ON state is generated by binding of a charged cofactor from the internal aqueous solution. This switches the internal head group from apolar to polar (red to green), which simultaneously activates the catalyst and provides a driving force for the directional translocation, anchoring the system in the inner leaflet of the membrane. In this ON state, the polar catalyst is exposed to the internal aqueous phase and turns over encapsulated substrate molecules to generate the output signal. By coupling each input molecular signal to the activation of a catalyst, the output signal is amplified, because each catalyst can turn over a large number of substrate molecules.

1.4.3.1 Transducer Design and Input

The differing solubility characteristics of polar and apolar head groups at lipid bilayer membrane interfaces are key features of the transducer: charged, polar moieties are preferentially located in the aqueous phase, while neutral, apolar moieties can enter the interior of the hydrophobic bilayer. Figure 6 shows two types of transducers that have been reported and use a membrane translocation mechanism.[115,116] These two transducers consist of similar components: 1) a polarity switchable head group (Figure 1.35 blue: charged, purple: neutral) which is responsive to different input signals, namely pH variation and metal ion binding; 2) a steroid core (spacer) that links the input responsive head group with a pro-catalyst and anchors the transducer in the bilayer membrane in a perpendicular orientation; 3) the pro-catalyst moiety (Figure 1.35 red) that can be switched to a charged state by the coordination of a zinc ion cofactor (Figure 1.35 green), which pulls the catalyst into the internal aqueous phase. Zinc binding also lowers the pK_a of the oxime from 11 to <6. If the pH on the inside of the vesicle is maintained at 7 by a buffer, cofactor binding will lead to deprotonation of the oxime and activation of the catalyst (the ON state).[117]

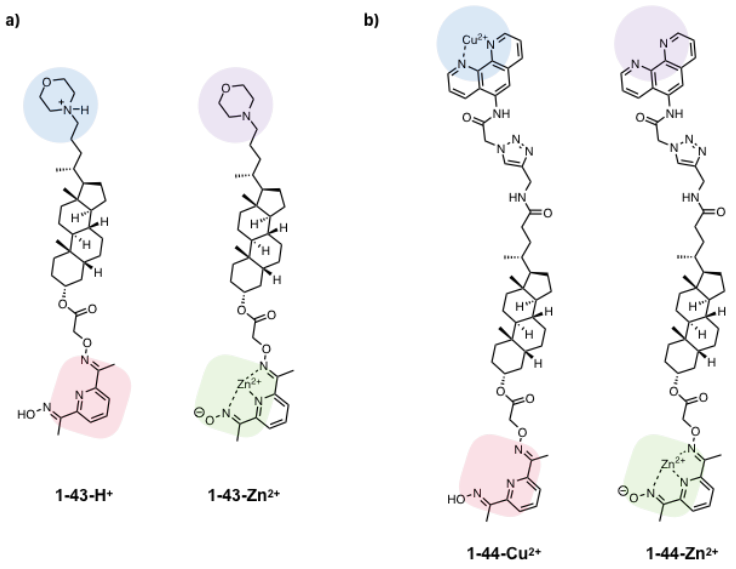

Figure 1.35 Molecular structure of two types of transducers. a) morpholine transducer **1-43**-H^+ (OFF state), the Zn^{2+}-activated catalyst **1-43**-Zn^{2+} (ON state); b) phenanthroline transducer **1-44** as the Cu^{2+} complex **1-44**-Cu^{2+} (OFF state), the Zn^{2+}-activated catalyst **1-44**-Zn^{2+} (ON state).

Transducer **1-43** consists of a morpholine moiety (Figure 1.35a blue), which acts as the sensor for the input signal. When the pH on the outside of the vesicle is below the pK_a of morpholine (~8), the charged head group will be held in the external aqueous phase (the OFF state). Raising the external pH will remove the charge and allow the neutral morpholine head group (Figure 1.35a purple) to enter the membrane. Transducer **1-44** consists of a phenanthroline moiety and binds with Cu^{2+} ions. When copper is bound, the head group is charged (Figure 1.35b

blue) and held out of the membrane in the aqueous phase. Displacement of the bound cation by adding EDTA in the extra-vesicle solution reveals the neutral phenanthroline head group (Figure 1.35b purple), which can enter the membrane and generate an output.

1.4.3.2 Substrate and Output

The encapsulated substrate **1-45** is non-fluorescent and can be hydrolysed by the zinc complex of the oxime catalyst at neutral pH to give a product **1-46**, which is highly fluorescent (Figure 1.36). Both substrate **1-45** and product **1-46** are highly charged at neutral pH and do not cross lipid bilayer membranes and can be encapsulated efficiently inside vesicles. Fluorescence spectroscopy was used to monitor the conversion of **1-45** into **1-46** inside the vesicles. In addition, the fluorescence excitation spectrum of **1-46** was used to quantify internal pH changes independently of the total product concentration. HPTS has a pK_a of ~7.3 and exhibits a pH-dependent absorption shift (Figure 1.36b), allowing ratiometric measurements using an excitation ratio of 460/405 nm.[118] The calibration curve can be obtained by plotting the pH of a lysed vesicle solution vs the fluorescence emission I_{460}/I_{405} (excitation at 460 nm and 405 nm, emission at 510 nm) of that solution by using a Henderson-Hasselbach type equation (Equation 1.1).[115]

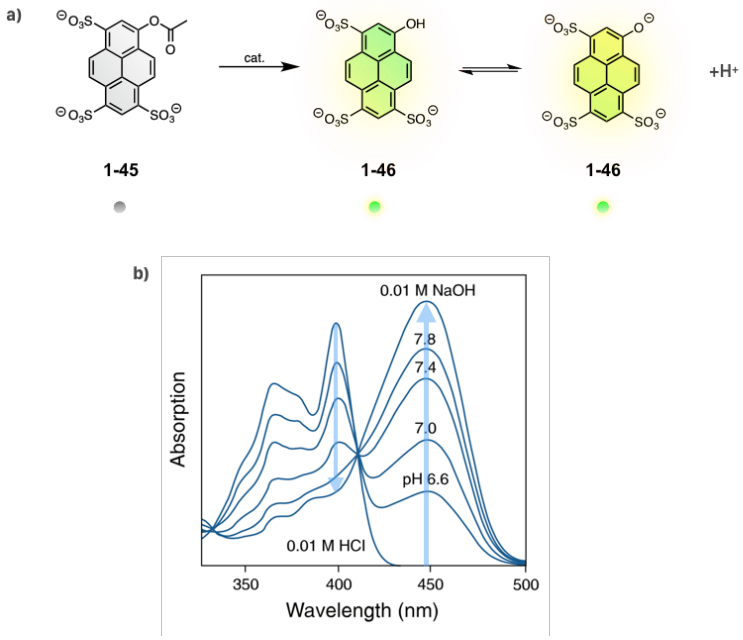

Figure 1.36 Hydrolysis of substrate **1-45** and use of its product **1-46** as a pH probe. a) The non-fluorescent substrate **1-45** can be hydrolysed to a highly fluorescent product **1-46**. b) **1-46** as a pH probe: excitation spectra of HPTS (emission at 510 nm). The ratio of the peaks at 460 nm and 405 nm can be used to determine the pH of the solution inside the vesicles. Change in relative fluorescence emission intensity at 510 nm, exciting at 415 nm, can be used to determine the conversion of the substrate independently of pH.

Equation 1.1

$$pH = b - log(\frac{a-x}{x}) \qquad x = \frac{I_{460}}{I_{405}}$$

All transmembrane signalling experiments were carried out in artificial vesicles (LUV) prepared by a standard extrusion. The membranes should be capable of decoupling different chemical events that occur on both sides of the vesicles. In addition, the vesicles should be impermeable to the substrate **1-45**, product **1-46**, the buffer, zinc (II) or copper (II) and EDTA. For the morpholine transducer system, maintaining a pH gradient is essential so that the pH on the outside and inside of the vesicles can be changed independently. A mixture with 3:2 ratio of 1,2-dioleoyl-*sn*-glycero-3-phosphocholine (DOPC) and 1,2-dioleoyl-*sn*-glycero-3-phosphoethanolamine (DOPE) can effectively perform this function.

1.4.3.3 Transmembrane Signalling Experiments

A representative result of transmembrane signalling experiment is shown in Figure 3.38. The vesicles are loaded with pH-sensitive morpholine transducer **1-43** at neutral pH. Raising external pH from 7 to 9 deprotonate the morpholine group and initiate the translocation of the transducer. Upon zinc(II)-binding, the catalytic head group of the transducer hydrolyses the encapsulated substrate **1-45** and generates the fluorescent product **1-46** (green data). It is important to note that, similar to biological signalling events, this process provides a mechanism for signal amplification: a single hydroxide ion, corresponding to the external input signal, can generate approximately five **1-46** as the internal output signal.

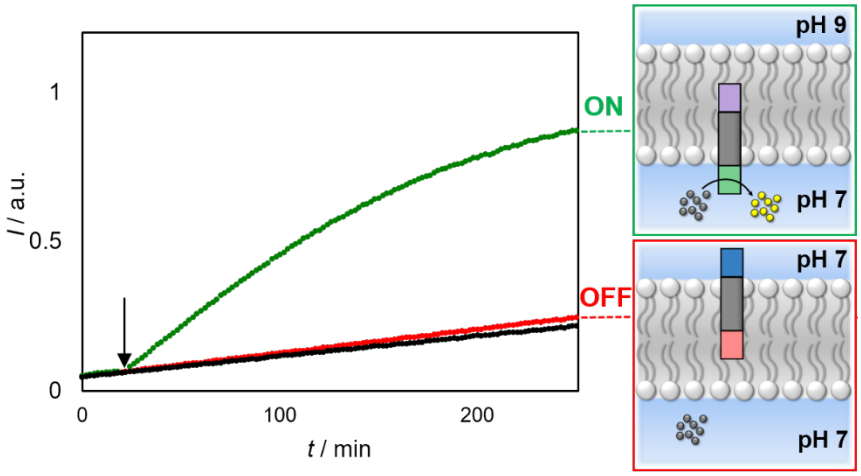

Figure 1.37 Transmembrane signal transduction experiment with pH-sensitive transducer **1-43.** Time dependence of the relative fluorescence emission intensity at 510 nm (exciting at 415 nm). Red data: vesicles with 2.5 mol% loading of **1-43** at pH 7. Green data: vesicles with 2.5 mol% loading of **1-43** initially incubated at an external pH of 7, and then raised to an external pH of 9 after 20 minutes (indicated by the black arrow). Black data: control vesicles prepared without transducer at pH 7. All experiments were conducted in 200 nm

DOPC/DOPE vesicles containing 250 μM substrate **1-45**, 250 μM $ZnCl_2$ and 100 mM HEPES buffer at pH 7. ©copyright (2017) Nature Publishing Group, reprint with permission.[115]

The signalling process is reversible and can be switched between ON and OFF states by altering the external pH of the vesicles, see Figure 1.38. At pH 7, the morpholine unit is protonated and the system is in the OFF state. Raising the external pH to 9 deprotonates the morpholine recognition head group and initiates the translocation. The catalytic head group is switched ON by binding to Zn^{2+} in the internal aqueous solution. Decreasing the external pH back to 7 re-protonates the morpholine recognition head group, which pulls the catalytic head group out of the internal compartment and switch the system to the OFF state. The cycle can continue until the encapsulated substrate is fully hydrolysed.

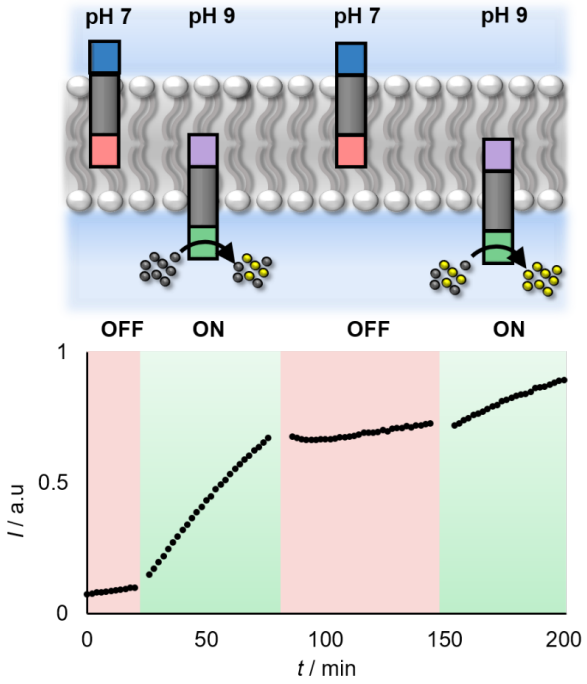

Figure 1.38 Reversible switching of transducer. Changing the external pH between 7 and 9 switches the system OFF and ON. The plot shows the time dependence of the relative fluorescence emission intensity at 510 nm (exciting at 415 nm) during two strokes of a reciprocating cycle in which the external pH was changed by addition of aliquots of sodium hydroxide and hydrochloric acid to the vesicle suspension. Experiment conducted in 200 nm DOPC/DOPE vesicles with 2.5 mol% loading of **1-43** that encapsulated 250 μM substrate **1-45**, 250 μM $ZnCl_2$ and 100 mM HEPES buffer. ©copyright (2017) Nature Publishing Group, reprint with permission.[115]

1.4.3.4 Controlled-Release

The translocation mechanism can also be used to trigger controlled release from vesicles by using the substrate **1-47**, see Figure 1.39.[115] An external input signal (hydroxide) switches the permeability of the recognition head group of a membrane-bound transducer and initiates the

transducer translocation. Upon cofactor binding from the internal aqueous solution, the catalytic head group is switched ON and catalyses the intra-vesicle generation of a surfactant (2-naphthoic acid). Permeabilization of the membrane by surfactant leads to cargo efflux. This system may provide a generic platform with which to develop triggered release applications such as for drug delivery.

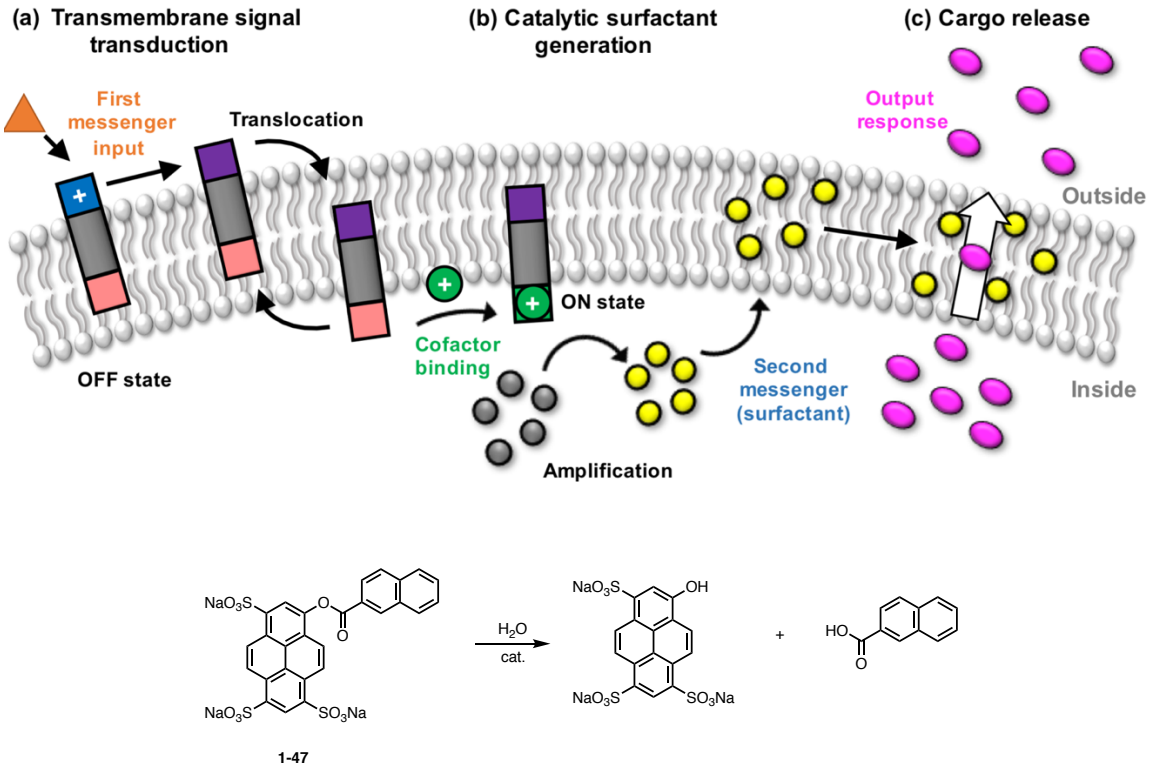

Figure 1.39 Triggered cargo release from vesicles using an artificial signal transduction mechanism. a) Transmembrane signal transduction: the input signal switches the external head group (blue) of a synthetic signal transducer embedded in the membrane from polar to apolar (purple), allowing it to translocate through the membrane. b) Catalytic surfactant generation: charged co-factor binding to the inner (catalytic) head group (red) activates the catalyst (green), turning on catalytic surfactant generation by catalysing the hydrolysis of a substrate (grey) into a surfactant (yellow). The surfactant disrupts the membrane and enhances the permeability of the lipid bilayers to polar solutes; c) Cargo release: cargo (pink) encapsulated in the vesicles are released through disordered lipid bilayers and an output is generated. d) Molecular structures of substrate **1-47** and hydrolysis products: HPTS and 2-naphthoic acid. ©copyright (2017) American Chemical Society, reprint with permission.[119]

1.5 Objectives

Vesicles in cells perform a large variety of functions, for example signalling, metabolism, cargo transport, temporary storage, and acting as reaction chambers. Artificial vesicles have the potential to mimic these functions as in the synthetic system, the compartmentalisation afforded by the bilayer membrane provides a similar metastable barrier to biological systems which allows an incompatible chemical process on the interior or exterior of vesicles to co-exist.

Therefore, there is huge potential to develop highly responsive vesicles that can be selectively activated by an extra-vesicle signal to achieve a well-defined function. Our ultimate goal is to develop highly tuneable and user-definable synthetic analogues that can effectively transduce and amplify a wide range of different external signals into various internal responses in artificial vesicles or living cells.

The potential biological applications using this transmembrane signal transduction mechanism are as follows: 1) **Detection and diagnostics**. Responsive vesicles could be introduced into a living organism as a means to examine organ function or other aspects of health, by sensing the presence of a specific metabolite or protein and subsequently transducing the chemical signals into an optical output *via* internal chromophore/fluorophore generation. 2) **Drug delivery**. This could be achieved through the controlled-release of anti-tumour drugs from responsive vesicles, which can sense the molecular differences between normal and cancerous tissue microenvironments and target the delivery. 3) **Cell modulation**. Direct insertion of artificial transducers into living cell membranes would enable these cells to respond to an input defined by the head group of the transducer. By attaching various catalytic domains that can generate specific biological messengers, the transducer can act as an artificial analogue of signalling proteins to regulate cell activity. Modulation of cell function could thus be achieved by the addition of the corresponding input.

Previous studies in the Hunter group have demonstrated the viability of the membrane translocation mechanism. In this dissertation, the main objective is to investigate the development of new external signal input modules and extend the scope of the translocation mechanism towards more biological systems.

References

(1) Berridge, M. J. Module 2: Cell Signalling Pathways. *Cell Signal. Biol.* **2014**, *6*, csb0001002. https://doi.org/10.1042/csb0001002.

(2) Littleton, J. T.; Ganetzky, B. Ion Channels and Synaptic Organization: Analysis of the Drosophila Genome. *Neuron* **2000**, *26* (1), 35–43. https://doi.org/10.1016/S0896-6273(00)81135-6.

(3) Murata, K.; Mitsuoka, K.; Hirai, T.; Walz, T.; Agre, P.; Heymann, J. B.; Engel, A.; Fujiyoshi, Y. Structural Determinants of Water Permeation through Aquaporin-1. *Nature* **2000**, *407* (6804), 599–605. https://doi.org/10.1038/35036519.

(4) Lodish, H.; Berk, A.; Zipursky, S. L.; Matsudaira, P.; Baltimore, D.; Darnell, J. *Molecular Cell Biology*, 4th ed.; W. H. Freeman, 2000.

(5) The Nobel Prize in Chemistry 2003 https://www.nobelprize.org/prizes/chemistry/2003/press-release/ (accessed Aug 15, 2019).

(6) Catterall, W. A. Structure and Function of Voltage-Gated Ion Channels. *Annu. Rev. Biochem.* **1995**, *64* (1), 493–531. https://doi.org/10.1146/annurev.bi.64.070195.002425.

(7) Lemoine, D.; Jiang, R.; Taly, A.; Chataigneau, T.; Specht, A.; Grutter, T. Ligand-Gated Ion Channels: New Insights into Neurological Disorders and Ligand Recognition. *Chem. Rev.* **2012**, *112* (12), 6285–6318. https://doi.org/10.1021/cr3000829.

(8) Jiang, Y.; Lee, A.; Chen, J.; Cadene, M.; Chait, B. T.; MacKinnon, R. Crystal Structure and

Mechanism of a Calcium-Gated Potassium Channel. *Nature* **2002**, *417* (6888), 515–522. https://doi.org/10.1038/417515a.

(9) Nielsen, S.; Frøkiær, J.; Marples, D.; Kwon, T.-H.; Agre, P.; Knepper, M. A. Aquaporins in the Kidney: From Molecules to Medicine. *Physiol. Rev.* **2002**, *82* (1), 205–244. https://doi.org/10.1152/physrev.00024.2001.

(10) Navale, A. M.; Paranjape, A. N. Glucose Transporters: Physiological and Pathological Roles. *Biophys. Rev.* **2016**, *8* (1), 5–9. https://doi.org/10.1007/s12551-015-0186-2.

(11) Sands, J. M. Mammalian Urea Transporters. *Annu. Rev. Physiol.* **2003**, *65* (1), 543–566. https://doi.org/10.1146/annurev.physiol.65.092101.142638.

(12) Andrade, S. L. A.; Einsle, O. The Amt/Mep/Rh Family of Ammonium Transport Proteins (Review). *Mol. Membr. Biol.* **2007**, *24* (5–6), 357–365. https://doi.org/10.1080/09687680701388423.

(13) PDB-101: Molecule of the Month: Glucose Transporters https://pdb101.rcsb.org/motm/208 (accessed Aug 17, 2019).

(14) Schlessinger, J. Cell Signaling by Receptor Tyrosine Kinases. *Cell* **2000**, *103* (2), 211–225. https://doi.org/10.1016/S0092-8674(00)00114-8.

(15) Locksley, R. M.; Killeen, N.; Lenardo, M. J. The TNF and TNF Receptor Superfamilies: Integrating Mammalian Biology. *Cell* **2001**, *104* (4), 487–501. https://doi.org/10.1016/s0092-8674(01)00237-9.

(16) The Nobel Prize in Chemistry 2012 https://www.nobelprize.org/prizes/chemistry/2012/summary/ (accessed Aug 18, 2019).

(17) The protein tyrosine kinase family of the human genome | Oncogene https://www.nature.com/articles/1203957 (accessed Aug 17, 2019).

(18) PDB101: Molecule of the Month: Epidermal Growth Factor http://pdb101.rcsb.org/motm/126 (accessed Aug 17, 2019).

(19) Hamm, H. E. The Many Faces of G Protein Signaling. *J. Biol. Chem.* **1998**, *273* (2), 669–672. https://doi.org/10.1074/jbc.273.2.669.

(20) Cabrera-Vera, T. M.; Vanhauwe, J.; Thomas, T. O.; Medkova, M.; Preininger, A.; Mazzoni, M. R.; Hamm, H. E. Insights into G Protein Structure, Function, and Regulation. *Endocr. Rev.* **2003**, *24* (6), 765–781. https://doi.org/10.1210/er.2000-0026.

(21) Hurley, J. H. Structure, Mechanism, and Regulation of Mammalian Adenylyl Cyclase. *J. Biol. Chem.* **1999**, *274* (12), 7599–7602. https://doi.org/10.1074/jbc.274.12.7599.

(22) Kaupp, U. B.; Seifert, R. Cyclic Nucleotide-Gated Ion Channels. *Physiol. Rev.* **2002**, *82* (3), 769–824. https://doi.org/10.1152/physrev.00008.2002.

(23) van der Pol, E.; Böing, A. N.; Harrison, P.; Sturk, A.; Nieuwland, R. Classification, Functions, and Clinical Relevance of Extracellular Vesicles. *Pharmacol. Rev.* **2012**, *64* (3), 676–705. https://doi.org/10.1124/pr.112.005983.

(24) The Nobel Prize in Physiology or Medicine 2013 https://www.nobelprize.org/prizes/medicine/2013/summary/%E2%80%9D (accessed Aug 18, 2019).

(25) Balazs, D. A.; Godbey, Wt. Liposomes for Use in Gene Delivery. *J. Drug Deliv.* **2011**, *2011*, 1–12. https://doi.org/10.1155/2011/326497.

(26) Cattel, L.; Ceruti, M.; Dosio, F. From Conventional to Stealth Liposomes: A New Frontier in Cancer Chemotherapy. *Tumori* **2003**, *89* (3), 237–249.

(27) Bulbake, U.; Doppalapudi, S.; Kommineni, N.; Khan, W. Liposomal Formulations in Clinical Use: An Updated Review. *Pharmaceutics* **2017**, *9* (2). https://doi.org/10.3390/pharmaceutics9020012.

(28) Nozaki, Y.; Tanford, C. Proton and Hydroxide Ion Permeability of Phospholipid Vesicles. *Proc. Natl. Acad. Sci.* **1981**, *78* (7), 4324–4328. https://doi.org/10.1073/pnas.78.7.4324.

(29) Stengel, G.; Zahn, R.; Höök, F. DNA-Induced Programmable Fusion of Phospholipid Vesicles. *J. Am. Chem. Soc.* **2007**, *129* (31), 9584–9585. https://doi.org/10.1021/ja073200k.

(30) Czogalla, A.; Grzybek, M.; Jones, W.; Coskun, Ü. Validity and Applicability of Membrane Model Systems for Studying Interactions of Peripheral Membrane Proteins with Lipids. *Biochim. Biophys. Acta BBA - Mol. Cell Biol. Lipids* **2014**, *1841* (8), 1049–1059. https://doi.org/10.1016/j.bbalip.2013.12.012.

(31) Kikuchi, J.; Ariga, K.; Ikeda, K. Signal Transduction Mediated by Artificial Cell-Surface Receptors: Activation of Lactate Dehydrogenase Triggered by Molecular Recognition and Phase Reorganization of Bile

Acid Derivatives Embedded in a Synthetic Bilayer Membrane. *Chem. Commun.* **1999**, No. 6, 547–548. https://doi.org/10.1039/a900083f.

(32) Barton, P.; Hunter, C. A.; Potter, T. J.; Webb, S. J.; Williams, N. H. Transmembrane Signalling. *Angew. Chem. Int. Ed.* **2002**, *41* (20), 3878–3881. https://doi.org/10.1002/1521-3773(20021018)41:20<3878::AID-ANIE3878>3.0.CO;2-F.

(33) Lim, C. W.; Ravoo, B. J.; Reinhoudt, D. N. Dynamic Multivalent Recognition of Cyclodextrin Vesicles. *Chem. Commun.* **2005**, No. 45, 5627–5629. https://doi.org/10.1039/B510540D.

(34) Lee, H.-K.; Park, K. M.; Jeon, Y. J.; Kim, D.; Oh, D. H.; Kim, H. S.; Park, C. K.; Kim, K. Vesicle Formed by Amphiphilc Cucurbit[6]Uril: Versatile, Noncovalent Modification of the Vesicle Surface, and Multivalent Binding of Sugar-Decorated Vesicles to Lectin. *J. Am. Chem. Soc.* **2005**, *127* (14), 5006–5007. https://doi.org/10.1021/ja042172s.

(35) Dijkstra, H. P.; Hutchinson, J. J.; Hunter, C. A.; Qin, H.; Tomas, S.; Webb, S. J.; Williams, N. H. Transmission of Binding Information across Lipid Bilayers. *Chem. – Eur. J.* **2007**, *13* (25), 7215–7222. https://doi.org/10.1002/chem.200601723.

(36) Voskuhl, J.; Ravoo, B. J. Molecular Recognition of Bilayer Vesicles. *Chem. Soc. Rev.* **2009**, *38* (2), 495–505. https://doi.org/10.1039/B803782P.

(37) Bernitzki, K.; Schrader, T. Entirely Artificial Signal Transduction with a Primary Messenger. *Angew. Chem. Int. Ed.* **2009**, *48* (43), 8001–8005. https://doi.org/10.1002/anie.200902973.

(38) Bernitzki, K.; Maue, M.; Schrader, T. Artificial Signal Transduction with Primary and Secondary Messengers. *Chem. – Eur. J.* **2012**, *18* (42), 13412–13417. https://doi.org/10.1002/chem.201200623.

(39) Gruber, B.; Balk, S.; Stadlbauer, S.; König, B. Dynamic Interface Imprinting: High-Affinity Peptide Binding Sites Assembled by Analyte-Induced Recruiting of Membrane Receptors. *Angew. Chem. Int. Ed.* **2012**, *51* (40), 10060–10063. https://doi.org/10.1002/anie.201205701.

(40) Banerjee, S.; Bhuyan, M.; König, B. Tb(III) Functionalized Vesicles for Phosphate Sensing: Membrane Fluidity Controls the Sensitivity. *Chem. Commun.* **2013**, *49* (50), 5681–5683. https://doi.org/10.1039/C3CC42132E.

(41) Müller, A.; König, B. Vesicular Aptasensor for the Detection of Thrombin. *Chem. Commun.* **2014**, *50* (84), 12665–12668. https://doi.org/10.1039/C4CC05221H.

(42) Peters, R. J. R. W.; Nijemeisland, M.; van Hest, J. C. M. Reversibly Triggered Protein–Ligand Assemblies in Giant Vesicles. *Angew. Chem. Int. Ed.* **2015**, *54* (33), 9614–9617. https://doi.org/10.1002/anie.201502920.

(43) Paleos, C. M.; Tsiourvas, D.; Sideratou, Z. Interaction of Vesicles: Adhesion, Fusion and Multicompartment Systems Formation. *ChemBioChem* **2011**, *12* (4), 510–521. https://doi.org/10.1002/cbic.201000614.

(44) Papahadjopoulos, D.; Nir, S.; Düzgünes, N. Molecular Mechanisms of Calcium-Induced Membrane Fusion. *J. Bioenerg. Biomembr.* **1990**, *22* (2), 157–179. https://doi.org/10.1007/BF00762944.

(45) Richard, A.; Marchi-Artzner, V.; Lalloz, M.-N.; Brienne, M.-J.; Artzner, F.; Gulik-Krzywicki, T.; Guedeau-Boudeville, M.-A.; Lehn, J.-M. Fusogenic Supramolecular Vesicle Systems Induced by Metal Ion Binding to Amphiphilic Ligands. *Proc. Natl. Acad. Sci.* **2004**, *101* (43), 15279–15284. https://doi.org/10.1073/pnas.0406625101.

(46) Jin, H.; Liu, Y.; Zheng, Y.; Huang, W.; Zhou, Y.; Yan, D. Cytomimetic Large-Scale Vesicle Aggregation and Fusion Based on Host–Guest Interaction. *Langmuir* **2012**, *28* (4), 2066–2072. https://doi.org/10.1021/la203857s.

(47) Caschera, F.; Noireaux, V. Integration of Biological Parts toward the Synthesis of a Minimal Cell. *Curr. Opin. Chem. Biol.* **2014**, *22*, 85–91. https://doi.org/10.1016/j.cbpa.2014.09.028.

(48) Hanczyc, M. M.; Szostak, J. W. Replicating Vesicles as Models of Primitive Cell Growth and Division. *Curr. Opin. Chem. Biol.* **2004**, *8* (6), 660–664. https://doi.org/10.1016/j.cbpa.2004.10.002.

(49) Akbarzadeh, A.; Rezaei-Sadabady, R.; Davaran, S.; Joo, S. W.; Zarghami, N.; Hanifehpour, Y.; Samiei, M.; Kouhi, M.; Nejati-Koshki, K. Liposome: Classification, Preparation, and Applications. *Nanoscale Res. Lett.* **2013**, *8* (1), 102. https://doi.org/10.1186/1556-276X-8-102.

(50) Lasic, D. D. The Mechanism of Vesicle Formation. *Biochem. J.* **1988**, *256* (1), 1–11. https://doi.org/10.1042/bj2560001.

(51) Mozafari, M. R. Liposomes: An Overview of Manufacturing Techniques. **2005**, *10* (4), 9.

(52) Pick, U. Liposomes with a Large Trapping Capacity Prepared by Freezing and Thawing of Sonicated Phospholipid Mixtures. *Arch. Biochem. Biophys.* **1981**, *212* (1), 186–194. https://doi.org/10.1016/0003-9861(81)90358-1.

(53) Ohsawa, T.; Miura, H.; Harada, K. Improvement of Encapsulation Efficiency of Water-Soluble Drugs in Liposomes Formed by the Freeze-Thawing Method. *Chem. Pharm. Bull. (Tokyo)* **1985**, *33* (9), 3945–3952. https://doi.org/10.1248/cpb.33.3945.

(54) Liu, L.; Yonetani, T. Preparation and Characterization of Liposome-Encapsulated Haemoglobin by a Freeze-Thaw Method. *J. Microencapsul.* **1994**, *11* (4), 409–421. https://doi.org/10.3109/02652049409034258.

(55) MacDonald, R. C.; MacDonald, R. I.; Menco, B. Ph. M.; Takeshita, K.; Subbarao, N. K.; Hu, L. Small-Volume Extrusion Apparatus for Preparation of Large, Unilamellar Vesicles. *Biochim. Biophys. Acta BBA - Biomembr.* **1991**, *1061* (2), 297–303. https://doi.org/10.1016/0005-2736(91)90295-J.

(56) Jousma, H.; Talsma, H.; Spies, F.; Joosten, J. G. H.; Junginger, H. E.; Crommelin, D. J. A. Characterization of Liposomes. The Influence of Extrusion of Multilamellar Vesicles through Polycarbonate Membranes on Particle Size, Particle Size Distribution and Number of Bilayers. *Int. J. Pharm.* **1987**, *35* (3), 263–274. https://doi.org/10.1016/0378-5173(87)90139-6.

(57) Zhu, T. F.; Szostak, J. W. Preparation of Large Monodisperse Vesicles. *PLOS ONE* **2009**, *4* (4), e5009. https://doi.org/10.1371/journal.pone.0005009.

(58) Szoka, F.; Papahadjopoulos, D. Procedure for Preparation of Liposomes with Large Internal Aqueous Space and High Capture by Reverse-Phase Evaporation. *Proc. Natl. Acad. Sci. U. S. A.* **1978**, *75* (9), 4194–4198.

(59) Deamer, D.; Bangham, A. D. Large Volume Liposomes by an Ether Vaporization Method. *Biochim. Biophys. Acta BBA - Biomembr.* **1976**, *443* (3), 629–634. https://doi.org/10.1016/0005-2736(76)90483-1.

(60) Schieren, H.; Rudolph, S.; Finkelstein, M.; Coleman, P.; Weissmann, G. Comparison of Large Unilamellar Vesicles Prepared by a Petroleum Ether Vaporization Method with Multilamellar Vesicles: ESR, Diffusion and Entrapment Analyses. *Biochim. Biophys. Acta* **1978**, *542* (1), 137–153. https://doi.org/10.1016/0304-4165(78)90240-4.

(61) Huang, C.-H. Phosphatidylcholine Vesicles. Formation and Physical Characteristics. *Biochemistry* **1969**, *8* (1), 344–352. https://doi.org/10.1021/bi00829a048.

(62) Finkelstein, M. C.; Weissmann, G. Enzyme Replacement via Liposomes Variations in Lipid Composition Determine Liposomal Integrity in Biological Fluids. *Biochim. Biophys. Acta BBA - Gen. Subj.* **1979**, *587* (2), 202–216. https://doi.org/10.1016/0304-4165(79)90354-4.

(63) Lesieur, S.; Grabielle-Madelmont, C.; Paternostre, M.; Ollivon, M. Study of Size Distribution and Stability of Liposomes by High Performance Gel Exclusion Chromatography. *Chem. Phys. Lipids* **1993**, *64* (1), 57–82. https://doi.org/10.1016/0009-3084(93)90058-B.

(64) Ruysschaert, T.; Marque, A.; Duteyrat, J.-L.; Lesieur, S.; Winterhalter, M.; Fournier, D. Liposome Retention in Size Exclusion Chromatography. *BMC Biotechnol.* **2005**, *5* (1), 11. https://doi.org/10.1186/1472-6750-5-11.

(65) Sakai, N.; Matile, S. Anion-Mediated Transfer of Polyarginine across Liquid and Bilayer Membranes. *J. Am. Chem. Soc.* **2003**, *125* (47), 14348–14356. https://doi.org/10.1021/ja037601l.

(66) The s-Block Elements in Biology https://saylordotorg.github.io/text_general-chemistry-principles-patterns-and-applications-v1.0/s25-05-the-s-block-elements-in-biolog.html (accessed Aug 19, 2019).

(67) Pressman, B. C. Biological Applications of Ionophores. *Annu. Rev. Biochem.* **1976**, *45* (1), 501–530. https://doi.org/10.1146/annurev.bi.45.070176.002441.

(68) Deber, C. M.; Young, M. E. M.; Tom-Kun, J. Synthetic Cation Transport Peptides: Calcium Transport across Phospholipid Membranes. *Biochemistry* **1980**, *19* (26), 6194–6198. https://doi.org/10.1021/bi00567a038.

(69) Drobnies, A. E.; Deber, C. M. Cation Transport Properties of a Synthetic Ca2+-Selective Peptide Ionophore in Phospholipid and Sarcoplasmic Reticulum Vesicles. *Biochim. Biophys. Acta BBA - Biomembr.* **1982**, *691* (1),

30–36. https://doi.org/10.1016/0005-2736(82)90210-3.

(70) Jin, T.; Kinjo, M.; Kobayashi, Y.; Hirata, H. Ion Transport Activity of Calix[n]Arene (N=4, 5, 6, 7, 8) Esters toward Alkali-Metal Cations in a Phospholipid Bilayer Membrane. *J. Chem. Soc. Faraday Trans.* **1998**, *94* (20), 3135–3140. https://doi.org/10.1039/a805101a.

(71) Tsukube, H. Armed Crown Ether Complexes in Supramolecular Assembly. *Coord. Chem. Rev.* **1996**, *148*, 1–17. https://doi.org/10.1016/0010-8545(95)01151-X.

(72) Tong, C. C.; Quesada, R.; Sessler, J. L.; Gale, P. A. Meso-Octamethylcalix[4]Pyrrole: An Old yet New Transmembrane Ion-Pair Transporter. *Chem. Commun.* **2008**, No. 47, 6321–6323. https://doi.org/10.1039/B814988G.

(73) Lisbjerg, M.; Valkenier, H.; Jessen, B. M.; Al-Kerdi, H.; Davis, A. P.; Pittelkow, M. Biotin[6]Uril Esters: Chloride-Selective Transmembrane Anion Carriers Employing C—H···Anion Interactions. *J. Am. Chem. Soc.* **2015**, *137* (15), 4948–4951. https://doi.org/10.1021/jacs.5b02306.

(74) Whitmarsh, S. D.; Redmond, A. P.; Sgarlata, V.; Davis, A. P. Cationic Cyclocholamides; Toroidal Facial Amphiphiles with Potential for Anion Transport. *Chem. Commun.* **2008**, No. 31, 3669–3671. https://doi.org/10.1039/B805777J.

(75) Díaz, R. I. S.; Regourd, J.; Santacroce, P. V.; Davis, J. T.; Jakeman, D. L.; Thompson, A. Chloride Anion Transport and Copper-Mediated DNA Cleavage by C-Ring Functionalized Prodigiosenes. *Chem. Commun.* **2007**, No. 26, 2701–2703. https://doi.org/10.1039/B701919J.

(76) Gale, P. A.; Garric, J.; Light, M. E.; McNally, B. A.; Smith, B. D. Conformational Control of HCl Co-Transporter: Imidazole Functionalised Isophthalamide vs. 2,6-Dicarboxamidopyridine. *Chem. Commun.* **2007**, No. 17, 1736–1738. https://doi.org/10.1039/B703259E.

(77) Leevy, W. M.; Johnson, J. R.; Lakshmi, C.; Morris, J.; Marquez, M.; Smith, B. D. Selective Recognition of Bacterial Membranes by Zinc(II)-Coordination Complexes. *Chem. Commun.* **2006**, No. 15, 1595–1597. https://doi.org/10.1039/B517519D.

(78) McNally, B. A.; Koulov, A. V.; Lambert, T. N.; Smith, B. D.; Joos, J.-B.; Sisson, A. L.; Clare, J. P.; Sgarlata, V.; Judd, L. W.; Magro, G.; et al. Structure–Activity Relationships in Cholapod Anion Carriers: Enhanced Transmembrane Chloride Transport through Substituent Tuning. *Chem. – Eur. J.* **2008**, *14* (31), 9599–9606. https://doi.org/10.1002/chem.200801163.

(79) Lai, X.-Z.; Feng, Y.; Pollard, J.; Chin, J. N.; Rybak, M. J.; Bucki, R.; Epand, R. F.; Epand, R. M.; Savage, P. B. Ceragenins: Cholic Acid-Based Mimics of Antimicrobial Peptides. *Acc. Chem. Res.* **2008**, *41* (10), 1233–1240. https://doi.org/10.1021/ar700270t.

(80) Mehiri, M.; Chen, W.-H.; Janout, V.; Regen, S. L. Molecular Umbrella Transport. *J. Am. Chem. Soc.* **2009**, *131* (4), 1338–1339. https://doi.org/10.1021/ja806476t.

(81) Ren, C.; Chen, F.; Ye, R.; Ong, Y. S.; Lu, H.; Lee, S. S.; Ying, J. Y.; Zeng, H. Molecular Swings as Highly Active Ion Transporters. *Angew. Chem. Int. Ed.* **2019**, *58* (24), 8034–8038. https://doi.org/10.1002/anie.201901833.

(82) Weber, M. E.; Wang, W.; Steinhardt, S. E.; Gokel, M. R.; Leevy, W. M.; Gokel, G. W. The Influence of Varied Amide Bond Positions on Hydraphile Ion Channel Activity. *New J. Chem.* **2006**, *30* (2), 177–184. https://doi.org/10.1039/B510863M.

(83) Tsikolia, M.; Hall, A. C.; Suarez, C.; Nylander, Z. O.; Wardlaw, S. M.; Gibson, M. E.; Valentine, K. L.; Onyewadume, L. N.; Ahove, D. A.; Woodbury, M.; et al. Synthesis and Characterization of a Redox-Active Ion Channel Supporting Cation Flux in Lipid Bilayers. *Org. Biomol. Chem.* **2009**, *7* (18), 3862–3870. https://doi.org/10.1039/B907350G.

(84) Otis, F.; Voyer, N.; Polidori, A.; Pucci, B. End Group Engineering of Artificial Ion Channels. *New J. Chem.* **2006**, *30* (2), 185–190. https://doi.org/10.1039/B509668E.

(85) Otis, F.; Racine-Berthiaume, C.; Voyer, N. How Far Can a Sodium Ion Travel within a Lipid Bilayer? *J. Am. Chem. Soc.* **2011**, *133* (17), 6481–6483. https://doi.org/10.1021/ja110336s.

(86) Vargas Jentzsch, A.; Matile, S. Transmembrane Halogen-Bonding Cascades. *J. Am. Chem. Soc.* **2013**, *135* (14), 5302–5303. https://doi.org/10.1021/ja4013276.

(87) McNally, B. A.; O'Neil, E. J.; Nguyen, A.; Smith, B. D. Membrane Transporters for Anions That Use a Relay Mechanism. *J. Am. Chem. Soc.* **2008**, *130* (51), 17274–17275. https://doi.org/10.1021/ja8082363.

(88) Matile, S. En Route to Supramolecular Functional Plasticity: Artificial β-Barrels, the Barrel-Stave Motif, and Related Approaches. *Chem. Soc. Rev.* **2001**, *30* (3), 158–167. https://doi.org/10.1039/B008101I.

(89) Matsubara, A.; Asami, K.; Akagi, A.; Nishino, N. Ion-Channels of Cyclic Template-Assembled Alamethicins That Emulate the Pore Structure Predicted by the Barrel-Stave Model. *Chem. Commun.* **1996**, No. 17, 2069–2070. https://doi.org/10.1039/CC9960002069.

(90) Sakai, N.; Matile, S. Synthetic Multifunctional Pores: Lessons from Rigid-Rod β-Barrels. *Chem. Commun.* **2003**, *0* (20), 2514–2523. https://doi.org/10.1039/B303649A.

(91) Goto, C.; Yamamura, M.; Satake, A.; Kobuke, Y. Artificial Ion Channels Showing Rectified Current Behavior. *J. Am. Chem. Soc.* **2001**, *123* (49), 12152–12159. https://doi.org/10.1021/ja010761h.

(92) Baginski, M.; Resat, H.; McCammon, J. A. Molecular Properties of Amphotericin B Membrane Channel: A Molecular Dynamics Simulation. *Mol. Pharmacol.* **1997**, *52* (4), 560–570. https://doi.org/10.1124/mol.52.4.560.

(93) Fuhrhop, J. Hinrich.; Liman, Ulrich.; Koesling, Volker. A Macrocyclic Tetraether Bolaamphiphile and an Oligoamino .Alpha.,.Omega.-Dicarboxylate Combine to Form Monolayered, Porous Vesicle Membranes, Which Are Reversibly Sealed by EDTA and Other Bulky Anions. *J. Am. Chem. Soc.* **1988**, *110* (20), 6840–6845. https://doi.org/10.1021/ja00228a037.

(94) Wilson, C. P.; Webb, S. J. Palladium(II)-Gated Ion Channels. *Chem. Commun.* **2008**, No. 34, 4007–4009. https://doi.org/10.1039/B809087D.

(95) Devi, U.; Brown, J. R. D.; Almond, A.; Webb, S. J. Pd(II)-Mediated Assembly of Porphyrin Channels in Bilayer Membranes. *Langmuir* **2011**, *27* (4), 1448–1456. https://doi.org/10.1021/la104152s.

(96) Jones, J. E.; Diemer, V.; Adam, C.; Raftery, J.; Ruscoe, R. E.; Sengel, J. T.; Wallace, M. I.; Bader, A.; Cockroft, S. L.; Clayden, J.; et al. Length-Dependent Formation of Transmembrane Pores by 310-Helical α-Aminoisobutyric Acid Foldamers. *J. Am. Chem. Soc.* **2016**, *138* (2), 688–695. https://doi.org/10.1021/jacs.5b12057.

(97) Langecker, M.; Arnaut, V.; Martin, T. G.; List, J.; Renner, S.; Mayer, M.; Dietz, H.; Simmel, F. C. Synthetic Lipid Membrane Channels Formed by Designed DNA Nanostructures. *Science* **2012**, *338* (6109), 932–936. https://doi.org/10.1126/science.1225624.

(98) Ishida, H.; Donowaki, K.; Inoue, Y.; Qi, Z.; Sokabe, M. Synthesis and Ion Channel Formation of Novel Cyclic Peptides Containing a Non-Natural Amino Acid. *Chem. Lett.* **1997**, *26* (9), 953–954. https://doi.org/10.1246/cl.1997.953.

(99) Fernandez-Lopez, S.; Kim, H.-S.; Choi, E. C.; Delgado, M.; Granja, J. R.; Khasanov, A.; Kraehenbuehl, K.; Long, G.; Weinberger, D. A.; Wilcoxen, K. M.; et al. Antibacterial Agents Based on the Cyclic d,l -α-Peptide Architecture. *Nature* **2001**, *412* (6845), 452–455. https://doi.org/10.1038/35086601.

(100) Sánchez-Quesada, J.; Kim, H. S.; Ghadiri, M. R. A Synthetic Pore-Mediated Transmembrane Transport of Glutamic Acid. *Angew. Chem. Int. Ed.* **2001**, *40* (13), 2503–2506. https://doi.org/10.1002/1521-3773(20010702)40:13<2503::AID-ANIE2503>3.0.CO;2-E.

(101) Gong, B.; Shao, Z. Self-Assembling Organic Nanotubes with Precisely Defined, Sub-Nanometer Pores: Formation and Mass Transport Characteristics. *Acc. Chem. Res.* **2013**, *46* (12), 2856–2866. https://doi.org/10.1021/ar400030e.

(102) Wei, X.; Zhang, G.; Shen, Y.; Zhong, Y.; Liu, R.; Yang, N.; Al-mkhaizim, F. Y.; Kline, M. A.; He, L.; Li, M.; et al. Persistent Organic Nanopores Amenable to Structural and Functional Tuning. *J. Am. Chem. Soc.* **2016**, *138* (8), 2749–2754. https://doi.org/10.1021/jacs.5b12698.

(103) Xin, P.; Kong, H.; Sun, Y.; Zhao, L.; Fang, H.; Zhu, H.; Jiang, T.; Guo, J.; Zhang, Q.; Dong, W.; et al. Artificial K+ Channels Formed by Pillararene-Cyclodextrin Hybrid Molecules: Tuning Cation Selectivity and Generating Membrane Potential. *Angew. Chem. Int. Ed.* **2019**, *58* (9), 2779–2784. https://doi.org/10.1002/anie.201813797.

(104) Boccalon, M.; Iengo, E.; Tecilla, P. Metal–Organic Transmembrane Nanopores. *J. Am. Chem. Soc.* **2012**, *134* (50), 20310–20313. https://doi.org/10.1021/ja310425j.

(105) Pérez, C.; Espínola, C. G.; Foces-Foces, C.; Núñez-Coello, P.; Carrasco, H.; Martín, J. D. A Synthetic Hydroxy Acid That Shows Tubular-Shaped Structure in Solid-State and Ionophoric Activity in Phospholipid Bilayers.

Org. Lett. **2000**, *2* (9), 1185–1188. https://doi.org/10.1021/ol005534j.

(106) Carrasco, H.; Foces-Foces, C.; Pérez, C.; Rodríguez, M. L.; Martín, J. D. Tubular Hydrogen-Bonded Networks Sustained by Water Molecules. *J. Am. Chem. Soc.* **2001**, *123* (48), 11970–11981. https://doi.org/10.1021/ja011028t.

(107) Kishikawa, K.; Isaka, M.; Takahashi, M.; Saito, K.; Kohmoto, S. Self-Assembly of Compact Molecules Possessing Two Carboxy and One Amide Groups into Tubular Nanostructures in Liquid Crystal Phases. *Chem. Lett.* **2011**, *40* (11), 1278–1279. https://doi.org/10.1246/cl.2011.1278.

(108) Saha, T.; Dasari, S.; Tewari, D.; Prathap, A.; Sureshan, K. M.; Bera, A. K.; Mukherjee, A.; Talukdar, P. Hopping-Mediated Anion Transport through a Mannitol-Based Rosette Ion Channel. *J. Am. Chem. Soc.* **2014**, *136* (40), 14128–14135. https://doi.org/10.1021/ja506278z.

(109) Saha, T.; Gautam, A.; Mukherjee, A.; Lahiri, M.; Talukdar, P. Chloride Transport through Supramolecular Barrel-Rosette Ion Channels: Lipophilic Control and Apoptosis-Inducing Activity. *J. Am. Chem. Soc.* **2016**, *138* (50), 16443–16451. https://doi.org/10.1021/jacs.6b10379.

(110) Cross, T. A.; Arseniev, A.; Cornell, B. A.; Davis, J. H.; Killian, J. A.; Koeppe, R. E.; Nicholson, L. K.; Separovic, F.; Wallace, B. A. Gramicidin Channel Controversy — Revisited. *Nat. Struct. Biol.* **1999**, *6* (7), 610–611. https://doi.org/10.1038/10650.

(111) Jones, T. L.; Fu, R.; Nielson, F.; Cross, T. A.; Busath, D. D. Gramicidin Channels Are Internally Gated. *Biophys. J.* **2010**, *98* (8), 1486–1493. https://doi.org/10.1016/j.bpj.2009.11.055.

(112) Lum, K.; Ingólfsson, H. I.; Koeppe, R. E.; Andersen, O. S. Exchange of Gramicidin between Lipid Bilayers: Implications for the Mechanism of Channel Formation. *Biophys. J.* **2017**, *113* (8), 1757–1767. https://doi.org/10.1016/j.bpj.2017.08.049.

(113) Huo, Y.; Zeng, H. "Sticky"-Ends-Guided Creation of Functional Hollow Nanopores for Guest Encapsulation and Water Transport. *Acc. Chem. Res.* **2016**, *49* (5), 922–930. https://doi.org/10.1021/acs.accounts.6b00051.

(114) Poli, M. D.; Zawodny, W.; Quinonero, O.; Lorch, M.; Webb, S. J.; Clayden, J. Conformational Photoswitching of a Synthetic Peptide Foldamer Bound within a Phospholipid Bilayer. *Science* **2016**, *352* (6285), 575–580. https://doi.org/10.1126/science.aad8352.

(115) Langton, M. J.; Keymeulen, F.; Ciaccia, M.; Williams, N. H.; Hunter, C. A. Controlled Membrane Translocation Provides a Mechanism for Signal Transduction and Amplification. *Nat. Chem.* **2017**, *9* (5), 426–430. https://doi.org/10.1038/nchem.2678.

(116) Langton, M. J.; Williams, N. H.; Hunter, C. A. Recognition-Controlled Membrane Translocation for Signal Transduction across Lipid Bilayers. *J. Am. Chem. Soc.* **2017**, *139* (18), 6461–6466. https://doi.org/10.1021/jacs.7b02345.

(117) Yatsimirsky, A. K.; Gómez-Tagle, P.; Escalante-Tovar, S.; Ruiz-Ramírez, L. Kinetics and Mechanism of Ester Hydrolysis by Metal Complexes of 2,6-Diacetylpyridine Dioxime. *Inorganica Chim. Acta* **1998**, *273* (1), 167–174. https://doi.org/10.1016/S0020-1693(97)05971-9.

(118) Clement, N. R.; Gould, J. M. Pyranine (8-Hydroxy-1,3,6-Pyrenetrisulfonate) as a Probe of Internal Aqueous Hydrogen Ion Concentration in Phospholipid Vesicles. *Biochemistry* **1981**, *20* (6), 1534–1538. https://doi.org/10.1021/bi00509a019.

(119) Langton, M. J.; Scriven, L. M.; Williams, N. H.; Hunter, C. A. Triggered Release from Lipid Bilayer Vesicles by an Artificial Transmembrane Signal Transduction System. *J. Am. Chem. Soc.* **2017**, *139* (44), 15768–15773. https://doi.org/10.1021/jacs.7b07747.

Freedom is nothing but a chance to be better.

Albert Camus

2

Maleimide Transducer

2.1 Introduction

In biology, signal transduction is a conversion process by which a stimulus is recognised and transmitted through a cell membrane. Membrane-spanning proteins respond to a large variety of input signals and give rise to well-defined biochemical cascade reactions in cells. The signalling events regulate almost all functions of the cell from basic survival to specific biochemical response. There are two major categories of signalling pathways: 1) direct mass transfer, where molecules pass through cell membranes such as membrane channels or transporters[1], or 2) indirect transfer, where signal input and output are separated by the membrane, such as observed in G protein-coupled receptor[2] or receptor tyrosine kinases[3]. Although numerous examples of synthetic membrane channels and transporters have been reported, signal transduction without mass transfer is considerably more challenging.

A novel transmembrane signalling mechanism was recently reported which operates by controlled translocation of a synthetic transducer across a vesicle lipid bilayer.[4] The external recognition head group of the transducer becomes membrane-permeable in response to an external chemical stimulus, which leads to membrane translocation, exposing a catalytic head group to the interior of the vesicle. Catalytic hydrolysis of an internal substrate generates an amplified output signal, which can also be used to trigger the release of the vesicle contents.[5] The choice of recognition head group can be used to make this system respond to different external stimuli, such as pH[4] or metal ions[6]. To generalise the concept of the translocation

mechanism, we aimed to develop a synthetic transducer that can be conveniently functionalised and respond to different stimuli. To achieve this goal, a "stem transducer" from which other specific input responsive transducers can be further derived is needed, together with a corresponding in-situ chemistry that allows the embedded "stem transducer" to be functionalised in the extra-vesicle solution.

Maleimide-sulfhydryl coupling is commonly used in biochemistry for labelling and crosslinking.[7] Sulfhydryl groups react specifically with maleimide units at neutral pH (6.5-7.5) and form a stable thioether linkage. We exploited this conjugation reaction and designed a maleimide transducer **2-1** as a "stem transducer". Compared to previously reported pH-controlled and molecular recognition-controlled transducers, the major difference of this maleimide transducer **2-1** is that the input responsive group is not directly attached to the transducer by organic synthesis, but can be attached *via* a thiol-maleimide *in-situ* conjugation on the vesicles, providing flexibility and ease of synthesis.

The approach to controlling membrane translocation of maleimide transducer **2-1** is illustrated in Figure 2.1. Similar to previous transducers, **2-1** consists of a steroid core which links two head groups: a pyridine-oxime pro-catalyst and a maleimide head group which is responsible for *in-situ* conjugation. However, as the maleimide moiety is soluble in the lipid bilayer, an extra piperazine moiety acting as a "safety catch" is included between the maleimide moiety and the steroid core. The piperazine should be protonated and membrane-impermeable at neutral pH, keeping the maleimide in the aqueous phase and available for reaction. Initially, the transducer is anchored at the external membrane-water interface (OFF state). The recognition group equipped with a thiol is added to the extra-vesicle solution and an *in-situ* maleimide-thiol conjugation reaction takes place. The excess amount of thiol can be easily removed by size exclusion chromatography. The recognition group should be membrane-impermeable in order to hold the transducer at the outer leaflet of the membrane. Raising the external pH deprotonates the piperazine unit and releases the "safety catch". An appropriate input switches the recognition group from membrane-impermeable to membrane-permeable and initiates the translocation, generating an ON state.

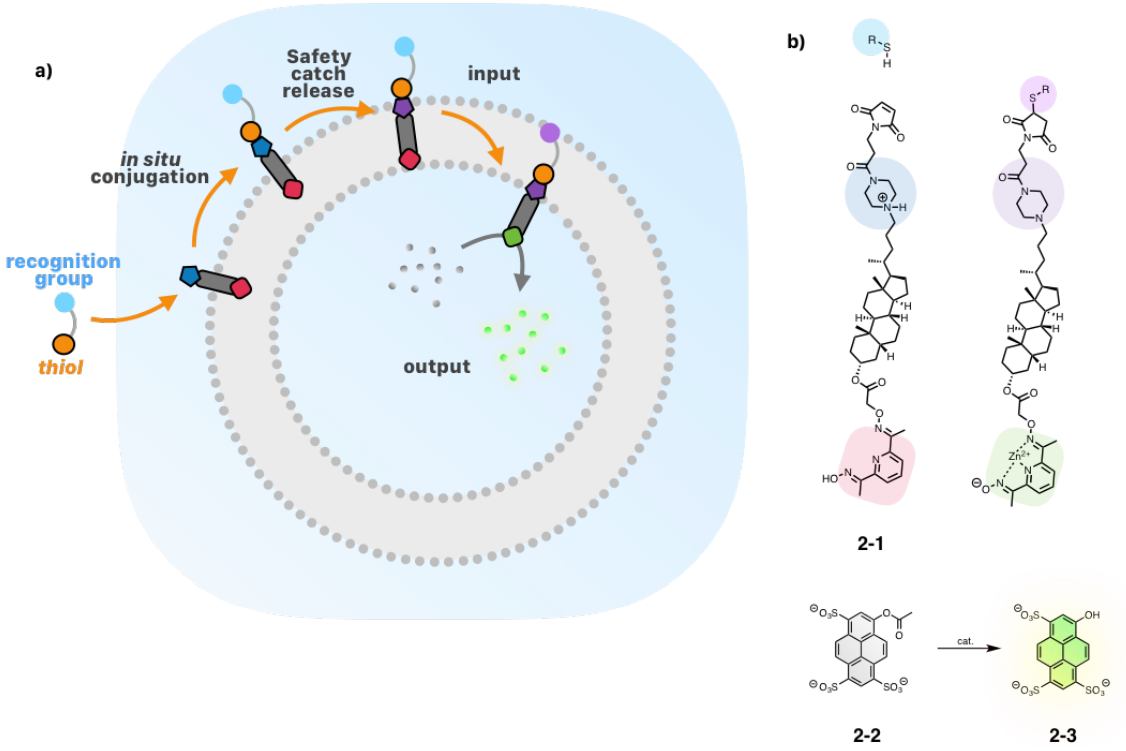

Figure 2.1 Schematic representation of maleimide transducer signal transduction system. a) The piperazine unit acts as a "safety catch" to ensure the maleimide moiety is held in the aqueous phase. The membrane-impermeable recognition group which bears a thiol moiety is attached to the maleimide transducer via thiol-maleimide in-situ conjugation by adding an excess amount of thiol into the vesicle suspension. The "safety catch" is released by raising the external pH and the conjugated recognition group takes over the role of anchoring the transducer on the outside of the membrane. A relevant input signal switches the recognition head group from membrane-impermeable to membrane-permeable, allowing it to enter the membranes. The other head group is a neutral pyridine-oxime pro-catalyst which can be switched to a charged activated state by coordination of a zinc (II) ion cofactor. This pulls the catalyst into the internal aqueous phase and catalyses the hydrolysis of encapsulated substrate to generate the output signal. b) Molecular structures of initial OFF state of maleimide transducer (**2-1**-H^+), thiol reagent and recognition group conjugated transducer with activated catalyst (RS-**2-1**-Zn^{2+}, ON state). R = recognition group.

2.2 Results and discussions

2.2.1 Synthesis of Maleimide Transducer

The maleimide head group (prone to nucleophilic attack) and oxime head group (good nucleophile) could make the maleimide transducer intrinsically unstable. To test the stability of transducer **2-1**, Pyridine-oxime derivative **2-4** and *N*-neopentyl maleimide **2-5** were synthesised as model compounds to assess the stability of transducer **2-1** (Scheme 2.1).

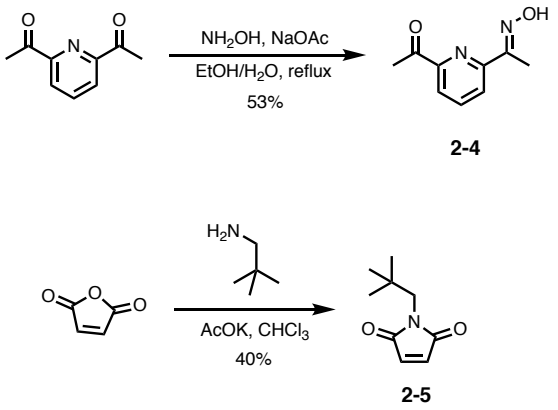

Scheme 2.1 Synthesis of pyridine-oxime derivative **2-4** and maleimide derivative **2-5**.

We then put compound **2-4** and **2-5** together in various conditions which they might encounter during synthesis. The ^{1}H NMR spectrum of the mixture was recorded to examine whether the sp^{2} CH of maleimide remained intact. The results are shown in Table 2.1. Results in Entry 1, 2 and 6 suggest that maleimide and oxime do not react with each other in organic solvents or in HEPES buffer solution. However, when potassium carbonate or sodium acetate was added into the mixture (Entry 3 and 4), the sp^{2} CH signal of maleimide decreased and multiple new peaks appeared. Addition of hydroxylamine into the mixture of 1 and 6 (Entry 5), maleimide (Entry 7) or compound 6 (Entry 8) also led to a decrease of the sp2 CH signal of maleimide, indicating that hydroxylamine or oxime is not compatible with maleimide in basic conditions. Entry 9 indicates that pyridine-oxime is stable in acidic conditions. Therefore, the maleimide head group should be protected in reactions that require the use of a base.

Table 2.1 Stability assay of model compounds **2-4** and **2-5** in various conditions.

Entry	Compound	Condition	Solvent	Result
1	**2-5**+**2-4**[a]	*r.t.*, 16 h	chloroform[b]	No reaction
2	**2-5**+**2-4**[a]	110 °C, 5 h	toluene	No reaction
3	**2-5**+**2-4**[a], K_2CO_3	60 °C, 16 h	dimethylformamide	Reacted[c]
4	**2-5**+**2-4**[a], NaOAc	*r.t.*, 48 h	chloroform/ethanol/water[b,e]	Reacted[d]
5	**2-5**+**1**[a], NH_2OH, NaOAc	60 °C, 16 h	chloroform/ethanol/water[b,e]	Reacted[c]
6	maleimide+**2-4**[a], HEPES	*r.t.*, 16 h	water[b]	No reaction
7	maleimide, NH_2OH, NaOAc	*r.t.*, 16 h	chloroform/ethanol/water[b,e]	Reacted[c]
8	**2-5**, NH_2OH, NaOAc	*r.t.*, 16 h	chloroform/ethanol/water[b,e]	Reacted[c]
9	**2-4**, HCl	*r.t.*, 16 h	methanol	No reaction

*(a) 1:1 ratio mixture; (b) Reaction carried out in deuterated solvent in a sealed NMR tube; (c) Decrease of the integral of the signal due to the sp2 CH (maleimide) observed; (d) Slow reaction, new peaks appeared after 24 h; (e) 1/1/0.1 ratio.

To avoid basic hydrolysis, we used furan to protect the maleimide motif by a Diels-Alder reaction (Scheme 2.3). Deprotection should be achieved via a retro-Diels-Alder reaction at elevated temperatures. The maleimide transducer was synthesised in seven steps from

lithocholic acid. EDC coupling of 1-*tert*-butyloxycarbonylpiperazine with lithocholic acid gave compound **2-8**. Reduction with boron trifluoride yielded compound **2-9**. Condensation with chloroacetyl chloride gave compound **2-10**. Functionalisation with pyridine-oxime **2-1** afforded compound **2-11**. After Boc-deprotection, furan protected maleimide **2-7** was attached to yield compound **2-12**. Condensation with hydroxylamine afforded the pyridine-oxime pro-catalyst **2-13**. Unfortunately, however, the final step of deprotection of **2-13** through a retro-Diels-Alder reaction was unsuccessful in toluene and in *N,N*-dimethylformamide. ^{1}H NMR spectra also suggested that degradation of the transducer occurred upon heating in solution. The deprotection step was then tested without solvent under high vacuum at 95°C, monitored by ^{1}H NMR and mass spectroscopy. Deprotection of the maleimide reached approximately 90% after heating for 10 h. However, significant degradation or polymerisation was observed. A pure sample of maleimide transducer **2-1** was isolated by reverse-phase HPLC in 15% yield.

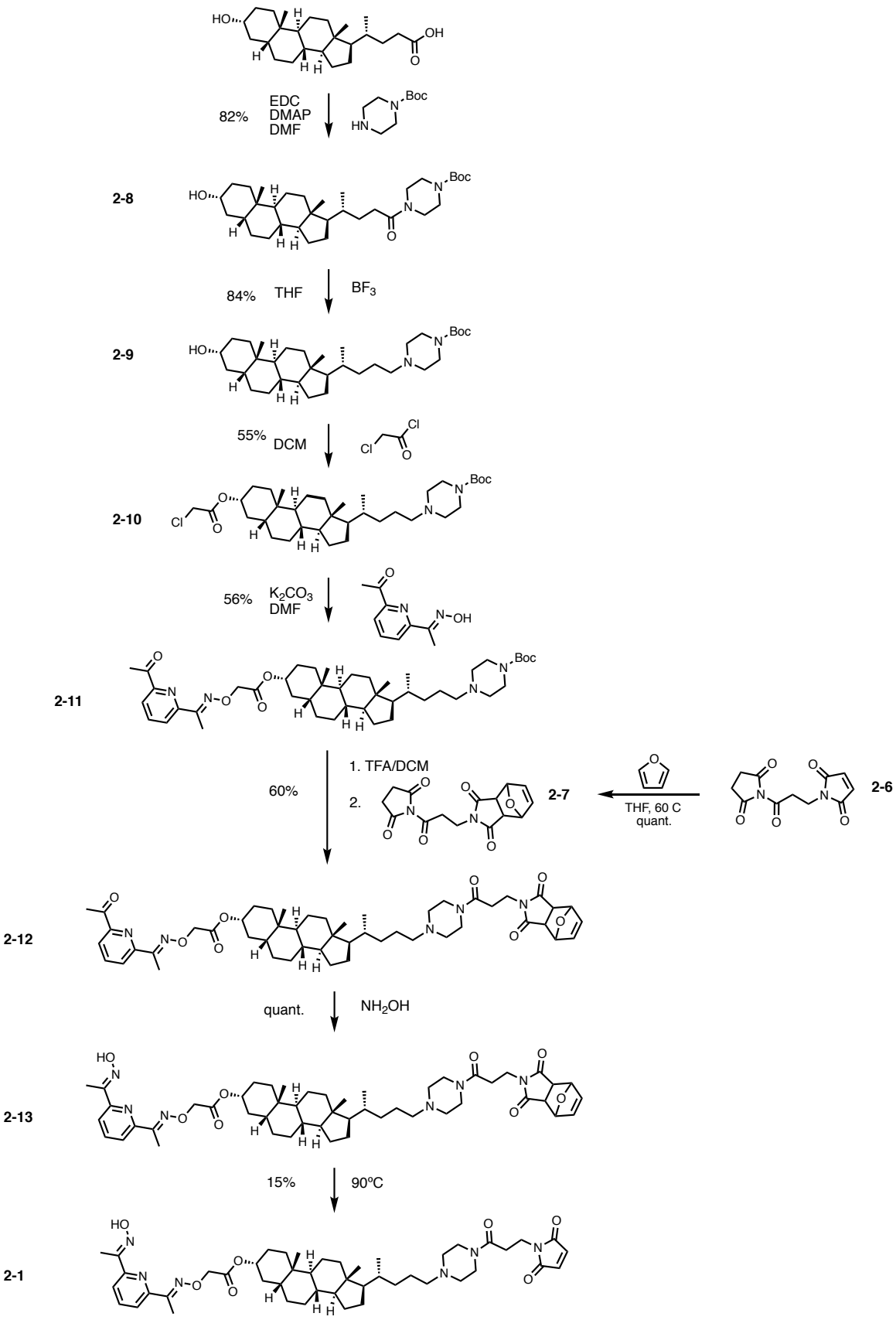

Scheme 2.3 Synthesis of maleimide transducer **2-1**.

2.2.2 Transmembrane Signalling Experiments

200 nm DOPC/DOPE (molar ratio 3:2) vesicles with 1 mol% loading of maleimide transducer containing 250 μM ester **2-2** and 250 μM zinc chloride in HEPES buffer at pH 7 were prepared. Raising the extra-vesicle pH to 10 deprotonates the piperazine group and therefore enables the translocation of the transducer, generating a rapid increase in the fluorescent emission, see Figures 2.2 red data. For the control systems lacking maleimide transducer **2-1**, a slow increase in fluorescent emission intensity was observed over a period of hours, which reflects the background rate of the hydrolysis of substrate **2-2** (Figure 2.2 grey data). When the external pH was raised to 10, a small increase of fluorescence was observed due to the pH jump inside the vesicles, as indicated in Figure 2.2b. This background rate of hydrolysis is comparable to that observed for vesicles with 1 mol% loading of transducer **2-1** without adding the external base pulse. Figure 2.3 shows an example of the change in excitation spectra of vesicles suspension at the beginning and the end of the experiment. These results confirm the catalytic activity of maleimide transducer as well as the viability of using the piperazine "safety catch" to lock the transducer at the external surface.

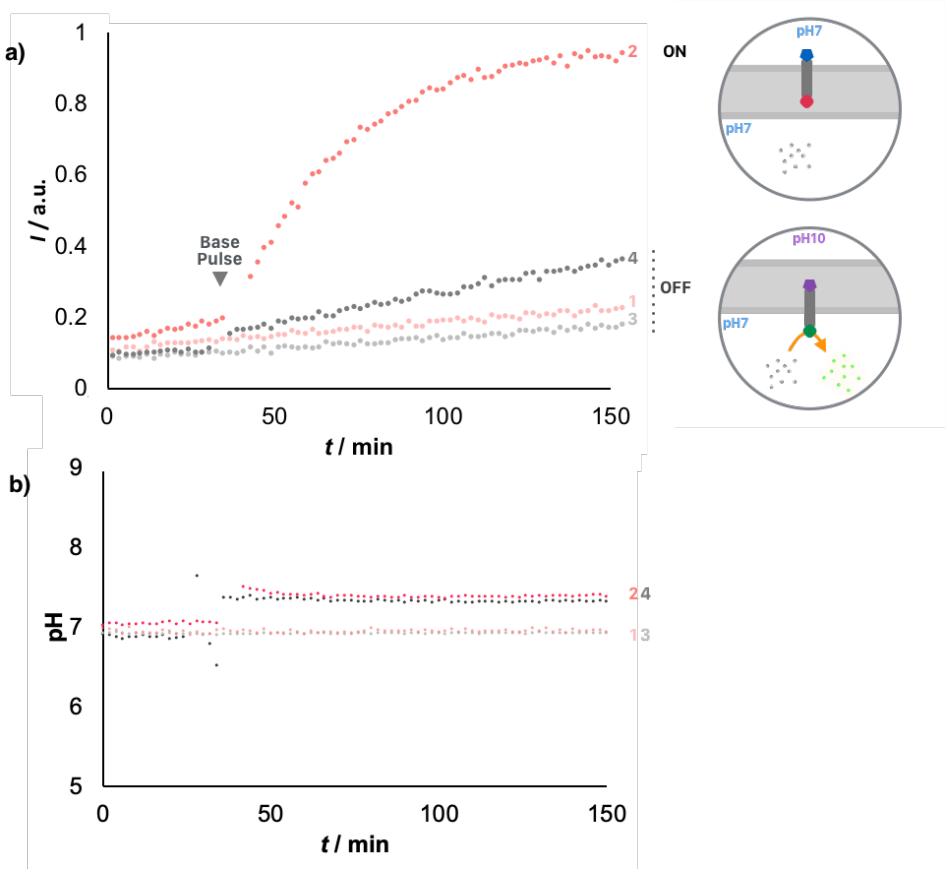

Figure 2.2 Transmembrane signal transduction using maleimide transducer **2-1** with pH sensitive "safety catch". a) Time dependence of the normalised fluorescence emission intensity at 510 nm (exciting at 415 nm). Red data: (1) vesicles with 1 mol% loading of maleimide transducer **2-1** at pH 7; (2) vesicles with 1 mol% loading of transducer **2-1** and the external pH was raised to pH 10 after 30 min, indicated by the arrow; Grey

data: (3) control vesicles prepared without transducer incubated at an external pH of 7; (4) control vesicles prepared without transducer and the external pH was raised to pH 10 after 30 min, indicated by the arrow. All experiments were conducted in 200 nm DOPC/DOPE vesicles containing 250 μM substrate **2-2**, 250 μM $ZnCl_2$ and 250 mM HEPES buffer at pH 7. b) Internal pH of vesicles.

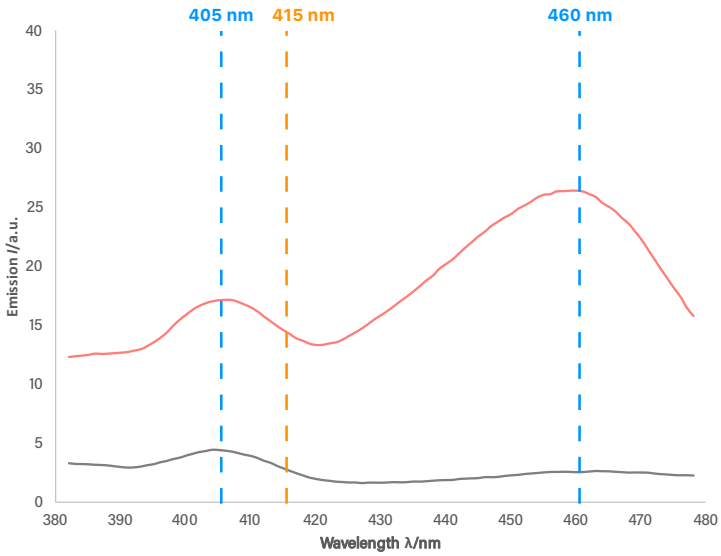

Figure 2.3 Change in excitation spectra of vesicle suspension with 1 mol% loading of transducer (external pH raised to 10) with time during the signalling experiment. Excitation spectra of the vesicle suspension (λ_{em} = 510 nm) at (grey) t = 0 and (red) t = 600 min.

To demonstrate the viability of performing thiol-maleimide in-situ conjugation at the vesicle surface, we designed a "molecular ruler" system (Figure 2.4). When the desired conjugation occurs with a thiol that bears a sulfonate group, the transducer should remain at the outer leaflet of the membrane as the sulfonate group is charged and membrane-impermeable. If the spacer between the thiol and sulfonate is short, raising the external pH to release the "safety catch" does not switch the system to an ON state because translocation is not possible. On the contrary, if the spacer is long enough to enable the conjugated maleimide transducer span the lipid bilayer, the catalytic head group can cross the membrane and be exposed to the internal aqueous solution, generating an ON state.

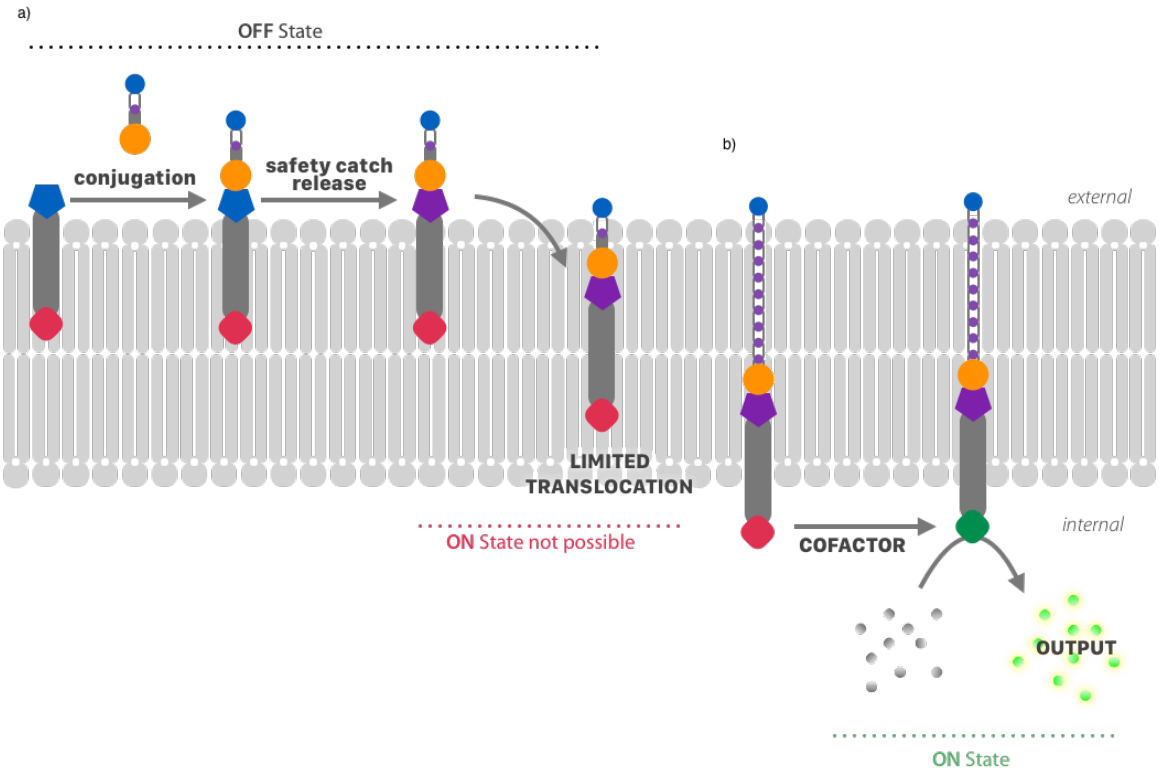

Figure 2.4 Proposed design of the molecular ruler. The "safety-catch" locks the transducer in the outer leaflet of the membrane, exposing the maleimide head group. Addition of thiol (illustrated as yellow circle) that bears a sulphonate group (small blue circle) and a membrane-permeable spacer (purple chain) undergoes in-situ maleimide-thiol conjugation and anchors the transducer in the outer leaflet of membrane as the sulfonate group remains charged and membrane-impermeable. a) If the maleimide transducer is conjugated with a short thiol, when the external pH is raised, the translocation of the transducer is limited due to the short length of the transducer. Therefore, an ON state cannot be achieved.; b) If the spacer of the thiol is long enough to enable the conjugated maleimide transducer cross the lipid bilayer, the catalytic head group can enter the internal aqueous solution and generates an output.

2-Mercaptoethanesulfonic acid, a short thiol reagent with sulfonate group, was selected to examine the above concept. Thiol-maleimide in-situ conjugation was performed by adding an excess amount (10^3-fold) of thiol into the vesicles and incubating at r.t. for 2 hours. The vesicles were then purified from the external solution by size exclusion chromatography and were suspended in a buffered solution at pH 7. The preliminary results are shown in Figure 2.5. For the control system lacking transducer **2-1**, after raising external pH from 7 to 10, an increased background rate for hydrolysis of the substrate **2-2** (Figure 2.5a grey data) was observed. A similar result was observed with the addition of thiol (Figure 2.5a yellow data), showing that thiol has no effect on the background hydrolysis rate. When the maleimide transducer **2-1** was included in the vesicles and subjected to thiol-maleimide in-situ conjugation, the results (Figure 2.5a green data) were similar to the control experiments. This is because when the thiol-maleimide reaction takes place, the sulphonate group makes the conjugate membrane-impermeable. As the length of the conjugate is not long enough to span the lipid bilayer, the catalytic head group cannot cross the membrane and be exposed to the inner surface, i.e. an

ON state is not achieved. After raising the external pH to 10, a small jump of internal pH (from 7.0 to 7.3) was observed in all of these four experiments. As the internal pH is comparable, the pH effect on the hydrolysis rate can be ruled out. These preliminary results suggest that it is feasible to perform thiol-maleimide in-situ conjugation in vesicle suspensions.

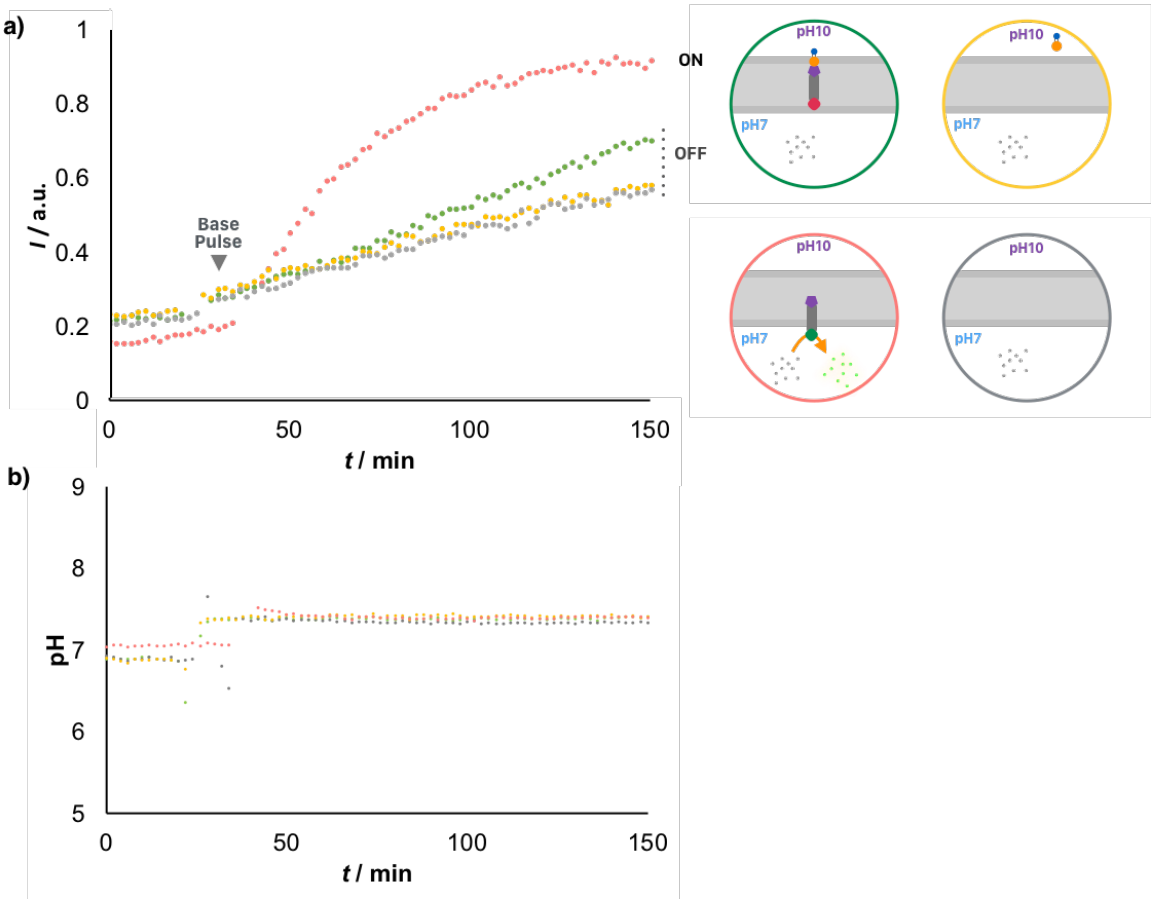

Figure 2.5 Transmembrane signal transduction of maleimide transducer **2-1** with *in-situ* thiol-maleimide conjugation (thiol: sodium methanethiolate). a) Time dependence of the normalised fluorescence emission intensity at 510 nm (exciting at 415 nm). Green data: vesicles with 1 mol% loading of **2-1** and addition of thiol. Yellow data: a control experiment without transducer, with addition of thiol. Red data: vesicles with 1 mol% loading of maleimide transducer **2-1**. Grey data: a control experiment without transducer. All experiments were conducted in 1 mM 200 nm DOPC/DOPE vesicles containing 250 μM substrate **2-2**, 250 μM $ZnCl_2$ and 250 mM HEPES buffer at pH 7, the pH of external solution was raised to 10 after approximately 30 min, indicated by an arrow. Experiments with addition of thiol (10^3 eq. relative to transducer **2-1**) was added and the vesicles were incubated at r.t. for 2 h prior to the measurement. b) internal pH of vesicles in green, yellow, red, and grey data, respectively.

However, although our preliminary results were convincing, the ON state achieved by removing the "safety-catch" of transducer **2-1** (Figure 2.5a red data) was not reproducible. A large number of repetitions, including variation in the loading of the transducer and the buffer concentration, were conducted but a reliable ON state could not be achieved. In addition, the change in the internal pH after the base pulse was variable. Figure 2.6 shows the distribution

of internal pH values measured in 27 repeats of the similar experiments with an external base pulse to pH 10. The internal pH increased from the initial value of 7.0 to as high as 8.0. If a stable internal pH cannot be maintained, the high internal pH could possibly result in a false-positive signal. Although in theory it is possible to examine the internal pH and eliminate these false positive results, the randomness of the internal pH jump makes it practically difficult to reproduce the result that has an internal pH of 7.3. One reason for the variability in the pH change is that the lipids were purchased from different suppliers and different batches and purities may maintain the pH gradient better.

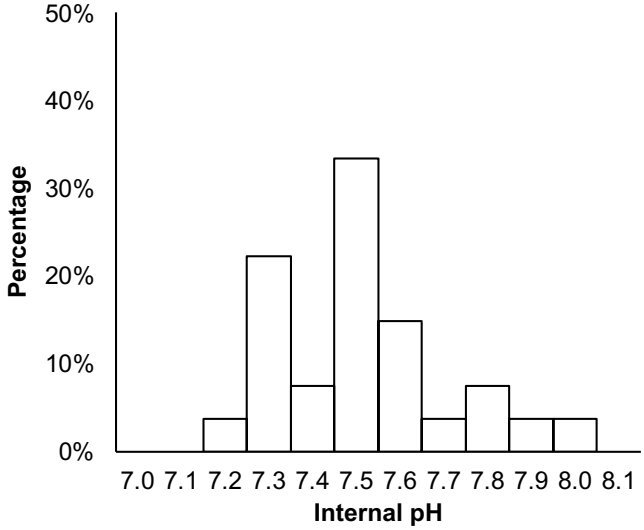

Figure 2.6 A statistic distribution (in percentage) of internal pH after the external base pulse to pH 10, out of 27 experiments. 1 mM 200 nm DOPC/DOPE vesicles containing 250 μM substrate **2-2**, 250 μM $ZnCl_2$ and 250 mM HEPES buffer at pH 7, the pH of external solution was raised to 10 by addition of sodium hydroxide.

2.3 Conclusion

To conclude, we have designed and synthesised a transducer featuring a maleimide head group with a piperazine unit acting as a "safety catch". In neutral pH, the piperazine unit is charged and membrane-impermeable, locking the transducer in the outer leaflet of the lipid bilayer. Preliminary results suggested the viability of the "safety catch" and demonstrated that the transducer could be functionalised with an in-situ thiol-maleimide conjugation reaction at the membrane surface. However, the ON state experiment could not be reproduced. Therefore, we cannot draw a conclusion on whether the in-situ thiol-maleimide reaction is a reliable technique for this particular system. Furthermore, the pH gradient was not maintained when external pH is raised to 10, which suggests that the system could generate false-positive signals due to high background hydrolysis rate. Having realised these challenges, we decided not to investigate further on systems that involve external addition of base.

References

(1) Catterall, W. A. Structure and Function of Voltage-Gated Ion Channels. *Annu. Rev. Biochem.* **1995**, *64* (1), 493–531. https://doi.org/10.1146/annurev.bi.64.070195.002425.

(2) Simon, M. I.; Strathmann, M. P.; Gautam, N. Diversity of G Proteins in Signal Transduction. *Science* **1991**, *252* (5007), 802–808. https://doi.org/10.1126/science.1902986.

(3) Schlessinger, J. Cell Signaling by Receptor Tyrosine Kinases. *Cell* **2000**, *103* (2), 211–225. https://doi.org/10.1016/S0092-8674(00)00114-8.

(4) Langton, M. J.; Keymeulen, F.; Ciaccia, M.; Williams, N. H.; Hunter, C. A. Controlled Membrane Translocation Provides a Mechanism for Signal Transduction and Amplification. *Nat. Chem.* **2017**, *9* (5), 426–430. https://doi.org/10.1038/nchem.2678.

(5) Langton, M. J.; Scriven, L. M.; Williams, N. H.; Hunter, C. A. Triggered Release from Lipid Bilayer Vesicles by an Artificial Transmembrane Signal Transduction System. *J. Am. Chem. Soc.* **2017**, *139* (44), 15768–15773. https://doi.org/10.1021/jacs.7b07747.

(6) Langton, M. J.; Williams, N. H.; Hunter, C. A. Recognition-Controlled Membrane Translocation for Signal Transduction across Lipid Bilayers. *J. Am. Chem. Soc.* **2017**, *139* (18), 6461–6466. https://doi.org/10.1021/jacs.7b02345.

(7) Ravasco, J. M. J. M.; Faustino, H.; Trindade, A.; Gois, P. M. P. Bioconjugation with Maleimides: A Useful Tool for Chemical Biology. *Chem. – Eur. J.* **2019**, *25* (1), 43–59. https://doi.org/10.1002/chem.201803174.

2.4 Supporting Information

2.4.1 Synthetic Procedures and Characterisation

Materials and Methods

^{1}H NMR and ^{13}C NMR spectra were recorded on a 400-MHz Bruker® spectrometer. Chemical shifts are reported as δ values in ppm. Microwave reactions were carried out on a Biotage® Initiator+ microwave reactor. Flash chromatography was carried out on an automated system (Combiflash® Rf+ Lumen™) using pre-packed cartridges of silica (25 µm PuriFlash® Column) or neutral alumina (50 µm Redi*Sep*® Rf Column). RF-HPLC was carried out on an Agilent 1100 Series HPLC Value System. SEC purification of the vesicles was carried out using GE Healthcare PD-10 desalting columns prepacked with Sephadex® G-25 medium. Melting point was measured on a Mettler-Toledo MP90 Melting Point System. Fluorescence spectra were recorded using a Cary Eclipse fluorescence spectrophotometer (Agilent Technologies) in Hellma® Analytics Suprasil® quartz cuvettes. Measurements of pH were conducted using a Mettler-Toledo SevenCompact™ pH meter equipped with an InLab® Micro electrode. Vesicles were assembled in Eppendorf® polypropylene DNA LoBind® polypropylene microcentrifuge tube and extruded as described below using Avanti® Polar Lipids extruder kits, equipped with Avestin® LiposoFast Liposome Factory 200 nm polycarbonate membranes with GE Healthcare Whatman® 10 mm polyester filter support. Sonication was carried out using an Elma® Transsonic 420 sonicator. Vortexing was carried out on a Heidolph™ Reax Top Vortex Mixer. Solutions or vesicles suspensions were transferred using Eppendorf Multipette® Xstream Pippette with Combitips Advanced® or Hamilton Microliter™ syringes. All reagents and solvents were used without further purification. Lipids were purchased from Sigma-Aldrich® and used without further purification.

Compound 2-5

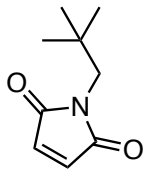

To a solution of maleic anhydride (2.0 g, 20.4 mmol) in chloroform (40 mL) was added the solution of neopentylamine (1.8 g, 20.4 mmol) in chloroform (5 mL). The mixture was stirred at r.t. for 90 min. The precipitate was filtrated and dissolved in glacial acetic (20 mL) acid with potassium acetate (400 mg, 4 mmol). The mixture was stirred under reflux for 2 h. The reaction mixture was then poured onto chilled sodium bicarbonate solution and extracted with diethyl ether, washed with brine, dried over magnesium sulphate and purified by flash column chromatography (silica gel, petroleum ether/ethyl acetate:9/1, R_f = 0.3) to afford a white crystal (267 mg, 8%).

^{1}H NMR (400 MHz, $CDCl_3$) δ (ppm): 6.71 (s, 2H), 3.32 (s, 2H), 0.92 (s, 9H).
^{13}C NMR (100 MHz, $CDCl_3$) δ (ppm): 171.6, 134.2, 49.3, 33.7, 28.2.
HR-MS (ES+): calcd. for $C_9H_{14}NO_2$: 168.1025, found: 168.1026.
FT-IR (ATR): ν_{max} 3105, 3091, 2957, 2910, 2872, 1697 cm^{-1}.
m.p.: 106.9 °C.

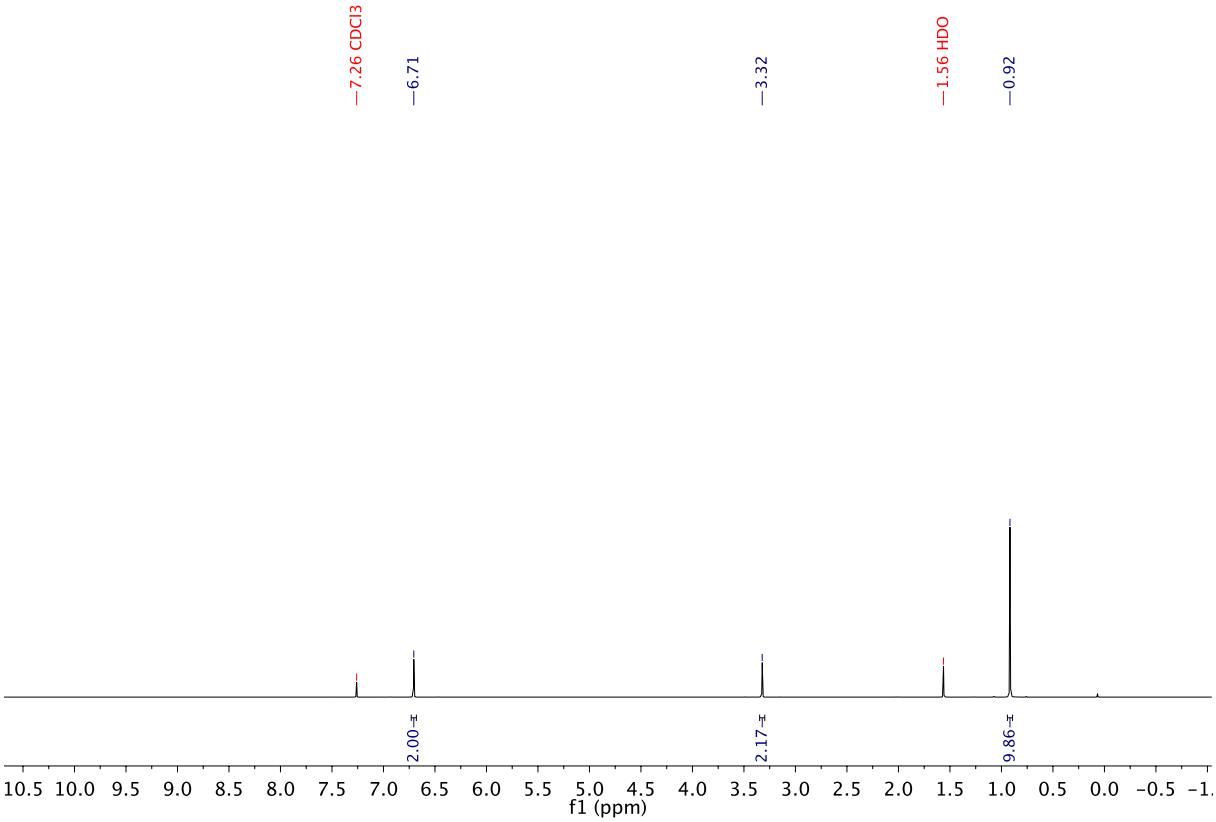

Figure S2.1 ^{1}H spectrum of compound **2-5**.

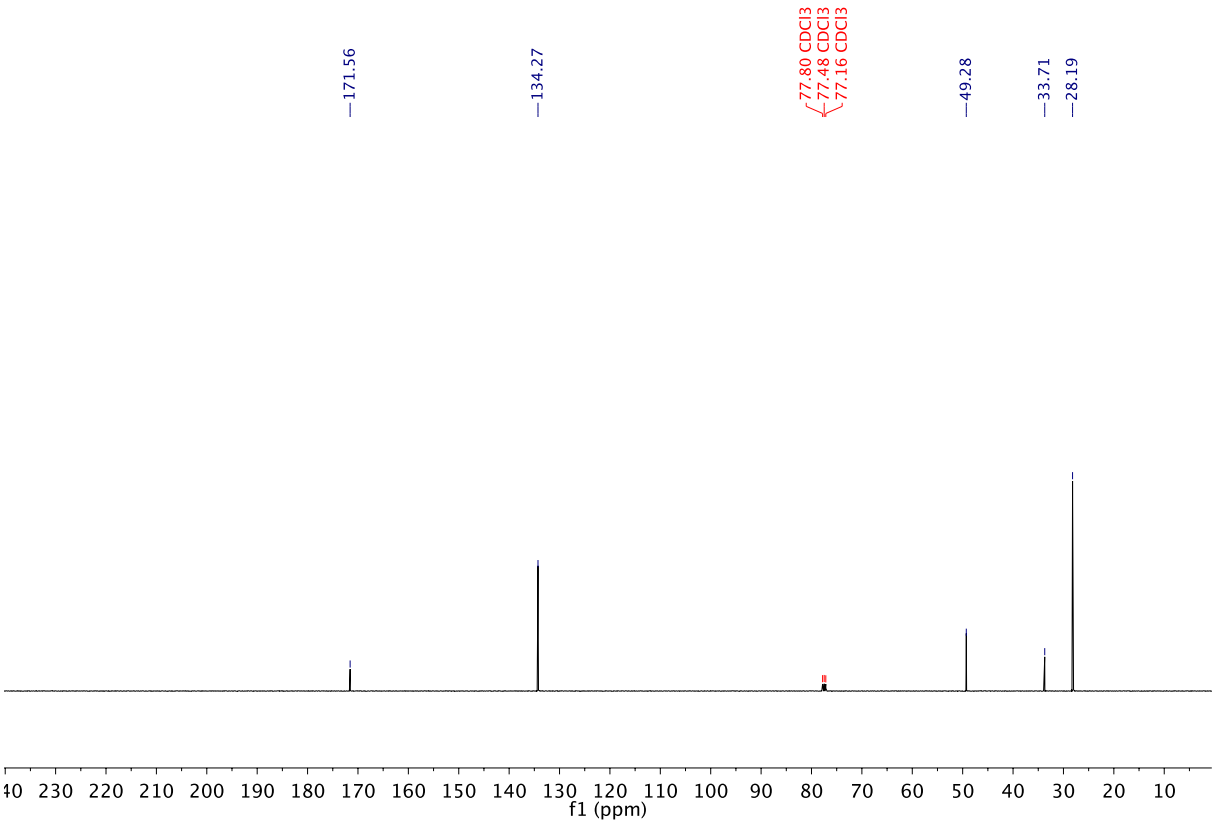

Figure S2.2 ^{13}C spectrum of compound **2-5**.

Compound 2-7

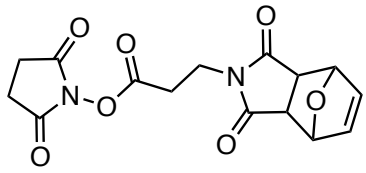

In a sealed bottle the solution of 3-maleimidopropionic acid *N*-hydroxy-succinimde ester **2-6** (100 mg, 0.376 mmol) in furan (15 mL) and tetrahydrofuran (5 mL) was stirred at 60 °C under microwave radiation for 2 h. After evaporation of solvent, the product was obtained as a pale yellow solid (145 mg, quant. yield).

^{1}H NMR (400 MHz, $CDCl_3$) δ (ppm): Endo-exo isomers were found with a ratio of 4:6. 6.50 (s, 0.8H), 6.41 (s, 1.2H), 5.31 (s, 1.2H), 5.27 (s, 0.8H), 3.88 (t, *J* = 7.1 Hz, 0.8H), 3.72 (t, *J* = 6.8 Hz, 1.2H), 3.55 (dd, *J* = 3.6, 1.6 Hz, 1.2H), 2.99 (t, *J* = 7.1 Hz, 0.8H), 2.91 (s, 1.2H), 2.88 (t, *J* = 6.8 Hz, 1.2H), 2.82-2.81 (m, 4H).
^{13}C NMR (100 MHz, $CDCl_3$) δ (ppm): Endo-exo isomers were found. 175.90/174.54, 168.88/168.86, 166.06/166.04, 136.67/134.71, 81.05/79.54, 47.68/46.13, 34.14/33.55, 29.08/28.68, 25.68.
HR-MS (ES+): calcd. for $C_{15}H_{15}N_2O_7$: 335.0879, found 335.0879.
FT-IR (ATR): ν_{max} 2954, 2850, 1818, 1779, 1730, 1694, 1538 cm^{-1}.

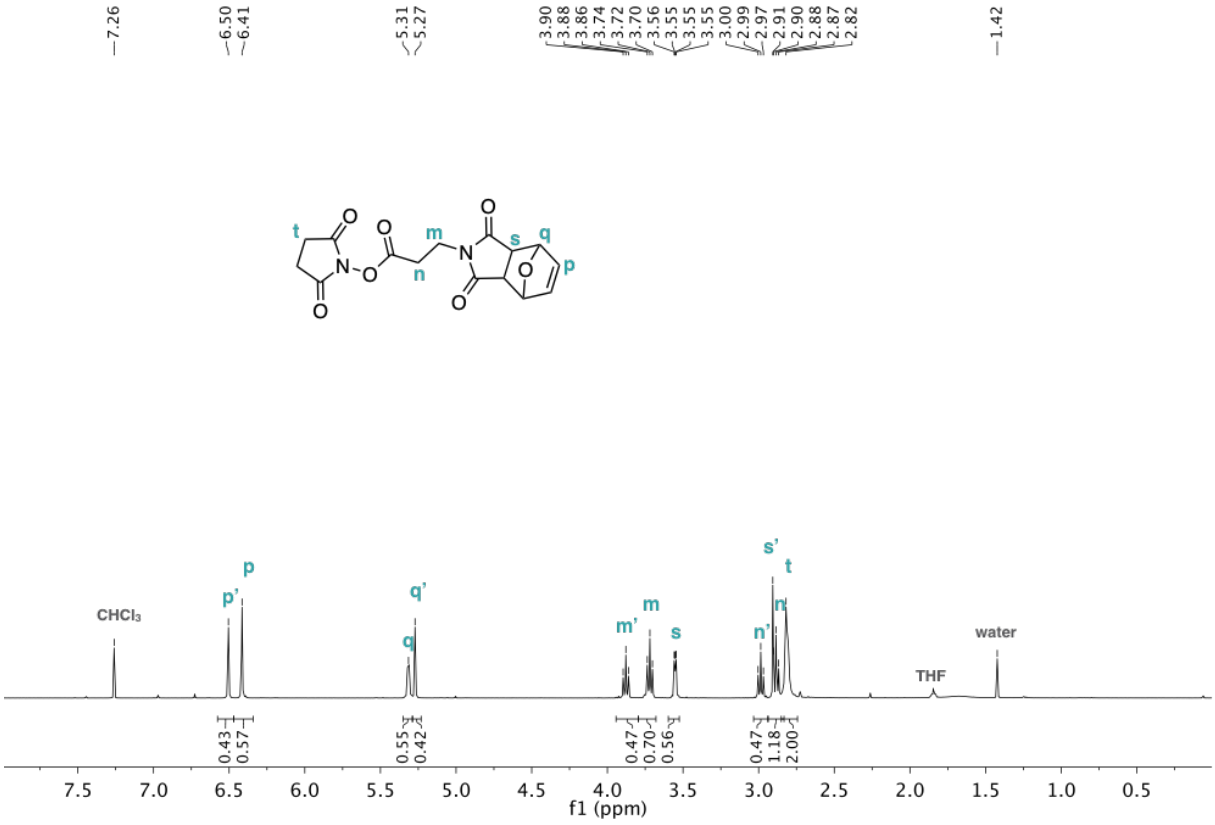

Figure S2.3 [1]H spectrum of compound **2-7**. (Prime notation indicates an endo/exo isomer)

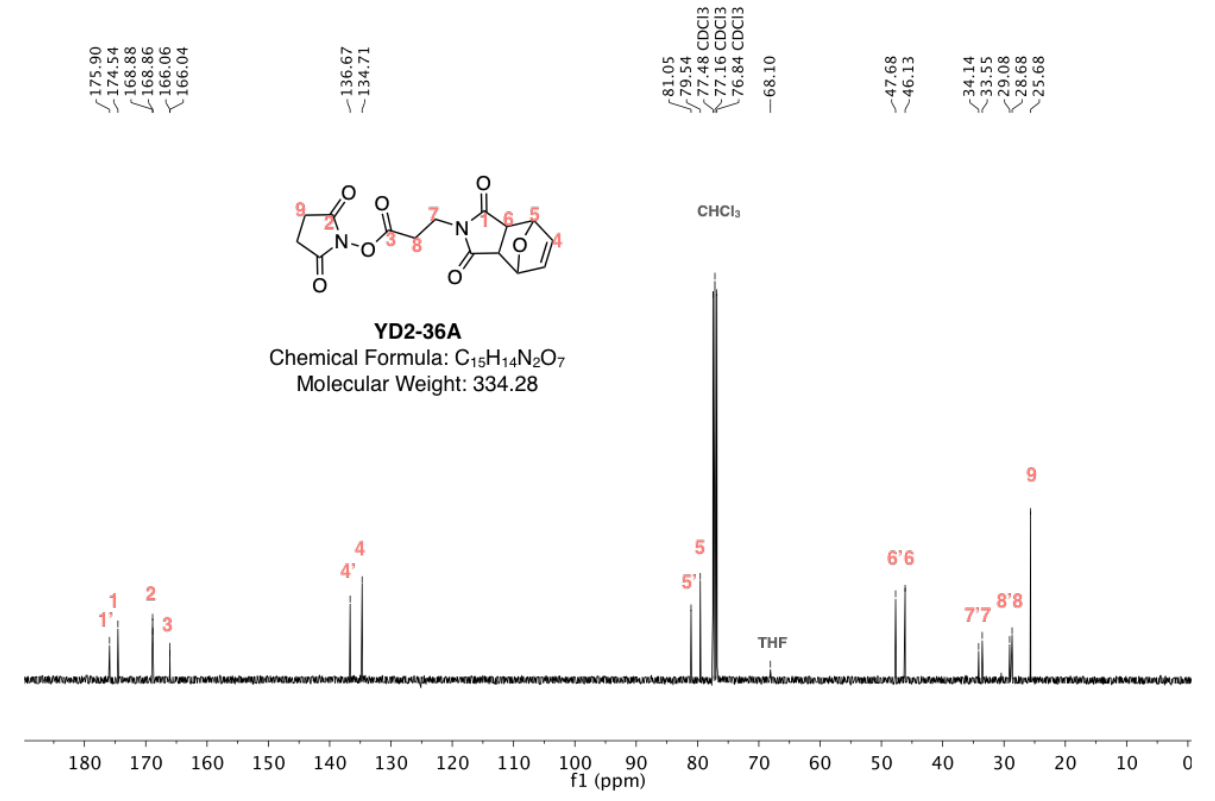

Figure S2.4 [13]C spectrum of compound **2-7**. (Prime notation indicates an endo/exo isomer)

Compound 2-8

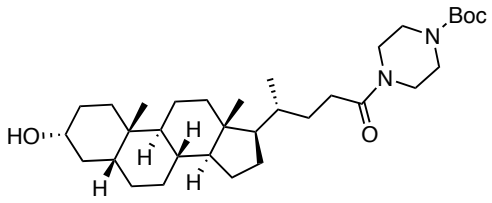

*Compound **2-8** has been previously characterised within the group (unpublished result).* The solution of lithocholic acid (2.00 g, 5.32 mmol), *N*-ethylcarbodiimide hydrochloride (1.53 g, 5.32 mmol), 1-boc-piperazine (1.50 g, 5.32 mmol) and 4-dimethylaminopyridine (10 mg) in anhydrous dimethylformamide (50 mL) was stirred at r.t. for 24 h, then diluted with ethyl acetate (100 mL) and washed with aqueous LiCl (5%, 10 × 25 mL) and brine (25 mL). The organic phase was dried over Na_2SO_4 and purified by flash chromatography (SiO_2, 0-15% gradient of methanol in dichloromethane) to afford the product as a white solid (2.37 g, 82% yield).

^{1}H NMR (400 MHz, $CDCl_3$) δ (ppm): 3.69-3.57 (m, 3H), 3.48- 3.39 (m, 6H), 2.39 (m, 1H), 2.24 (m, 1H), 1.97 (dt, 1H), 1.92-0.92 (m, 41H), 0.66 (s, 3H).
^{13}C NMR (100 MHz, CDCl3) δ (ppm): 172.3, 154.6, 80.3, 71.8, 56.5, 56.0, 45.5, 42.8, 42.1, 41.3, 40.4, 40.2, 36.5, 35.9, 35.6, 35.4, 34.6, 31.4, 30.5, 30.4, 28.4, 28.3, 27.2, 26.4, 24.2, 23.4, 20.8, 18.5, 12.1. *(This characterisation was conducted by Peter Bolgar)*
HR-MS (ES+): calcd. for $C_{33}H_{57}N_2O_4$: 545.4318, found: 545.4323.
FT-IR (ATR): ν_{max} 3421, 2924, 2860, 1697, 1635 cm^{-1}.

Compound 2-9

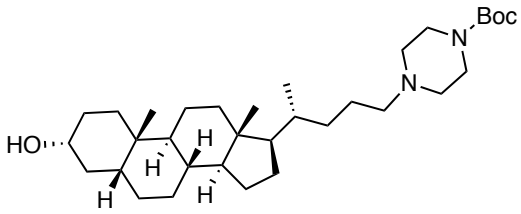

BH_3-THF (1M, 50 mL) was added to compound **2-8** (2.30 g, 4.22 mmol) with external cooling, then refluxed for 3 h. Methanol (60 mL) was added to quench the reaction and the crude was purified by flash chromatography (silica, 0-50% gradient of ethyl acetate in petroleum ether) to afford the product as a white solid (1.88 g, 84% yield).

^{1}H NMR (400 MHz, $CDCl_3$) δ (ppm): 3.68-3.56 (m, 5H), 2.97-2.81 (m, 2H), 2.76-2.58 (m, 4H), 1.96-0.90 (m, 50H), 0.62(s, 3H).
^{13}C NMR (100 MHz, $CDCl_3$) δ (ppm): 154.44, 80.52, 71.89, 65.36, 57.37, 57.28, 56.57, 56.23, 56.21, 42.84, 42.19, 40.52, 40.27, 36.54, 35.94, 35.68, 35.45, 34.67, 33.58, 30.64, 28.45, 27.30, 26.52, 24.30, 23.48, 19.50, 19.44, 18.73, 12.16.
HR-MS (ES+): calcd. for $C_{33}H_{59}O_3N_2$: 531.4520, found: 531.4516.
FT-IR (ATR): ν_{max} 3438, 2926, 2864, 2372, 1690 cm^{-1}.

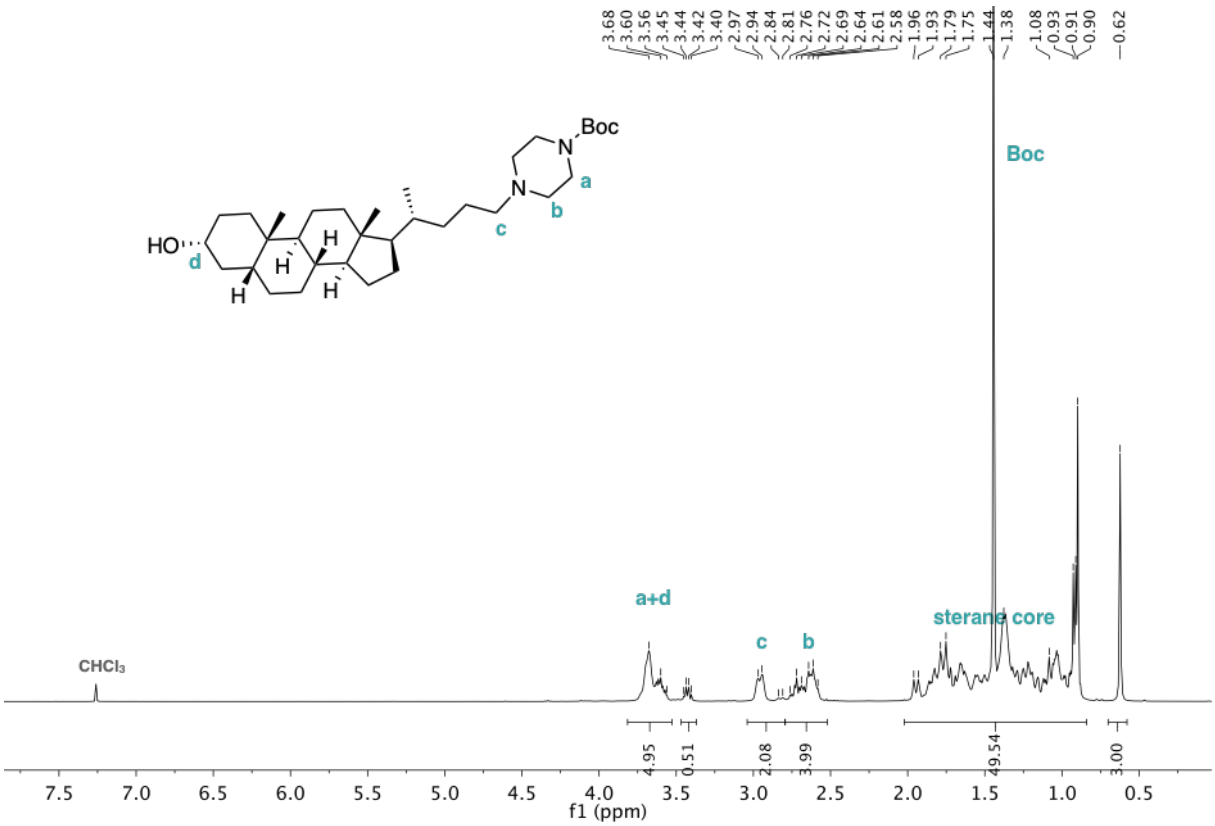

Figure S2.5 ^{1}H spectrum of compound **2-9**.

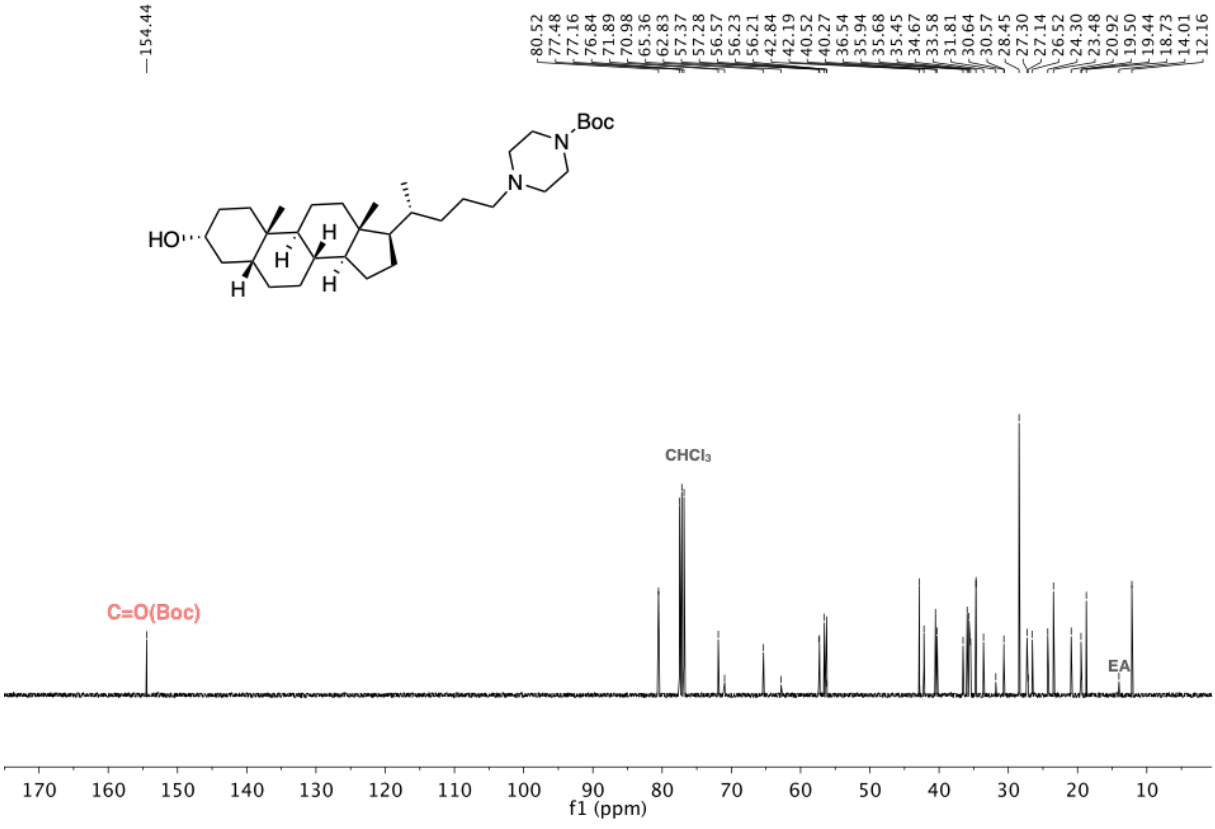

Figure S2.6 ^{13}C spectrum of compound **2-9**.

Compound 2-10

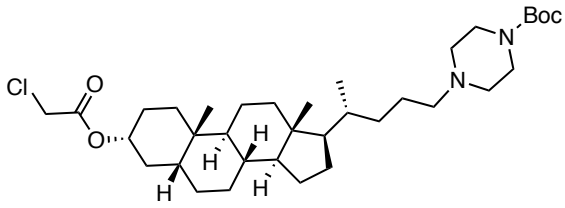

To a solution of compound **2-9** (400 mg, 0.754 mmol), DMAP (9 mg, 0.075 mmol) and triethylamine (0.31 mL, 2.262 mmol) in dichloromethane (20 mL) was added a solution of chloroacetyl chloride (0.12 mL, 1.508 mmol) 10 mL of dichloromethane (10 mL) with external cooling. The reaction was then stirred at r.t. for 24 h. After quenching with methanol (2 mL), the solvent was evaporated and the crude was purified by flash chromatography (silica, 0-5% gradient of methanol in dichloromethane) to afford the product as a white solid (253.2 mg, 55% yield).

^{1}H NMR (400 MHz, $CDCl_3$) δ (ppm): 4.83-4.80 (m, 1H), 4.03 (s, 1H), 3.76-3.56 (m, 4H), 3.26-3.22 (m, 2H), 2.97-2.79 (m, 4H), 2.04-0.93 (m, 47H), 0.65 (s, 3H).
^{13}C NMR (100 MHz, $CDCl_3$) δ (ppm): 166.57, 154.04, 80.57, 76.45, 60.17, 58.36, 56.21, 55.87, 53.73, 53.69, 42.52, 41.66, 41.03, 40.21, 39.88, 35.54, 35.25, 34.70, 34.34, 33.11, 31.81, 28.10, 26.75, 26.24, 26.07, 23.94, 23.06, 20.62, 18.74, 18.41, 11.85.
HR-MS (ES+): calcd. for $C_{35}H_{60}N_2O_4Cl$: 607.4260, found: 607.4242.
FT-IR (ATR): ν_{max} 2934, 2866, 2455, 1748, 1696 cm^{-1}.

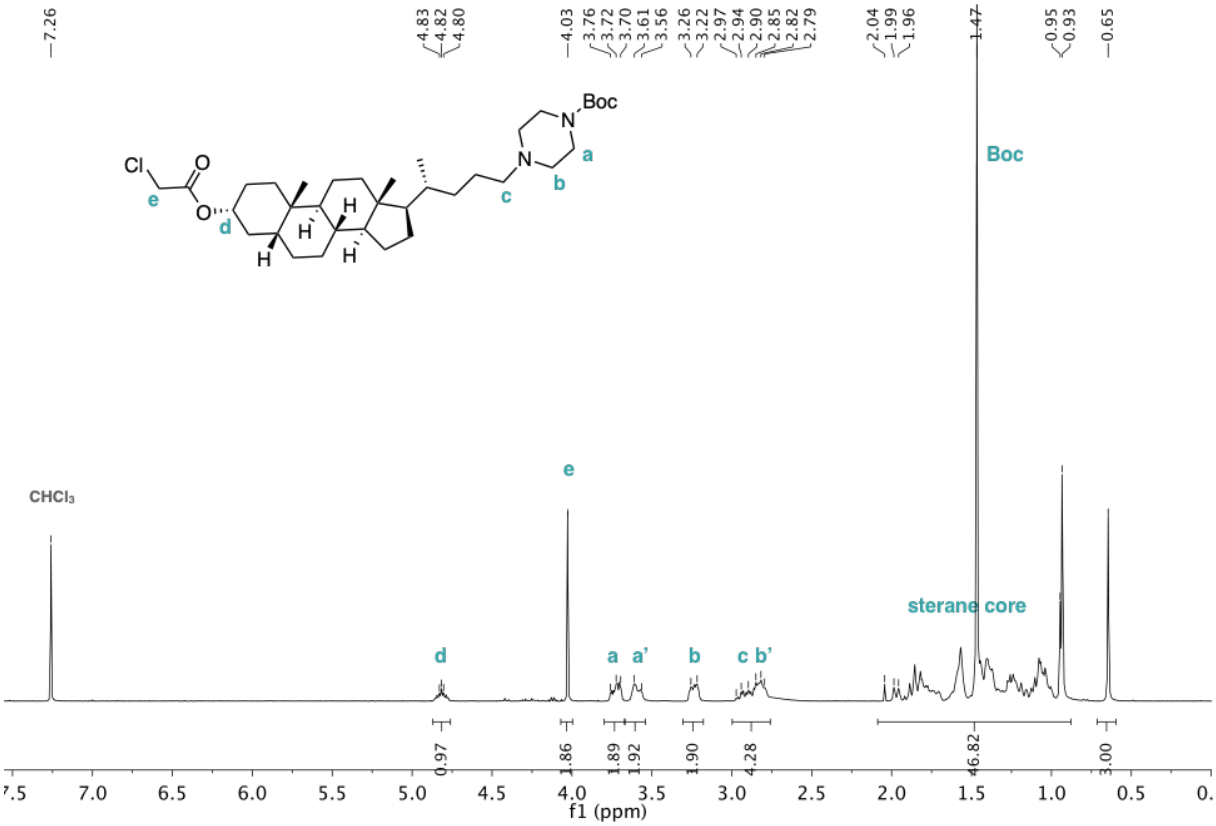

Figure S2.7 ^{1}H spectrum of compound **2-10**.

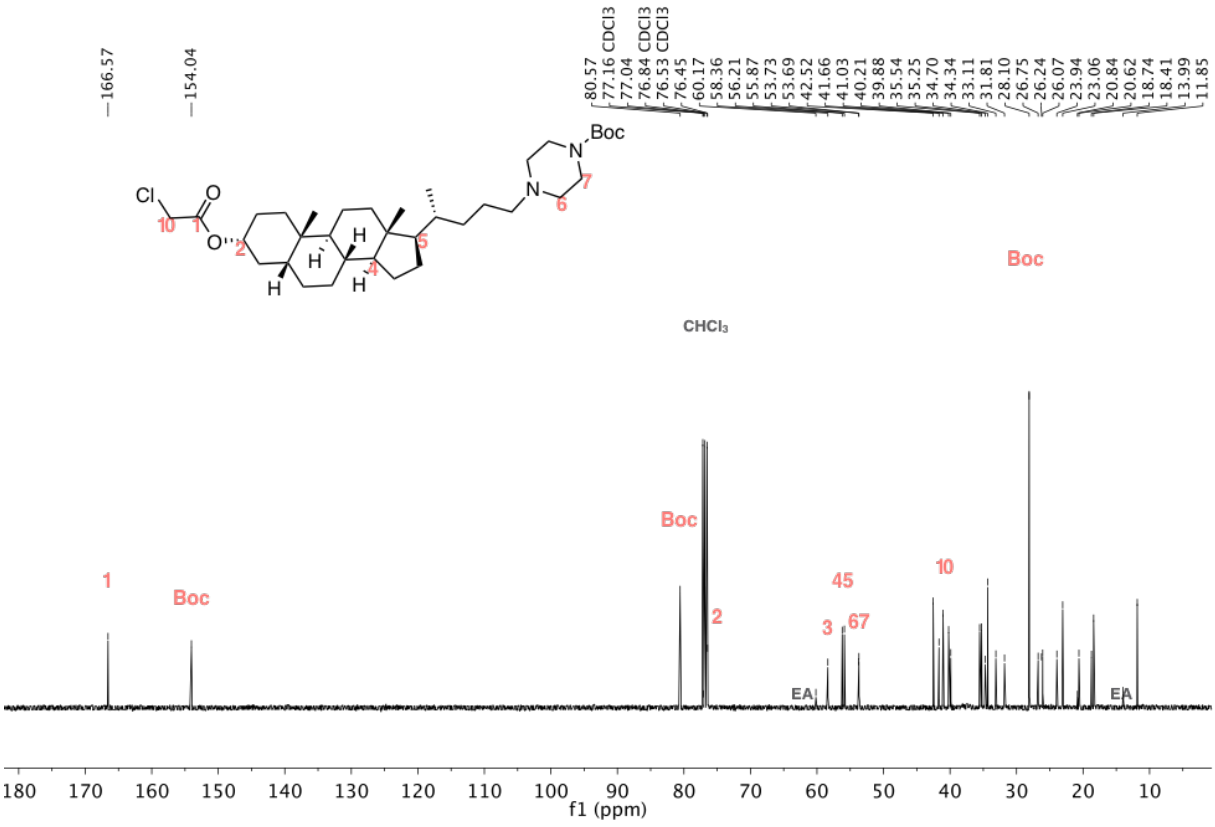

Figure S2.8 ^{13}C spectrum of compound **2-10**.

Compound 2-11

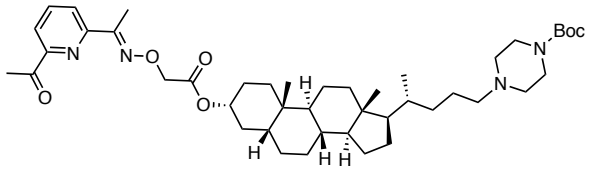

The solution of compound **2-10** (100 mg, 0.165 mmol), compound **2-4** (146 mg, 0.823 mmol) and potassium carbonate (158 mg, 1.15 mmol) in anhydrous dimethylformamide (10 mL) was stirred at r.t. for 48 h. The reaction mixture was diluted with ethyl acetate (50 mL) and washed with lithium chloride (5% aq., 5 x 10 mL), sodium carbonate (sat. aq., 3 x 10 mL) and brine (10 mL). After evaporation of solvent, the crude was purified by flash chromatography (neutral alumina, 0-15% gradient of ethyl acetated in petroleum ether then silica, 0-30% gradient of ethyl acetate in petroleum ether) to afford the product as a white solid (65 mg, 53% yield).

^{1}H NMR (400 MHz, $CDCl_3$) δ (ppm): 8.06 (d, *J* = 7.9 Hz, 1H), 7.97 (d, *J* = 7.9 Hz, 1H), 7.78 (d, *J* = 7.9 Hz, 1H), 4.82 (s, 1H), 4.73 (s, 1H), 3.74-3.57 (m, 4H), 3.24-3.20 (m, 2H), 2.91-2.84 (m, 4H), 2.40 (s, 3H), 2.45 (s, 3H), 1.96-0.91 (m, 47H), 0.62 (s, 3H).

^{13}C NMR (100 MHz, $CDCl_3$) δ (ppm): 200.12, 169.41, 157.11, 154.35, 153.20, 152.64, 137.04, 124.13, 121.59, 80.88, 75.35, 71.42, 58.67, 56.55, 56.19, 54.05, 54.02, 42.82, 41.96, 40.53, 40.22, 35.85, 35.55, 35.06, 34.66, 33.42, 32.30, 28.41, 28.39, 27.08, 26.70, 26.39, 25.76, 24.26, 23.39, 20.92, 19.05, 18.72, 12.16, 11.26.

HR-MS (ES+): calcd. for $C_{44}H_{69}N_4O_6$: 749.5200, found: 749.5217.

FT-IR (ATR): ν_{max} 2931, 2867, 2467, 1753, 1798, 1579 cm^{-1}.

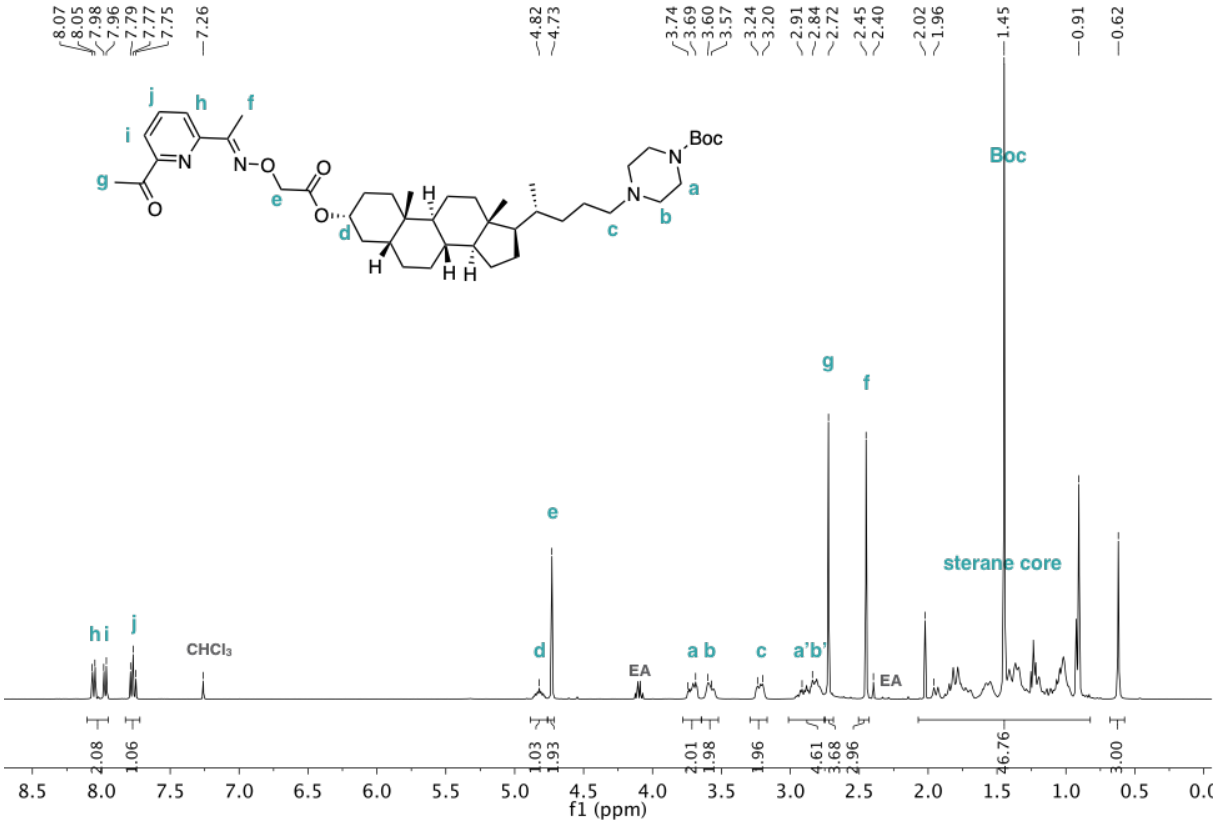

Figure S2.9 ^{1}H spectrum of compound **2-11**.

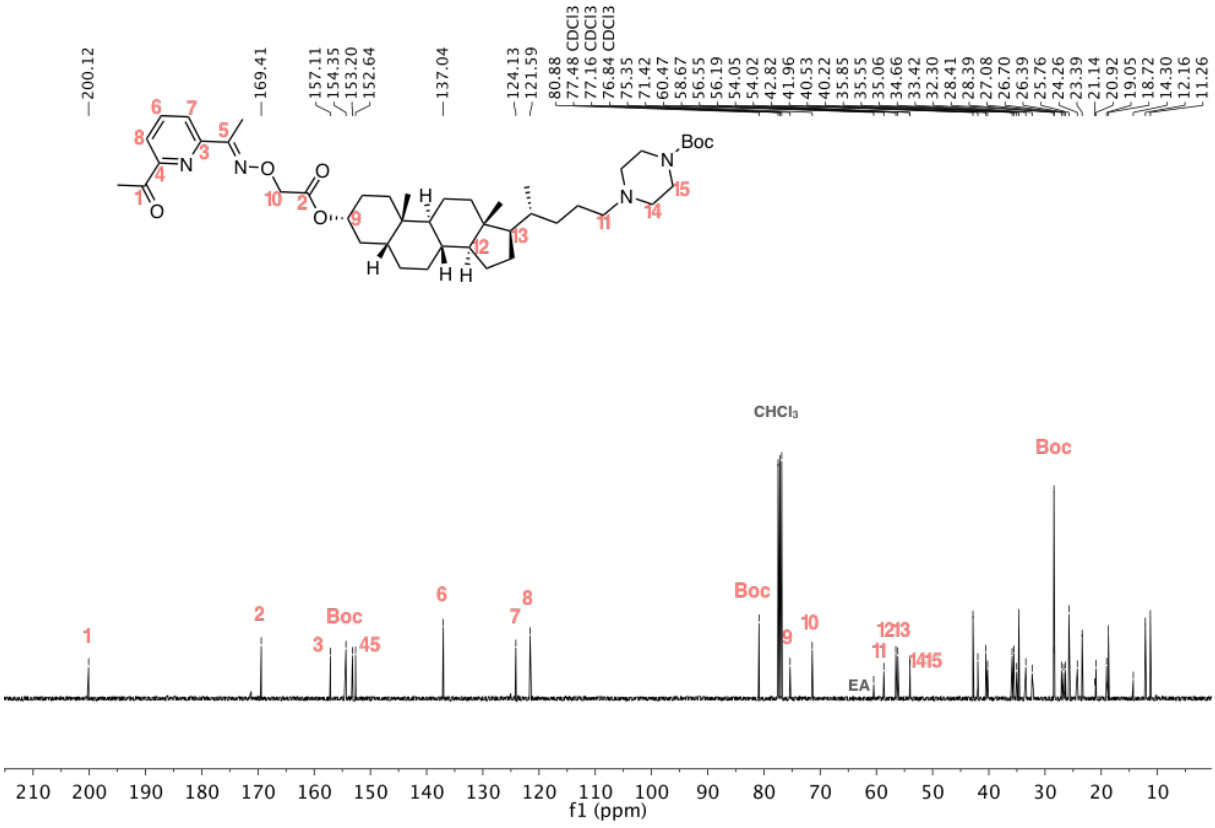

Figure S2.10 ^{13}C spectrum of compound **2-11**.

Compound 2-11 (deprotected)

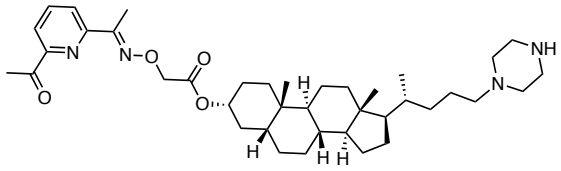

The solution of compound **2-11** (65 mg, 0.08 mmol) and trifluoroacetic acid (1 mL, 13.1 mmol) in dichloromethane (10 mL) was stirred at r.t. for 1 h. The reaction was quenched with sodium hydroxide (2 M, aq., 6 mL) then washed with sodium bicarbonate (sat., aq., 3 x 10 mL), brine (10 mL) and dried over anhydrous sodium sulphate. After evaporation of solvent the product was obtained as white solid (60.2 mg, quant. yield) and used for the next step without further purification.

^{1}H NMR (400 MHz, $CDCl_3$) δ (ppm): 8.06 (d, *J* = 7.9 Hz, 1H), 7.98 (d, *J* = 7.9 Hz, 1H), 7.77 (t, *J* = 7.9 Hz, 1H), 4.83 (m, 1H), 4.73 (s, 1H), 3.22-3.17 (m, 4H), 2.97-2.84 (m, 4H), 2.73 (s, 3H), 2.45 (s, 3H), 1.96-0.91 (m, 37H), 0.63 (s, 3H).
^{13}C NMR (100 MHz, $CDCl_3$) δ (ppm): 200.00, 169.29, 157.01, 153.10, 152.55, 136.93, 124.02, 121.49, 75.26, 71.32, 56.51, 56.45, 56.15, 42.73, 42.69, 41.87, 40.44, 40.13, 35.76, 35.56, 34.96, 34.57, 33.33, 32.21, 28.29, 26.99, 26.61, 26.30, 25.65, 24.17, 23.29, 20.82, 18.67, 18.62, 12.06, 12.03, 11.16.
HR-MS (ES+): calcd. for $C_{39}H_{61}O_4N_4$: 649.4687, found: 649.4681.
FT-IR (ATR): ν_{max} 2932, 2865, 1753, 1699, 1578 cm^{-1}.

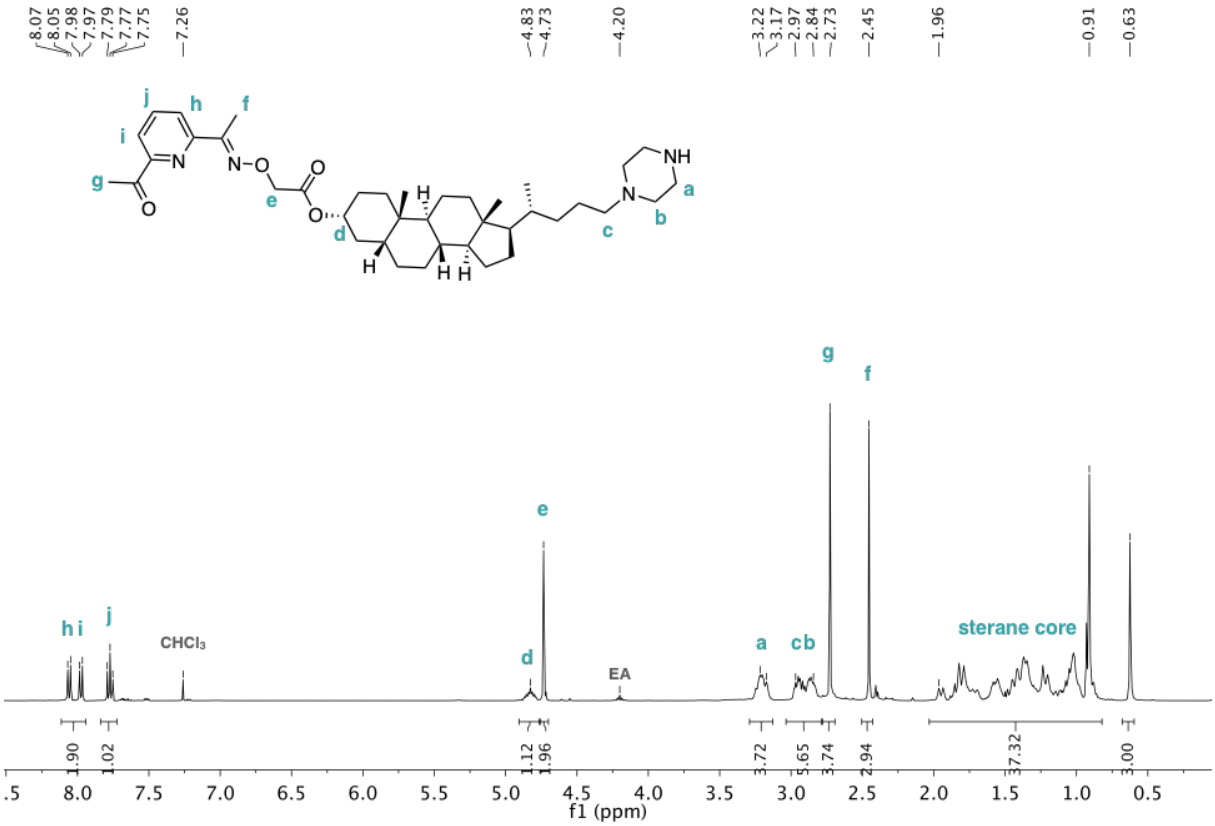

Figure S2.11 ^{1}H spectrum of compound **2-11** (deprotected).

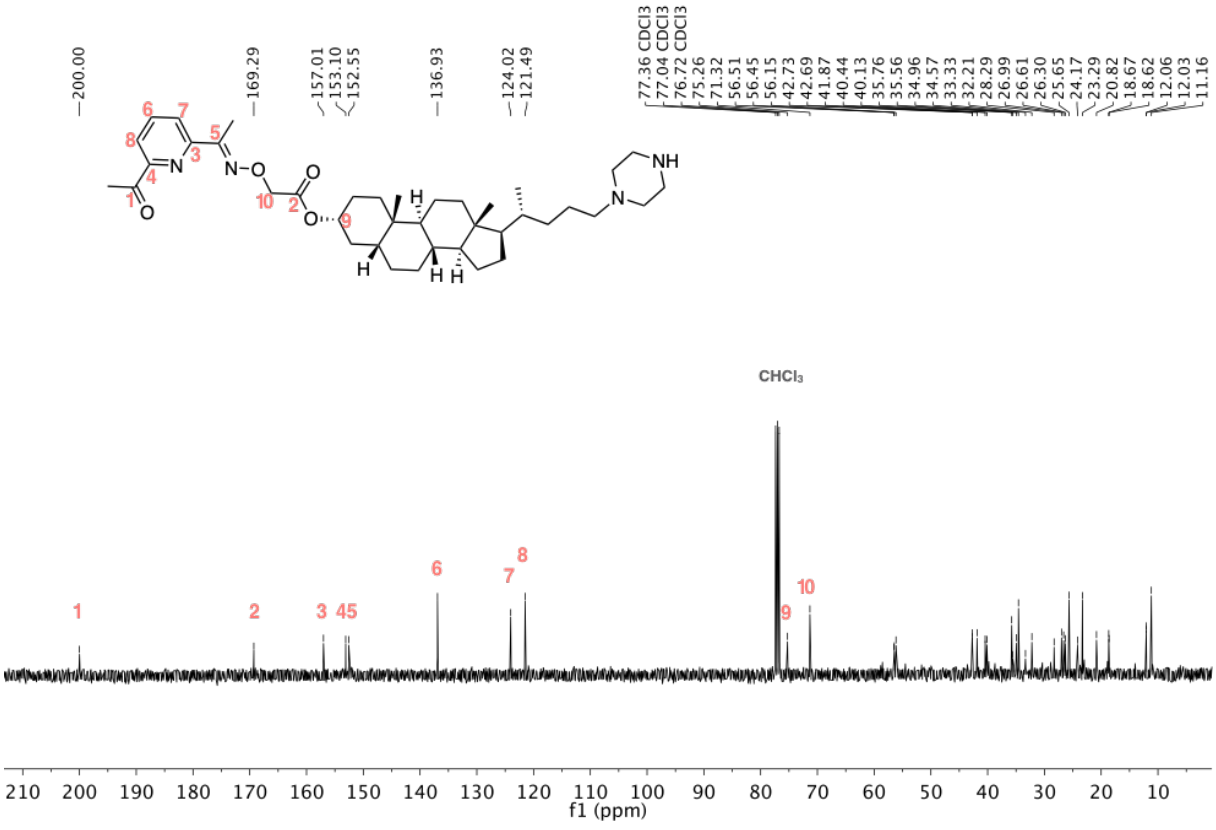

Figure S2.12 ^{13}C spectrum of compound **2-11** (deprotected).

Compound 12

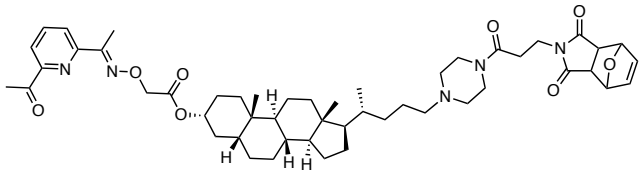

The solution of deprotected compound **2-11** (60 mg, 0.092 mmol), compound **2-7** (145 mg, 0.433 mmol) and triethylamine (0.038 mL, 0.277 mmol) in anhydrous dimethylformamide (10 mL) was stirred at r.t. for 24 h. The reaction mixture was diluted with ethyl acetate (25 mL), washed with lithium chloride (5%, aq., 5 x 10 mL), brine (10 mL) and dried over anhydrous sodium sulphate. After evaporation of solvent, the crude was purified by flash chromatography (silica, 0-10% gradient of methanol in dichloromethane) to afford the product as a white solid (35 mg, 44% yield).

^{1}H NMR (400 MHz, $CDCl_3$) δ (ppm): Two endo-exo isomers were found with a ratio of 8:2. 8.06 (d, *J* = 7.9 Hz, 1H), 7.98 (d, *J* = 7.9 Hz, 1H), 7.78 (t, *J* = 7.9 Hz, 1H), 6.50 (s, 1.6H), 6.38 (s, 0.4H), 5.29 (s, 0.4H), 5.26 (s, 1.6H), 4.91-4.78 (m, 1H), 4.74 (s, 2H), 3.80 (t, *J* = 7.9 Hz, 1.6H), 3.61-3.44 (m, 4.8H), 2.84 (s, 1.6H), 2.73 (s, 3H), 2.59 (t, *J* = 7.9 Hz, 1.6H), 2.46-2.31 (m, 9.4H), 1.97-0.91 (m, 40H), 0.63 (s, 3H).
^{13}C NMR (100 MHz, $CDCl_3$) δ (ppm): 200.17, 176.14/174.83, 169.44, 168.15, 157.16, 153.24, 152.69, 137.06, 136.66/134.53, 124.17, 121.63, 81.04, 75.42, 71.46, 59.10, 56.65, 56.27, 47.57, 42.82, 42.02, 40.59, 40.28, 35.90, 35.74, 35.35, 35.11, 34.71, 32.35, 30.73, 30.50, 29.82, 28.43, 27.14, 26.75, 26.45, 25.79, 24.32, 23.44, 22.81, 22.75, 20.96, 18.82, 12.16, 11.30.
HR-MS (ES+): calcd. for $C_{50}H_{70}N_5O_8$: 868.3236, found: 868.5224.
FT-IR (ATR): ν_{max} 2931, 2865, 1752, 1608, 1641, 1578 cm^{-1}.

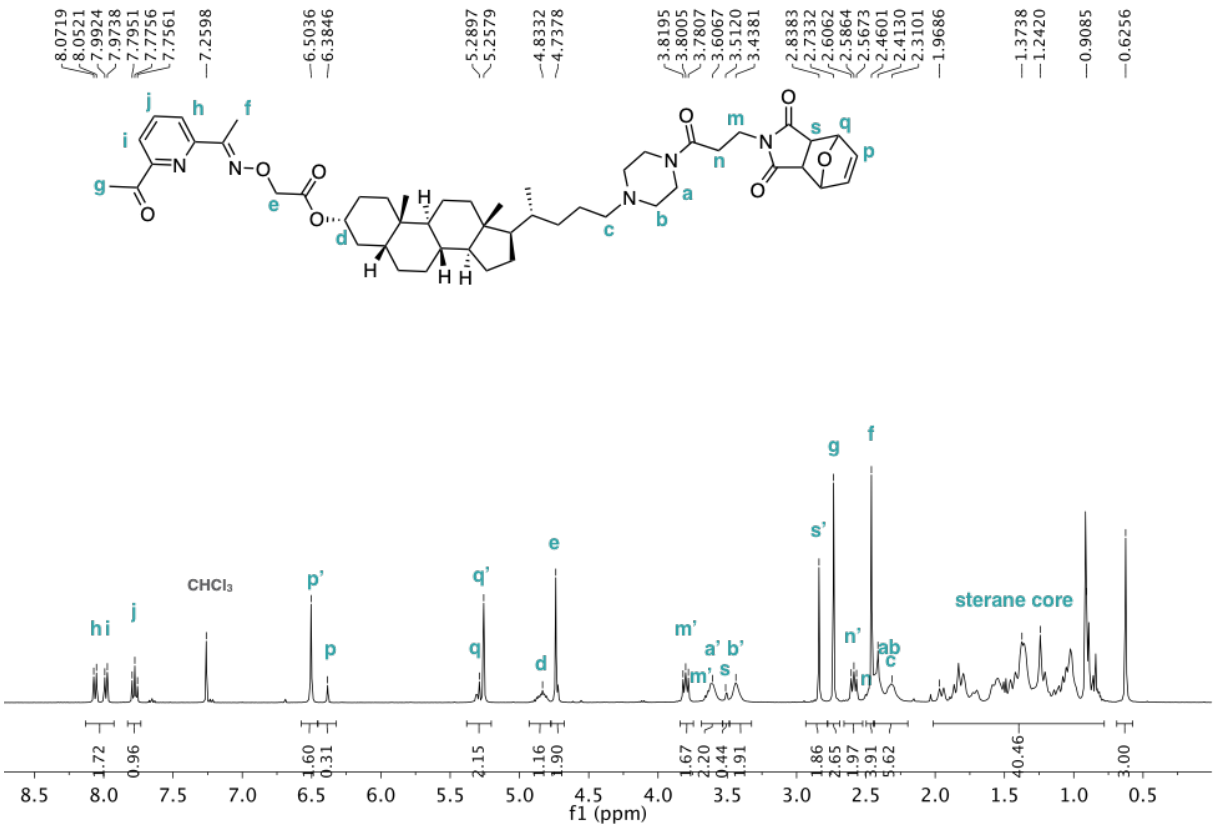

Figure S2.13 [1]H spectrum of compound **2-12**.

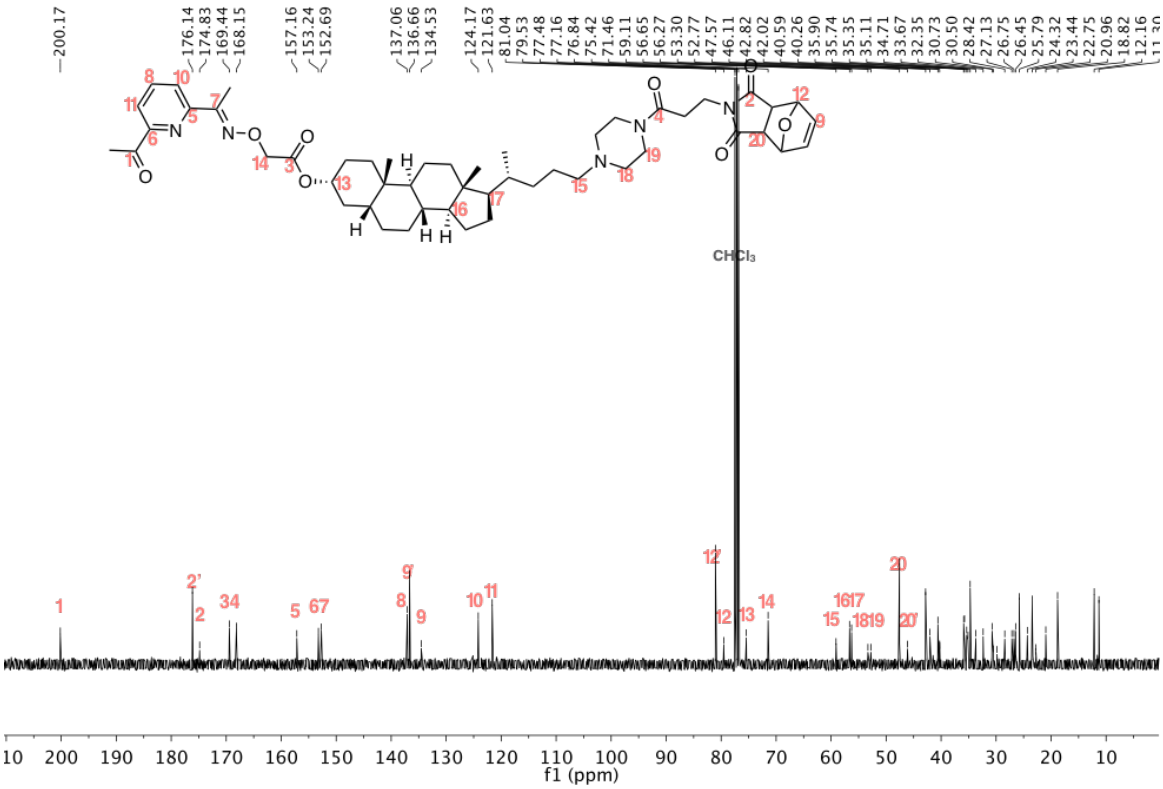

Figure S2.14 [13]C spectrum of compound **2-12**.

Compound 2-13

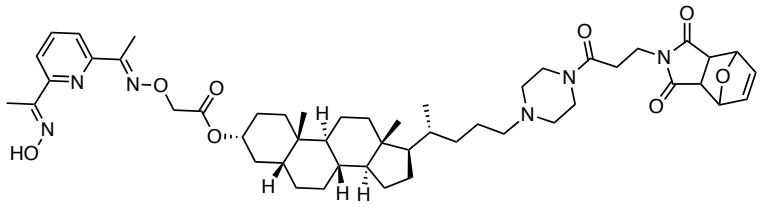

To a solution of compound **2-12** (17.5 mg, 0.0346 mmol) in chloroform/ethanol (1:1, 5 mL) was added a solution of hydroxylamine hydrochloride (2.8 mg, 0.0692 mmol) and sodium acetate (1.4 mg, 0.0346 mmol) in water (0.5 mL). The reaction mixture was sealed and stirred at 60 °C under microwave radiation for 5 h. After dilution with chloroform (30 mL), the mixture washed with water (2 x 10 mL), brine (10 mL) and dried over anhydrous sodium sulphate. The crude was purified by flash chromatography (neutral alumina, 0-20% gradient of methanol in dichloromethane) to afford the product as a white solid (12 mg, 67% yield).

^{1}H NMR (400 MHz, $CDCl_3$) δ (ppm): Endo-exo isomers + *Z-E* isomers. 8.01-7.77 (m, 2H), 7.68-7.52 (m, 1H), 6.50/6.39 (2s, 2H), 5.32/5.26 (2s, 2H), 4.74-4.73 (m, 3H), 3.83-3.52 (m, 7H), 2.84 (s, 2H), 2.62-2.35 (m, 13H), 1.83-0.63 (m, 46H), 0.57 (s, 3H).
^{13}C NMR (100 MHz, $CDCl_3$) δ (ppm): 176.17, 170.10, 168.26, 157.81, 152.64, 136.68, 136.34, 120.06, 119.89, 81.06, 77.48, 75.31, 71.36, 56.36, 47.60, 42.86, 42.63, 41.76, 40.43, 40.07, 35.92, 35.78, 35.33, 35.00, 34.90, 34.73, 34.60, 32.12, 30.74, 28.20, 27.15, 27.11, 27.07, 26.45, 26.31, 24.29, 23.44, 20.83, 19.64, 18.99, 18.79, 12.12, 11.30, 10.22.
MS (ES-): calcd. for $C_{50}H_{69}N_6O_8$: 882.1, found: 882.2.
FT-IR (ATR): ν_{max} 3460, 2933, 2866, 1754, 1708, 1641, 1573 cm^{-1}.

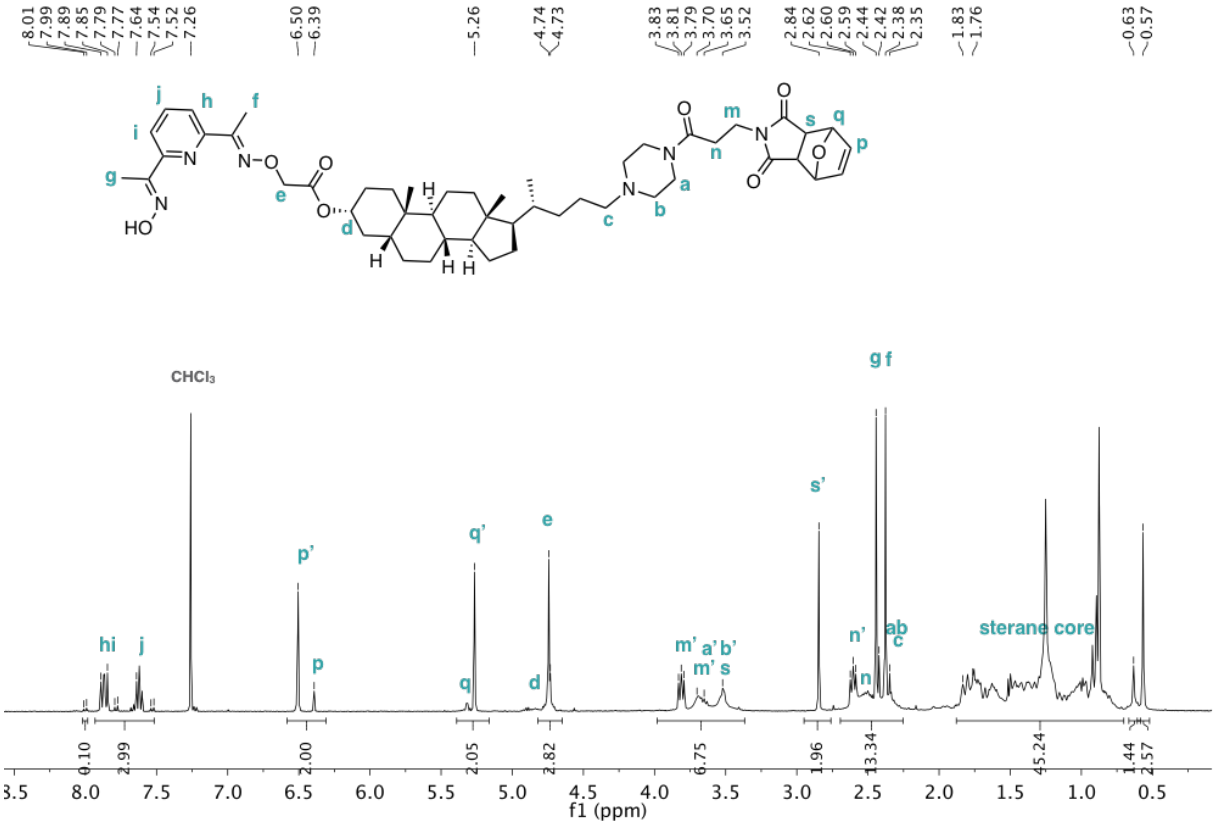

Figure S2.15 ^{1}H spectrum of compound **2-13**.

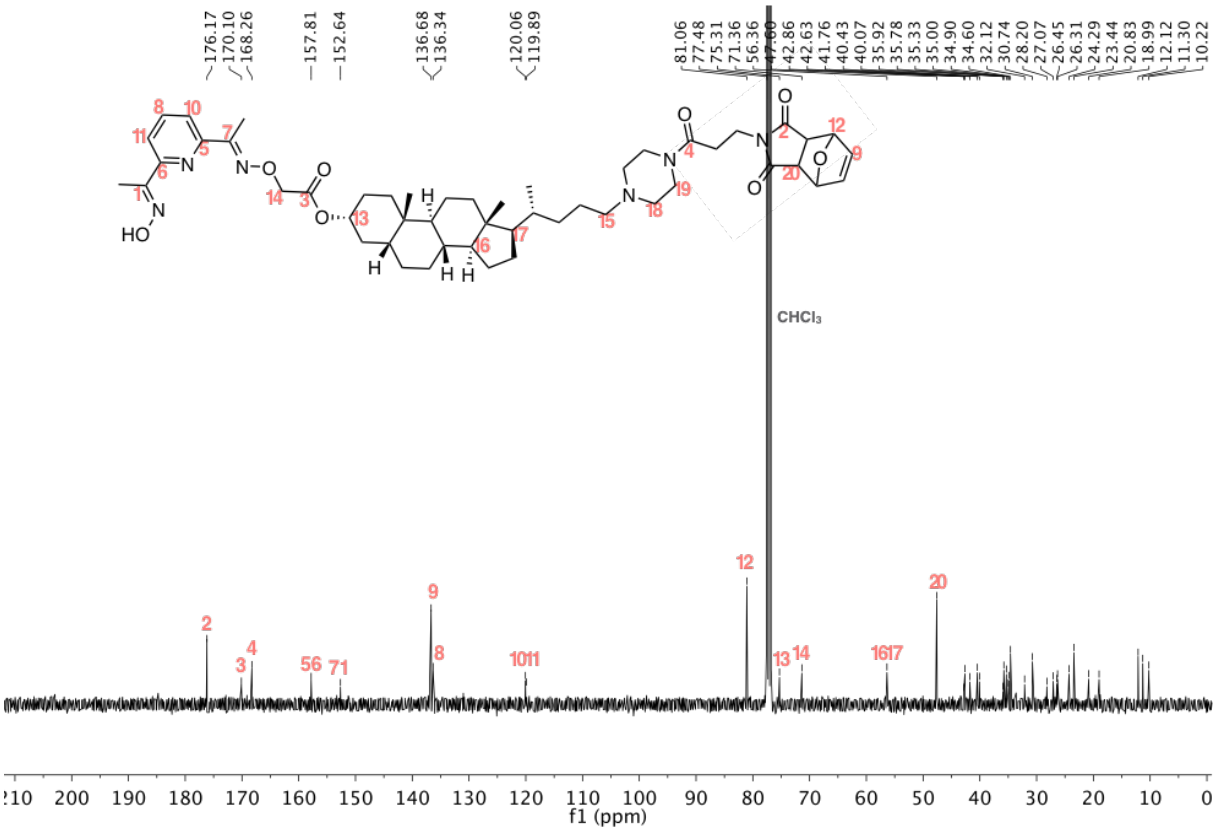

Figure S2.16 ^{13}C spectrum of compound **2-13**.

Compound 2-1

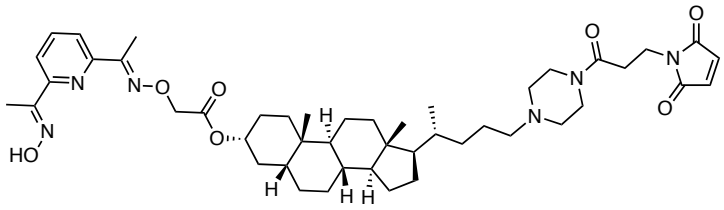

Compound **2-13** (12 mg, 0.136 mmol) was heated at 95 °C *in vacuo* for 10 h. The residue was purified by RF-HPLC (XBridge® BEH C8 2.5 µm Column, solvent A: water + 0.1% formic acid; solvent B: acetonitrile +0.1% formic acid; 47.5% isocratic gradient of solvent B in solvent A, retention time: 2 min) to afford the product as a white solid (0.73 mg, 6 % yield).

^{1}H NMR (400 MHz, $CDCl_3$) δ (ppm): *Z*-*E* isomers. 7.97-7.85 (m, 2H), 7.72-7.61 (m, 1H), 6.71 (s, 2H), 4.84-4.74 (m, 3H), 3.85-3.54 (m, 6H), 2.92-2.55 (m, 7H), 2.44 (s, 3H), 2.38 (s, 3H), 2.04-0.63 (m, 41H), 0.58 (s, 3H).
^{13}C NMR (100 MHz, $CDCl_3$) δ (ppm): 170.67, 170.10, 168.32, 157.82, 157.35, 153.94, 152.68, 136.35, 134.42, 122.22, 120.09, 75.30, 71.37, 56.63, 56.38, 53.57, 42.65, 41.76, 40.44, 40.08, 35.92, 35.78, 35.70, 35.02, 34.91, 34.60, 34.20, 33.45, 32.12, 31.56, 28.21, 27.06, 26.77, 26.32, 24.29, 23.44, 20.83, 18.76, 12.19, 12.12, 11.30, 10.23.
HR-MS (ES+): calcd. for $C_{46}H_{67}N_6O_7$: 815.5066, found: 815.5047.
FT-IR (ATR): ν_{max} 3461, 2934, 2865, 1754, 1708, 1640, 1571 cm^{-1}.

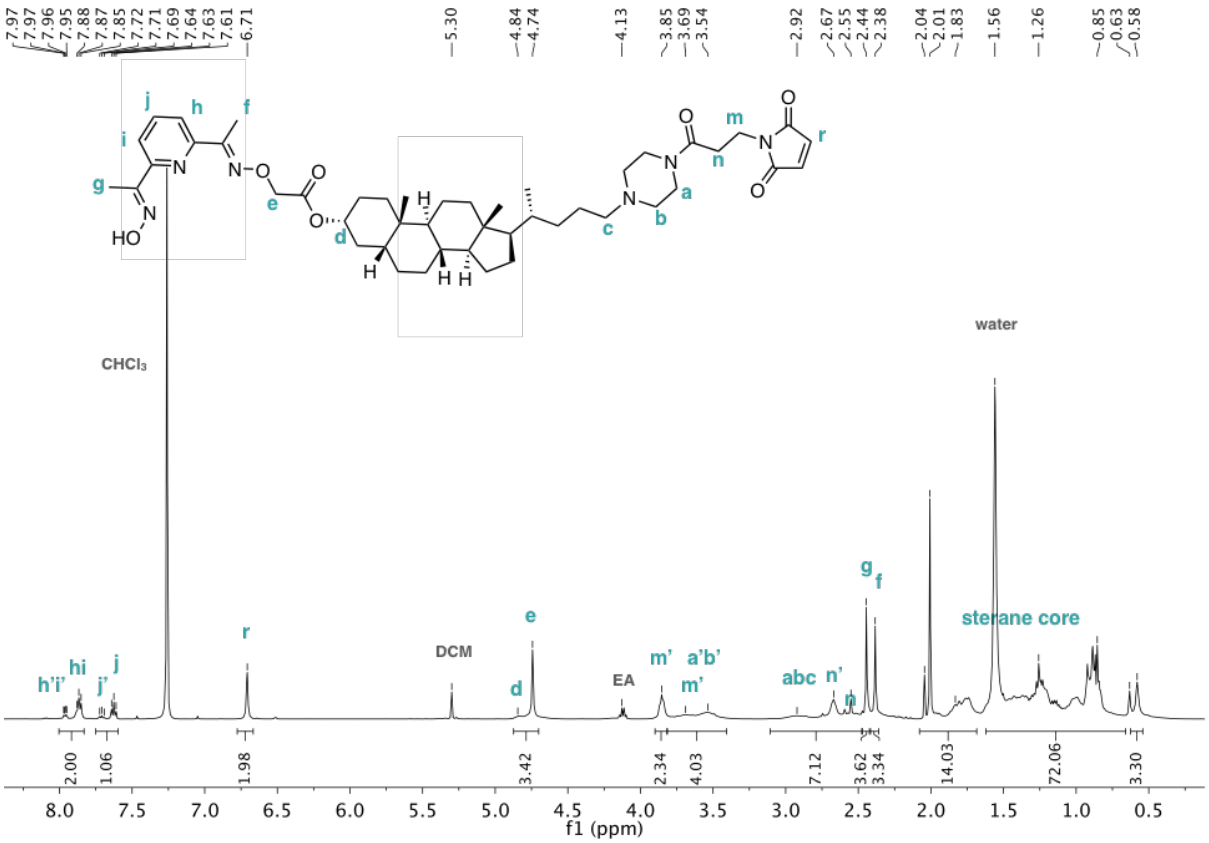

Figure S2.17 ^{1}H spectrum of compound **2-1**.

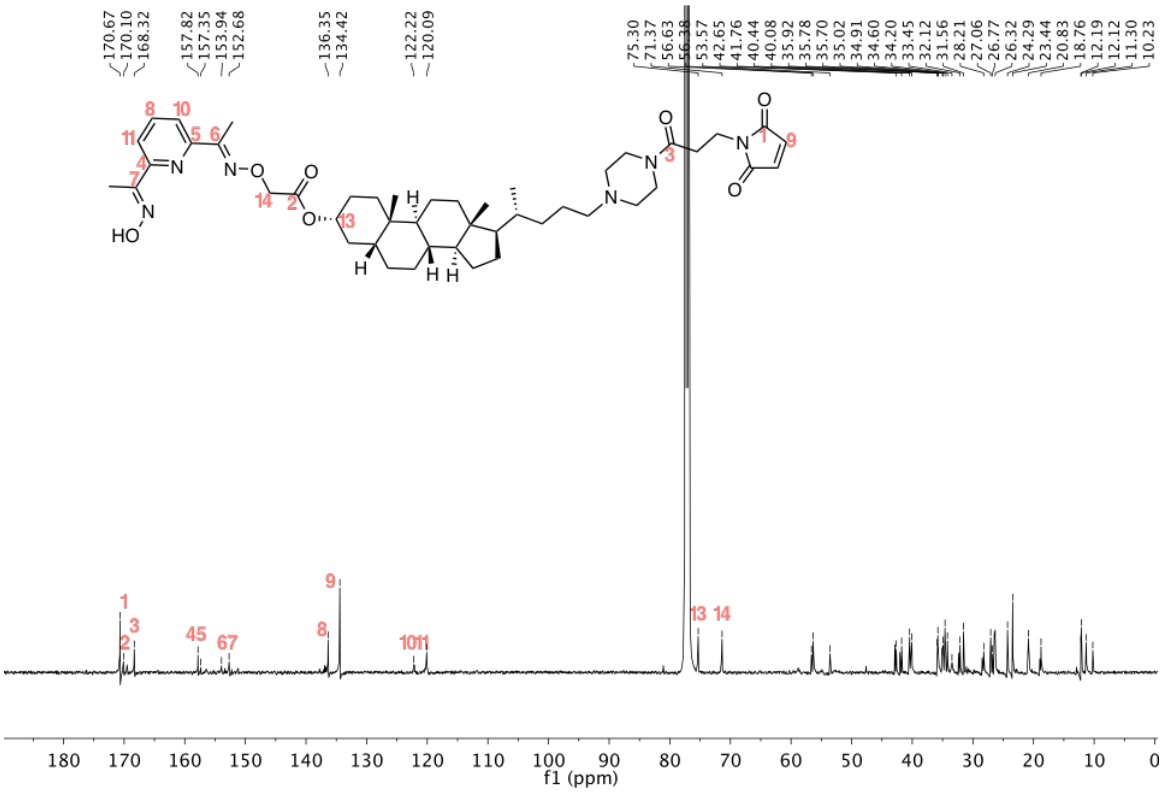

Figure 2-18 ^{13}C spectrum of compound **2-1**.

2.4.2 Vesicle Experiments

General Protocol for Vesicle Preparation

To a 1.5 mL microcentrifuge tube was added a chloroform solution of lipids (DOPC/DOPE in a 3:2 ratio) in order to obtain a final lipid concentration of 1 mM in 3.5 mL (final elution volume). The solvent was evaporated using a dry nitrogen stream and dried under high vacuum for at least 2 h to yield a thin lipid film. To the microcentrifuge containing the lipids was added 25 mM HEPES 150 mM NaCl buffer (0.5 mL) at pH 7, as well as stock solutions of ester substrate and zinc chloride as appropriate to reach final concentrations of 250 µM. After swelling for 1 min, the suspension was subjected to 5 cycles of freeze-thaw using liquid nitrogen and 35 °C water bath. The suspension was extruded for 19 times through a 200 nm polycarbonate filter in an extruder apparatus, and then the vesicles were separated by a bulk solution using prepacked SEC columns eluting with the same HEPES buffer at pH 7.

Fluorescence Measurements

Fluorescence excitation experiments were recorded using the following parameters: emission wavelength = 510 nm, excitation range 380–480 nm, recorded at 2-minute intervals. At the end of the experiment, 5% Triton X-100 (50 µL) and 1 M NaOH (50 µL) was added to lyse the vesicles and hydrolyze all of the remaining substrates. The emission measured at this end point was used to normalise the data taking into account of the dilution factor.

Safety-Catch (Figure 2.2)

OFF state red data (1): To a 1 mL fluorescence cuvette was added 1 mM vesicle suspensions with 1 mol% loading of maleimide transducer **2-1** (800 µL); **ON state red data (2)**: An aliquot of 1 mM NaOH was added to the above OFF state vesicle suspensions to raise the external pH to 10 at *t* = 40 min; **OFF state grey data (3)**: To a 1 mL fluorescence cuvette was added 1 mM vesicle suspensions without loading of maleimide transducer **2-1** (800 µL); **OFF state grey data (4)**: An aliquot of 1 mM NaOH was added to the above OFF state vesicle suspensions (3) to raise the external pH to 10 at *t* = 40 min;

***In-Situ* Thiol Conjugation (Figure 2.5)**

OFF state grey data: To a 1 mL fluorescence cuvette was added 1 mM vesicle suspensions without loading of maleimide transducer **2-1** (800 µL). An aliquot of 1 mM NaOH was added to the vesicle suspensions to raise the external pH to 10 at *t* = 40 min; **ON state red data**: To

a 1 mL fluorescence cuvette was added 1 mM vesicle suspensions with 1 mol% loading of maleimide transducer **2-1** (800 µL). An aliquot of 1 mM NaOH was added to the vesicle suspensions to raise the external pH to 10 at *t* = 40 min; **OFF state green data**: To a 1 mL fluorescence cuvette was added 1 mM vesicle suspensions with 1 mol% loading of maleimide transducer **2-1** (800 µL). 10^3 eq. of 2-mercaptoethanesulfonic acid (relative to **2-1**) was added externally and the vesicle suspension was incubated at r.t. for 2 h before the start of the fluorescence measurement. An aliquot of 1 mM NaOH was added to the vesicle suspensions to raise the external pH to 10 at *t* = 40 min; **OFF state yellow data**: To a 1 mL fluorescence cuvette was added 1 mM vesicle suspensions with 1 mol% loading of maleimide transducer **2-1** (800 µL). 10^3 eq. of 2-mercaptoethanesulfonic acid (relative to **2-1** in green data) was added externally and the vesicle suspension was incubated at r.t. for 2 h before the start of the fluorescence measurement. An aliquot of 1 mM NaOH was added to the vesicle suspensions to raise the external pH to 10 at *t* = 40 min

People face trade-offs, and the cost of something is what you give up to get it.
Gregory Mankiw

3

Carboxylic Acid Transducer

3.1 Introduction

Development of effective therapy for malignant tumours is one of the biggest challenges in research as well as in the clinic. One major difference between many solid tumours and the surrounding normal tissue is the acidic extracellular pH (range from 5.7 to 7.8), because of high concentration of acidic metabolites such as lactic acid.[1] Moreover, changes in pH are also encountered in the process of endocytosis where pH can drop as low as 6.0-6.5 in early endosomes and 4.5-5.5 in late endosomes and lysosomes, as shown in Figure 3.1.[2] Therefore, this acidic external vesicle pH can be exploited as a drug-release trigger. Recent therapeutic approaches have been designed to target the tumour pH through low-pH activation of drug release from micelles and nanoparticles.[3]

We have recently developed a novel transmembrane signalling mechanism by controlling the movement of a synthetic transducer across a vesicle lipid bilayer.[4,5] The external recognition head group of the transducer becomes membrane-permeable in response to an external chemical stimulus, which leads to membrane translocation, exposing a catalytic head group to the interior of the vesicle. Catalytic hydrolysis of an internal substrate generates an amplified output signal, which can also be used to trigger the release of the vesicle contents[6], see Figure 3.2. In this case, one of the products generated by substrate hydrolysis is a surfactant, which disrupts the membrane and enhances the permeability of the lipid bilayers to polar solutes; The cargo encapsulated in the vesicles are subsequently released through the disordered membranes.

We therefore designed a carboxylic acid transducer using this translocation mechanism in an attempt to trigger drug release from artificial vesicles.

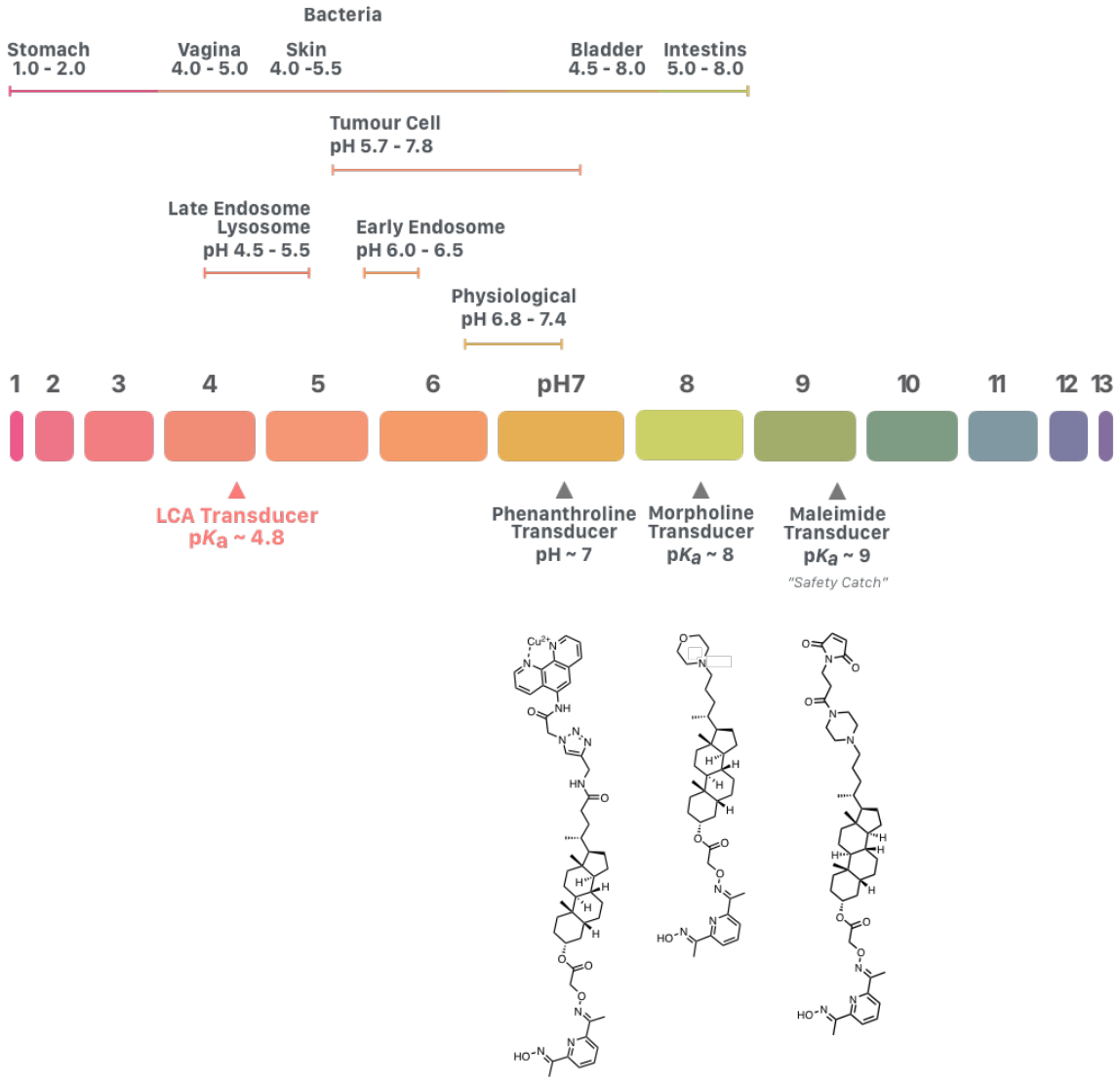

Figure 3.1 Various biological pH values and the pK_a value of the head groups of synthetic transducers.

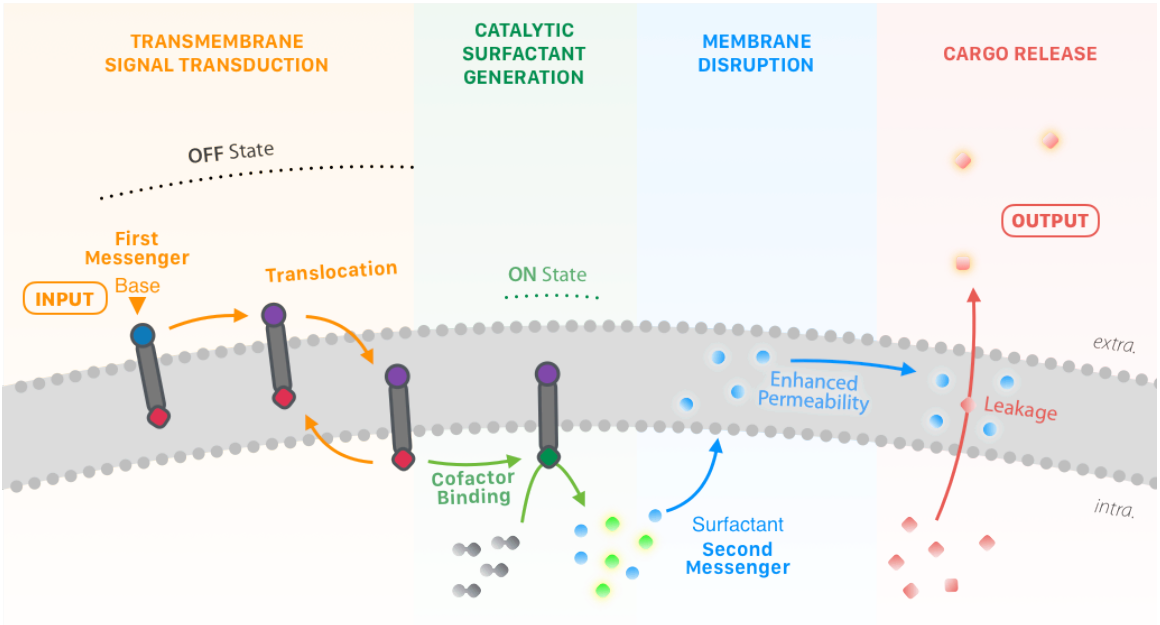

Figure 3.2 Triggered cargo release from vesicles using an artificial signal transduction mechanism. Transmembrane signal transduction: the input signal switches the external head group (blue) of a synthetic signal transducer from polar to apolar (purple), allowing the translocation of the transducer across the membrane. Catalytic surfactant generation: charged co-factor binding to the inner (catalytic) head group (red) activates the catalyst (green), leading to hydrolysis of a substrate (grey) into a surfactant (blue) and fluorophore (green). Membrane disruption: The surfactant disrupts the membrane and enhances the permeability of the lipid bilayers to polar solutes; Cargo release: cargo (pink) encapsulated in the vesicles are released through disordered lipid bilayers and an output is generated.

The designed chemical structure of carboxylic acid transducer **3-1** and the corresponding signalling experiments for anti-tumour drug release is illustrated in Figure 3.2. Transducer **3-1** consists of a polarity switchable carboxylic acid group with pK_a value of 4.8 (in aqueous solution) and a steroid core spacer which links to a pyridine-oxime pro-catalyst. Vesicles contain substrate **3-3**, and water-soluble anti-tumour drug, for example doxorubicin (DXR)[7]. In the initial pH neutral state, carboxylic acid transducer is embedded on the outside leaflet of the lipid bilayer as the carboxylic acid group is deprotonated. Concurrence of acidic microenvironments in tumour tissue protonates the transducer, which gives a neutral carboxylic acid group and allows the transducer to translocate the membrane and turn on the hydrolysis reaction of substrate **3-2** inside the vesicles. The surfactant **3-4** subsequently dissolves into the lipid bilayer and increases the membrane permeability to the polar contents. Drugs encapsulated in the vesicles are released through the disordered membrane and are preferably administrated into the nearby tumour cells.

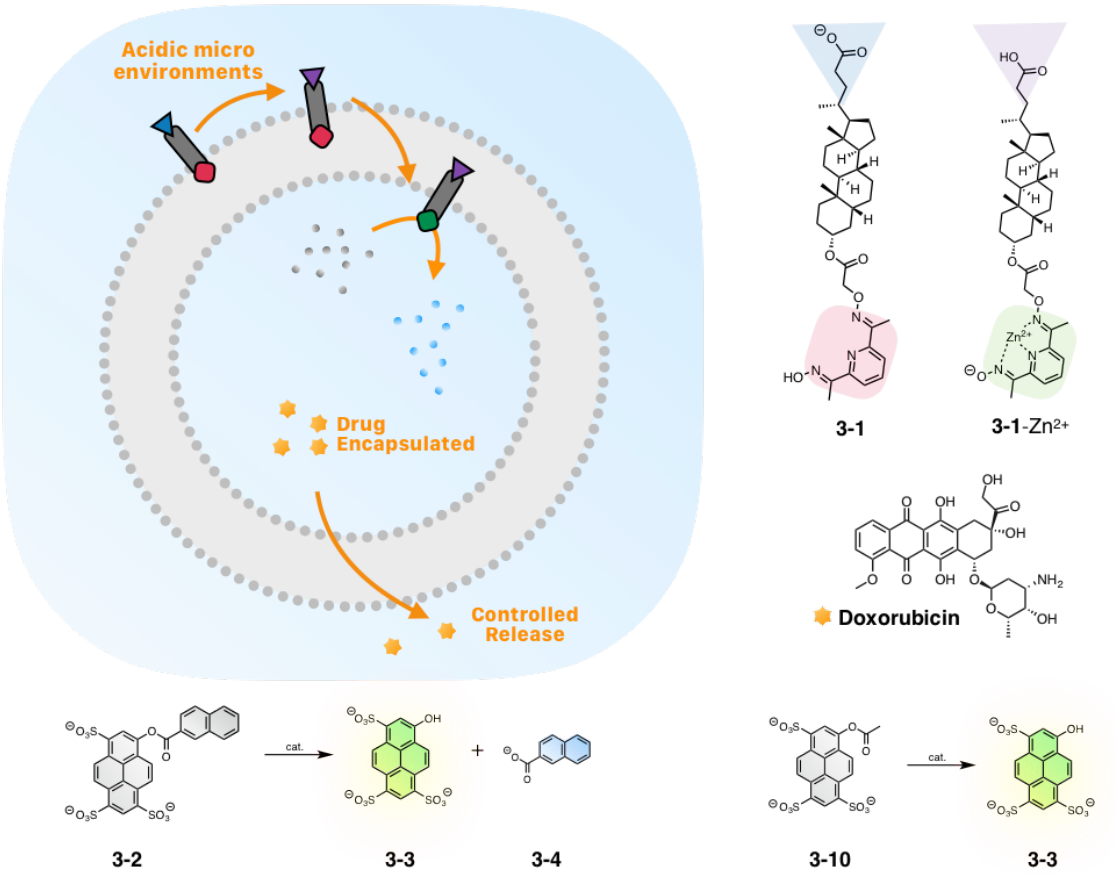

Figure 3.3 A designed controlled release of anti-tumour drug triggered by transmembrane signal transduction using carboxylic acid transducer. Vesicles are loaded with water-soluble anti-tumour drug, zinc ions and a hydrolysable substrate. At physiological pH, the carboxylic acid group of carboxylic acid transducer **3-1** is deprotonated (blue) and stays in the outside leaflet of the vesicle membrane. Concurrence of acidic microenvironments in tumour tissue protonates the transducer, and the neutral carboxylic acid group (purple) allows the transducer to translocate the membrane. Binding of zinc ions to the inner catalytic head group (red) activates the catalyst (green), turning on surfactant generation by catalysing the hydrolysis of the substrate (grey) into a surfactant (light blue). The surfactant subsequently dissolves into the lipid bilayer and increase the membrane permeability to polar solutes. Drugs encapsulated in the vesicles are released through the disordered membrane and target the nearby tumour cells.

3.2 Results and Discussions

3.2.1 Synthesis of Carboxylic Acid Transducer

Carboxylic acid transducer **3-1** was synthesised in five steps from lithocholic acid, see Scheme 3.1. Condensation of chloroacetyl chloride gave **3-5**. Esterification of carboxylic acid group with tert-butyl alcohol gave **3-6**. Functionalisation with pyridine mono-oxime **3-7** gave **3-8**. TFA deprotection of tert-butyl group gave transducer **3-9**. Condensation of hydroxylamine gave transducer **3-1**. Substrates **3-2** and **3-10** are previously reported.

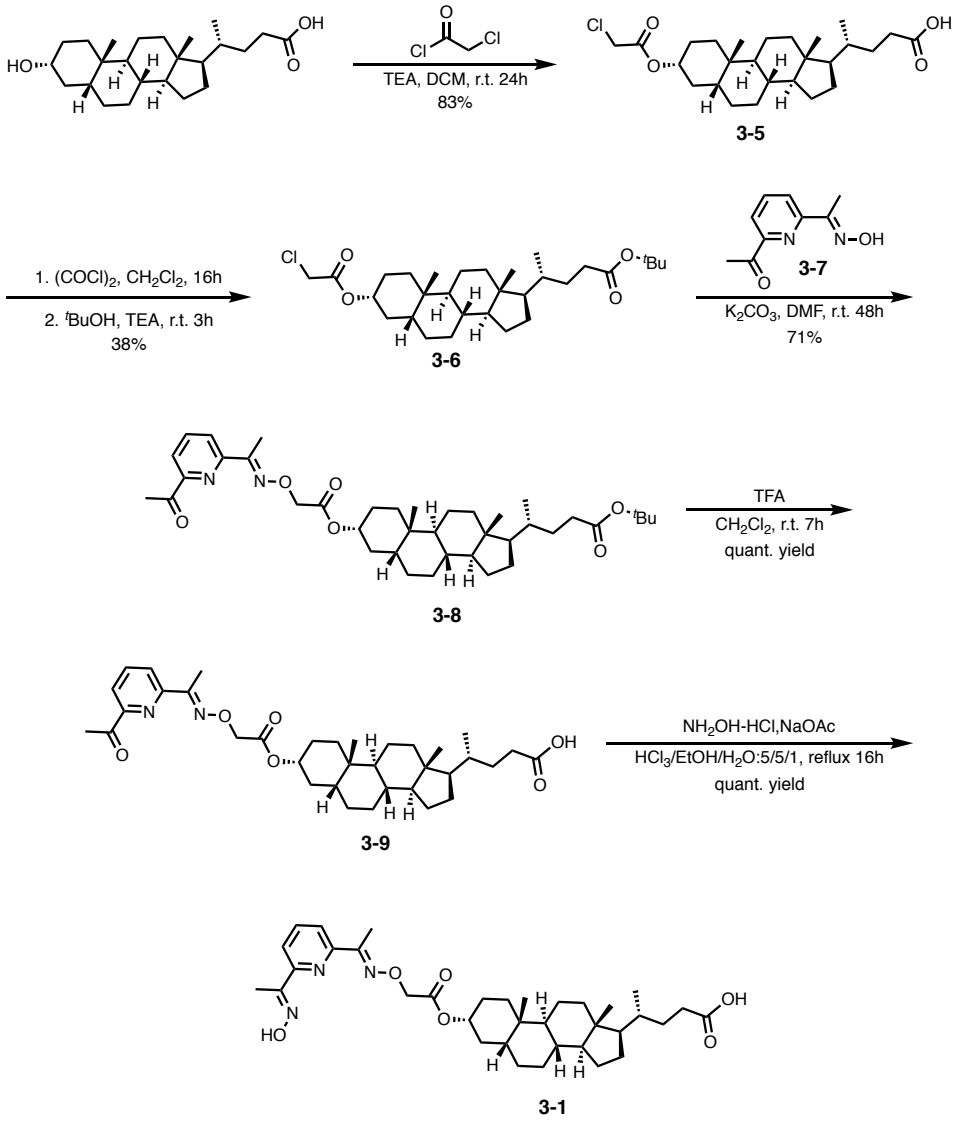

Scheme 3.1 Synthesis of carboxylic acid transducer **3-1**.

3.2.2 Signalling Experiments

DOPC/DOPE vesicles (molar ratio: 3/2) with 5 mol% loading of the carboxylic acid transducer **3-1** were assembled at neutral pH with encapsulation of 250 µM substrate **3-10** and 250 µM zinc chloride in HEPES buffer saline. At pH 7 and the carboxylic acid group should be deprotonated and membrane-impermeable. An external acid pulse with addition of hydrochloric acid should protonate the carboxylate anion and initiate the translocation. However, no turn ON was observed after the acid pulse, see Figure 3.4.

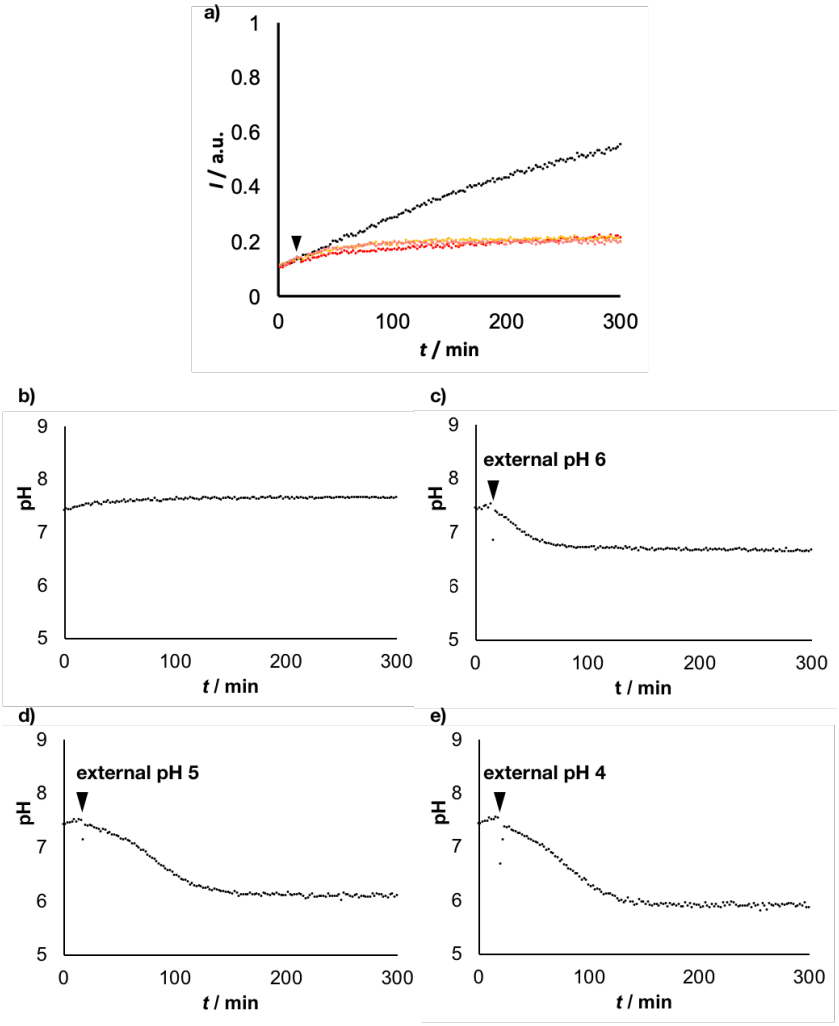

Figure 3.4 Attempted signalling experiments (HEPES buffer). Time dependence of the normalized fluorescence emission intensity at 510 nm (exciting at 415 nm). Experiments were conducted in 200 nm DOPC/DOPE vesicles (molar ratio: 3/2, 2 mM lipid concentration) with 5 mol% loading of carboxylic acid transducer **3-1** containing 250 µM substrates **3-10**, 250 µM zinc chloride, and 250 mM HEPES buffer 150 mM NaCl at pH 7. Black data: background hydrolysis of substrate **3-10** in vesicles at pH 7. Yellow/pink/red data: external addition of HCl at t = 20 min (indicated by an arrow) to reach pH 6, 5, and 4, respectively. b), c), d) and e): Time dependence of internal vesicle pH, calculated from fluorescence emission intensity at 510 nm (exciting at 405 nm and 460 nm). External addition of HCl at *t* = 20 min to reach pH 6, 5, and 4, respectively.

Previously, Dr Flore Keymeulen discovered that, at pH 5, the catalytic hydrolysis rate of pyridine-oxime catalytic head group for substrate **3-10** in water is approximately 500 times slower than the hydrolysis rate at pH 7 (unpublished results). This indicates that the effectiveness of the catalytic head group is pH-dependent. The product HPTS is a pH indicator. The HPTS fluorescence emission ratio at 510 nm between excitation at 405 and 460 nm can be used for calculating the internal vesicle pH.[4] After the acid pulse, the internal vesicle pH dropped to pH 6.5 when external vesicle pH was 5 (Figure 3.4d), and it dropped to pH 5.5 when external vesicle pH was 4 (Figure 3.4e). Therefore, even when the transducer is in the ON state, i.e. the transducer has translocated across the lipid bilayer and bound to zinc(II) at the inner surface of the membrane, the significantly slow rate of hydrolysis makes the system OFF. The lipid used in these experiments was a mixture of DOPC/DOPE in 3:2 molar ratio which failed to maintain the internal vesicles pH at pH 7.

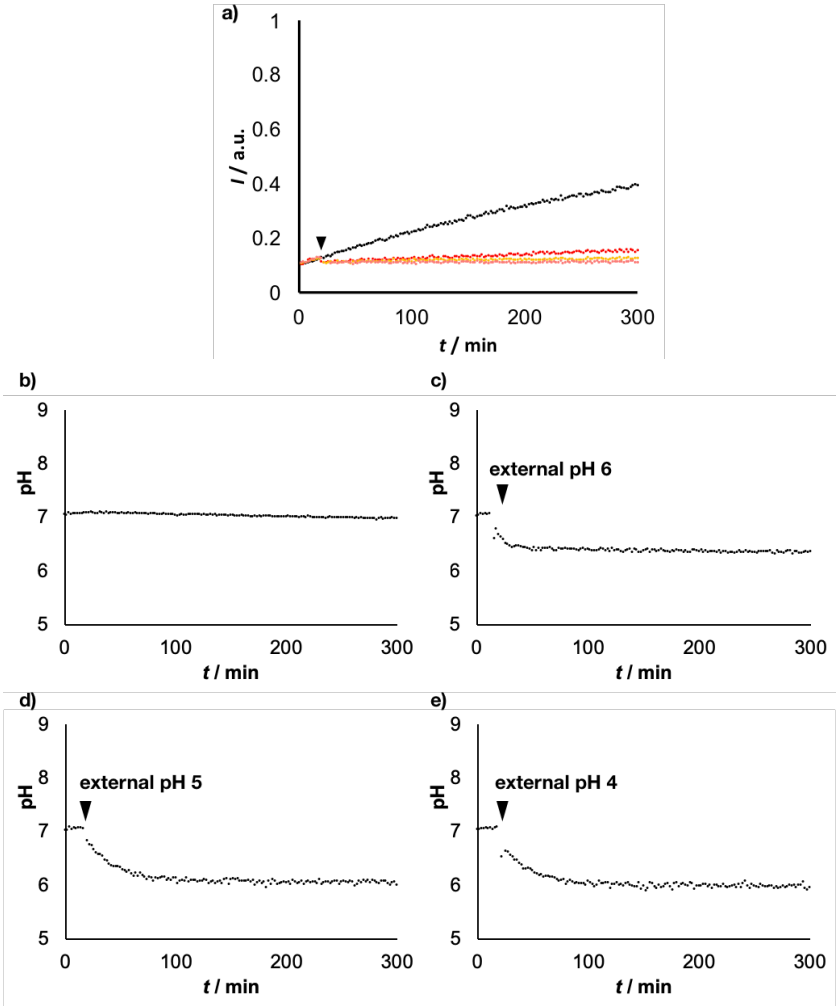

Figure 3.5 Attempted signalling experiments (MES buffer). Time dependence of the normalized fluorescence emission intensity at 510 nm (exciting at 415 nm). Experiments were conducted in 200 nm DOPC/DOPE vesicles (molar ratio: 3/2, 2 mM lipid concentration) with 5 mol% loading of carboxylic acid transducer **3-1** containing 250 μM substrate **3-10**, 250 μM zinc chloride, and 250 mM MES buffer 150 mM NaCl at pH 7.

Black data: background hydrolysis. Yellow/Magenta/Red data: external addition of HCl to reach pH 6, 5, and 4, respectively. b), c), d) and e): Time dependence of internal vesicle pH, calculated from fluorescence emission intensity at 510 nm (exciting at 405 nm and 460 nm). External addition of HCl at *t* = 20 min to reach pH 6, 5, and 4, respectively.

We then made several attempts to improve the maintenance of pH gradient across the membrane by changing buffer, raising buffer concentration to increase buffering capacity, and altering lipid composition. For example, MES has p*K*a value of 6.15 at 20 °C compared to p*K*a 7.5 of HEPES. Thus the useful pH buffering range of MES buffer more suitable than HEPES in acidic environments. Figure 3.5 shows a vesicle experiment with 5 mol% loading of the carboxylic acid transducer using MES buffer. The external vesicle pH decreased to pH 6, 5, and 4 after the acid pulse. However, the internal vesicle pH dropped rapidly to pH 6 or less.

Several pH gradient assays were conducted to test how different lipid compositions maintain the pH gradient. We assembled vesicles with different lipids encapsulating 250 uM HPTS in the buffer and followed the internal vesicle pH change after the acid pulse. For example, Figure 3.6 - 3.8 show pH gradient assays of vesicles with lipid composition of DOPC/cholesterol:2/1, POPC (100%), and DOPC/DOPE/cholesterol: 50/34/16, respectively. Unfortunately, none of these systems was able to maintain a stable pH gradient for the duration of the signalling experiments when external vesicle pH is at pH 4 (p*K*a of the carboxylic acid group is ~4.7). Potentially, the carboxylic acid transducer could act as a proton carrier to shuffle the proton from one side to another via a flip-flop mechanism, as observed for lipid translocation in the lipid bilayer membrane.[8]

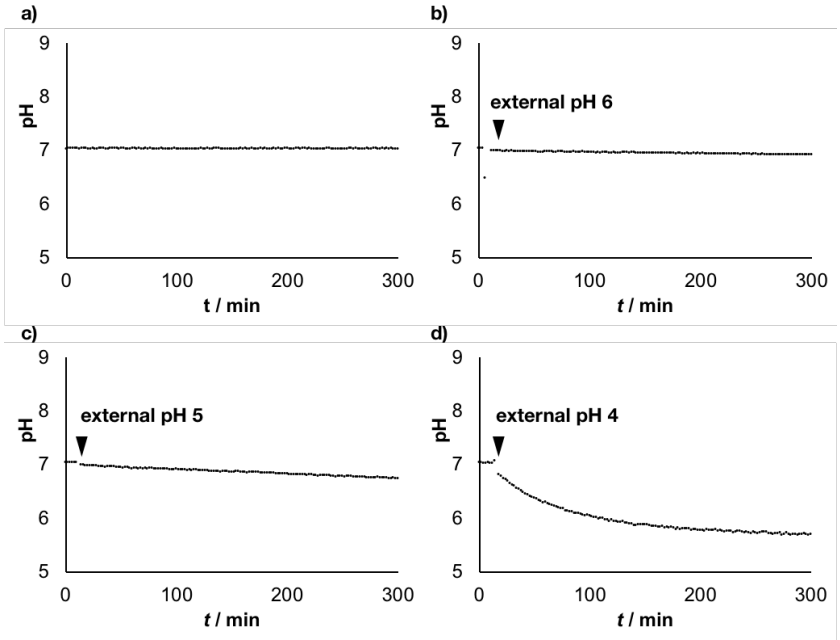

Figure 3.6 pH gradient test (lipid composition: DOPC/cholesterol). Time dependence of internal vesicle pH calculated from fluorescence emission intensity at 510 nm (exciting at 405 nm and 460 nm). Experiments were conducted in 200 nm DOPC/cholesterol vesicles (molar ratio: 2/1, 1 mM lipid concentration) containing

250 μM HPTS, 250 μM zinc chloride, and 250 mM HEPES buffer 150 mM NaCl at pH 7. a) without external addition of HCl. b), c), and d) external addition of HCl at *t* = 20 min to reach pH 6, 5, and 4, respectively.

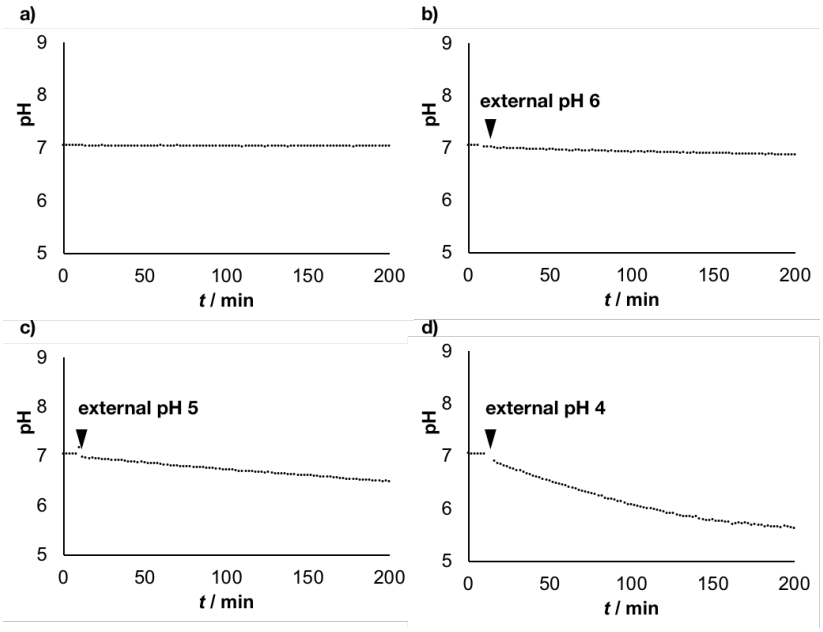

Figure 3.7 pH gradient test (lipid composition: DOPC). Time dependence of internal vesicle pH calculated from fluorescence emission intensity at 510 nm (exciting at 405 nm and 460 nm). Experiments were conducted in 200 nm DOPC vesicles (1 mM lipid concentration) containing 250 μM HPTS, 250 μM zinc chloride, and 250 mM HEPES buffer 150 mM NaCl at pH 7. a) without external addition of HCl. b), c), and d) external addition of HCl at t = 20 min to reach pH 6, 5, and 4, respectively.

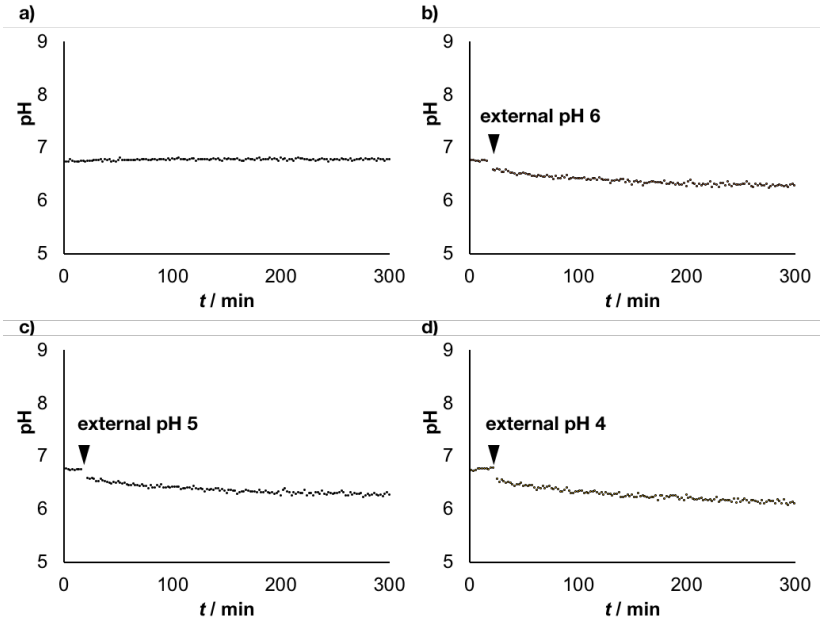

Figure 3.8 pH gradient test (lipid composition: DOPC/DOPE/cholesterol). Time dependence of internal vesicle pH calculated from fluorescence emission intensity at 510 nm (exciting at 405 nm and 460 nm).

Experiments were conducted in 200 nm DOPC/DOPE/cholesterol vesicles (50/34/16, 1 mM lipid concentration) containing 250 μM HPTS, 250 μM zinc chloride, and 250 mM HEPES buffer 150 mM NaCl at pH 7. a) without external addition of HCl. b), c), and d) external addition of HCl at t = 20 min to reach pH 6, 5, and 4, respectively.

3.2.3 *In-situ* EDC coupling at membrane surface

Whereas pH gradient is challenging to maintain as well as the catalytic head group is very much less effective in acidic pH environment, we proposed a signalling system using *in-situ* carbodiimide coupling chemistry at membrane surface to avoid the change of pH as a trigger for translocation, see Figure 3.10. The carboxylic acid transducer at neutral pH is deprotonated and exposes the carboxylate ion at the membrane surface. EDC is a water-soluble carbodiimide and works by activating carboxylic group for amide formation with primary amine. N-hydroxysuccinimide (NHS) can be included in the EDC coupling protocols to improve the coupling efficiency. The resulting *O*-acrylisourea and sulfo-NHS ester are both charged and therefore membrane-impermeable, maintaining the transducer at the outer surface of the membrane. These intermediates are relatively unstable but highly reactive. Addition of a membrane-permeable primary amine would yield a stable amide conjugate that is overall neutral, initiating the membrane translocation and generate the ON state.

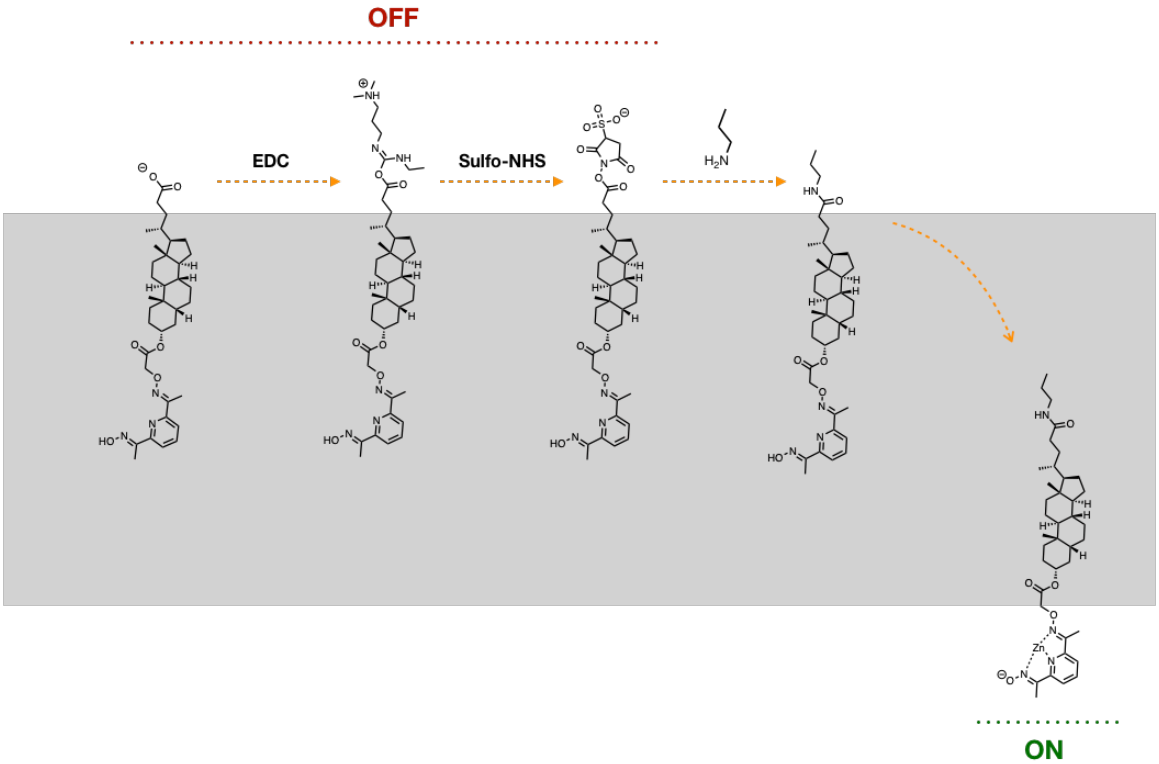

Figure 3.9 Proposed *in-situ* EDC coupling of carboxylic acid transducer **3-1** with a membrane-permeable amine. The carboxylic acid transducer is deprotonated in neutral pH. *In-situ* reaction with EDC and sulfo-NHS should generate a membrane-impermeable activated intermediate. Further reaction with a membrane-soluble amine should lead to formation of a neutral amide bond, initiating the translocation of the transducer.

For the attempted signalling experiments, we assembled POPC vesicles with 5 mol% loading of carboxylic acid transducer **3-1** in HEPES buffer saline. An excess amount of EDC/NHS was added externally followed by addition of propylamine, and the fluorescent emission of the product HPTS in the vesicles was measured, see Figure 3.10. Two control experiments were conducted at the same time: 1) vesicles with external addition of EDC/NHS, and 2) vesicles with external addition of propylamine. These experiments were designed to rule out any effects that EDC/NHS or propylamine may cause on the hydrolysis of substrate **3-10**. Unfortunately, no sign of switching to ON state was achieved in this attempted signalling experiment. It is possible that carboxylic acid transducer is not fully exposed at the membrane surface so that the *in-situ* reaction did not occur or did not occur effectively as designed.

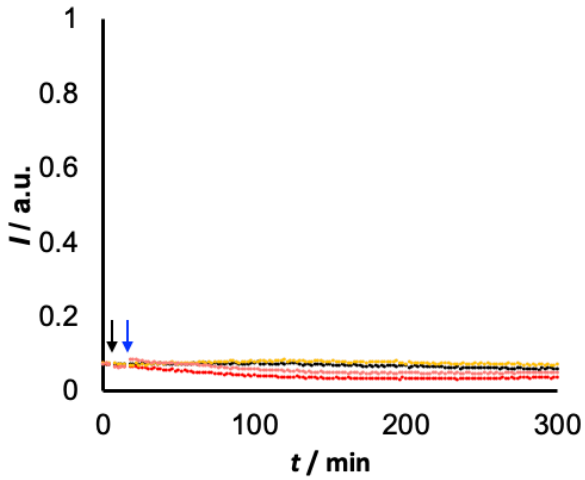

Figure 3.10 Attempted *in-situ* EDC coupling and signalling experiment. Time dependence of the normalized fluorescence emission intensity at 510 nm (exciting at 415 nm). Experiments were conducted in 200 nm POPC vesicles (1 mM lipid concentration) with 5 mol% loading of carboxylic acid transducer **3-1** containing 250 μM substrate **3-10**, 250 μM zinc chloride, and 250 mM MES buffer 150 mM NaCl at pH 7. Black data: background hydrolysis of substrate **3-10** in vesicles. Red data: external addition of 2 mM EDC/NHS (40 eq. relative to transducer **3-1**) at t = 5 min (indicated by the black arrow) and 2 mM propylamine (40 eq. relative to transducer **3-1**) at t = 15 min (indicated by the blue arrow). Yellow data: a control experiment with external addition of 2 mM EDC/NHS (40 eq. relative to transducer **3-1**) at t = 5 min. Pink data: a control experiment with external addition of 2 mM propylamine in DMSO (40 eq. relative to transducer **3-1**) at t = 15 min.

3.3 Conclusion

In this chapter, a transducer with a carboxylic acid head group was designed and synthesised in an attempt to conduct signal transduction across the membrane in acidic pH condition. As the pK_a of carboxylic group is approximately 4.7, external pH should decrease to 4 to protonate the majority of the transducers and enable the translocation. However, lowering extravesicular pH from neutral to pH 4 resulted in undesired rapid pH decrease inside the vesicles because 1) transducer could act as a proton transporter through a flip-flop mechanism, and 2) even the membrane without the loading of transducer could not maintain a stable pH gradient.

Unfortunately, catalytic hydrolysis of substrate **3-10** is significantly slowed down at pH <6, making the ON/OFF state of the system undistinguishable. Various lipids compositions and buffers solutions were examined to try to maintain a pH gradient across the membrane but with little success. We then changed the signalling design from a pH-responsive system to an amine-responsive one using an *in-situ* EDC/sulpho-NHS coupling chemistry. The highly active EDC/NHS intermediate should be charged and membrane-impermeable. Coupling with a membrane-soluble amine would form a stable amide bond and initiate the translocation of the transducer. However, the observed negative results suggest that carboxylic acid transducer might not be fully exposed to the internal aqueous solution, making the *in-situ* reaction difficult to occur at the membrane surface. We therefore stopped further investigation on this carboxylic acid transducer.

References

(1) Tannock, I. F.; Rotin, D. Acid PH in Tumors and Its Potential for Therapeutic Exploitation. *Cancer Res.* **1989**, *49* (16), 4373–4384.

(2) Sorkin, A.; Von Zastrow, M. Signal Transduction and Endocytosis: Close Encounters of Many Kinds. *Nat. Rev. Mol. Cell Biol.* **2002**, *3* (8), 600–614. https://doi.org/10.1038/nrm883.

(3) Mura, S.; Nicolas, J.; Couvreur, P. Stimuli-Responsive Nanocarriers for Drug Delivery. *Nat. Mater.* **2013**, *12* (11), 991–1003. https://doi.org/10.1038/nmat3776.

(4) Langton, M. J.; Keymeulen, F.; Ciaccia, M.; Williams, N. H.; Hunter, C. A. Controlled Membrane Translocation Provides a Mechanism for Signal Transduction and Amplification. *Nat. Chem.* **2017**, *9* (5), 426–430. https://doi.org/10.1038/nchem.2678.

(5) Langton, M. J.; Williams, N. H.; Hunter, C. A. Recognition-Controlled Membrane Translocation for Signal Transduction across Lipid Bilayers. *J. Am. Chem. Soc.* **2017**, *139* (18), 6461–6466. https://doi.org/10.1021/jacs.7b02345.

(6) Langton, M. J.; Scriven, L. M.; Williams, N. H.; Hunter, C. A. Triggered Release from Lipid Bilayer Vesicles by an Artificial Transmembrane Signal Transduction System. *J. Am. Chem. Soc.* **2017**, *139* (44), 15768–15773. https://doi.org/10.1021/jacs.7b07747.

(7) Tacar, O.; Sriamornsak, P.; Dass, C. R. Doxorubicin: An Update on Anticancer Molecular Action, Toxicity and Novel Drug Delivery Systems. *J. Pharm. Pharmacol.* **2013**, *65* (2), 157–170. https://doi.org/10.1111/j.2042-7158.2012.01567.x.

(8) Allhusen, J. S.; Conboy, J. C. The Ins and Outs of Lipid Flip-Flop. *Acc. Chem. Res.* **2017**, *50* (1), 58–65. https://doi.org/10.1021/acs.accounts.6b00435.

3.4 Supporting Information

3.4.1 Synthetic procedures and characterizations

Materials and methods

^{1}H NMR and ^{13}C NMR spectra were recorded on a 400-MHz Bruker® spectrometer. Chemical shifts are reported as δ values in ppm. Flash chromatography was carried out on an automated system (Combiflash® Rf+ Lumen™) using pre-packed cartridges of silica (25 µm PuriFlash® Column) or neutral alumina (50 µm RediSep® Rf Column). GPC purification of the vesicles was carried out using GE Healthcare PD-10 desalting columns prepacked with Sephadex® G-25 medium. Fluorescence spectra were recorded using a Cary Eclipse fluorescence spectrophotometer (Agilent Technologies) in Hellma® Analytics Suprasil® quartz cuvettes. Measurements of pH were conducted using a Mettler-Toledo SevenCompact™ pH meter equipped with an InLab® Micro electrode. Vesicles were assembled in Eppendorf® polypropylene Protein LoBind® polypropylene microcentrifuge tube and extruded as described below using Avanti® Polar Lipids extruder kits, equipped with Avestin® LiposoFast Liposome Factory 200 nm polycarbonate membranes with GE Healthcare Whatman® 10 mm polyester filter support. Solutions or vesicles suspensions were transferred using Eppendorf Multipette® Xstream Pippette with Combitips Advanced® or Hamilton Microliter™ syringes. All reagents and solvents were used without further purification. Chemicals were purchased from Sigma-Aldrich® and used without further purification.

Synthesis and Characterizations

Compound 3-2

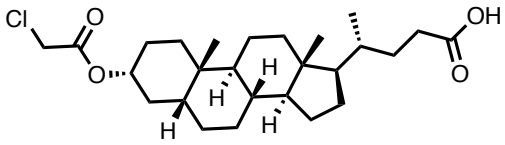

To a solution of lithocholic acid (1.0 g, 2.655 mmol) in tetrahydrofuran (20 mL) was added chloroacetyl chloride (0.6 g, 5.311 mmol) with external cooling. The reaction mixture was stirred over night at room temperature. After the reaction was quenched by methanol (2 mL) with external cooling, the solvent was removed in vacuo. The crude was purified by flash chromatography (silica, methanol in dichloromethane: 0 – 20%) to yield a white solid (1.05 g, 83%).

^{1}H NMR (400 MHz, CDCl3) δ (ppm): 4.81 (m, 1H), 4.03 (s, 2H), 2.42 – 2.22 (m, 2H), 1.98 – 0.91 (m, 32H), 0.65 (s, 3H).
^{13}C NMR (100 MHz, CDCl3) δ (ppm): 180.5, 167.0, 76.9, 56.7, 56.2, 43.0, 42.1, 41.4, 40.6, 40.3, 36.0, 35.5, 35.1, 34.8, 32.2, 31.2, 31.0, 28.4, 27.2, 26.7, 26.5, 24.4, 23.5, 21.1, 18.5, 12.3.
HR-MS (MS+): calcd. for $C_{26}H_{41}{}^{35}ClO_4$: 452.2693, found: 452.2690.
FT-IR (ATR): ν_{max} 2957, 2927, 2903, 2866, 2847, 1750, 1700 cm^{-1}.

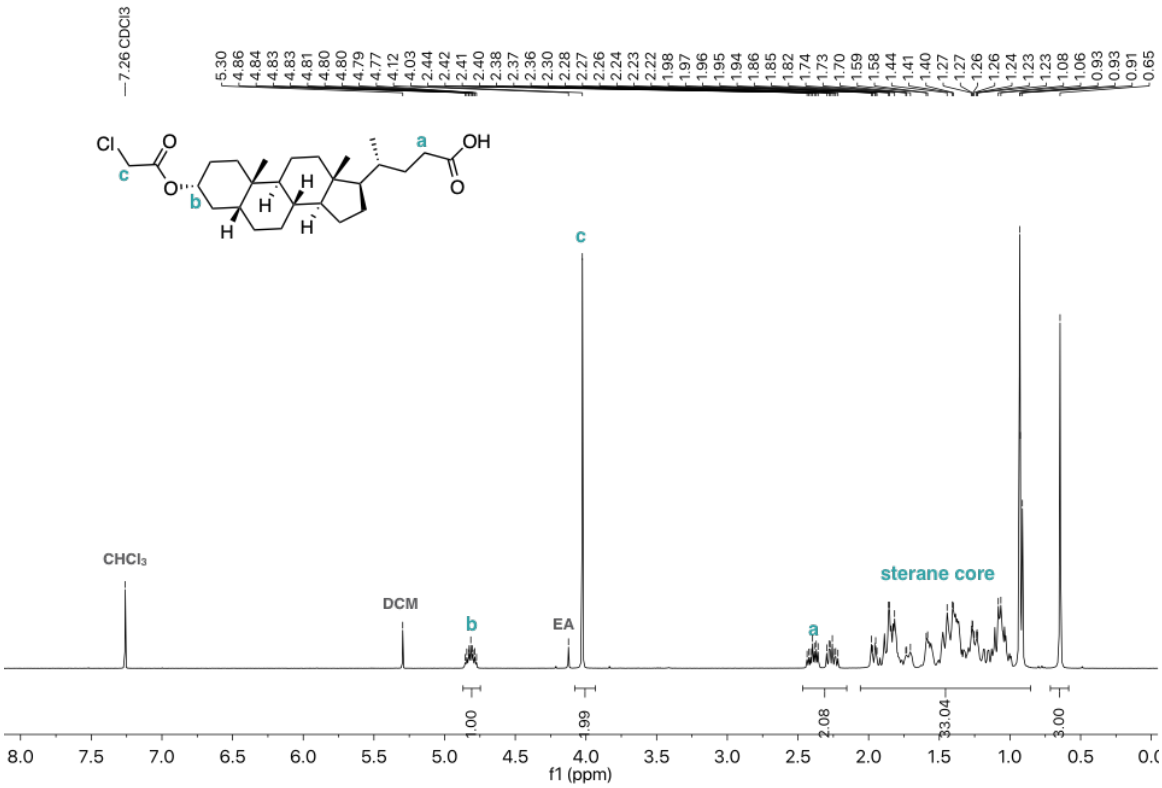

Figure S3.1 ^{1}H NMR spectrum of compound **3-2**.

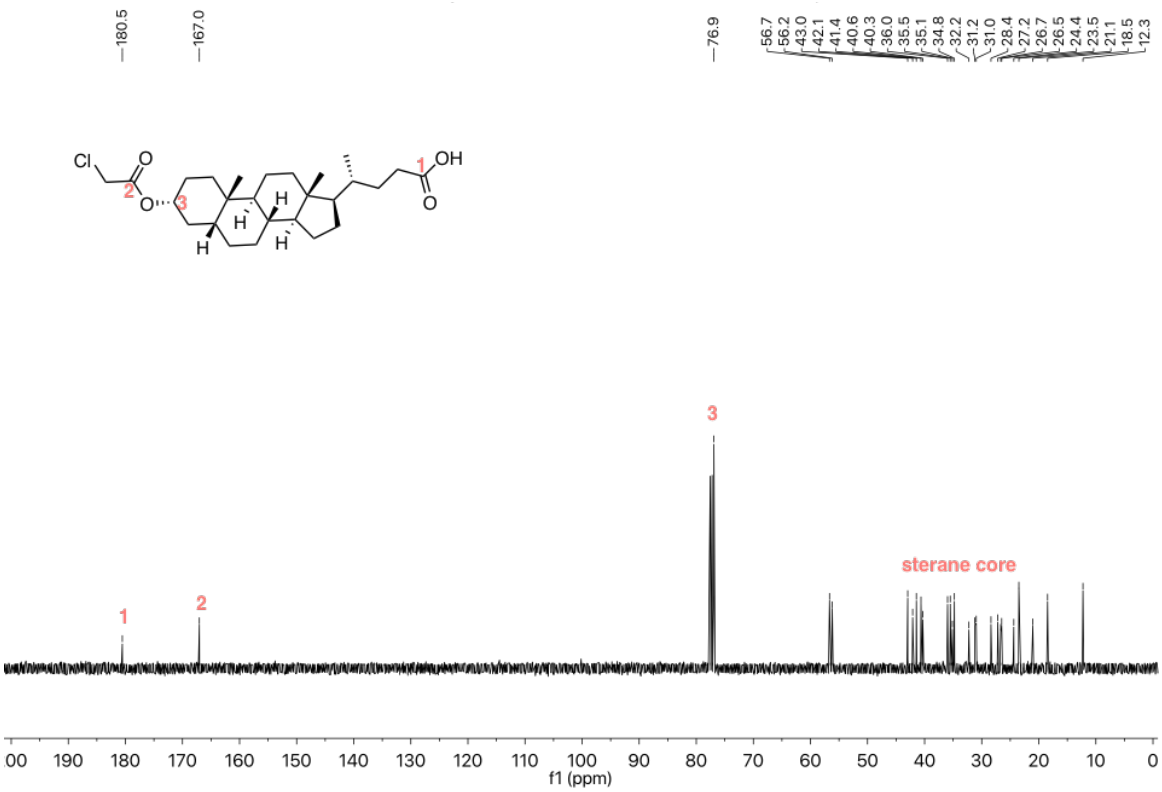

Figure S3.2 ^{13}C NMR spectrum of compound **3-2**.

Compound **3-3**

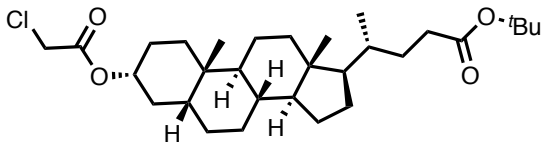

To an anhydrous solution of compound **3-2** (100 mg, 0.22 mmol) in dichloromethane (2 mL) was added one drop of dimethylformamide and oxalyl chloride (130 mg, 0.88 mmol) at 0 °C. The mixture was stirred at r.t. for 2 h. *Tert*-butyl alcohol (49 mg, 0.66 mmol) and triethylamine (66 mg, 0.66 mmol) were added and the reaction was stirred at r.t. overnight. The reaction mixture was diluted with dichloromethane, washed with hydrochloric acid (1 M), sodium bicarbonate (sat.), and brine, and the solvent was evaporated. The residue was purified by flash column chromatography (silica, petroleum ether/ethyl acetate:9/1, R_f = 0.5) to afford a white solid (43.1 mg, 38% yield).

^{1}H NMR (400 MHz, CDCl3) δ (ppm): 4.80 (m, 1H), 4.02 (s, 2H), 2.28-1.94 (m, 2H), 1.97 – 0.89 (m, 41H), 0.65 (s, 3H).

^{13}C NMR (100 MHz, CDCl3) δ (ppm): 173.5, 166.6, 79.7, 76.5, 56.3, 55.9, 42.5, 41.7, 41.0, 40.2, 39.9, 35.6, 35.1, 34.7, 34.4, 32.4, 31.8, 30.9, 28.0, 27.9, 26.8, 26.3, 26.1, 24.0, 23.1, 20.7, 18.1, 11.8.

HR-MS (ES+): calcd. for $C_{30}H_{49}ClO_4$: 508.3319, found: 508.3327.

FT-IR (ATR): ν_{max} 2973, 2956, 2925, 2866, 1750, 1724, 1468, 1449, 1421, 1407, 1372, 1317, 1230, 1193 cm^{-1}.

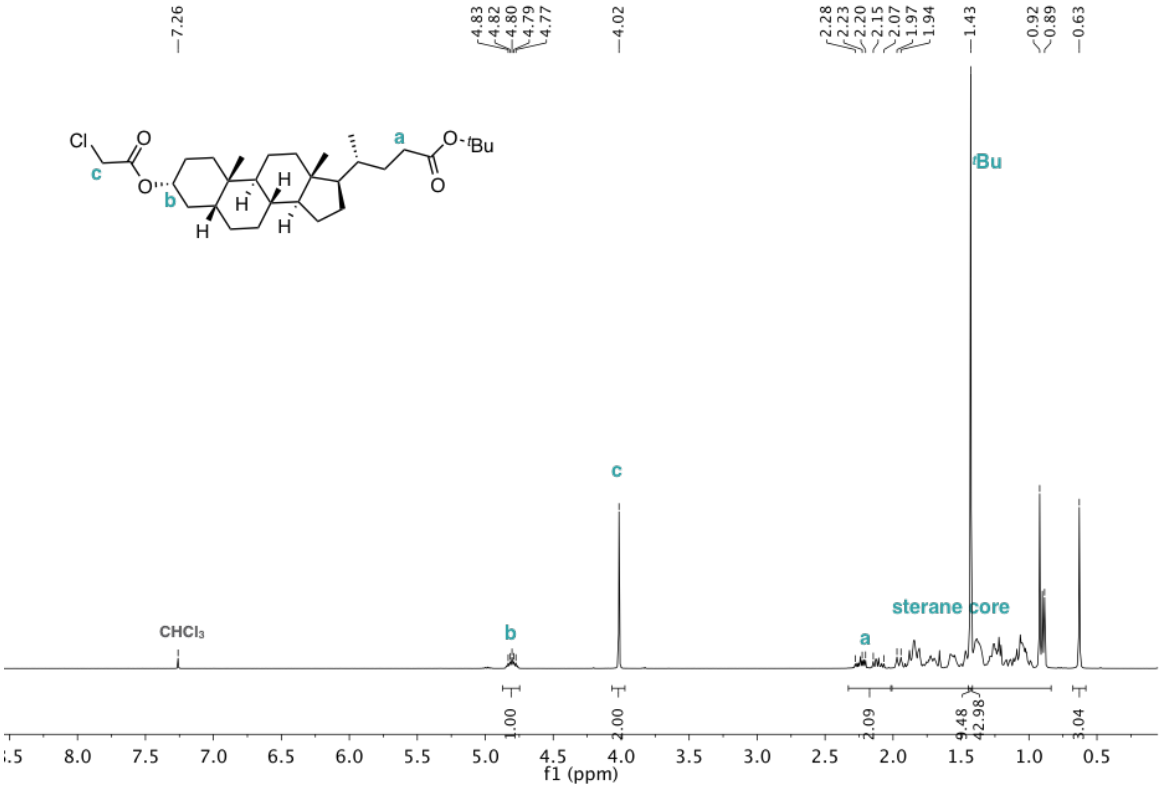

Figure S3.3 [1]H NMR spectrum of compound **3-3**.

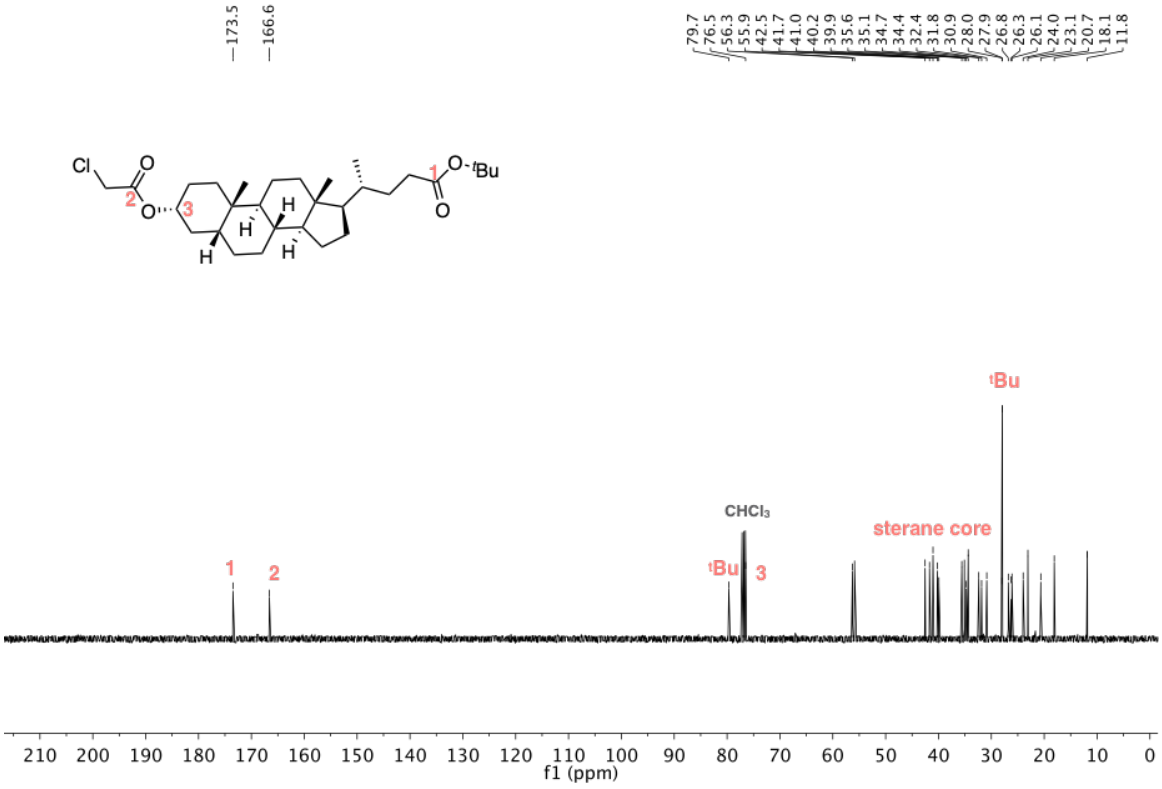

Figure S3.4 [13]C NMR spectrum of compound **3-3**.

Compound 3-5

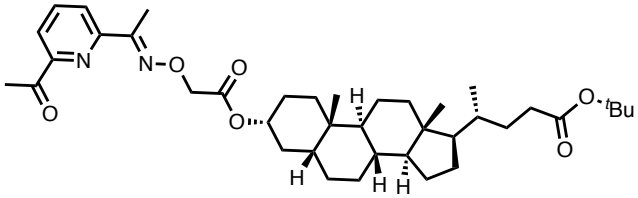

To a solution of compound **3-3** (40 mg, 0.079 mmol) in dimethylformamide (1 mL) was added potassium carbonate (54 mg, 0.393 mmol) and stirred for 15 min before a solution of compound **3-4** (42 mg, 0.236 mmol) in dimethylformamide (7 mL). The mixture was stirred at r.t. overnight. The reaction mixture was centrifuged, and the supernatant was diluted with ethyl acetate (25 mL), washed with lithium chloride (15% aq.) and brine, and the solvent was evaporated. The residue was purified by flash column chromatography (silica, petroleum ether/ethyl acetate:9/1) to afford a white solid (37 mg, 71% yield). Compound **3-4** co-eluted with the product. The product was used in the next step without further purification.

^{1}H NMR (400 MHz, CDCl3) δ (ppm): 7.98 (d, *J* = 7.8 Hz, 1H), 7.77 (t, *J* = 7.8 Hz, 1H), 4.89 – 4.76 (m, 1H), 4.74 (s, 2H), 2.78 (s, 1H), 2.73 (s, 3H), 2.46 (s, 3H), 2.34 – 2.07 (m, 2H), 1.94 – 0.91 (m, 45H), 0.62 (s, 3H).

^{13}C NMR (100 MHz, CDCl3) δ (ppm): 200.1, 173.8, 169.4, 157.1, 153.2, 152.7, 137.0, 124.2, 121.6, 80.0, 75.4, 71.4, 56.6, 56.2, 42.8, 42.0, 40.6, 40.3, 35.9, 35.4, 35.1, 34.7, 32.7, 32.3, 31.2, 28.2, 27.1, 26.7, 26.4, 25.8, 25.7, 24.3, 23.4, 21.0, 18.4, 12.2, 11.3.

HR-MS (ES+): calcd. for $C_{39}H_{58}N_2O_6$: 650.4295, found: 650.4296.

FT-IR (ATR): ν_{max} 2973, 2956, 2925, 2866, 1750, 1723, 1468, 1449, 1421, 1407, 1372, 1230, 1193 cm^{-1}.

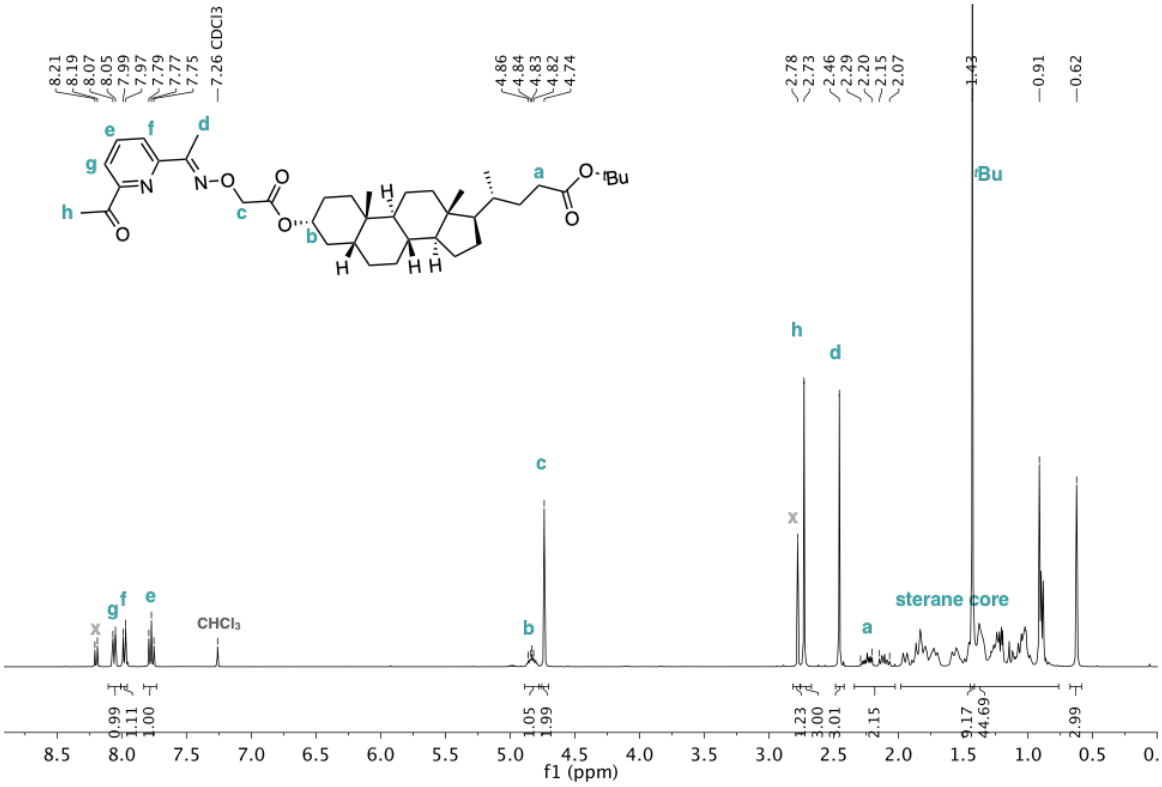

Figure S3.5 [1]H NMR spectrum of compound **3-5**.

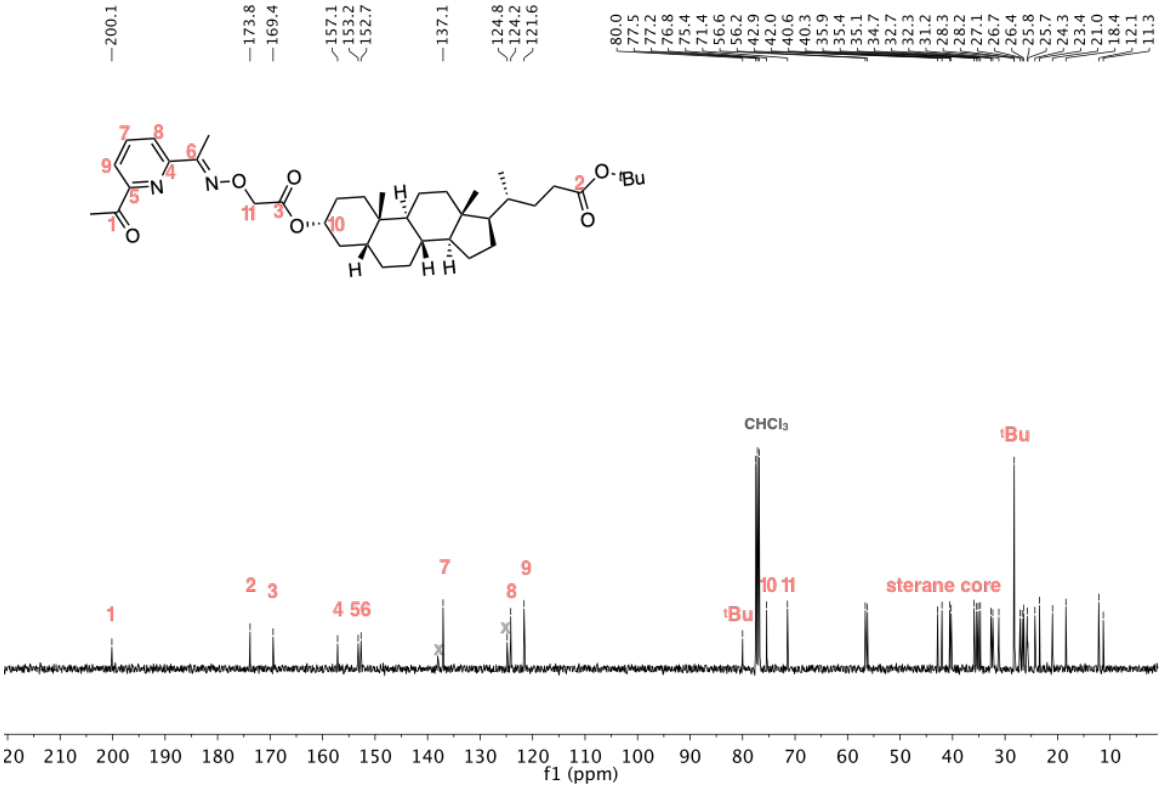

Figure S3.6 [13]C NMR spectrum of compound **3-5**.

Compound 3-6

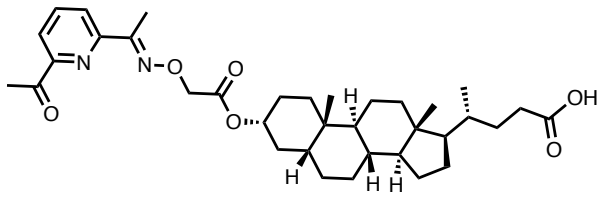

To a solution of compound 26 (37 mg, 0.062 mmol) in dichloromethane (5 mL) was added trifluoroacetic acid (1 mL) and stirred at r.t. for 7 h. The reaction mixture was diluted with ethyl acetate (30 mL), washed with sodium bicarbonate (sat.) and brine, dried over anhydrous sodium sulphate, and the solvent was evaporated. The residue was purified by flash column chromatography (silica, dichloromethane/methanol:9/1) to afford a white solid (30 mg, 89% yield).

^{1}H NMR (400 MHz, CDCl3) δ (ppm): 8.06 (d, *J* = 7.6 Hz, 1H), 7.98 (d, *J* = 7.6 Hz, 1H), 7.77 (t, *J* = 7.8 Hz, 1H), 4.89 – 4.76 (m, 1H), 4.74 (s, 2H), 2.78 (s, 1H), 2.73 (s, 3H), 2.46 (s, 3H), 2.34 – 2.02 (m, 2H), 1.96 – 0.88 (m, 45H), 0.62 (s, 3H).
^{13}C NMR (100 MHz, CDCl3) δ (ppm): 200.3, 180.0, 169.5, 157.2, 153.3, 152.7, 137.1, 124.2, 121.7, 75.4, 71.5, 56.6, 56.1, 42.9, 42.0, 40.6, 40.3, 35.9, 35.4, 35.1, 34.7, 32.4, 31.1, 30.9, 28.3, 27.1, 26.8, 26.4, 25.8, 24.3, 23.4, 21.0, 18.4, 12.2, 11.3.
HR-MS (ES+): calc.d for $C_{35}H_{51}N_2O_6$: 595.3747, found: 595.3752.
FT-IR (ATR): ν_{max} 2934, 2866, 1756, 1735, 1703, 1578, 1450, 1378, 1284, 1233, 1205, 1130, 1087 cm^{-1}.

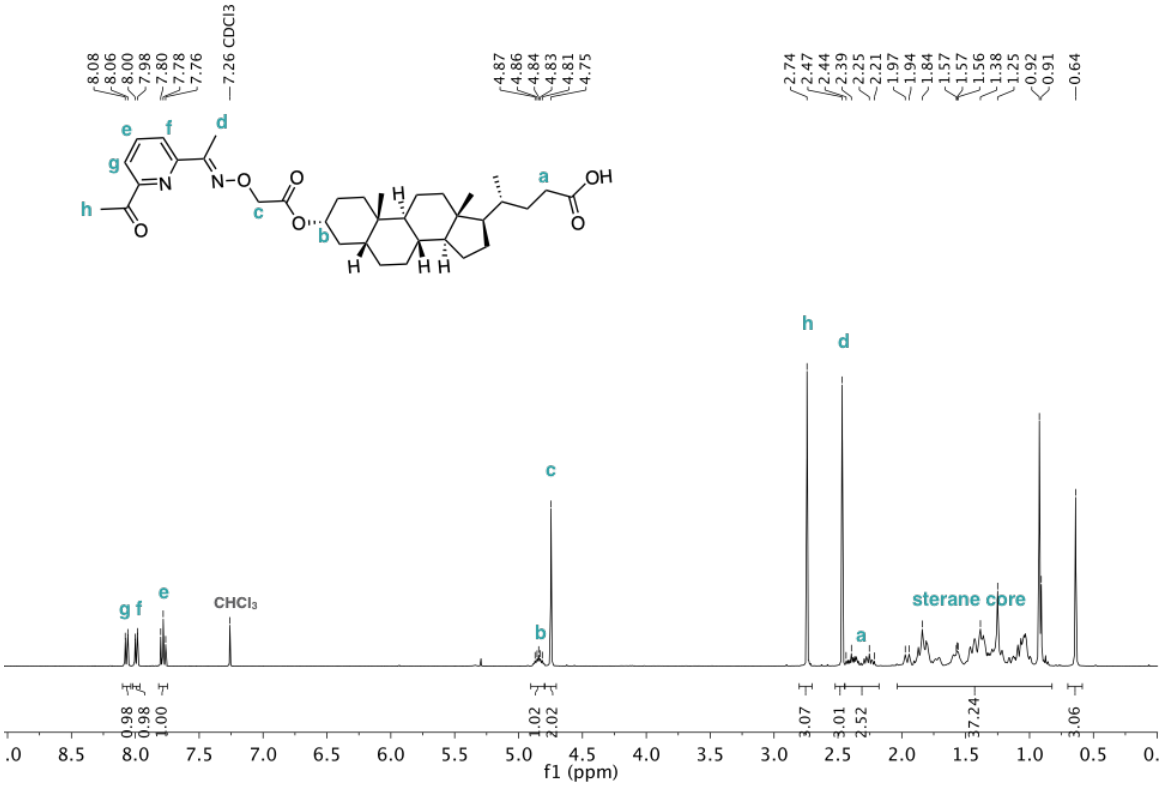

Figure S3.7 [1]H NMR spectrum of compound **3-6**.

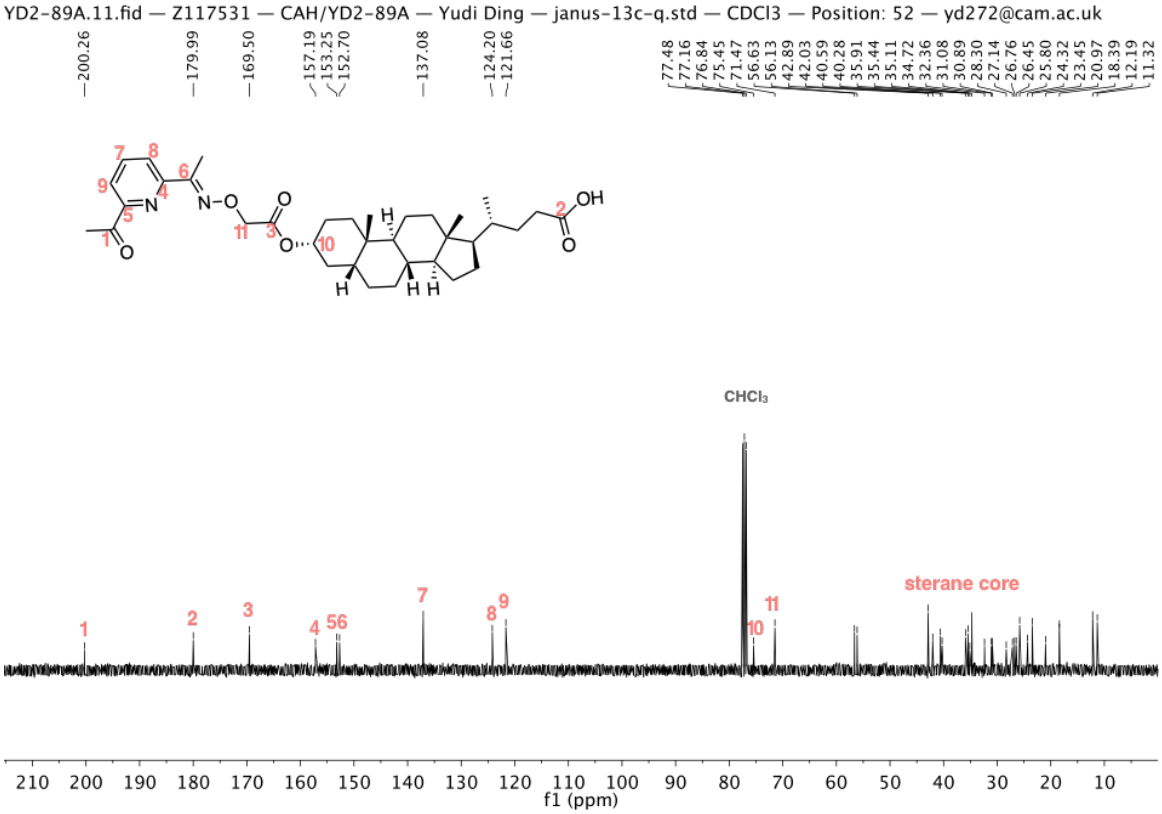

Figure S3.8 [13]C NMR spectrum of compound **3-6**.

Compound 3-1

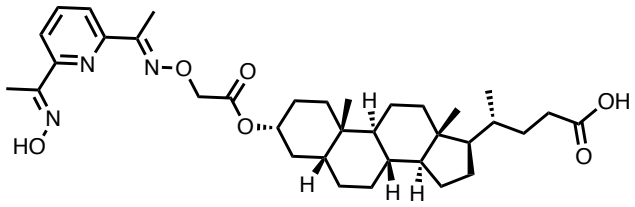

To a chloroform/ethanol:1/1 solution (10 mL) of compound **3-6** (30 mg, 0.050 mmol) was added an aqueous solution (1 mL) of hydroxylamine (3.5 mg, 0.050 mmol) and sodium acetate (4.1 mg, 0.050 mmol). The reaction mixture was stirred at 60 °C overnight. The reaction mixture was diluted with chloroform (30 mL), washed with water (10 mL x 3) and brine, dried over anhydrous sodium sulphate, and the solvent was evaporated to afford a white solid (67 mg, 43% yield).

^{1}H NMR (400 MHz, CDCl3) δ (ppm): 6.00 (t, *J* = 7.5 Hz, 1H), 7.86 – 7.63 (m, 2H), 4.87 – 4.79 (m, 1H), 4.74 (s, 2H), 2.44 (s, 3H), 2.42 (s, 3H), 1.96 – 1.82 (m, 4H), 1.57 – 0.92 (m, 33H), 0.63 (s, 3H) .

^{13}C NMR (100 MHz, CDCl3) δ (ppm): 179.7, 169.6, 157.6, 156.8, 152.8, 136.6, 120.7, 120.3, 77.2, 75.3, 71.3, 56.5, 55.9, 42.7, 41.8, 40.4, 40.1, 35.8, 35.3, 35.0, 34.6, 32.2, 30.9, 29.7, 28.2, 27.0, 26.6, 26.3, 24.2, 23.3, 20.8, 18.3, 12.0, 11.3, 10.9.

HR-MS (ES+): calcd. for $C_{35}H_{51}N_3O_6$: 609.3778, found: 609.3779.

FT-IR (ATR): ν_{max} 2925, 2864, 1753, 1734, 1704, 1570, 1453, 1424, 1365, 1284, 1258, 1204, 1159, 1132, 1081, 1021 cm^{-1}.

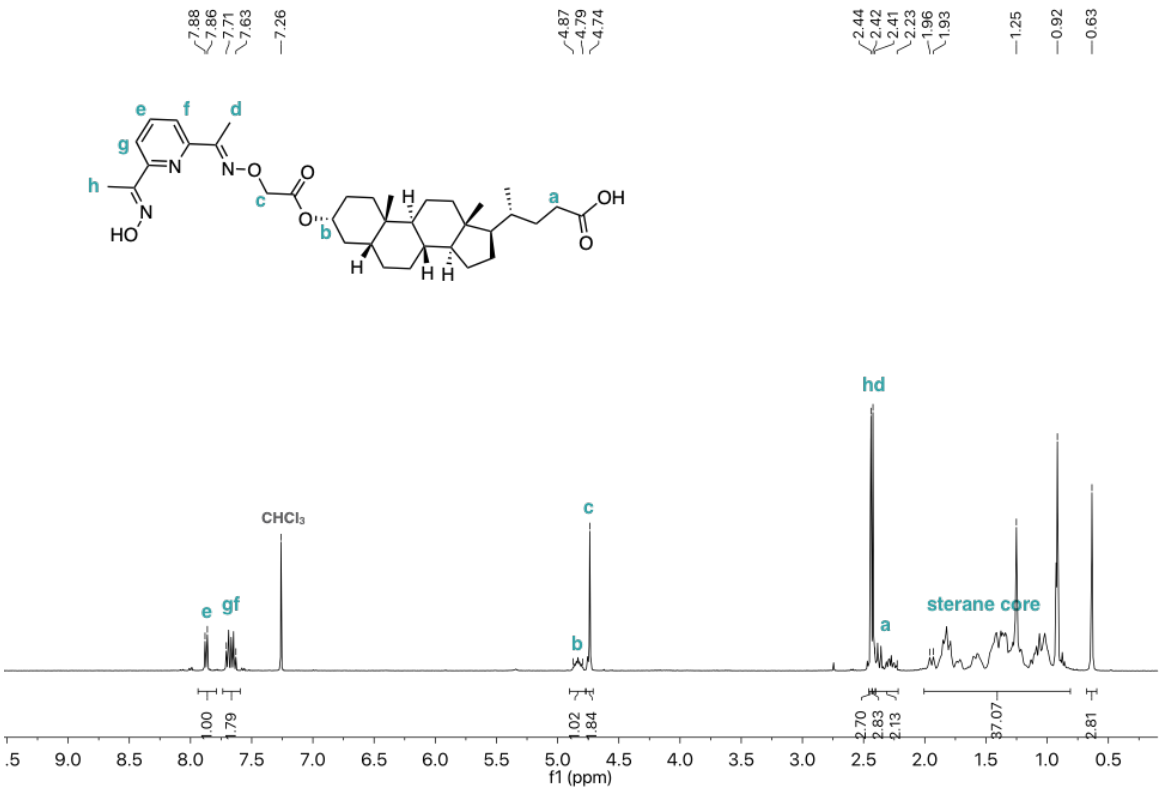

Figure S3.9 ^{1}H NMR spectrum of compound **3-1**.

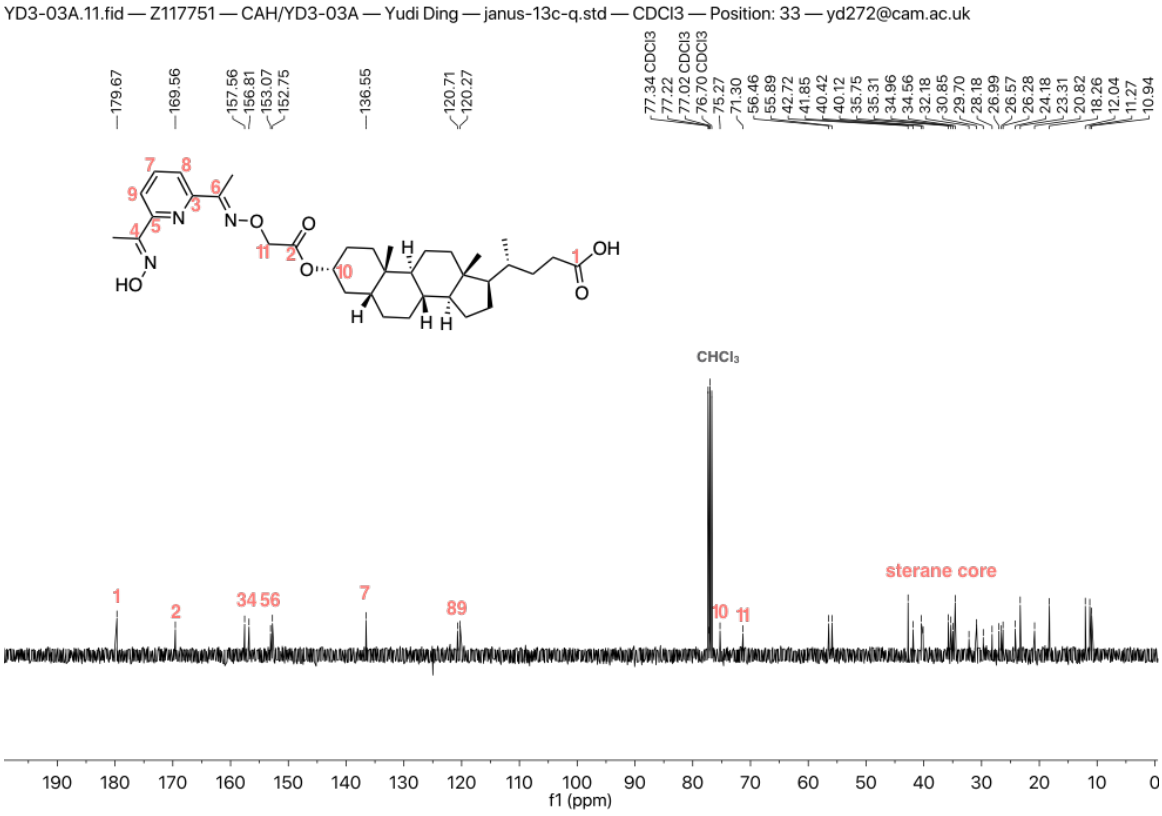

Figure S3.10 ^{13}C NMR spectrum of compound **3-1.**

3.4.2 Vesicle Experiments

General Protocol for Vesicle Preparation

To a 1.5 mL microcentrifuge tube was added a chloroform solution of lipids in order to obtain a final lipid concentration of 1 mM in 3.5 mL (final elution volume). The solvent was evaporated using a dry nitrogen stream and dried under high vacuum for at least 2 h to yield a thin lipid film. To the microcentrifuge containing the lipids was added 25 mM HEPES 150 mM NaCl buffer (0.5 mL) at pH 7, as well as stock solutions of ester substrate and zinc chloride as appropriate to reach final concentrations of 250 µM. After swelling for 1 min, the suspension was subjected to 5 cycles of freeze-thaw using liquid nitrogen and 35 °C water bath. The suspension was extruded for 19 times through a 200 nm polycarbonate filter in an extruder apparatus, and then the vesicles were separated by a bulk solution using prepacked SEC columns eluting with the same HEPES buffer at pH 7.

Fluorescence Measurements

Fluorescence excitation experiments were recorded using the following parameters: emission wavelength = 510 nm, excitation range 380–480 nm, recorded at 2-minute intervals. At the end of the experiment, 5% Triton X-100 (50 µL) and 1M NaOH (50 µL) was added to lyse the vesicles and hydrolyze all of the remaining substrates. The emission measured at this end point was used to normalize the data taking into account of the dilution factor.

OFF State

To a 1 mL fluorescence cuvette was added 1 mM vesicle suspensions with 1 mol% loading of carboxylic acid transducer **3-1** (800 µL).

Attempted ON State

An aliquot of 1 mM HCl was added to the vesicle suspensions described above to lower the external pH to 6, 5, or 4 at t = 20 min.

Attempted *In-situ* EDC Coupling (Figure 3.10)

OFF state background hydrolysis of substrate **3-10** in vesicles (black data): to a 1 mL fluorescence cuvette was added 1 mM vesicle suspensions with 1 mol% loading of carboxylic acid transducer **3-1** (800 µL). **Attempted ON state** (red data): to the above described vesicle suspension was added 40 eq. of EDC/NHS (1:1, relative to **3-1**) at t = 5 min, and 40 eq. of

propylamine (relative to **3-1**) at *t* = 15 min; **OFF state control experiment with EDC coupling** (yellow): to the above described vesicle suspension was added 40 eq. of EDC/NHS (1:1, relative to **3-1**) at *t* = 5 min; **OFF state control experiment with propylamine** (pink data): to the above described vesicle suspension was added 40 eq. of propylamine (relative to **3-1**) at *t* = 15 min.

This page is intentionally left blank

Doubt everything. Find your own light. Pain is Certain. Suffering is optional.
Gautama Buddha

4

Desthiobiotin Transducer

4.1 Introduction

Cell membranes coordinate a large variety of biological processes by selectively recognizing and responding to different external stimuli, and membrane-spanning proteins play a vital role in these signalling pathways. Direct mass transfer by carrier proteins or by channels allows exchange of molecules between the inside and outside of the cell.[1] For signalling pathways that do not involve direct mass transfer, an external signal induces dimerization or conformational changes in membrane-spanning proteins that result in a cascade of reactions on the inner side of the membrane.[2,3] Although numerous examples of synthetic membrane channels and transporters have been reported[4–10], signal transduction without mass transfer is considerably more challenging[11–16].

We have recently reported a novel transmembrane signalling mechanism, which operates by controlled translocation of a synthetic transducer across a vesicle lipid bilayer (Figure 1).[17,18] The external recognition head group of the transducer becomes membrane permeable in response to an external chemical stimulus, which leads to membrane translocation, exposing a catalytic head group to the interior of the vesicle. Catalytic hydrolysis of an internal substrate generates an amplified output signal, which can also be used to trigger the release of the vesicle contents.[19] The choice of recognition head group can be used to make this system respond to different external stimuli, such pH[17] or metal ions[18]. Here, we extend the scope of the signal transduction system by using ligand-protein binding as the input signal. We show that

multivalent interactions at lipid bilayer interfaces lead to dramatic changes in protein-ligand binding affinities and exploit this phenomenon to achieve signal transduction processes between two different populations of vesicles.

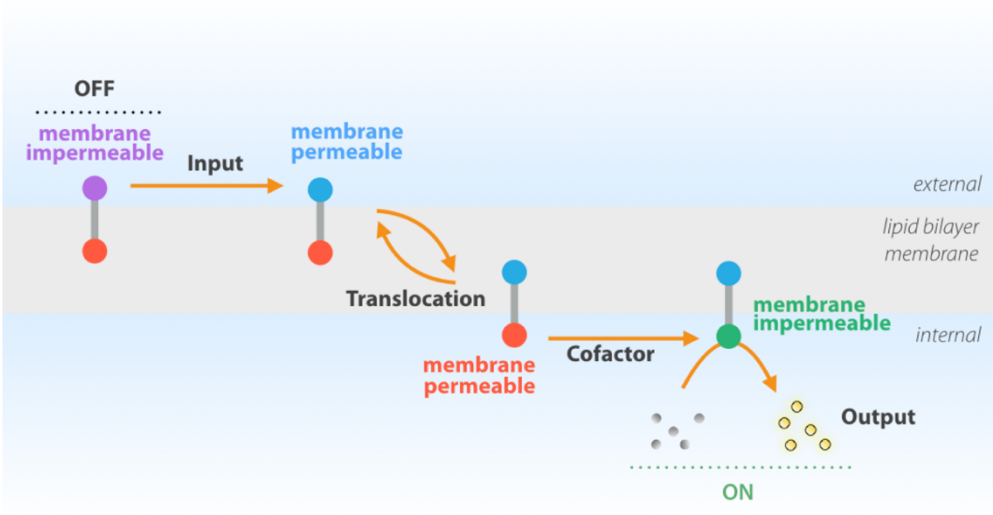

Figure 4.1 Signal transduction via membrane translocation. The transducer has two switchable head groups. In the OFF state, the recognition head group is membrane impermeable and sits in the external aqueous phase (purple), and the internal pro-catalyst head group sits in the membrane (red). An external signal switches the recognition head group to membrane permeable (blue), allowing translocation of the transducer across the bilayer. Binding of a charged cofactor to the catalytic head group (green) generates the ON state, where the catalyst turns over an encapsulated substrate (grey) to generate an amplified output signal (yellow).

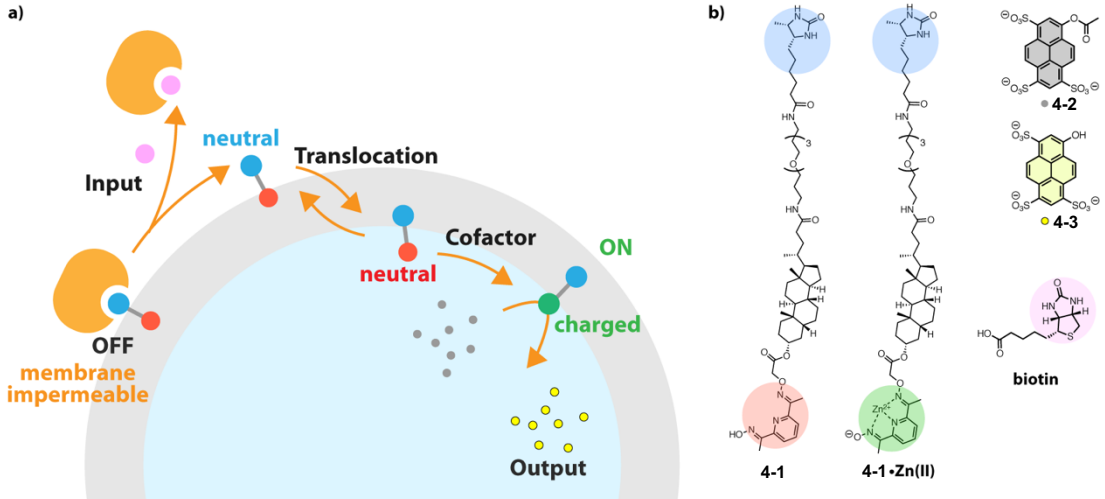

Figure 4.2 a) An artificial signal transduction system that responds to protein-ligand binding. In the initial OFF state, the protein-transducer complex is anchored in the outer leaflet of the vesicle bilayer and the catalytic head group (red) is buried in the membrane. The input is a competing ligand (pink) that binds the protein (orange), displacing the transducer head group (blue) and allowing it to enter the membrane. Translocation followed by binding of a charged cofactor (Zn^{2+}) from the internal aqueous solution of the vesicle activates the catalytic head group (green), which hydrolyses an internal substrate (grey) to generate an amplified output signal (yellow). b) Molecular structure of transducer **4-1**, the corresponding zinc complex, substrate **4-2**, fluorescent hydrolysis product **4-3**, and biotin.

The avidin-biotin system is a well-exploited and reliable biotechnology tool used in a broad range of applications such as biochemical assays[20], diagnosis[21], and affinity purification[22]. Avidins are water soluble proteins that have an extremely high affinity for biotin (K_d ~ 0.01 pM) and a somewhat lower affinity for desthiobiotin (K_d ~ 10 pM).[23] The desthiobiotin-avidin-biotin system is ideally suited to construction of a transducer with a recognition head group that responds to biotin as a molecular input signal. The approach is illustrated in Figure 4.2a. Desthiobiotin is used as the recognition head group on transducer **4-1**, and assembly of vesicles in the presence of avidin should lead to the OFF state, because the desthiobiotin-avidin complex is not membrane permeable. Addition of the higher affinity ligand, biotin (pink), to the external solution should displace the protein from the vesicles, allowing the relatively non-polar desthiobiotin to enter the membrane. Translocation of the transducer followed by binding of zinc ion cofactors to the internal catalytic head group will initiate hydrolysis of ester substrate **4-2** inside the vesicles. The output signal in the ON state is the fluorescent emission from the hydrolysis product **4-3**.

The molecular structure of transducer **4-1** is shown in Figure 4.2b. The hydrophobic steroid core provides the membrane anchor, and the pyridine oxime moiety is the pro-catalyst head group that will be activated by coordination to zinc ions. The desthiobiotin recognition head group is attached via a PEG linker to make sure it can reach the avidin binding site without steric clashes between the protein and the membrane (see Supporting Information). We used NeutrAvidin as the protein component of this system, because it has a low isoelectric point (pI = 6.3), which minimizes protein aggregation at neutral pH.

4.2 Results and Discussion

4.2.1 Synthesis

Synthesis of ester substrate **4-2** was described previously. Transducer **4-1** was synthesized from lithocholic acid in four steps as shown in Scheme 1. Coupling of the alcohol with chloroacetyl chloride, followed by EDC coupling of the carboxylic acid with *N*-Boc-4,7,10-trioxa-1,13-tridecanediamine **4-5** gave intermediate **4-6**. Deprotection of the amine followed by EDC coupling with desthiobiotin **4-7** gave **4-8**. Functionalization with pyridine dioxime **4-9** ligand gave transducer **4-1**.

A membrane-anchored biotin derivative was required for the signalling experiments described below. Compound **4-10** was therefore synthesized from lithocholic acid using the route shown in Scheme 4.2. The carboxylic acid group of lithocholic acid was converted to the corresponding amine in two steps, and then EDC coupling was used to attach biotin.

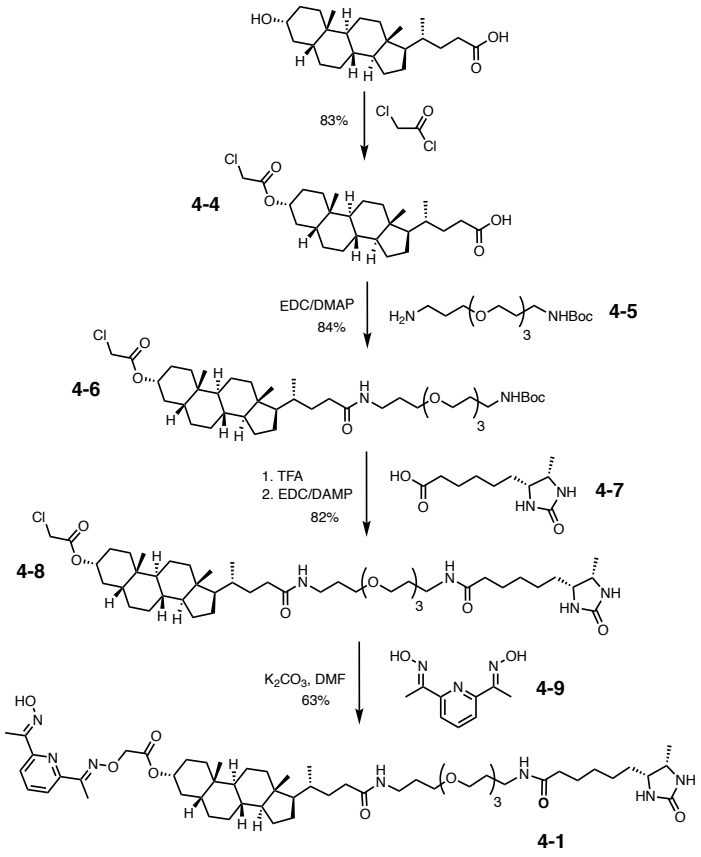

Scheme 4.1 Synthesis of Desthiobiotin Transducer **4-1**.

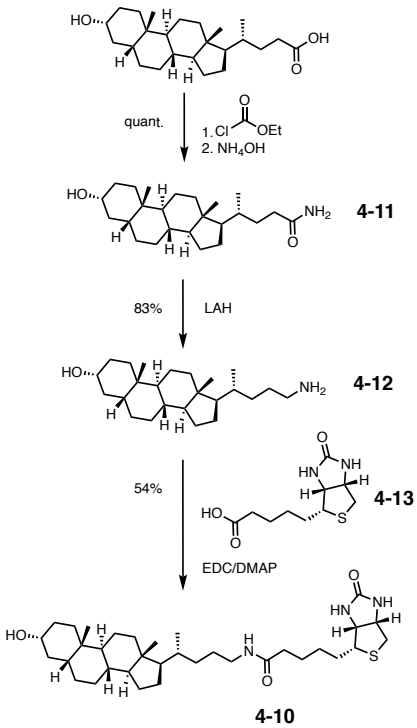

Scheme 4.2 Synthesis of Biotin Derivative **4-10**.

4.2.2 Characterization of the Input Signal

In order to confirm that NeutrAvidin binds transducer **4-1**, a 4'-hydroxyazobenzene-2-carboxylic acid (HABA) binding assay was first conducted in solution. HABA has a UV absorption maximum at 348 nm, which moves to 500 nm when it binds to NeutrAvidin.[24] Figure 3 shows the result of titrating a solution of transducer **4-1** in DMSO into a phosphate buffer solution of the HABA-NeutrAvidin complex at pH 7. The absorption at 500 nm decreased linearly with the amount of transducer until 4 equivalents had been added. Addition of just DMSO to the same solution had no effect on the absorption at 500 nm. This result indicates that, as expected, NeutrAvidin binds four equivalents of transducer **4-1** with a high affinity. Note that NeutrAvidin has four identical biotin binding sites, which will become important for understanding the signalling experiments below.

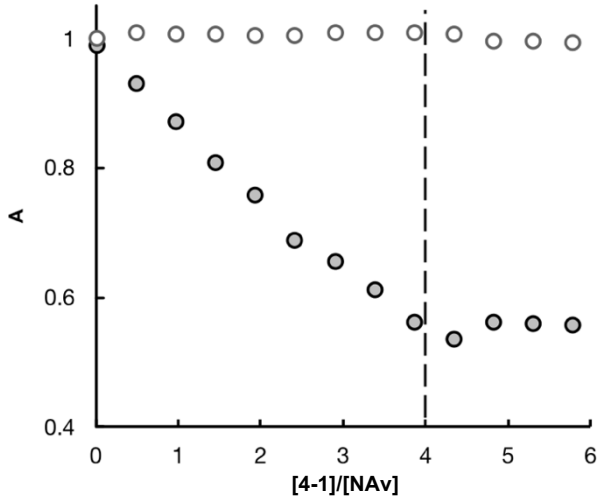

Figure 4.3 UV/vis absorption titration of transducer **4-1** in DMSO solution (filled circles) or just DMSO (open circles) into a mixture of 0.3 mM HABA and 8.3 μM NeutrAvidin in 100 mM phosphate buffer with 150 mM NaCl at pH 7. The UV/vis absorption at 500 nm is plotted as a function of the ratio of transducer [**4-1**] to protein [NAv].

To confirm that NeutrAvidin also binds transducer **4-1** when it is embedded in a vesicle membrane, we used a Förster resonance energy transfer (FRET) assay. A NeutrAvidin-TexasRed conjugate is commercially available, and nitrobenzoxadiazole (NBD) is a complementary dye suitable for FRET experiments.[25] We prepared one set of phosphatidylcholine vesicles loaded with transducer **4-1** and a C6-Ceramide derivative of NBD and another set of vesicles loaded with only the dye. The NeutrAvidin-TexasRed conjugate was added to both sets of vesicles, and the results are shown in Figure 4.4. For the vesicles that did not contain transducer **4-1**, no change in the NBD fluorescence was observed, which indicates that the protein does not bind to the vesicles (Figure 4.4a). In contrast, when transducer **4-1** was also present in the vesicles, addition of NeutrAvidin-TexasRed resulted in

quenching of the NBD fluorescence. The transducer-dependent quenching indicates that the protein does indeed bind to the membrane-anchored transducer, and that this inter-action brings to the two dyes into sufficiently close proximity for FRET (Figure 4.4b). These results suggest that the NeutrAvidin•**4-1** complex should provide a usable OFF state for signal transduction experiments.

NeutrAvidin makes a 1:4 complex with **4-1**, so there are four membrane-anchors exposed on the surface of complex, and there is potential for the complex to cross-link vesicles. Careful control of stoichiometry was therefore required. For example, for the experiment shown in Figure 4.4, an excess of protein was used, and no vesicle aggregation was observed.

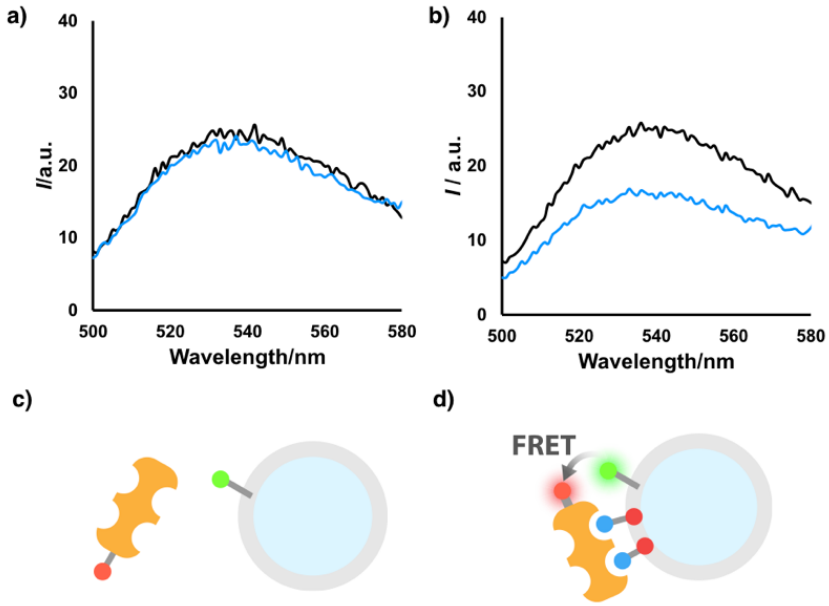

Figure 4.4 Fluorescence spectra (excitation at 330 nm, emission at 540 nm) of 0.01 mM 200 nm POPC vesicles with 2.5 mol% loading of NBD C6-Ceramide containing 25 mM HEPES buffer 150 mM NaCl at pH 7: a) without transducer **4-1**, and b) with 5 mol% loading of transducer **4-1**. Black: initial emission spectra, blue: spectra after addition of 0.5 μM NeutrAvidin-TexasRed (1 eq. relative to 1). Schematic illustrations are shown in c) and d), respectively.

The same FRET assay was used to test the effect of biotin on the interaction between NeutrAvidin and transducer **4-1.** Vesicles loaded with transducer **4-1** and NBD C6-Ceramide were prepared, and the NeutrAvidin-TexasRed conjugate was added. The fluorescence quenching described above was observed, which confirms that the protein binds to the membrane-anchored transducer on the surface of the vesicles. Then biotin was added, but no change in fluorescence was observed (Figure 4.5a). If biotin were to dissociate NeutrAvidin from the vesicles, then the FRET between TexasRed and NBD would be abolished, which suggests that membrane-anchored desthiobiotin outcompetes biotin for protein binding. In solution, biotin binds NeutrAvidin with a 1,000-fold higher affinity than desthiobiotin. A

possible reason for the change in relative affinity in the case of membrane-anchored ligands is that NeutrAvidin has four binding sites and vesicles present multiple ligands on their surface, so multivalent interactions are possible. The protein has two binding sites on one face and two on the opposite face, so we suggest that two desthiobiotin moieties bind cooperatively to two protein binding sites at the vesicle surface, leading to an enhanced binding affinity for membrane-anchored desthiobiotin relative to solution-phase biotin (Figure 4.5c).[26,27]

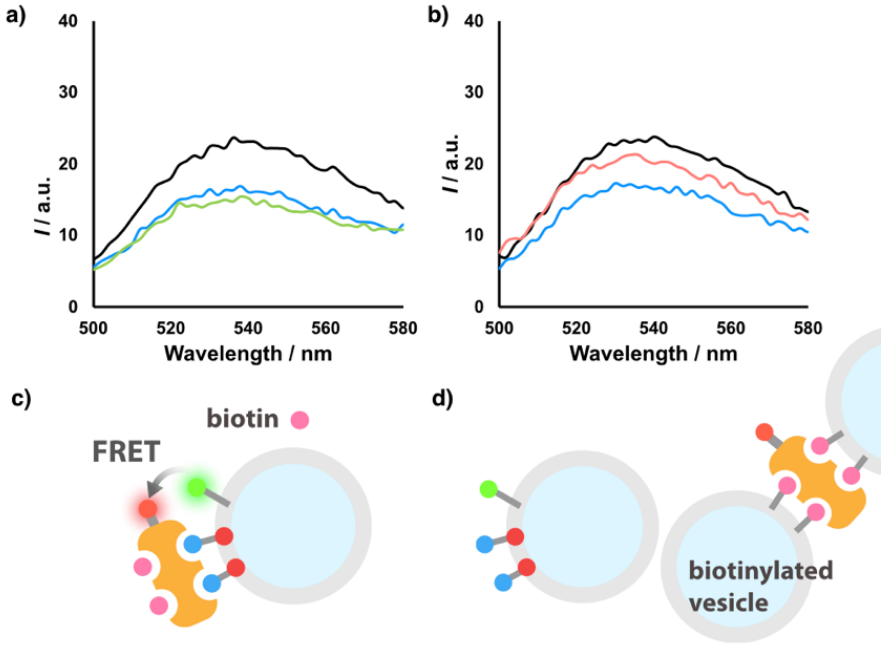

Figure 4.5 Fluorescence spectra (excitation at 330 nm, emission at 540 nm) of 0.01 mM 200 nm POPC vesicles with 2.5 mol% NBD C6-Ceramide and 5 mol% transducer **4-1** containing 25 mM HEPES buffer 150 mM NaCl at pH 7: a) initial spectrum (black), spectrum after addition of 0.42 μM NeutrAvidin-TexasRed (1 eq. relative to **4-1**) (blue), and spectrum after subsequent addition of 1.68 μM biotin (4 eq. relative to NeutraAvidin-TexasRed) (green), and b) initial spectrum (black), spectrum after addition of 0.42 μM NeutrAvidin-TexasRed (1 eq. relative to **4-1**) (blue), and spectrum after subsequent addition of vesicles with 5 mol% biotin derivative **4-10** to reach a bulk concentration of 1.68 μM **4-10** (4 eq. relative to NeutraAvidin-TexasRed) (red). Schematic illustrations are shown in c) and d), respectively.

If anchoring desthiobiotin in a membrane increases the apparent binding affinity for NeutrAvidin, the same should be true of biotin. To test this hypothesis, we used vesicles loaded with membrane-anchored biotin as the input signal to displace NeutrAvidin from the transducer. The FRET experiment described above was repeated, but instead of adding biotin to displace the NeutrAvidin from the membrane-anchored transducer, vesicles loaded with 5 mol% of biotin derivative **4-10** were added. The results are shown in Figure 4.5b. In this case, the fluorescence of the NBD present in the transducer-loaded vesicles was restored. This result shows that vesicles containing biotin derivative **4-10** remove NeutrAvidin from vesicles containing transducer **4-1**. In other words, multivalent biotin vesicles outcompete multivalent desthiobiotin vesicles, as expected from the solution-phase binding affinities. The fact that **4-**

10 binds NeutrAvidin without the PEG linker used in **4-1** suggests that a linker is not required for protein binding at the membrane interface. However, Figure **4.**5b shows that the fluorescence is not fully restored by the biotin vesicles, which could be due to a relatively small difference in the protein binding affinities of the two vesicle-anchored ligands.

In these experiments, the protein was present in excess relative to **4-1** to avoid cross-linking of the vesicles, so the other protein binding sites were initially empty. Addition of the biotin vesicles could cause cross-linking due to multivalent interactions at both vesicle membrane interfaces, but an excess of biotin was used relative to transducer **4-1**, and no aggregation was observed on the timescale of the measurements. The reorganization of multivalent interactions that would lead to vesicle aggregation appears to be relatively slow. However, when solutions containing both sets of vesicles were stored overnight, visible flocculation was observed indicating that aggregation of this system does take place on longer timescales.

4.2.3 Transmembrane Signalling Experiments

Before carrying out signalling experiments, we tested the catalytic activity of the transducer in the ON and the OFF states. Vesicles were prepared containing 250 μM ester **2** and 250 μM zinc chloride in HEPES buffer at pH 7. When transducer **4-1** was added to this solution, it inserted into the membrane and initiated catalysis of ester hydrolysis inside the vesicles (green data in Figure 4.6a). This system corresponds to the ON state of the signal transduction system and shows that the desthiobiotin head group does not interfere with catalysis. When the NeutrAvidin•**1** complex was added to the vesicle solution, no increase in the background rate of hydrolysis of substrate 4-**2** inside the vesicles was observed (black data in Figure 4.6a). This system corresponds to the OFF state of the signal transduction system and shows that protein binding holds the catalytic head group inside the membrane, preventing translocation. Vesicle cross-linking in this OFF state was avoided by adding an excess of the NeutrAvidin•**4-1** complex to ensure that the surfaces of the vesicles were saturated.

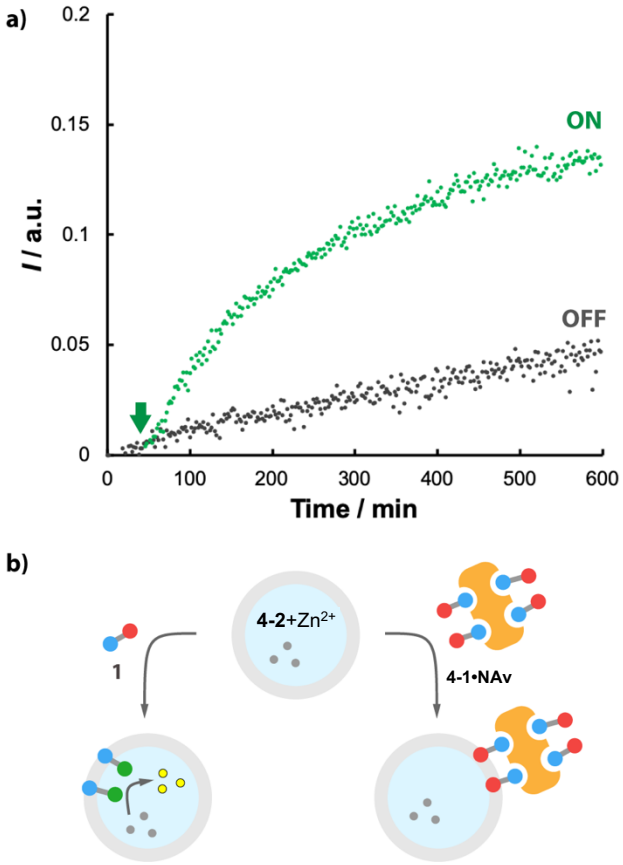

Figure 4.6 a) Time dependence of the normalized fluorescence emission intensity at 510 nm (exciting at 415 nm). The ON state (green) was obtained by adding transducer **4-1** in DMSO to vesicles to reach 10 mol% loading in lipids and a bulk concentration of 10 μM **4-1** (addition at time point indicated by the arrow). The OFF state (black) was obtained by adding the NeutrAvidin•**4-1** complex (16.7 μM protein, 66.8 μM **4-1**, i.e. 0.25 eq. of protein eq. relative to **4-1**). All experiments were conducted in 0.1 mM 200 nm DOPC/DOPE vesicles containing 250 μM **4-2**, 250 μM zinc chloride, and 25 mM HEPES buffer 150 mM NaCl at pH 7. b) Schematic illustration.

Having demonstrated that the ON and OFF states function as anticipated, we then attempted to switch between these two states by using external signals to initiate signal transduction. The ON state was assembled as described above, and NeutrAvidin was added to the vesicle suspension after two hours. Figure 4.7a shows that addition of the protein efficiently switches the system from the ON to the OFF state.

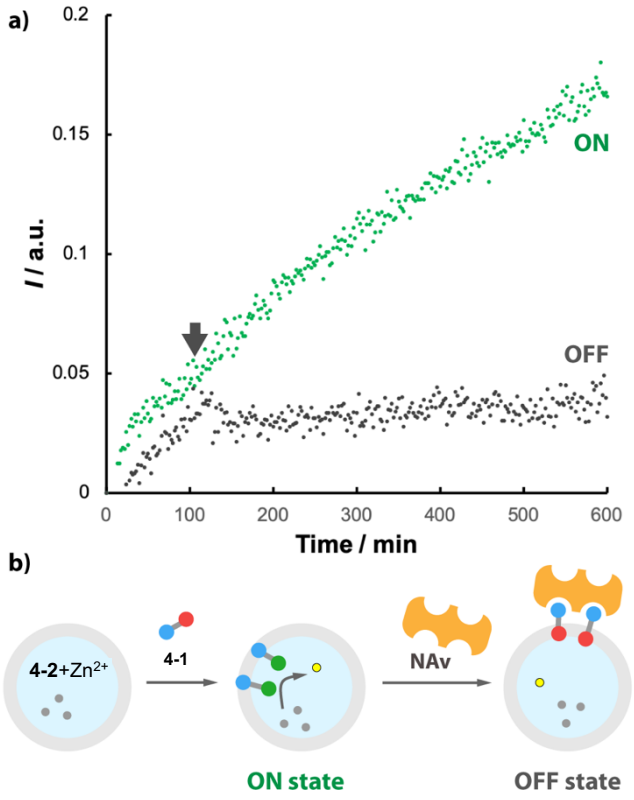

Figure 4.7 a) Time dependence of the normalized fluorescence emission intensity at 510 nm (exciting at 415 nm). The ON state (green) was obtained by adding transducer **4-1** in DMSO to vesicles to reach 10 mol% loading in lipids and a bulk concentration of 1 μM **4-1**. After 100 minutes, 2 μM NeutrAvidin was added (2 eq. relative to **4-1**) to generate the OFF state (black, addition indicated by the arrow). All experiments were conducted in 0.01 mM 200 nm DOPC/DOPE vesicles containing 250 μM 2, 250 μM zinc chloride, and 25 mM HEPES buffer 150 mM NaCl at pH 7. b) Schematic illustration.

Having demonstrated that the ON and OFF states function as anticipated, we then attempted to switch between these two states by using external signals to initiate signal transduction. The ON state was assembled as described above, and NeutrAvidin was added to the vesicle suspension after two hours. Figure 4.7a shows that addition of the protein efficiently switches the system from the ON to the OFF state. In this case, two equivalents of protein relative to transducer **4-1** were used to avoid vesicle cross-linking, and this stoichiometry is more effective at suppressing the reaction than the 0.25 equivalents of NeutrAvidin used for the experiments shown in Figure 4.6a.

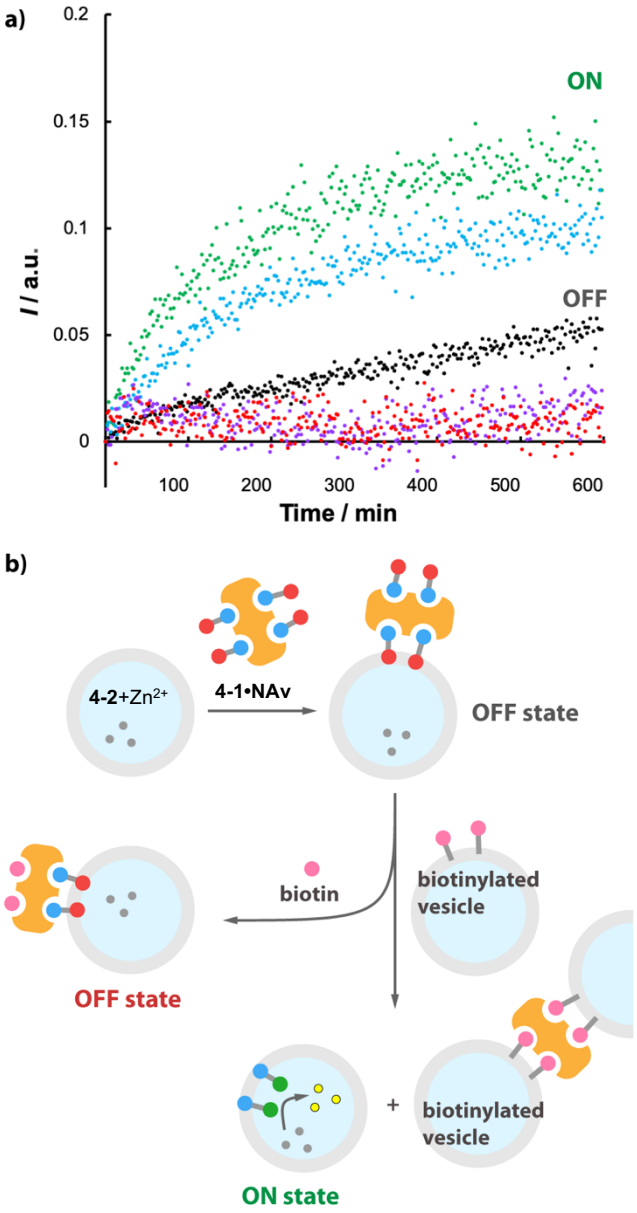

Figure 4.8 a) Time dependence of the normalized fluorescence emission intensity at 510 nm (exciting at 415 nm). The OFF state (black) was obtained by adding NeutrAvidin•**4-1** 1:4 complex (16.7 μM protein, 66.8 μM **4-1**, i.e. 0.25 eq. of protein eq. relative to **4-1**) to 0.1 mM DOPC/DOPE vesicles containing 250 μM **4-2**, 250 μM zinc chloride, and 25 mM HEPES buffer 150 mM NaCl at pH 7. Addition to the OFF vesicle solution of either 67 μM biotin (4 eq. relative to NeutrAvidin, red) or 1 mM biotin (60 eq. relative to NeutrAvidin, purple) biotin both gave OFF states. Addition to the OFF vesicle solution of different amounts of 200 nm DOPC/DOPE vesicles loaded with 10 mol% of biotin derivative **4-10** (green) or 5 mol% of biotin derivative **4-10** (blue) to reach bulk concentrations of 67 μM **4-10** (4 eq. relative to NeutrAvidin) both gave ON states. b) Schematic illustration.

To demonstrate switching from the OFF to the ON state, the OFF state was assembled as described above by adding the NeutrAvidin•**4-1** complex to vesicles containing substrate **4-2** and zinc ions. Figure 4.8a shows the effect of adding biotin to this system. Biotin slightly reduced the background rate of substrate hydrolysis (red data), but did not generate an ON state, as expected from the FRET experiments described above. Even a saturated solution of 1

mM biotin produced no signs of an ON signal (purple data). However, addition of vesicles loaded with 10 mol% of biotin derivative **4-10** lead to a rapid increase in fluorescence emission characteristic of the ON state (green data in Figure 4.8a). When the loading of **4-10** in the biotin vesicles was lowered to 5 mol%, an ON state was also obtained, albeit with lower catalyst activity (blue data). This result suggests that the affinity of the biotin vesicles for NeutrAvidin can be controlled with vesicle loading by changing the effective molarity for the cooperative binding interactions at the membrane interface. The timescale for the signalling experiments is significantly longer than for the FRET experiments, so flocculation was sometimes observed at the end of these experiments, presumably due to vesicle cross-linking. The experiments shown in Figure 4.8 indicate that signalling molecules displayed on the surface of one set of vesicles are able to initiate catalytic substrate turnover inside a second set of different vesicles. This process is reminiscent of the kind of complex cell-to-cell signalling processes found in biological organisms.

4.3 Conclusions

The system described here constitutes the first example of a synthetic construct where cooperative interactions at membrane interfaces have been used to trigger transmembrane signal transduction. A molecular signal (biotin) displayed on the external surface of one population of vesicles was used to trigger a catalytic process on the inside of a second population of vesicles. The key recognition event is the exchange of proteins (NeutrAvidin) bound to vesicles displaying desthiobiotin to vesicles displaying biotin. The desthiobiotin•NeutrAvidin complex was used to anchor a synthetic transducer in the outer leaflet of the vesicles, and when the protein was displaced, the transducer translocated across the bilayer to expose a catalytic head group to the internal vesicle solution. As a result, an ester substrate encapsulated on the inside of this second population of vesicles was hydrolysed to give a fluorescent product, which constitutes an amplified output signal. NeutrAvidin has four ligand binding sites, and multivalent interactions with the membrane-anchored ligands leads to very high binding affinities. Thus biotin, which has a dissociation constant three orders of magnitude higher than desthiobiotin, did not displace NeutrAvidin from the membrane-anchored transducer, and membrane-anchored biotin was required to generate the input signal. These findings extend the scope of artificial signal transduction from purely synthetic assemblies into more sophisticated systems, which opens up the potential for future development of responsive vesicles in bionanotechnology.

References

(1) Sakai, N.; Houdebert, D.; Matile, S. Voltage-Dependent Formation of Anion Channels by Synthetic Rigid-Rod Push–Pull β-Barrels. *Chem. – Eur. J.* **2003**, *9* (1), 223–232. https://doi.org/10.1002/chem.200390016.

(2) Simon, M. I.; Strathmann, M. P.; Gautam, N. Diversity of G Proteins in Signal Transduction. *Science* **1991**, *252* (5007), 802–808. https://doi.org/10.1126/science.1902986.

(3) Schlessinger, J. Cell Signaling by Receptor Tyrosine Kinases. *Cell* **2000**, *103* (2), 211–225. https://doi.org/10.1016/S0092-8674(00)00114-8.

(4) Bennett, I. M.; Farfano, H. M. V.; Bogani, F.; Primak, A.; Liddell, P. A.; Otero, L.; Sereno, L.; Silber, J. J.; Moore, A. L.; Moore, T. A.; et al. Active Transport of Ca 2+ by an Artificial Photosynthetic Membrane. *Nature* **2002**, *420* (6914), 398–401. https://doi.org/10.1038/nature01209.

(5) Matile, S.; Sakai, N. The Characterization of Synthetic Ion Channels and Pores. In *Analytical Methods in Supramolecular Chemistry*; John Wiley & Sons, Ltd, 2012; pp 711–742. https://doi.org/10.1002/9783527644131.ch15.

(6) Fyles, T. M. Synthetic Ion Channels in Bilayer Membranes. *Chem. Soc. Rev.* **2007**, *36* (2), 335–347. https://doi.org/10.1039/B603256G.

(7) Davis, J. T.; Okunola, O.; Quesada, R. Recent Advances in the Transmembrane Transport of Anions. *Chem. Soc. Rev.* **2010**, *39* (10), 3843–3862. https://doi.org/10.1039/B926164H.

(8) Matile, S.; Jentzsch, A. V.; Montenegro, J.; Fin, A. Recent Synthetic Transport Systems. *Chem. Soc. Rev.* **2011**, *40* (5), 2453–2474. https://doi.org/10.1039/C0CS00209G.

(9) Gale, P. A. From Anion Receptors to Transporters. *Acc. Chem. Res.* **2011**, *44* (3), 216–226. https://doi.org/10.1021/ar100134p.

(10) Stanzl, E. G.; Trantow, B. M.; Vargas, J. R.; Wender, P. A. Fifteen Years of Cell-Penetrating, Guanidinium-Rich Molecular Transporters: Basic Science, Research Tools, and Clinical Applications. *Acc. Chem. Res.* **2013**, *46* (12), 2944–2954. https://doi.org/10.1021/ar4000554.

(11) Grimaldi, J. J.; Boileau, S.; Lehn, J.-M. Light-Driven, Carrier-Mediated Electron Transfer across Artificial Membranes. *Nature* **1977**, *265* (5591), 229–230. https://doi.org/10.1038/265229a0.

(12) Barton, P.; Hunter, C. A.; Potter, T. J.; Webb, S. J.; Williams, N. H. Transmembrane Signalling. *Angew. Chem. Int. Ed.* **2002**, *41* (20), 3878–3881. https://doi.org/10.1002/1521-3773(20021018)41:20<3878::AID-ANIE3878>3.0.CO;2-F.

(13) Dijkstra, H. P.; Hutchinson, J. J.; Hunter, C. A.; Qin, H.; Tomas, S.; Webb, S. J.; Williams, N. H. Transmission of Binding Information across Lipid Bilayers. *Chem. – Eur. J.* **2007**, *13* (25), 7215–7222. https://doi.org/10.1002/chem.200601723.

(14) Bernitzki, K.; Schrader, T. Entirely Artificial Signal Transduction with a Primary Messenger. *Angew. Chem. Int. Ed.* **2009**, *48* (43), 8001–8005. https://doi.org/10.1002/anie.200902973.

(15) Bernitzki, K.; Maue, M.; Schrader, T. Artificial Signal Transduction with Primary and Secondary Messengers. *Chem. – Eur. J.* **2012**, *18* (42), 13412–13417. https://doi.org/10.1002/chem.201200623.

(16) Poli, M. D.; Zawodny, W.; Quinonero, O.; Lorch, M.; Webb, S. J.; Clayden, J. Conformational Photoswitching of a Synthetic Peptide Foldamer Bound within a Phospholipid Bilayer. *Science* **2016**, *352* (6285), 575–580. https://doi.org/10.1126/science.aad8352.

(17) Langton, M. J.; Keymeulen, F.; Ciaccia, M.; Williams, N. H.; Hunter, C. A. Controlled Membrane Translocation Provides a Mechanism for Signal Transduction and Amplification. *Nat. Chem.* **2017**, *9* (5), 426–430. https://doi.org/10.1038/nchem.2678.

(18) Langton, M. J.; Williams, N. H.; Hunter, C. A. Recognition-Controlled Membrane Translocation for Signal Transduction across Lipid Bilayers. *J. Am. Chem. Soc.* **2017**, *139* (18), 6461–6466. https://doi.org/10.1021/jacs.7b02345.

(19) Langton, M. J.; Scriven, L. M.; Williams, N. H.; Hunter, C. A. Triggered Release from Lipid Bilayer Vesicles by an Artificial Transmembrane Signal Transduction System. *J. Am. Chem. Soc.* **2017**, *139* (44), 15768–15773. https://doi.org/10.1021/jacs.7b07747.

(20) Bratthauer, G. L. The Avidin–Biotin Complex (ABC) Method and Other Avidin–Biotin Binding Methods. In *Immunocytochemical Methods and Protocols*; Oliver, C., Jamur, M. C., Eds.; Methods in Molecular Biology; Humana Press: Totowa, NJ, 2010; pp 257–270. https://doi.org/10.1007/978-1-59745-324-0_26.

(21) Jain, A.; Cheng, K. The Principles and Applications of Avidin-Based Nanoparticles in Drug Delivery and Diagnosis. *J. Control. Release Off. J. Control. Release Soc.* **2017**, *245*, 27–40. https://doi.org/10.1016/j.jconrel.2016.11.016.

(22) Bayer, E. A.; Wilchek, M. Application of Avidin—Biotin Technology to Affinity-Based Separations. *J. Chromatogr. A* **1990**, *510*, 3–11.

https://doi.org/10.1016/S0021-9673(01)93733-1.

(23) Hirsch, J. D.; Eslamizar, L.; Filanoski, B. J.; Malekzadeh, N.; Haugland, R. P.; Beechem, J. M.; Haugland, R. P. Easily Reversible Desthiobiotin Binding to Streptavidin, Avidin, and Other Biotin-Binding Proteins: Uses for Protein Labeling, Detection, and Isolation. *Anal. Biochem.* **2002**, *308* (2), 343–357. https://doi.org/10.1016/S0003-2697(02)00201-4.

(24) Livnah, O.; Bayer, E. A.; Wilchek, M.; Sussman, J. L. The Structure of the Complex between Avidin and the Dye, 2-(4'-Hydroxyazobenzene) Benzoic Acid (HABA). *FEBS Lett.* **1993**, *328* (1–2), 165–168. https://doi.org/10.1016/0014-5793(93)80986-5.

(25) Wong, A. P.; Groves, J. T. Molecular Topography Imaging by Intermembrane Fluorescence Resonance Energy Transfer. *Proc. Natl. Acad. Sci. U. S. A.* **2002**, *99* (22), 14147–14152. https://doi.org/10.1073/pnas.212392599.

(26) Doyle, E. L.; Hunter, C. A.; Phillips, H. C.; Webb, S. J.; Williams, N. H. Cooperative Binding at Lipid Bilayer Membrane Surfaces. *J. Am. Chem. Soc.* **2003**, *125* (15), 4593–4599. https://doi.org/10.1021/ja021048a.

(27) Yang, D.; Kroe-Barrett, R.; Singh, S.; Roberts, C. J.; Laue, T. M. IgG Cooperativity – Is There Allostery? Implications for Antibody Functions and Therapeutic Antibody Development. *mAbs* **2017**, *9* (8), 1231–1252. https://doi.org/10.1080/19420862.2017.1367074.

4.4 Supporting Information

4.4.1 Molecular modelling

There is no NeutrAvidin•biotin crystal structure available in the PDB bank, so the X-ray crystal structure of the avidin•biotin complex (PDB entry: 2AVI) was used to assess an appropriate length of linker to ensure that the membrane would not interfere with binding. NeutrAvidin is a deglycosylated version of avidin. The structure of the transducer **4-1** was built and energy minimized in an extended conformation using Avogadro. The amide group of the linker unit of transducer **4-1** was superimposed with the carboxylate group of biotin in the binding pocket of avidin using VMD (Figure S4.1). The dihedral angle adjustment function was used to manually configurate the bond angles of the rest of the transducer so that the steroid core extended towards outside of the protein. The resulting structure suggests that the linker used in transducer **4-1** is long enough to allow protein binding to the dethiobiotin unit simultaneously with anchoring of the steroid in the lipid bilayer of vesicles (Figure S4.2).

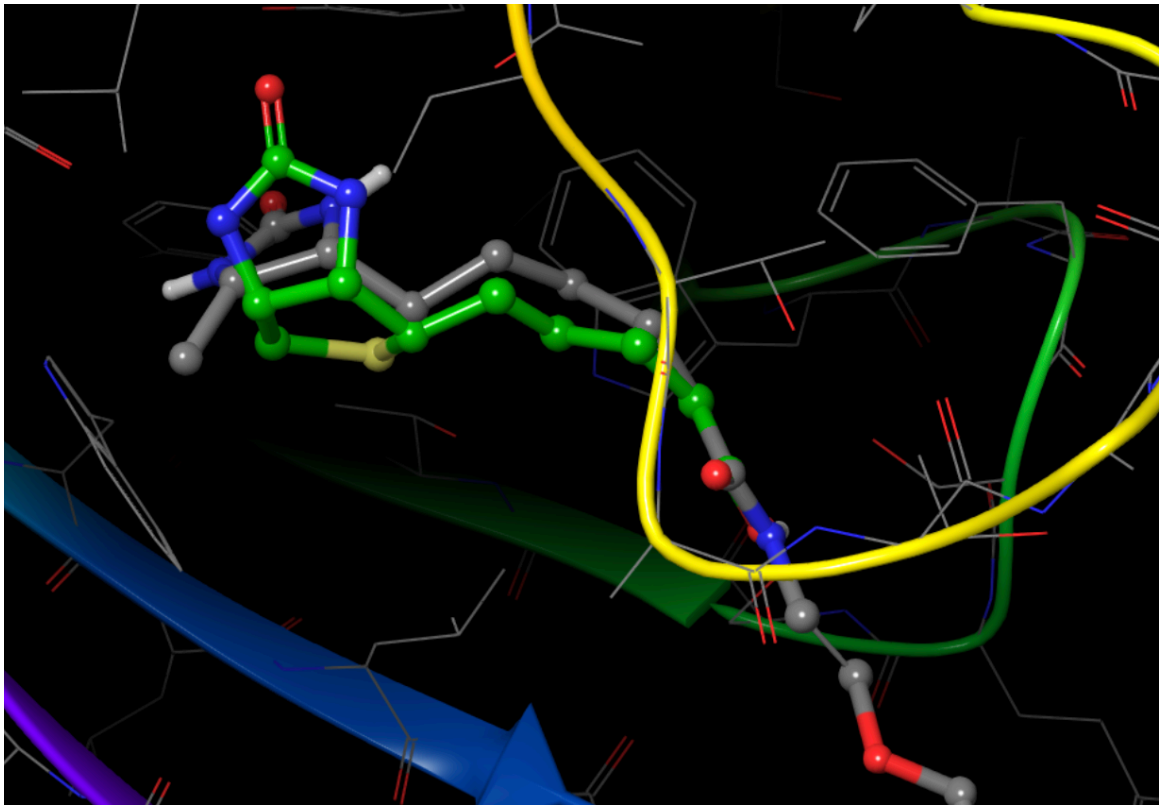

Figure S4.1 The binding pocket of the Avidin•**4-1** model. The amide group of the linker of **4-1** was superimposed with the carboxylate group of biotin in the binding pocket of avidin.

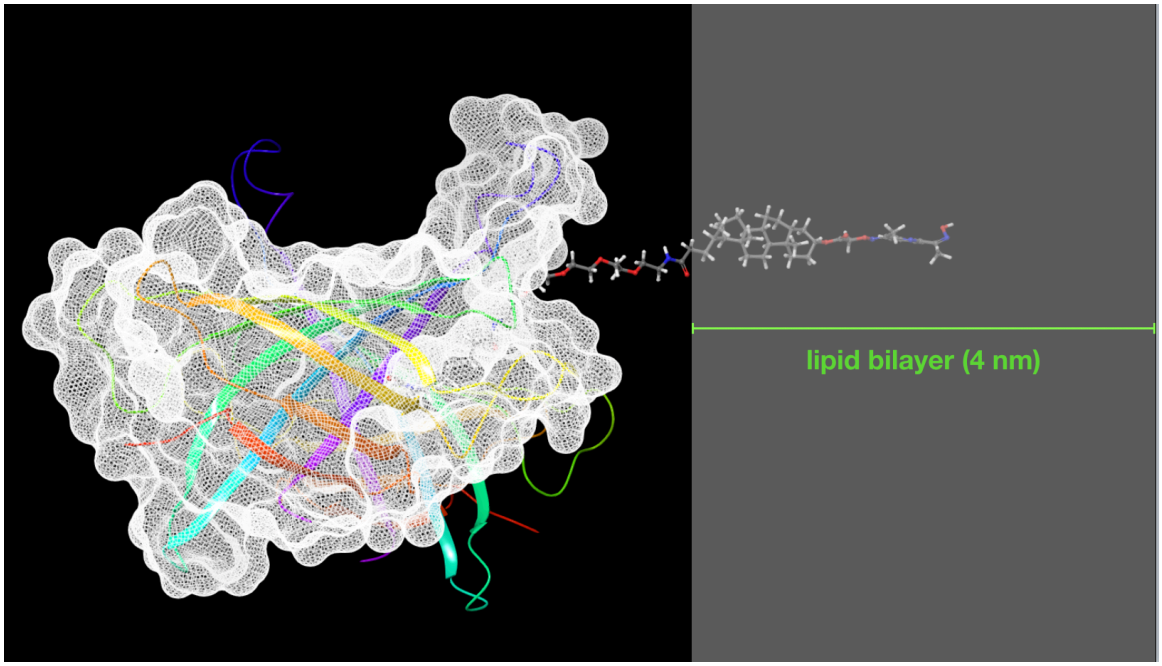

Figure S4.2 Model of the Avidin•**4-1** complex at a DOPC/DOPE lipid bilayer interface, which is 4 nm thick.[1]

4.4.2 Synthetic Procedures and Characterizations

Materials and methods

^{1}H NMR and ^{13}C NMR spectra were recorded on a 400-MHz Bruker® spectrometer. Chemical shifts are reported as δ values in ppm. Flash chromatography was carried out on an automated system (Combiflash® Rf+ Lumen™) using pre-packed cartridges of silica (25 µm PuriFlash® Column) or neutral alumina (50 µm RediSep® Rf Column). GPC purification of the vesicles was carried out using GE Healthcare PD-10 desalting columns prepacked with Sephadex® G-25 medium. Fluorescence spectra were recorded using a Cary Eclipse fluorescence spectrophotometer (Agilent Technologies) in Hellma® Analytics Suprasil® quartz cuvettes. pH measurements were conducted using a Mettler-Toledo SevenCompact™ pH meter equipped with an InLab® Micro electrode. Vesicles were assembled in Eppendorf® polypropylene Protein LoBind® polypropylene microcentrifuge tube and extruded as described below using Avanti® Polar Lipids extruder kits, equipped with Avestin® LiposoFast Liposome Factory 200 nm polycarbonate membranes with GE Healthcare Whatman® 10 mm polyester filter support. Solutions or vesicles suspensions were transferred using Eppendorf Multipette® Xstream Pippette with Combitips Advanced® or Hamilton Microliter™ syringes. All reagents and solvents were used without further purification. Chemicals were purchased from Sigma-Aldrich® and used without further purification.

Synthetic procedures

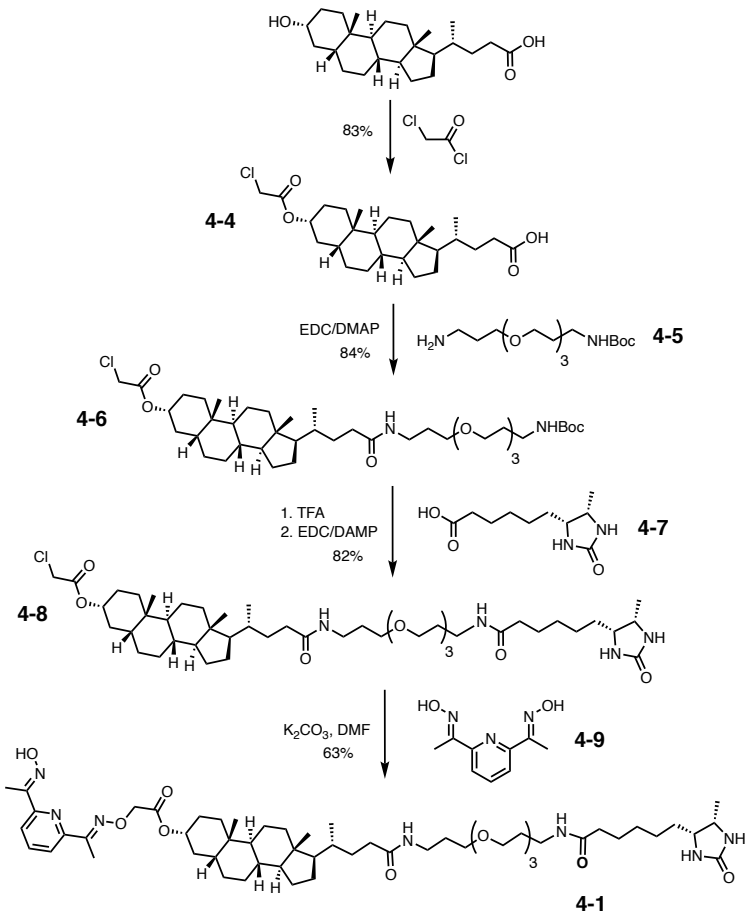

Scheme S4.1 Synthesis of desthiobiotin transducer **4-1**.

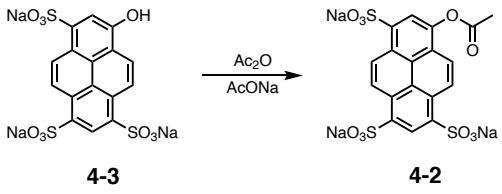

Scheme S4.2 Synthesis of ester substrate **4-2**.

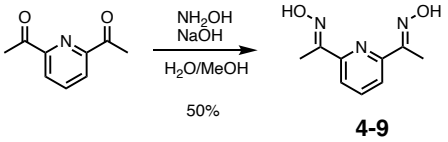

Scheme S4.3 Synthesis of pyridine-oxime **4-9**.

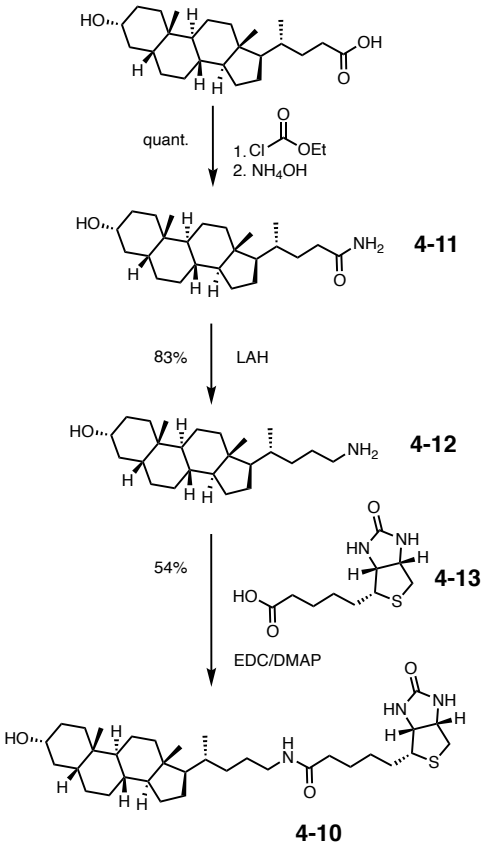

Scheme S4.4 Synthesis of biotin derivative **4-10**.

Characterizations

Compound 4-4

(see Compound **3-2**)

Compound 4-6

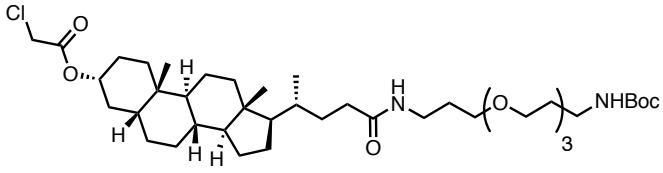

A mixture of compound **4-4** (100 mg, 0.221 mmol), *N*-Boc-4,7,10-trioxa-1,13-tridecanediamine **4-5** (71 mg, 0.221 mmol), EDC (52 mg, 0.265 mmol) and 4-dimethylaminopyridine (1 mg, cat.) in dichloromethanem (3 mL) was stirred at room temperature overnight. The reaction mixture was diluted with 25 mL of dichloromethane, then washed with 1 M hydrochloric acid (10 mL × 2), sodium bicarbonate (sat., 10 mL), brine (10 mL) and dried over anhydrous sodium sulfate. The solvent was removed in vacuo and the crude was purified by flash chromatography (neutral alumina, methanol in dichloromethane 0 – 5%) to afford the product as a colorless oil (140 mg, 84%).

^{1}H NMR (400 MHz, $CDCl_3$) δ (ppm): 6.11 (s, 1H), 4.94 (s, 1H), 4.81 (m, 1H), 4.03 (s, 2H), 3.66 – 3.53 (m, 13H), 3.38 – 3.23 (m, 2H), 3.21 – 3.20 (m, 2H), 2.25 – 2.17 (m, 2H), 1.77 – 0.90 (m, 43H), 0.62 (s, 3H).

^{13}C NMR (100 MHz, $CDCl_3$) δ (ppm): 173.4, 166.8, 156.0, 77.2, 70.5, 70.5, 70.2, 70.1, 69.6, 56.4, 56.1, 42.7, 41.9, 41.2, 40.4, 40.1, 37.9, 37.5, 35.7, 35.5, 34.9, 34.5, 33.7, 32.0, 31.9, 31.8, 29.7, 29.0, 28.4, 28.2, 26.9, 26.9, 26.4, 26.3, 24.1, 23.2, 22.8, 22.5, 20.8, 18.4, 12.0.

HR-MS (ES+): calcd. for $C_{41}H_{71}N_2O_8{}^{35}Cl^{23}Na$: 777.4785, found: 777.4791.

FT-IR (ATR): ν_{max} 3341, 2936, 2866, 1711, 1653, 1526, 1449, 1364, 1276, 1252, 1174 cm^{-1}.

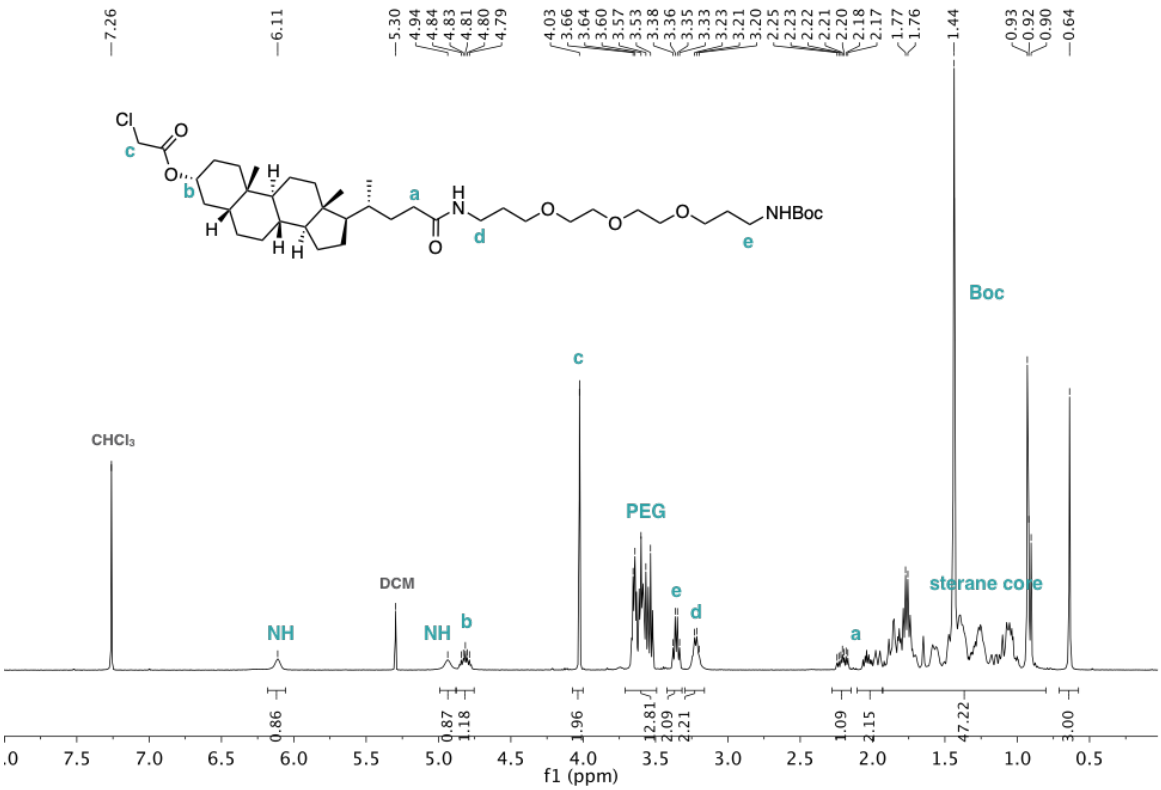

Figure S4.3 ^{1}H NMR spectrum of compound **4-6**.

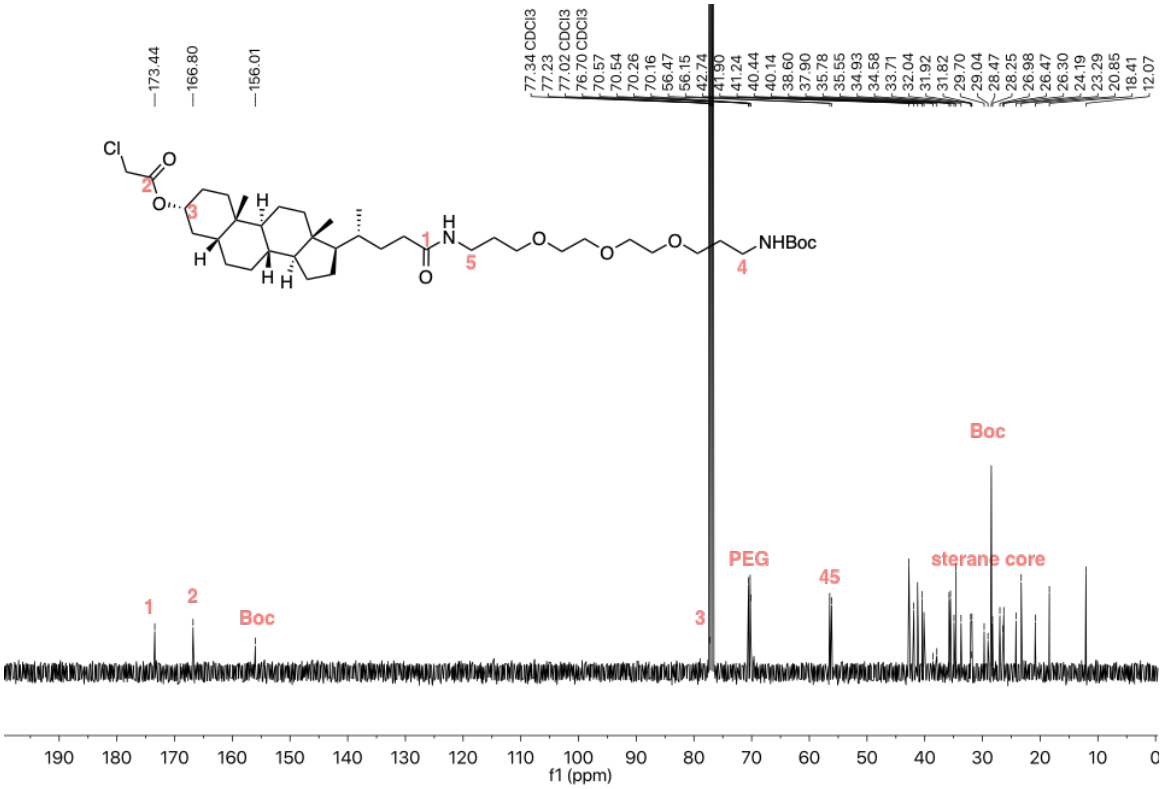

Figure S4.4 ^{13}C NMR spectrum of compound **4-6**.

Compound 4-8

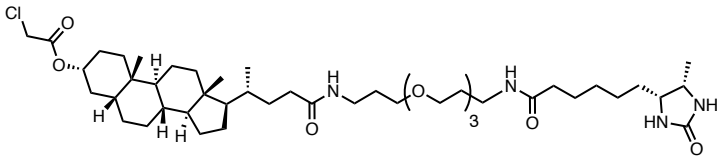

A solution of compound **4-6** (100 mg, 0.132 mmol) and 1 mL of trifluoroacetic acid in dichloromethane (10 mL) was stirred at room temperature for 2 h. The reaction mixture was evaporated and re-dissolved in dichloromethane (50 mL) before washed with sodium bicarbonate (sat., 20 mL × 3), brine (20 mL) and dried over anhydrous sodium sulfate. The solvent was evaporated, and the product was used directly in the next step. A solution of deprotected **4-6** (71 mg, 0.108 mmol), D-desthiobiotin **4-7** (26 mg, 0.119 mmol), EDC (18.5 mg, 0.119 mmol) and 4-dimethylaminopyridine (1 mg, cat.) in 5 mL of dichloromethane was stirred at room temperature overnight. The reaction mixture was diluted with 50 mL of dichloromethane, then washed with 1 M hydrochloric acid (20 mL × 3), sodium bicarbonate (sat., 20 mL), brine (20 mL) and dried over anhydrous sodium sulfate. The solvent was removed in vacuo and the crude was purified by flash chromatography (silica, methanol in dichloromethane 0 – 5%) to afford the product as a colorless oil (75 mg, 82%).

^{1}H NMR (400 MHz, $CDCl_3$) δ (ppm): 6.48 (s, 1H), 6.27 (s, 1H), 5.33 (s, 1H), 4.83 – 4.77 (m, 1H), 4.68 (s, 1H), 4.02 (s, 1H), 3.84 – 3.81 (m, 1H), 3.68 – 3.55 (m, 13H), 3.35 – 3.32 (m, 4H), 2.24 – 0.89 (m, 52H), 0.62 (s, 3H).

^{13}C NMR (100 MHz, $CDCl_3$) δ (ppm): 173.7, 172.9, 166.8, 163.4, 76.7, 70.5, 70.4, 70.4, 70.1, 70.0, 69.9, 56.4, 56.1, 56.0, 51.4, 42.7, 41.9, 41.3, 40.4, 40.1, 37.8, 37.6, 36.3, 35.7, 35.6, 34.9, 34.6, 33.7, 32.0, 31.9, 29.5, 29.1, 29.0, 28.9, 28.3, 27.0, 26.5, 26.3, 26.0, 25.4, 24.2, 23.3, 20.8, 18.4, 15.8, 12.1.

HR-MS (ES+): calcd. for $C_{46}H_{80}N_4O_8{}^{35}Cl$: 851.5639, found: 851.5641.

FT-IR (ATR): ν_{max} 3302, 2931, 2864, 1702, 1646, 1545, 1447, 1377, 1351, 1323, 1284, 1253, 1194, 1106, 1001 cm^{-1}.

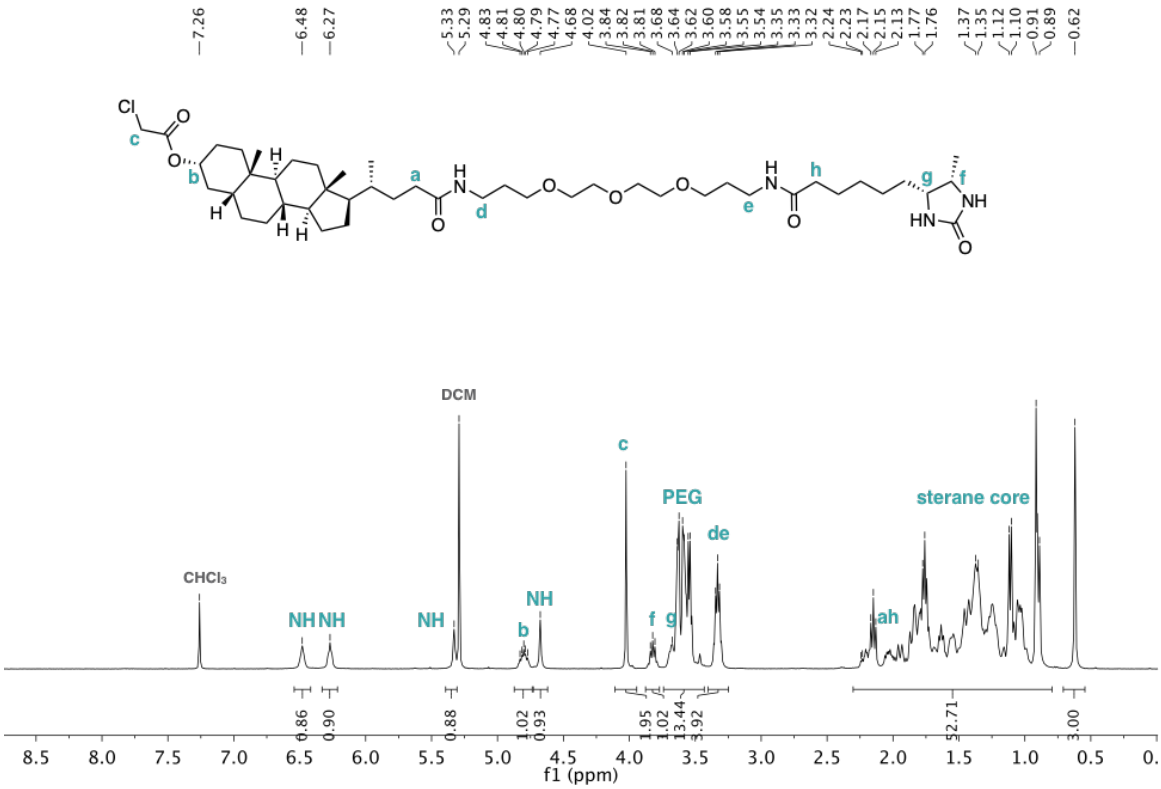

Figure S4.5 [1]H NMR spectrum of compound **4-8**.

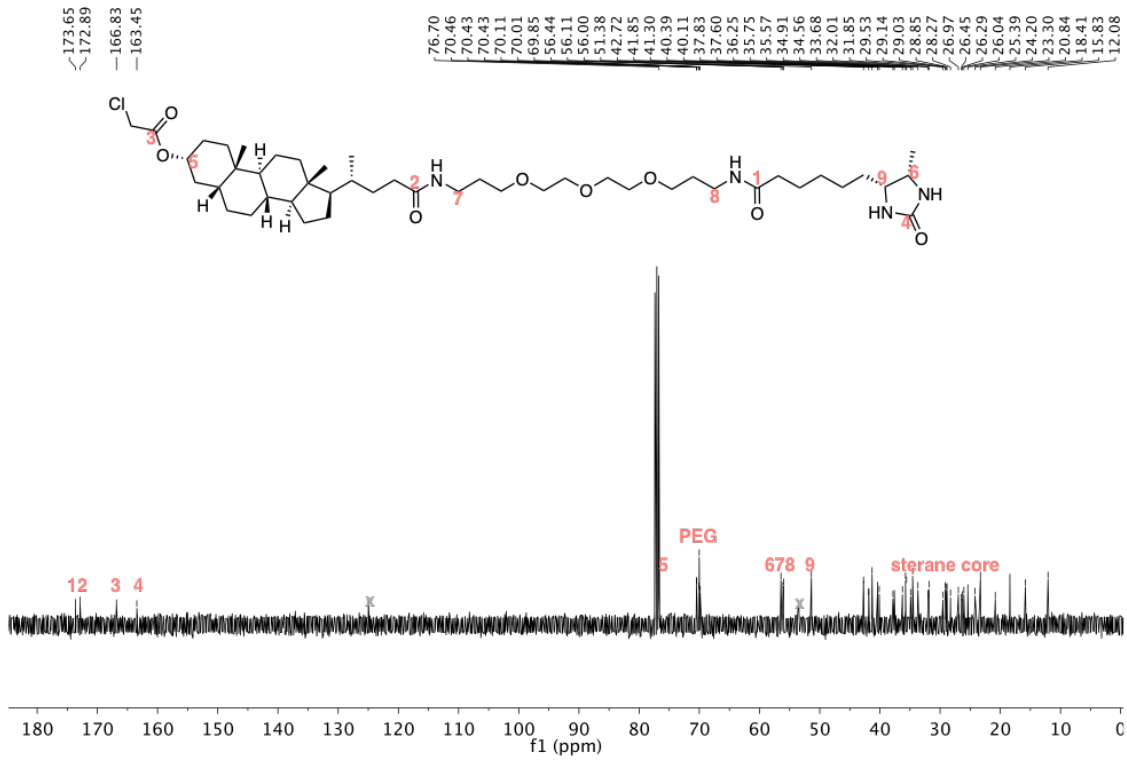

Figure S4.6 [13]C NMR spectrum of compound **4-8**.

Compound 4-9

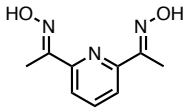

Compound **4-9** has been previously described.[2,3] A solution of 2,6-diacetylpyridine (100 mg, 0.613 mmol), hydroxylamine (104 mg, 1.53 mmol) and sodium hydroxide (61.2 mg, 1.533 mmol) in water/methanol:1/1 was refluxed overnight. The crude was filtered and recrystallized in methanol to afford a white solid as product (60 mg, 50%).

^{1}H NMR (400 MHz, DMSO-d_6) δ (ppm): 11.77 (s, 2H), 8.08-8.01 (m, 3H), 2.50 (s, 6H).
^{13}C NMR (100 MHz, DMSO-d_6) δ (ppm): 154.3, 153.5, 136.9, 119.2, 10.2. MS (ES+): 194.2 ($M\text{-}H^{+}$).
All characterization data match with literature.

Desthiobiotin transducer 4-1

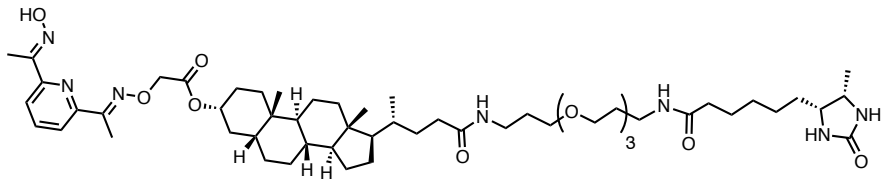

A solution of compound **4-9** (19 mg, 0.099 mmol) and potassium carbonate (2 mg, 0.164 mmol) in dimethylformamide (1 mL) was stirred at room temperature for 15 min and was added a solution of compound **4-8** (28 mg, 0.033 mmol) in dimethylformamide (1 mL). The reaction mixture was stirred at room temperature overnight. The reaction mixture was diluted with 50 mL of ethyl acetate and washed with hydrochloric acid (1M, 5 mL), lithium chloride (5% aq., 5 mL × 5), sodium bicarbonate (sat., 5 mL), brine (5 mL) and dried over anhydrous sodium sulfate. The solvent was removed and the product as a colorless oil (19 mg, 63%).

^{1}H NMR (400 MHz, $CDCl_3$) δ (ppm): 6.48 (s, 1H), 6.27 (s, 1H), 5.33 (s, 1H), 4.83 – 4.77 (m, 1H), 4.68 (s, 1H), 4.02 (s, 1H), 3.84 – 3.81 (m, 1H), 3.68 – 3.55 (m, 13H), 3.35 – 3.32 (m, 4H), 2.24 – 0.89 (m, 52H), 0.62 (s, 3H).

^{13}C NMR (100 MHz, $CDCl_3$) δ (ppm): 174.4, 174.4, 172.9, 169.8, 157.7, 153.8, 152.7, 152.6, 136.1, 120.1, 119.9, 75.1, 71.3, 70.5, 70.4, 70.2, 70.0, 70.0, 69.9, 56.4, 56.1, 55.7, 51.4, 42.6, 41.6, 40.4, 40.1, 37.9, 37.7, 36.3, 35.6, 35.4, 34.8, 34.6, 34.4, 33.2, 32.0, 31.8, 29.5, 29.1, 28.9, 28.2, 26.9, 26.4, 26.2, 26.1, 25.4, 24.1, 23.3, 20.7, 18.3, 15.8, 12.0, 11.2, 10.3.

HR-MS (ES-) calcd. for $C_{55}H_{89}N_7O_{10}$: 1007.6671, found: 1007.6661.

FT-IR (ATR): ν_{max} 3302, 2931, 2864, 1702, 1646, 1545, 1447, 1377, 1351, 1323, 1284, 1253, 1194, 1106, 1001 cm^{-1}.

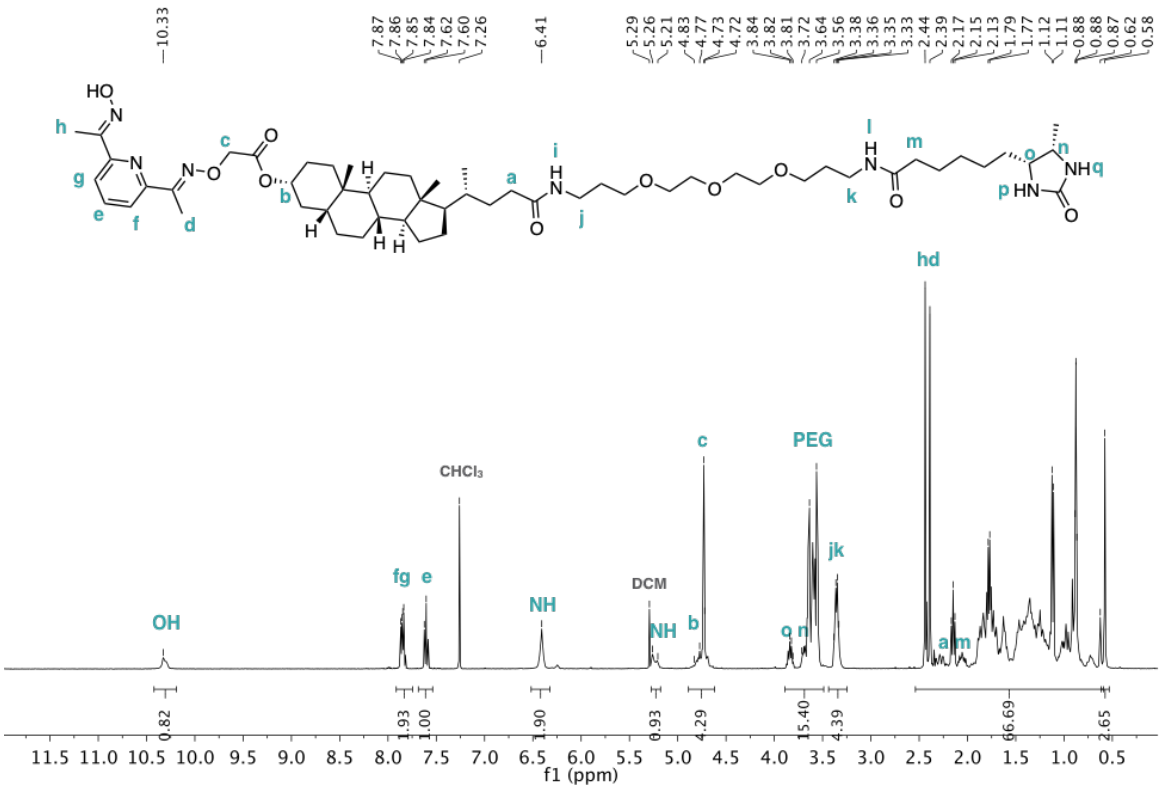

Figure S4.7 ^{1}H NMR spectrum of desthiobiotin transducer **4-1**.

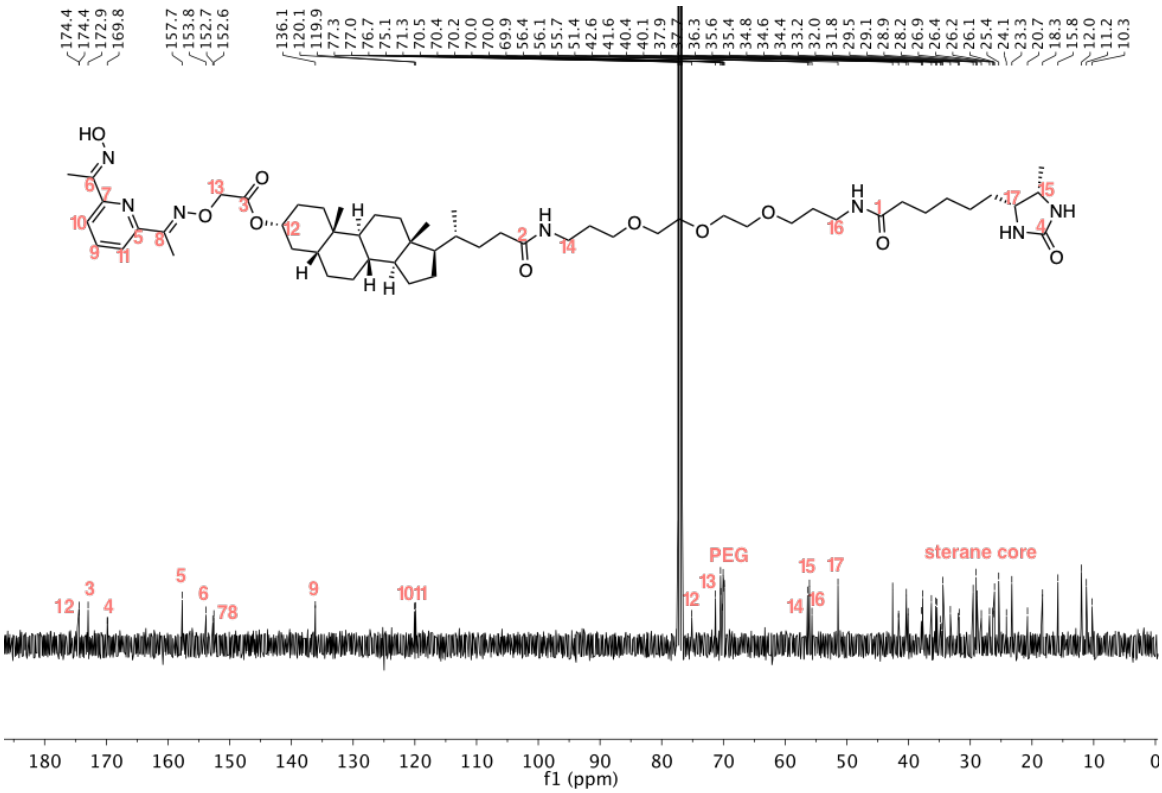

Figure S4.8 ^{13}C NMR spectrum of desthiobiotin transducer **4-1**.

Biotin derivative 4-10

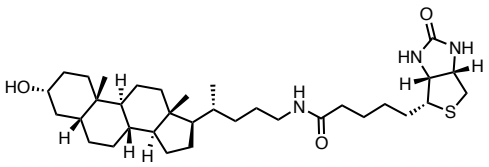

A reaction mixture of compound **4-12** (50.0 mg, 0.138 mmol), D-biotin (30.5 mg, 0.124 mmol), EDC (39.7 mg, 0.207 mmol), 4-dimethylaminopyridine (1 mg, cat.) in dimethylformamide (2 mL) was stirred at room temperature overnight. The reaction mixture was diluted with 50 mL of ethyl acetate, washed with hydrochloric acid (1 M, 5 mL), lithium chloride (5% aq., 5 mL × 5), sodium bicarbonate (sat., 5 mL), brine (5 mL), and dried over anhydrous sodium sulfate. After evaporation of solvent, the crude was purified by flash chromatography (basic alumina, methanol in dichloromethane: 0 – 10%) to afford the product as a colorless gel (39 mg, 54%).

^{1}H NMR (400 MHz, $CDCl_3$) δ (ppm): 6.30 (s, 1H), 6.00 (t, ^{3}J = 5.8 Hz, 1H), 5.52 (s, 1H), 4.50 (dd, ^{3}J = 7.4, 4.9 Hz, 1H), 4.30 (dd, ^{3}J = 7.4, 4.9 Hz, 2H), 3.64 – 3.58 (m, 1H), 3.25 – 3.12 (m, 2 H), 2.91 (dd, ^{3}J = 12.8, 4.9 Hz, 1H), 2.74 (d, ^{3}J = 12.8 Hz, 1H), 2.19 (t, ^{3}J = 7.4 Hz, 2H), 1.96 – 0.89 (m, 41H), 0.63 (s, 3H).
^{13}C NMR (100 MHz, $CDCl_3$) δ 173.0, 163.7, 71.7, 61.8, 60.1, 56.5, 56.0, 55.5, 42.6, 42.0, 40.6, 40.4, 40.2, 40.0, 36.4, 36.1, 35.8, 35.4, 35.3, 34.5, 33.1, 30.5, 28.3, 28.2, 28.1, 27.1, 26.4, 26.1, 25.7, 24.2, 23.3, 20.8, 18.6, 12.0.
HR-MS (MS+): calcd. for $C_{34}H_{57}N_3O_3S$: 587.4121, found: 587.4112.
FT-IR (ATR): ν_{max} 3271, 2925, 2860, 1696, 1643, 1551, 1449, 1375, 1365, 1330, 1306, 1262, 1214, 1163, 1068, 1037 cm^{-1}.

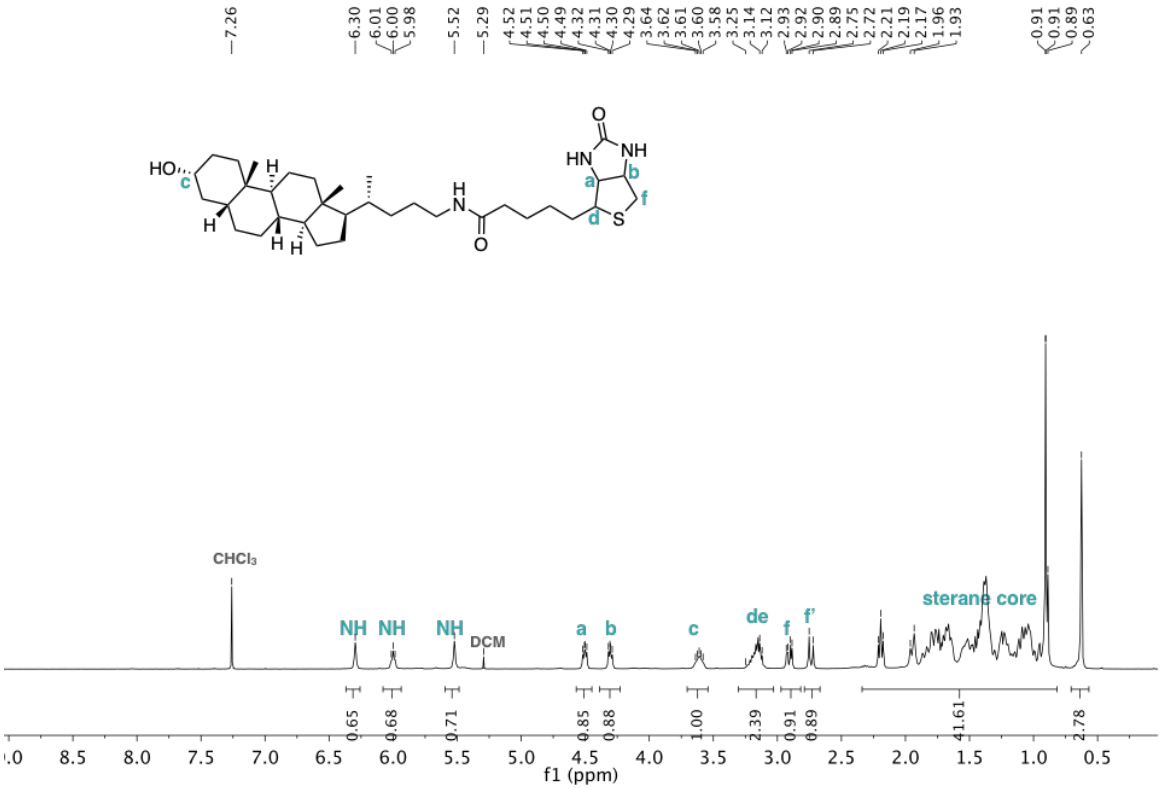

Figure S4.9 ^{1}H NMR spectrum of biotin derivative **4-10**.

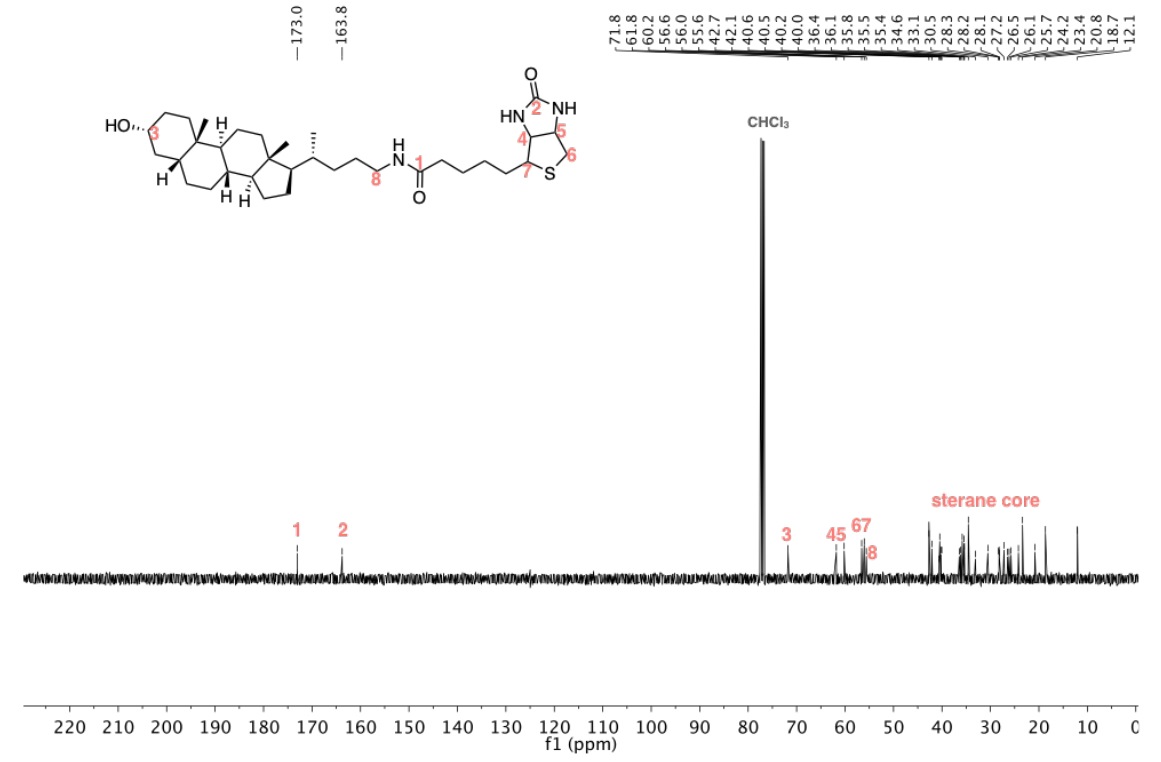

Figure S4.10 ^{13}C NMR spectrum of biotin derivative **4-10**.

Compound 4-11

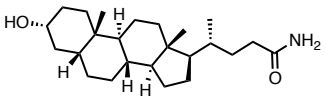

Compound **4-11** has been previously described.[4] To a solution of lithocholic acid (3.0 g, 7.97 mmol) and triethylamine (1.6 mL, 11.5 mmol) in tetrahydrofuran was added ethyl chloroformate (2 mL, 21.0 mmol) with external cooling. The reaction was further stirred at room temperature for 15 min. Cold concentrated ammonium hydroxide was added with external cooling until pH is basic. The precipitate was filtered, washed with cold water, and dried in vacuo to afford the product as a white solid (3.0 g, quant.).

^{1}H NMR (400 MHz, DMSO-d_6) δ (ppm): 7.22 (br, 2H), 6.64 (br, 1H), 3.40 – 3.33 (m, 1H), 2.09-0.87 (m, 34H), 0.61 (s, 3H).
HR-MS (MS-): calcd. for $C_{24}H_{41}NO_2$: 375.3137, found: 375.3142.
FT-IR (ATR): ν_{max} 3379, 3214, 2930, 2863, 1665, 1626, 1446, 1407, 1377, 1334, 1303, 1252, 1189, 1167, 1088, 1069, 1044 cm^{-1}.
All characterization data match with literature.

Compound 4-12

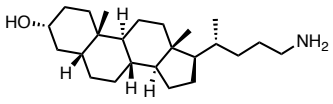

Compound **4-12** has been previously described.[4] To a solution of lithium aluminum hydride in tetrahydrofuran (1M, 20 mL) was added a solution of compound 4-11(2.5 g, 6.65 mmol) in tetrahydrofuran (100 mL), and the reaction mixture was refluxed overnight. The reaction mixture was diluted with 80 mL of ethyl acetate, and was added water (0.76 mL), sodium hydroxide (15% aq., 0.76 mL), water (2.28 mL), in this order respectively and stirred for 15 min. Anhydrous magnesium sulfate was added and the reaction mixture was stirred for further 15 min. The product was filtered, washed with cold water, dried in vacuo to afford the product as a pale yellow solid (2.0 g, 83%).

^{1}H NMR (400 MHz, DMSO-d_6) δ (ppm): 3.65 – 3.60 (m, 1H), 2.04 – 0.92 (m, 37H), 0.64 (s, 3H).
HR-MS (MS+): calcd. for $C_{24}H_{43}NO$: 361.3345, found: 361.3341.
FT-IR (ATR): ν_{max} 2935, 2860, 1579, 1564, 1548, 1461, 1446, 1375, 1365, 1067, 1057, 1013 cm^{-1}.
All characterization data match with literature.

4.4.3 Vesicle Experiments

General protocol for vesicle preparation

To a 1.5 mL microcentrifuge tube was added a chloroform solution of lipids (DOPC/DOPE in a 3:2 ratio) in order to obtain a final lipid concentration of 1 mM in 3.5 mL (final elution volume). The solvent was evaporated using a dry nitrogen stream and dried under high vacuum for at least 2 h to yield a thin lipid film. To the microcentrifuge containing the lipids was added 0.5 mL of 25 mM HEPES 150 mM NaCl buffer at pH 7, as well as stock solutions of ester substrate and zinc chloride as appropriate to reach final concentrations of 250 µM. After swelling for 1 min, the suspension was subjected to 5 cycles of freeze-thaw using liquid nitrogen and 35 °C water bath. The suspension was extruded for 19 times through a 200 nm polycarbonate filter in an extruder apparatus, and then the vesicles were separated by a bulk solution using prepacked SEC columns eluting with the same HEPES buffer at pH 7. Vesicles suspensions can be further diluted using HEPES buffer to 0.1 mM lipid concentration.

Fluorescence Measurements

Substrate **4-2** hydrolyses slowly in water, and there is some batch to batch variation in the background rate of hydrolysis inside vesicles, so a separate control experiment was carried out for each kinetic run. For each fluorescence experiment, a sample of the same batch of vesicles containing **4-2** was monitored to measure the background hydrolysis rate in the absence of any catalysis. These data were subtracted from the fluorescence data recorded in the catalysis experiment to remove the effects of background hydrolysis. At the end of the experiment, 5% Triton X-100 (50 µL) and 1M NaOH (50 µL) was added to lyse the vesicles and hydrolyze all of the remaining substrate **4-2**. The emission measured at this end point was used to normalize the data taking into account of the dilution factor.

ON State

To a 1 mL fluorescence cuvette was added 800 µL of 0.1 mM vesicles described above. 1 mM **4-1** solution in DMSO was added to the vesicles suspension to reach 10 mol% loading of **4-1** relative to lipids.

OFF State

NeutrAvidin•**4-1** 1:4 complex solution was prepared by adding 4 eq. of **4-1** (1 mM DMSO solution) to 16.7 µM protein solution in HEPES buffer. To a 1 mL fluorescence cuvette was added 800 µL of 16.7 µM NeutrAvidin•**4-1** 1:4 complex solution in HEPES buffer. 1 mM 200 nm DOPC/DOPE:3/2 vesicles containing 250 µM substrate **4-2** and 250 µM zinc chloride in 25 mM HEPES 150 mM NaCl was added to the cuvette to reach a final lipid concentration of 0.1 mM.

ON—OFF Switching

To a 1 mL fluorescence cuvette was added 800 µL of 0.01 mM 200 nm DOPC/DOPE:3/2 vesicles containing 250 µM substrate **4-2** and 250 µM zinc chloride in 25 mM HEPES 150 mM NaCl. 0.1 mM Transducer **4-1** solution in DMSO was added to the vesicle suspension using Hamilton syringes to reach 10 mol% loading of **4-1** relative to lipids. After 100 minutes, 83.3 µM NeutrAvidin solution in HEPES buffer was added to reach a final protein concentration of 2 µM (2 eq. relative to **4-1**).

Attempted OFF-ON Switching with Biotin

To the OFF State vesicles described above was added 1 mM biotin solution in HEPES buffer to reach 66.8 µM final concentration of biotin (4 eq. relative to NeutrAvidin).

OFF-ON Switching with Biotinylated Vesicles

To the OFF State vesicles described above was added 1 mM (lipid concentration) of biotinylated vesicles to reach 66.8 µM of 10 in final bulk concentration, 4 eq. relative to NeutrAvidin. Biotinylated vesicles were prepared in the same manner with 10 mol% of biotin derivate **4-10** in the chloroform solution of lipids. Flocculation occurs in this experiment, but the timescale is hours and is variable. The results presented are for at least three repetitions of the experiment before flocculation occurred.

References

(1) Dahmani, I.; Ludwig, K.; Chiantia, S. Influenza A Matrix Protein M1 Induces Lipid Membrane Deformation via Protein Multimerization. *Biosci. Rep.* **2019**, *39* (8), BSR20191024. https://doi.org/10.1042/BSR20191024.

(2) Aakeröy, C. B.; Sinha, A. S. Synthesis of Ketoximes via a Solvent-Assisted and Robust Mechanochemical Pathway. *RSC Adv.* **2013**, *3* (22), 8168–8171. https://doi.org/10.1039/C3RA40585K.

(3) Glynn, C. W.; Turnbull, M. M. Complexes of 2,6-Diacetylpyridine Dioxime (DapdoH2). Crystal Structures of [M(DapdoH2)2](ClO4)2 (M=Cu and Mn). 10.

(4) Joachimiak, R.; Piasecka, M.; Paryzek, Z. Synthesis of Novel Amide-Linked Dimers of Lithocholic Acid. *J. Chem. Res.* **2008**, *2008* (5), 260–265. https://doi.org/10.3184/030823408X318325.

This page is intentionally left blank

The truth is rarely pure and never simple.

Oscar Wilde

5

Galactose Transducer

5.1 Introduction

Cell signalling is a fundamental process by which cells communicate with other cells via their microenvironments. The majority of enzymes are involved with cell signalling pathways and enzyme-linked receptors response to extracellular signal proteins that promote the growth, proliferation, differentiation, and many other functions of cells.[1] The catalytic activity of enzymes also amplifies the signal detected by a single receptor. For example, upon activation, one adenylyl cyclase can produce a large quantity of cyclic adenosine monophosphate (cAMP) molecules. These so-called secondary messengers can further activate downstream signalling proteins (such as glycogen phosphorylase) and, after multiple enzymatic reactions with intermediate protein kinases, lead to catalytic production of as many as tens of thousands of glucose molecules in the cell.[2]

β-Galactosidase is an important enzyme for human and many other animals as it hydrolyses the β-galactosidic bond of lactose to galactose and glucose, providing energy to cells. The enzymatic cleavage reaction catalysed by β-galactosidase is highly efficient – one individual protein can hydrolyse several thousand substrate molecules per minute.[3] Although lactose would probably be the natural substrate of β-galactosidase, the enzyme is promiscuous for the non-galactose part of the substrate.[4] In general, any structure that has β-D-galactopyranosides with an oxygen glycosidic bond can be catalysed for hydrolysis by β-galactosidase.

We have recently reported a novel transmembrane signalling mechanism, which operates by controlled translocation of a synthetic transducer across a vesicle lipid bilayer.[5,6] The external recognition head group of the transducer becomes membrane-permeable in response to an external chemical stimulus, which leads to membrane translocation, exposing a catalytic head group to the interior of the vesicle. Catalytic hydrolysis of an internal substrate generates an amplified output signal. In this chapter, we report the studies of an artificial transmembrane signalling system that responds to β-galactosidase as the input signal, which operates by using transducers which consist of β-galactose unit as recognition head group, see Figure 5.1. The galactose head group is hydrophilic and membrane-impermeable, locking the transducer at the external surface of the vesicles. In the presence of the enzyme, the *O*-glycosidic bond of the transducer should be cleaved at the membrane surface and reveal a neutral phenol head group. The new head group is considerably less hydrophilic, leading to translocation of the transducer across the membrane and exposing a catalytic head group to the interior of the vesicle. Upon cofactor (zinc ion) binding, the catalytic head group is activated and hydrolyses an internal substrate, generating an amplified output signal.

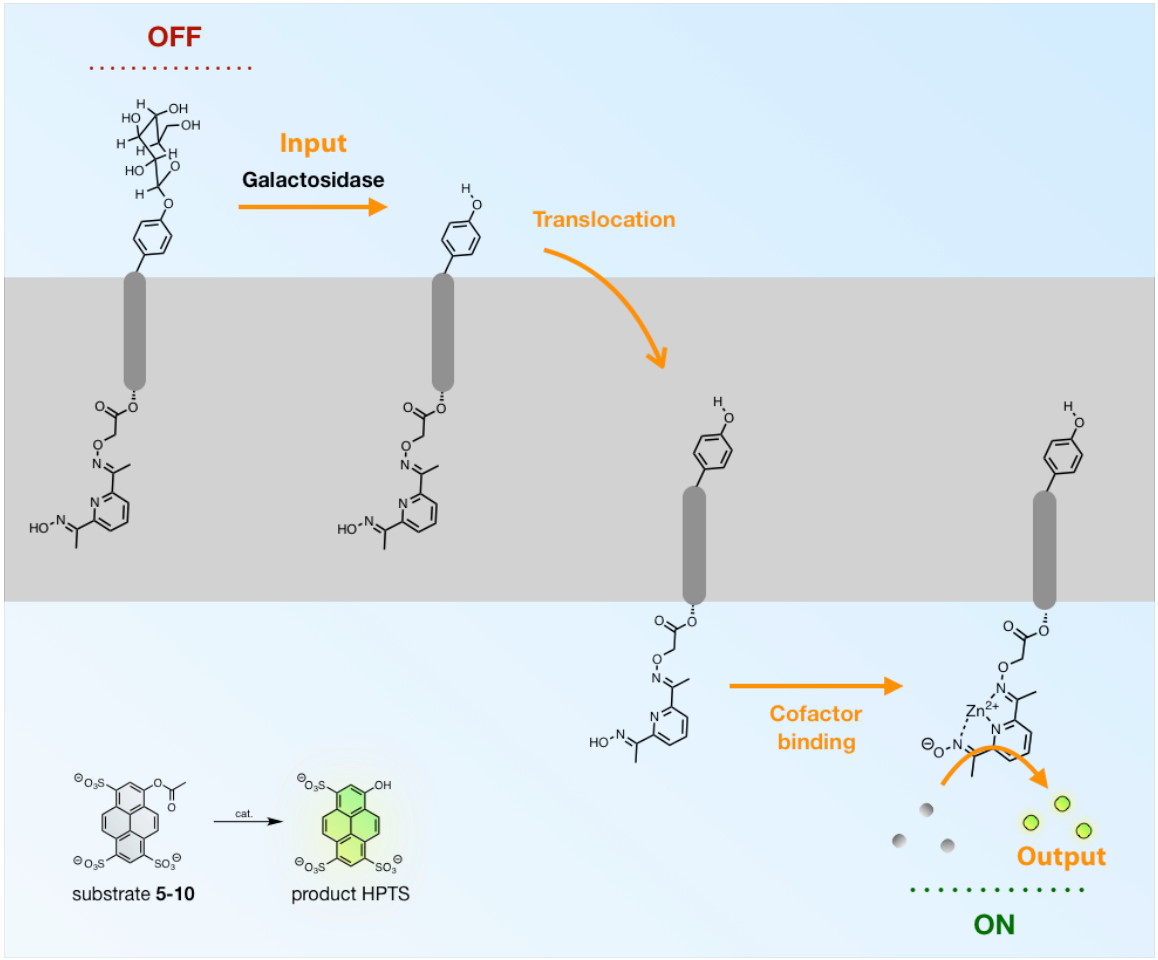

Figure 5.1 Concept of β-galactose transducer transmembrane signalling. Galactose unit is hydrophilic and membrane-impermeable, achieving the OFF state of β-galactose transducer. Enzymatic cleavage of the β-

galactose yields membrane-permeable transducer with a phenol unit and initiate the translocation. Cofactor binding from the internal solution turns ON the catalytic hydrolysis of the encapsulated substrates (grey, non-fluorescent, substrate **5-10**) and generates an amplified output (green, fluorescent, HPTS).

5.2 Results and Discussion

5.2.1 Synthesis of Short/Long Galactose, Phenol, and Hydrazide Transducers

Hydrazides are aldehyde-reactive chemical groups commonly used in biomolecular probes for labelling and crosslinking carbonyls on biomacromolecules such as glycoproteins and polysaccharides.[7] Hydrazide reacts with aldehydes in acidic conditions to form a sufficiently stable conjugate for most biological applications. Dr Istvan Kocsis successfully synthesised two hydrazide transducers: a short hydrazide transducer **5-1**, and a long transducer **5-4** with a polyethylene glycol linker (unpublished results). Both transducers have a hydrazide head group on one end, opposite to the catalytic head group. The synthesis of these two transducers is shown in the Supporting Information. We then used these transducers as precursors for β-galactose transducers.

To use the hydrazide-aldehyde reaction to attach a galactose unit onto the hydrazide transducers, we synthesised β-galactose-*O*-benzaldehyde **5-9** in two steps from 4-hydroxybenzaldehyde, see Scheme 5.2. Condensation with acetobromo-α-D-galactose gave acetyl protected intermediate **5-8**. Hydrolysis with sodium methoxide gave the desired compound **5-9**. Reaction between β-galactose-*O*-benzaldehyde **5-9** and hydrazide transducers **5-1** and **5-4** was done in ethanolic solutions with catalytic amount of acetic acid. Similarly, 4-hydroxybenzaldehyde was used to obtain phenol transducers which are the equivalent of the enzymatic hydrolysis products. The reactions were monitored by LC-MS to ensure that all hydrazide starting materials were consumed (see Supporting Information). As galactose-aldehyde derivative **5-9** is highly water-soluble and does not become involved in the hydrolysis reaction, the excess amount of **5-9** was not separated from the product.

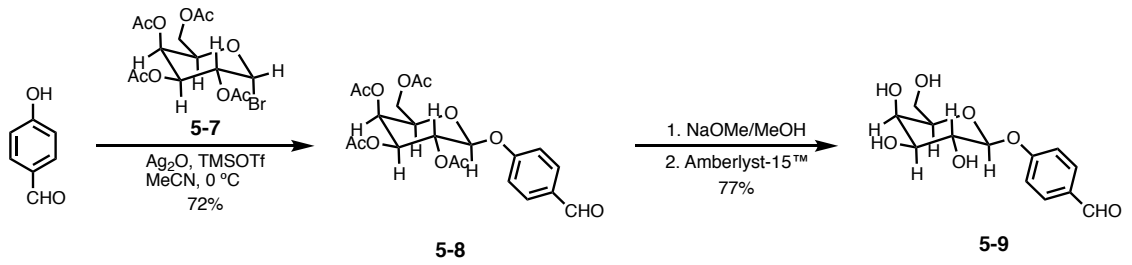

Scheme 5.1 Synthesis of β-galactose-*O*-benzaldehyde derivative **5-9**.

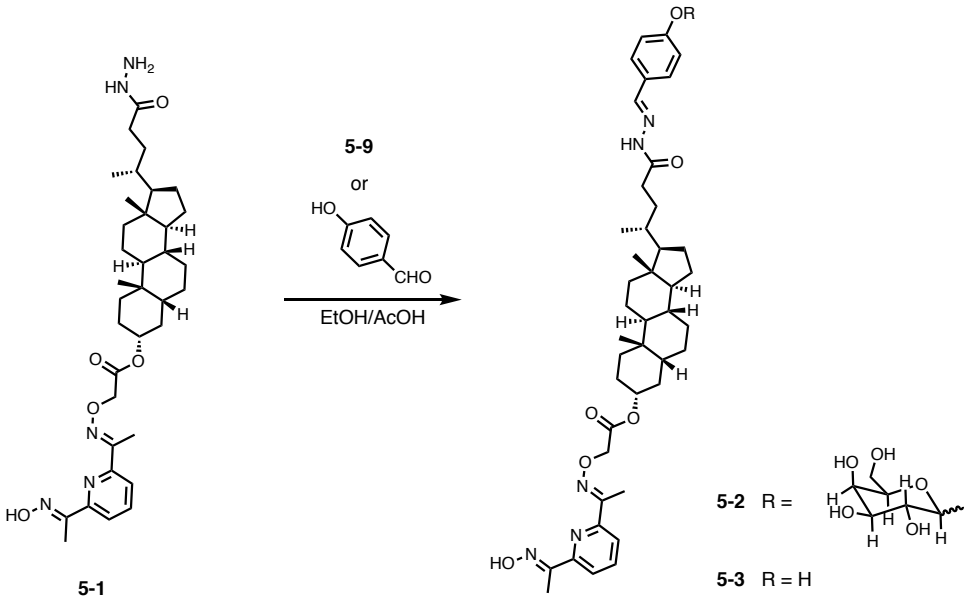

Scheme 5.2 Illustration of the conjugation reaction of short β-galactose transducer **5-2** and short phenol (ON state galactose) transducer **5-3**.

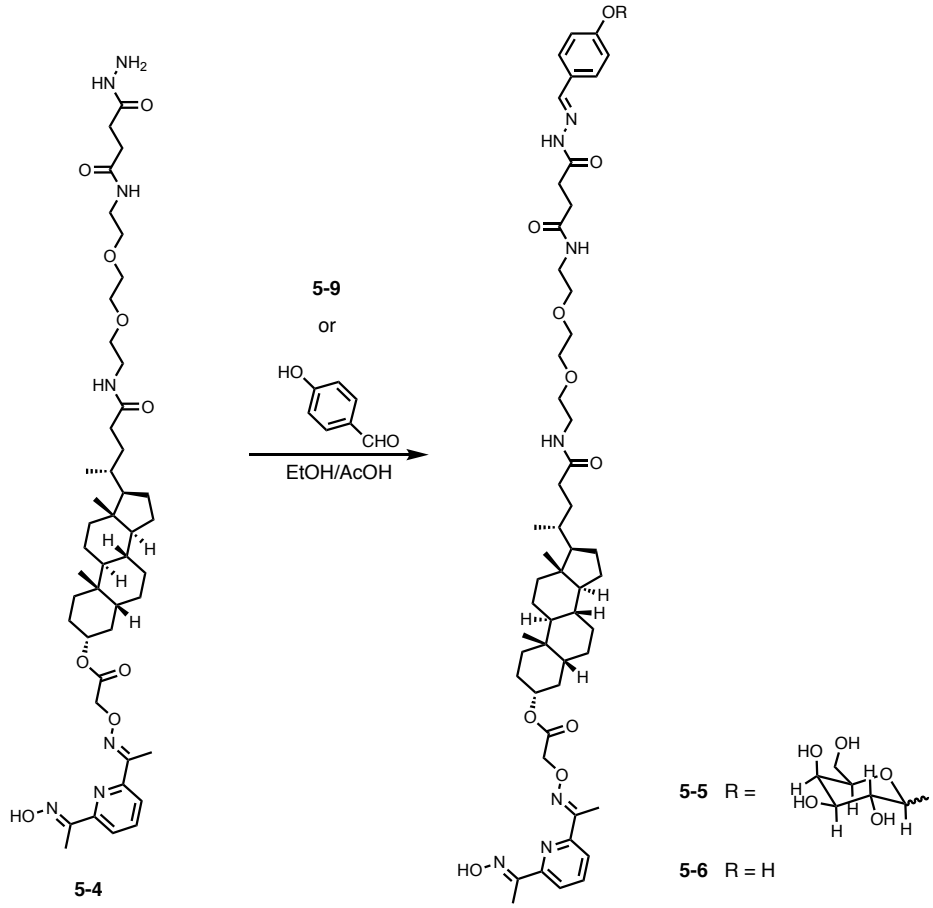

Scheme 5.3 Illustration of the conjugation reaction of long β-galactose transducer **5-5** and long phenol (ON state galactose) transducer **5-6**.

5.2.2 Transmembrane Signalling experiments

5.2.2.1 Signalling experiments with short transducers

There are two ways to load transducer onto vesicle membranes: pre-incorporation and external addition. For the pre-incorporation method, the transducer was mixed with lipids in organic solvents before rehydration and extrusion. This should give a statistical 50/50 distribution of transducer at both leaflets of the membrane. As for external addition method, the transducer was dissolved in water-miscible organic solvents such as methanol or dimethyl sulfoxide (DMSO) and this solution was added externally to the vesicle suspensions after extrusion and purification. We discovered that membrane-embedded transducer might act as a cation transporter to carry Zn^{2+} across the membrane. In order to distinguish the catalytic activity from the metal transport ability of transducers, we have designed experiments to decouple the two process and examine each of them individually.

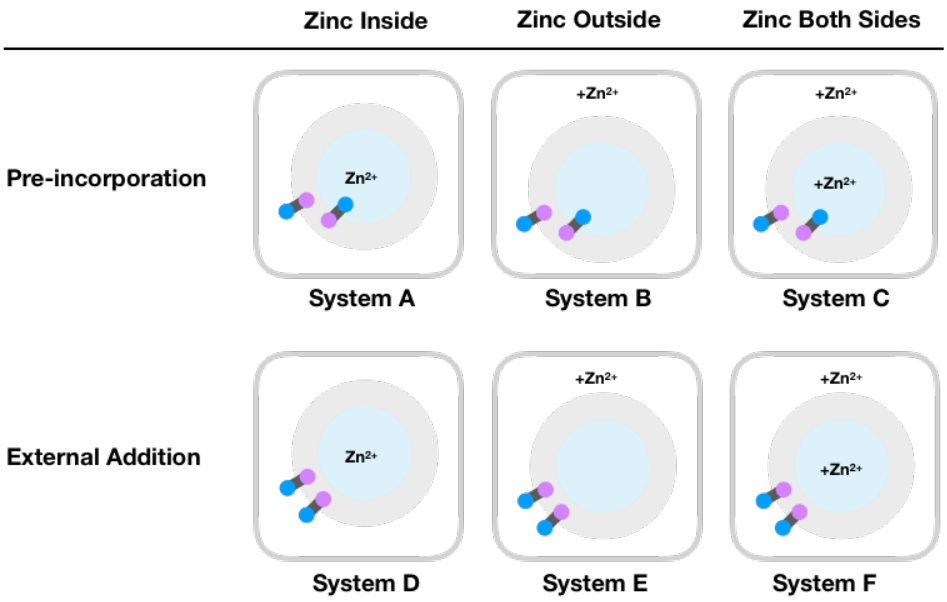

Figure 5.2 Schematic illustration of vesicles signalling experiments. Transducer loading techniques: pre-incorporation or external addition. Zinc chloride: no zinc inside (added at rehydration of lipids), zinc outside (added after vesicles were purified), or zinc both sides.

There are six possible ways to assemble the signalling systems, see Figure 5.2. The ways of loading of Zn^{2+} in the system could be one of the following:

1) Zn^{2+} only encapsulated inside the vesicles. This can be achieved by adding zinc chloride at the lipid rehydration stage; or

2) Zn^{2+} only in the extravesicular solution. This can be achieved by external addition of zinc chloride to a vesicle suspension; or

3) Zn^{2+} on both sides of the membrane.

There are two ways of loading transducer into lipid bilayers:

1) Pre-incorporating transducer. It is important to note that this pre-incorporation method should give a statistical 50/50 distribution of transducer at both leaflets of the membrane; or

2) External addition of transducers in DMSO to vesicle suspensions. This would result in an initial loading of transducers at only the outer leaflet of the membrane.

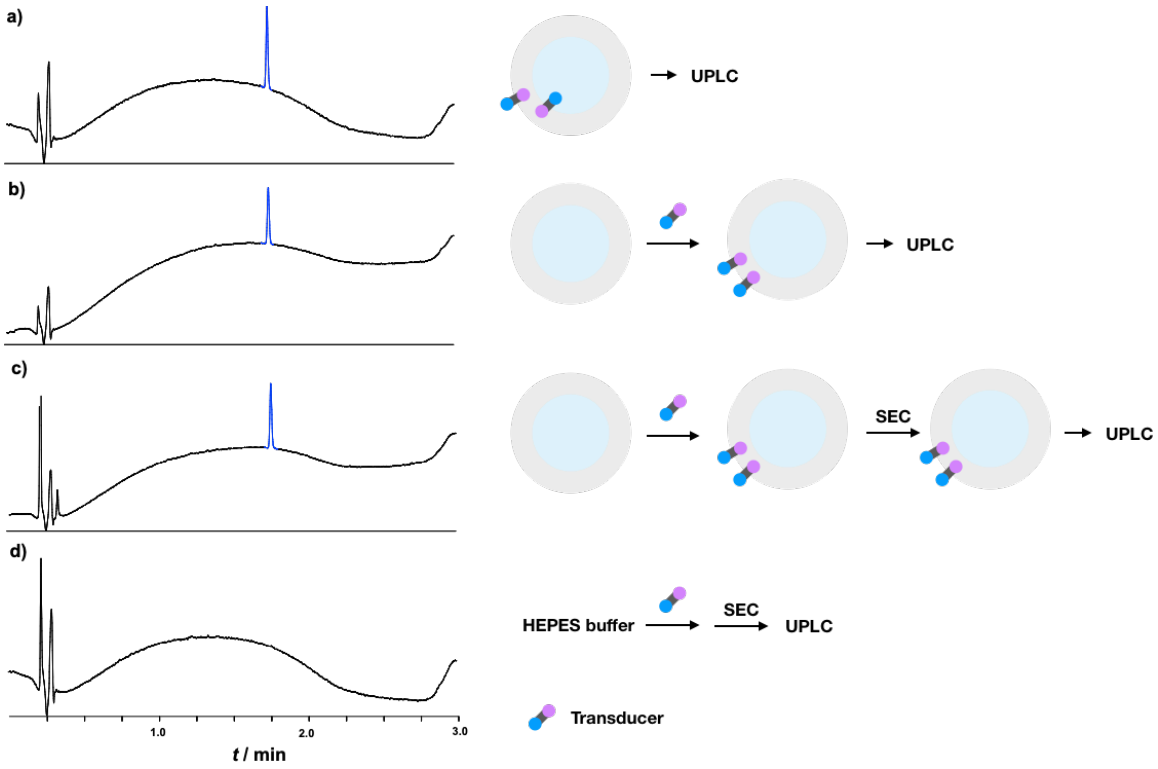

Figure 5.3 Transducer loading test. UPLC traces of short β-galactose transducer **5-2** (retention time: 1.81 min). a) Pre-incorporation of 5 mol% transducer in 1 mM 200 nM POPC vesicles in HEPES buffer. b) external addition of 5 mol% of transducer in DMSO to 1 mM 200 nM POPC vesicles suspension. c) vesicles with external addition of 5 mol% of transducer after size exclusion chromatography. This figure is scaled up to reflect on the dilution factor (dilution factor = 2, for 0.5 mL loading volume and 1 mL elusion volume of SEC). d) A control experiment with the same amount of transducer added to HEPES buffer (without vesicles) and after size exclusion chromatography. Column: ACQUITY UPLC® CSH C18, 2.1x 50 mm, 1.7 µm, 130 Å. Solvent A: 2 mM ammonium acetate in water/acetonitrile (95:5); Solvent B: acetonitrile. Gradient: 5-95% B over 1 min. Flow rate: 0.6 mL/min. This experiment was done in collaboration with Dr Istvan Kocsis.

Together with Dr Istvan Kocsis, we proved that transducer could be incorporated into membrane with both loading techniques, see Figure 5.3. 1 mM 1-palmitoyl-2-oleoyl-glycero-3-phosphocholine (POPC) vesicles were prepared with pre-incorporation and external loading (5 mol% relative to lipid) of galactose transducer **5-2** and the vesicles were directly injected into UPLC with C18 column, traces see Figure 5.3a and 5.3b, respectively. The signal at t = 1.81 (blue) is the UV absorption of transducer **5-2**. The sample using external addition method was further purified by size exclusion chromatography, and the resulting vesicles suspension

was re-injected into UPLC (Figure 5.3c). No significant loss of transducer was observed as the absorption level is the same before and after the size exclusion chromatography (SEC). Addition of transducer **5-2** to HEPES buffer led to precipitation and after SEC the transducer is eliminated from the solution, therefore no signal was seen in Figure 5.3d.

Before conducting any experiments, we can predict possible outcomes of the above-mentioned systems based on several general assumptions:

Premise 1. Substrate **5-10** and Zn^{2+} are charged and do not cross the lipid bilayer membrane;

Premise 2. Catalytic hydrolysis of substrate **5-10** must arise from the zinc-bound pyridine-oxime head group of transducers, provided that there is no pH change in the system);

Premise 3. The zinc(II)-binding of the pyridine-oxime head group should follow a standard binding isotherm, and a higher Zn^{2+} concentration results in higher molar fraction of zinc-bound pyridine-oxime compared to unbound pyridine-oxime, leading to higher catalytic hydrolysis activity.

Therefore, based on these premises we can infer that:

Inference 1. To catalytically hydrolyse the Substrate **5-10** (achieving an ON state), the pyridine-oxime head group must be present at the inner surface of the membrane;

Inference 2. To catalytically hydrolyse the Substrate **5-10** (achieving an ON state), the Zn^{2+} concentration inside the vesicles must be high enough to allow some of pyridine-oxime head group of the transducer to be active.

According to literature[8], the binding constant for Zn^{2+} and pyridine-dioxime $K = 4.1 \times 10^4$ M^{-1} at pH 7. Assuming the same binding constant is the same in vesicles, at 250 μM $ZnCl_2$, 90% of the pyridine-oxime head group should bind to Zn^{2+}. If Zn^{2+} transport across the takes place, this would dilute the internal Zn^{2+} concentration ~ 500 times (for 0.1 mM POPC 200 nm vesicles), resulting only 2% zinc(II)-bound pyridine-oxime head group being active in the system. Therefore, Zn^{2+} transport would switch the system to the OFF state if there is no Zn^{2+} outside the vesicles, even when translocation of transducer takes place.

For six system setups described in Figure 5.2, each of the system could be either ON or OFF. This leads to $2^6 = 64$ total combinations of results on a particular transducer. For better clarity, we assigned each set of results with a binary code where "0" represents the signalling system is OFF compared to the background whilst "1" represents ON, see table 5.1. For example, code 011000 represent the following set of results: System A – OFF, System B – ON, System C – ON, System D – OFF, System E – OFF, System F – OFF. However, not all of the outcomes are logical and actually the vast majority are not possible. We can quickly rule out systems that are not logical by examining the following contradictions:

Contradiction 1. E1F0: According to Premise 3, if external addition of zinc chloride to vesicles suspension generates an ON state (E1), having zinc chloride on both sides of the membranes must generate an ON state (F1). This is because, for the same loading of the transducer, the internal Zn^{2+} concentration in System E must be less than or equal to that in System F. Therefore, E1F0 is not a logical outcome;

Contradiction 2. D1F0: For the same reasons in Contradiction 1, if external addition of transducer to vesicles encapsulating zinc chloride generates an ON state (D1), adding transducer to a system with zinc chloride on both sides of the membranes must generate an ON state (F1);

Contradiction 3. C0F1: If external addition of transducer to vesicles generates an ON state (F1), the same system must be ON if the transducer is pre-incorporated (C1). This is because, according to Inference 1, the transducer must cross the membrane to the inner surface of vesicles to achieve an ON state in System F. As pre-incorporation of vesicles gives 50/50 distribution of transducer directly in both leaflets of membranes, System C must be ON. Therefore, C0F1 is not a logical outcome;

Contradiction 4. B0E1: For the same reasons in Contradiction 3, if external addition of transducer and zinc chloride to vesicles generates an ON state (E1), external addition of zinc chloride to vesicles with pre-incorporated transducer must be ON (B1).

Contradiction 5. A1B1: If external addition of zinc chloride to vesicles with pre-incorporated transducer generates an ON state (B1), transport of Zn^{2+} must take place in System A, B and C. Thus internally loaded Zn^{2+} in System A must be able to be transported to the outside of the vesicles, resulting a 500 times dilution in Zn^{2+} concentration as discussed before. This will turn the system to OFF state (A0). Therefore, A1B1 is not a logical outcome;

Contradiction 6. D1E1: If external addition of transducer and zinc chloride to vesicles generates an ON state (E1), transducer can cross the membrane as well as transport Zn^{2+}. As discussed above, internal Zn^{2+} concentration in System D must be diluted that the system is OFF (D0). Therefore, D1E1 is not a logical outcome;

Contradiction 7. A0B0C1: For the same reasons in Contradiction 5, A0C1 means the system can transport Zn^{2+}. Therefore, System B must be ON (B1) as externally added Zn^{2+} should be transported into the vesicles.

Contradiction 8. B1E0F1: As discussed above, F1 means transducer can cross the membrane, B1 means transducer can transport Zn^{2+}, therefore System E must be ON (E1).

 Pre-incorporation of transducer: System A (zinc inside), System B (zinc outside), System C (zinc both sides); External addition of transducer: System D (zinc inside), System E (zinc outside), System F (zinc both sides).

Taking into account of these contradictions, a summary of these predictions is shown in Table 5.1. Apart from **Entry 0** (000000) where the transducer is inactive in all systems, there are in total four possible outcomes:

Entry 24 (011000): Membrane pre-incorporated transducer can transport Zn^{2+} but transducer cannot cross the membrane. Whether externally loaded transducer can transport Zn^{2+} cannot be determined;

Entry 27 (011011): Transducer can cross the membrane as well as transport Zn^{2+};

Entry 40 (101000): Membrane pre-incorporated transducer cannot transport Zn^{2+}, neither can it cross the membrane. Whether externally loaded transducer can transport Zn^{2+} cannot be determined;

Entry 45 (101101): Membrane pre-incorporated transducer cannot transport Zn^{2+} but transducer can cross the membrane.

We then conducted signalling experiments with three short transducers in hand, namely short galactose transducer **5-2**, short hydrazide transducer **5-1**, and short phenol (ON state galactose) transducer **5-3**. The results are shown in Figure 5.4.

We observed that the hydrolysis rate in ON states might vary. For short galactose transducer **5-2**, it seems counter-intuitive that System B (membrane pre-incorporated transducer with external addition of zinc chloride) achieved higher hydrolysis rate than System C (membrane pre-incorporated transducer with zinc chloride on both sides of the vesicles) as internal Zn^{2+} in System B should be less than or equal to System C. However, we need to acknowledge that, compared to System B and D where vesicles are of the same batch, vesicles in System B and C cannot be prepared in the same batch. Although we followed the same protocol for all vesicle preparations, it is practically impossible to obtain two identical sets of vesicles. Therefore, we can assign both System B and C in ON state and the rest of the systems in OFF state. This is in line with above predicted outcome Entry 24. These results suggest that the short galactose transducer **5-2** is able to transport Zn^{2+} when pre-incorporated in the membrane but cannot cross the lipid bilayer when externally added to the membrane. A possible transport mechanism is discussed further in following sections.

As for short hydrazide transducer **5-1**, it is straightforward to distinguish the ON/OFF states (Figure 5.3b). We immediately recognise this system follows the outcome Entry 24, the same as short galactose transducer **5-2**. These results suggest that the short hydrazide transducer cannot cross the membrane either, despite the hydrazide group being neutral at pH 7 (as a reference, pK_a of acyl hydrazides is <4)[9]. One possible explanation is that hydrazide functional group may be very well solvated in aqueous phase with in total 3 hydrogen bond donors and 3 hydrogen bond acceptors.

Surprisingly, the short phenol transducer **5-3** generates similar results as the other two transducers, see Figure 5.3c, indicating that the transducer cannot cross the lipid bilayer. It is possible that the pK_a of the hydroxyl group is reduced by the electron-withdrawing group (as a reference, pK_a of 4-hydroxybenzaldehyde is 7.61 in water at 25°C)[10], and therefore the hydroxyl group could be deprotonated, making the transducer membrane-impermeable.

Table 5.1 A binary code table for theoretical outcomes of system A-F. "0" represents the signalling system is OFF compared to background whilst "1" represents ON.

Entry	A	B	C	D	E	F	Possible outcome?	Zinc transport pre-incorporation	Zinc transport external loading	Transducer translocation
0	**0**	**0**	**0**	**0**	**0**	**0**	**Possible**	**Cannot determine**	**Cannot determine**	**Cannot determine**
1	0	0	0	0	0	1	Not Possible C/F			
2	0	0	0	0	1	0	Not possible E/F			
3	0	0	0	0	1	1	Not possible C/F			
4	0	0	0	1	0	0	Not possible D/F			
5	0	0	0	1	0	1	Not possible C/F			
6	0	0	0	1	1	0	Not possible E/F			
7	0	0	0	1	1	1	Not possible C/F			
8	0	0	1	0	0	0	Not possible A/B/C			
9	0	0	1	0	0	1	Not possible A/B/C			
10	0	0	1	0	1	0	Not possible E/F			
11	0	0	1	0	1	1	Not possible B/E			
12	0	0	1	1	0	0	Not possible D/F			
13	0	0	1	1	0	1	Not possible A/B/C			
14	0	0	1	1	1	0	Not possible E/F			
15	0	0	1	1	1	1	Not possible A/B/C			
16	0	1	0	0	0	0	Not possible B/C			
17	0	1	0	0	0	1	Not possible C/F			
18	0	1	0	0	1	0	Not possible E/F			
19	0	1	0	0	1	1	Not possible C/F			
20	0	1	0	1	0	0	Not possible D/F			
21	0	1	0	1	0	1	Not possible C/F			
22	0	1	0	1	1	0	Not possible E/F			
23	0	1	0	1	1	1	Not possible C/F			
24	**0**	**1**	**1**	**0**	**0**	**0**	**Possible**	**Yes**	**Cannot determine**	**No**
25	0	1	1	0	0	1	Not possible D/F			
26	0	1	1	0	1	0	Not possible E/F			
27	**0**	**1**	**1**	**0**	**1**	**1**	**Possible**	**Yes**	**Yes**	**Yes**
28	0	1	1	1	0	0	Not possible D/F			
29	0	1	1	1	0	1	Not possible B/E/F			
30	0	1	1	1	1	0	Not possible E/F			
31	0	1	1	1	1	1	Not possible D/E			
32	1	0	0	0	0	0	Not possible A/C			
33	1	0	0	0	0	1	Not possible C/F			
34	1	0	0	0	1	0	Not possible E/F			
35	1	0	0	0	1	1	Not possible C/F			
36	1	0	0	1	0	0	Not possible D/F			
37	1	0	0	1	0	1	Not possible C/F			
38	1	0	0	1	1	0	Not possible E/F			
39	1	0	0	1	1	1	Not possible C/F			
40	**1**	**0**	**1**	**0**	**0**	**0**	**Possible**	**No**	**Cannot determine**	**No**
41	1	0	1	0	0	1	Not possible D/F			
42	1	0	1	0	1	0	Not possible E/F			
43	1	0	1	0	1	1	Not possible D/F			
44	1	0	1	1	0	0	Not possible C/F			
45	**1**	**0**	**1**	**1**	**0**	**1**	**Possible**	**No**	**No**	**Yes**
46	1	0	1	1	1	0	Not possible E/F			
47	1	0	1	1	1	1	Not possible D/E			
48	1	1	0	0	0	0	Not possible A/C			
49	1	1	0	0	0	1	Not possible C/F			
50	1	1	0	0	1	0	Not possible E/F			
51	1	1	0	0	1	1	Not possible C/F			
52	1	1	0	1	0	0	Not possible D/F			
53	1	1	0	1	0	1	Not possible C/F			
54	1	1	0	1	1	0	Not possible E/F			
55	1	1	0	1	1	1	Not possible C/F			
56	1	1	1	0	0	0	Not possible A/B			
57	1	1	1	0	0	1	Not possible B/E/F			
58	1	1	1	0	1	0	Not possible E/F			
59	1	1	1	0	1	1	Not possible D/F			
60	1	1	1	1	0	0	Not possible A/B			
61	1	1	1	1	0	1	Not possible A/B			
62	1	1	1	1	1	0	Not possible E/F			
63	1	1	1	1	1	1	Not possible D/E			

Pre-incorporation of transducer: System A (zinc inside), System B (zinc outside), System C (zinc both sides);
External addition of transducer: System D (zinc inside), System E (zinc outside), System F (zinc both sides).

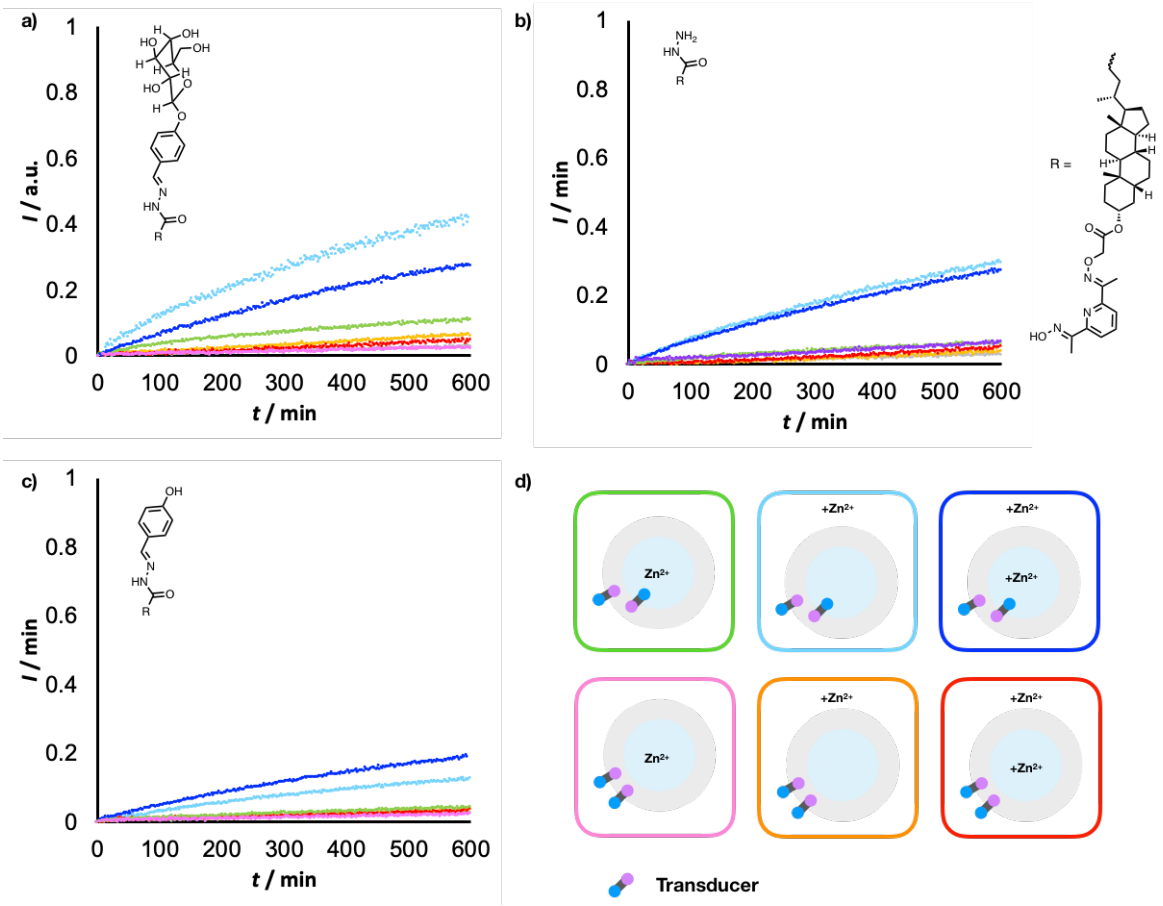

Figure 5.4 Signalling experiment of a) short galactose transducer **5-2**, b) short hydrazide transducer **5-1**, and c) short phenol transducer **5-3**. Time dependence of the normalized fluorescence emission intensity at 510 nm (exciting at 415 nm) of 0.1 mM 200 nm POPC vesicles containing 250 μM substrate **5-10** substrate in 25 mM HEPES buffer 150 mM NaCl at pH 7. Grey data: background hydrolysis of substrate **5-10** in POPC vesicles. For all systems: transducer loading is 5 mol%, $ZnCl_2$ concentration is 250 μM. d) Schematic illustration.

5.2.2.2 Signalling experiments with long transducers

Due to the small quantity of long hydrazide transducer **5-4** isolated (by Dr Istvan Kocsis), we did not have enough material to conduct signalling experiments with long transducers using the pre-incorporation methods (System A, B, and C) as they require significantly larger amount of materials than the external addition methods. However, for long galactose transducer **5-5**, System E with externally loaded transducer and zinc chloride generates an ON state. As galactose head group is hydrophilic and membrane-impermeable, according to Inference 1, the ON state can be only achieved if the pyridine-oxime catalytic head group crosses the membrane and reaches the inner surface of a vesicle. The fact that System E is in an ON state means that transducer can transport Zn^{2+} across the lipid bilayer. As discussed before, Zn^{2+} transport leads to 500 times dilution of Zn^{2+} concentration inside the vesicles in System D, effectively shutting down the catalytic activity of transducer and generating an OFF state.

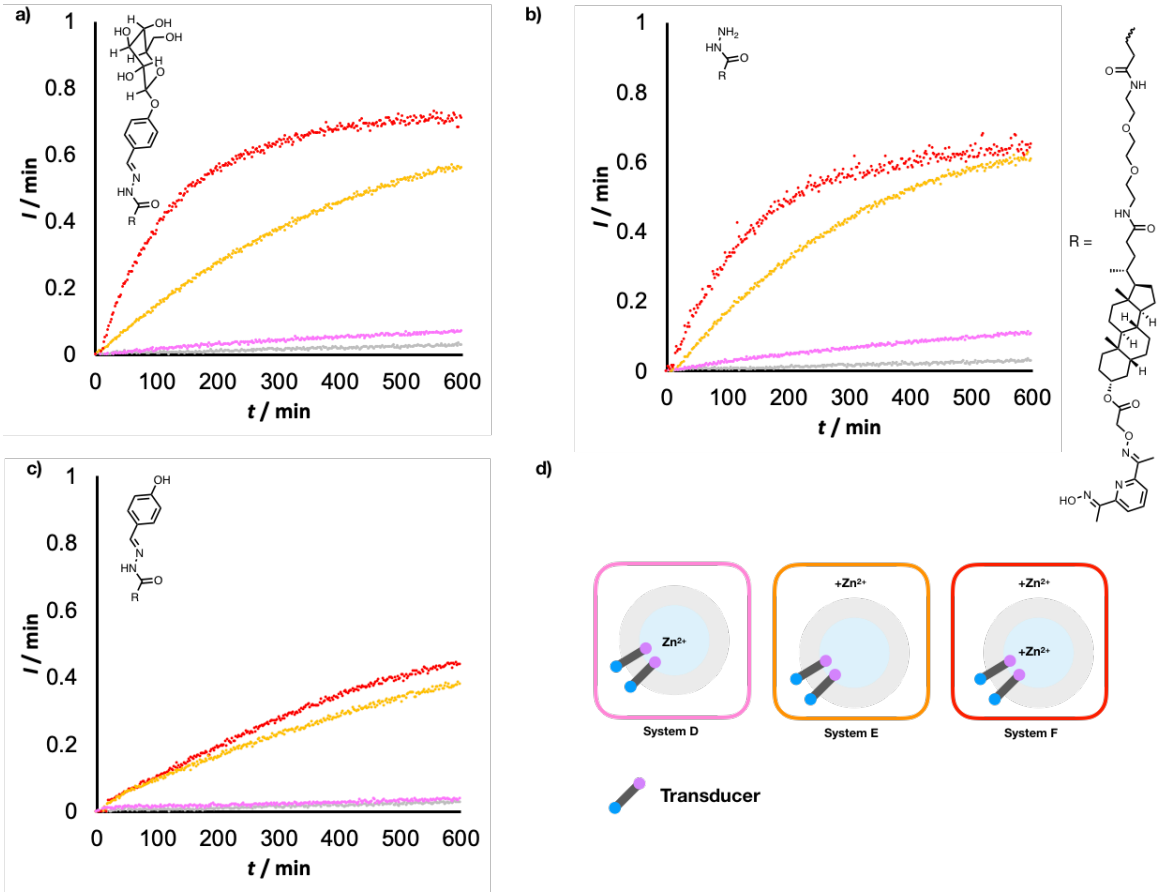

Figure 5.5 Signalling experiment of a) long galactose transducer **5-5**, b) long hydrazide transducer **5-4**, and c) long phenol transducer **5-6**. Time dependence of the normalized fluorescence emission intensity at 510 nm (exciting at 415 nm) of 200 nm POPC vesicles (0.1 mM lipid concentration) containing 250 μM substrate **5-10** in 25 mM HEPES buffer 150 mM NaCl at pH 7. Grey data: background hydrolysis of substrate **5-10** in POPC vesicles. For all systems: transducer loading is 5 mol%, $ZnCl_2$ concentration is 250 μM. d) Schematic illustration.

Similar to long galactose transducer **5-5**, long hydrazide transducer **5-4** and long phenol transducer **5-6** also generate an ON state in System E but remained in OFF state in System D, indicating both transducers can transport Zn^{2+} as well as span the lipid bilayer. According to a Chemdraw model shown in Figure 5.4, long transducers could indeed span the membrane.

Pre-incorporation of transducer: System A (zinc inside), System B (zinc outside), System C (zinc both sides); External addition of transducer: System D (zinc inside), System E (zinc outside), System F (zinc both sides).

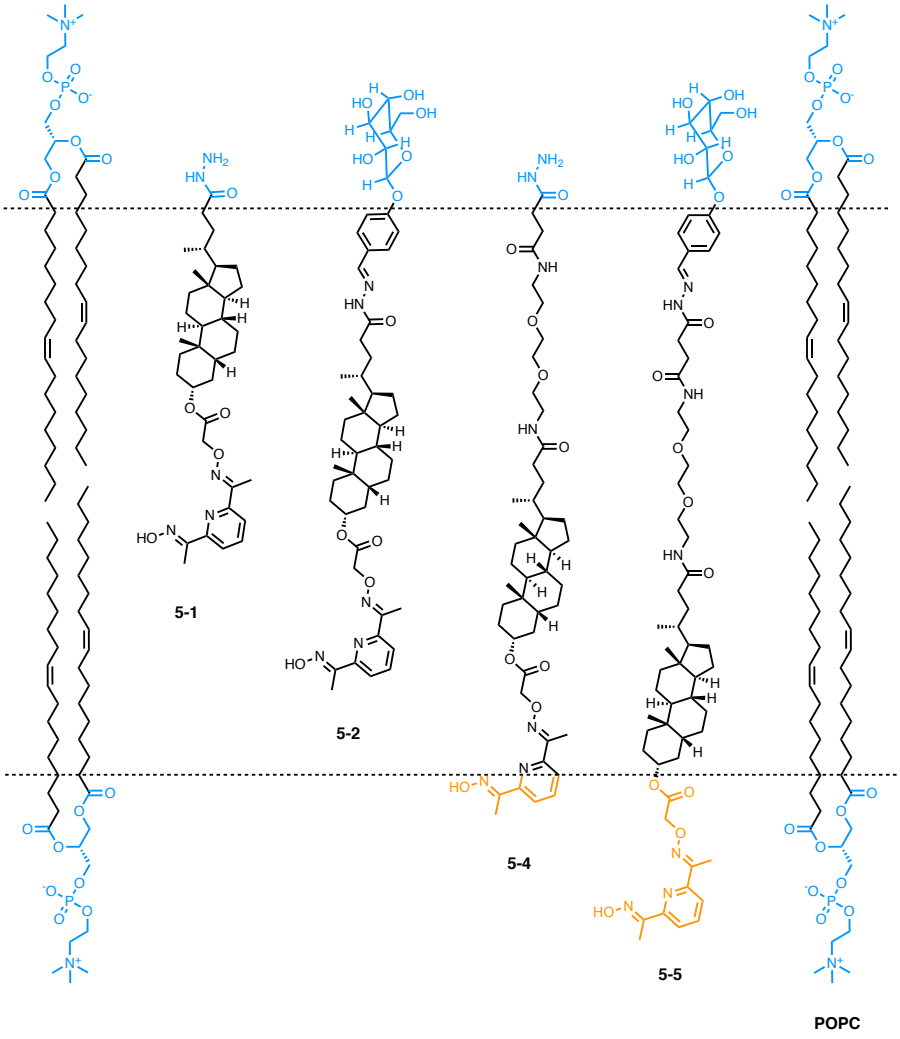

Figure 5.6 A Chemdraw model depicting the length of short hydrazide transducer **5-1**, short galactose transducer **5-2**, long hydrazide transducer **5-4**, and long galactose transducer **5-5** in comparison with POPC lipids. The hydrophilic region is shown in blue, catalytic head group of **5-4** and **5-5** that are outside the hydrocarbon region is shown in orange.

5.2.3 Fluorescence Quenching Assay

Ms Lucia Trevisan's work suggested that HPTS fluorescence emission can be quenched by transducer-Cu^{2+} complex (unpublished results). To further investigate the metal transport ability of six transducers, we designed an HPTS-transducer-Cu^{2+} fluorescence quenching assay. 0.1 mM POPC vesicles encapsulating 250 μM HPTS in HEPES buffer saline at neutral pH were assembled and suspended in the same buffer solution. 10 μM $CuCl_2$ was added from the outside of the vesicles. Transducers were then added to the vesicle suspensions and the fluorescence emission intensity of HPTS was monitored, see Figure 5.7. When long transducers were added to the vesicle suspension, we immediately observed a decrease of fluorescence emission to less than 20% of initial emission, indicating that long transducers can effectively shuffle Cu^{2+} across the membrane and expose the oxime complex to the interior

solution. However, for the system with short transducers, the fluorescence emission intensity of HPTS slowly decreased over time. This means that externally loaded short transducers have limited ability to carry Cu^{2+} across the lipid bilayer compared to long transducers. Based on these observations, we can conclude that the long transducers are able to span the membrane and conduct Cu^{2+} transport, whilst the short transducers cannot span or cross the membrane, see Figure 5.8.

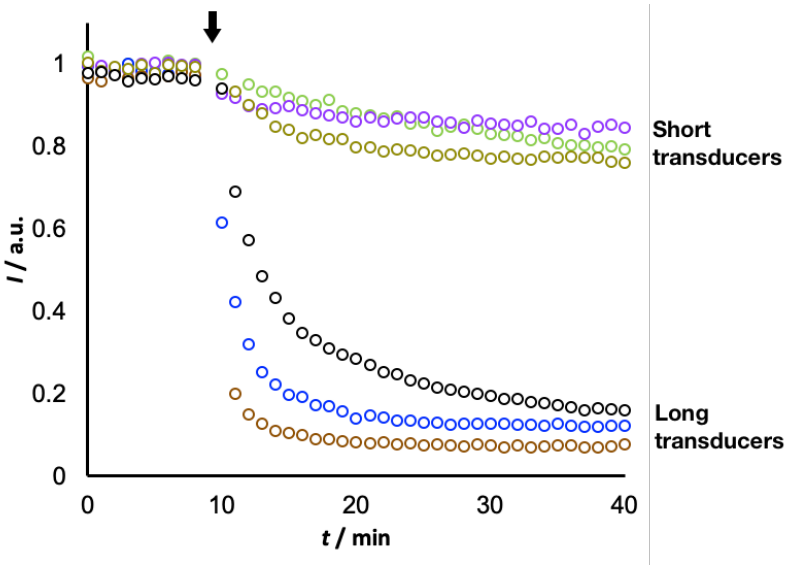

Figure 5.7 Copper transport assay. (Green: short galactose transducer; Purple: short hydrazide transducer; Dark green: short phenol transducer; Blue: long galactose transducer; Brown: long hydrazide transducer; Black: long phenol transducer). Time dependence of the normalized fluorescence emission intensity at 510 nm (exciting at 415 nm) of 0.1 mM POPC 200 nm vesicles encapsulating 250 μM HPTS in 25 mM HEPES 150 NaCl buffer at pH 7. 10 μM $CuCl_2$ is added externally at t = 0 min. An aliquot of transducer (1mM in DMSO) was added at t = 10 min (indicated by an arrow) to reach 5 μM bulk concentration (5 mol% loading relative to POPC lipids).

We then examined Cu^{2+} transport of the system with pre-incorporated short galactose transducer, see Figure 5.9. This system showed rapid transport of Cu^{2+}. As galactose head group is hydrophilic and membrane-impermeable, external loading of transducer locks the transducer at the outer leaflet of the membrane, whilst pre-incorporation of transducer gives a 50/50 distribution of transducer in both leaflets. We hypothesised that the rapid Cu^{2+} transport is due to a transducer relay mechanism that is only achievable when the transducer is present in both leaflets of the lipid bilayer, see Figure 5.10.[11] The pyridine oxime catalytic head group of the transducer is amphiphilic and can partition between aqueous-membrane interface and membrane hydrocarbon environment. When there is a concentration gradient of Cu^{2+} across the membrane, the pyridine-oxime head group binds Cu^{2+} and brings it into the membrane. Sequentially, another transducer in the other side of the membrane with opposite orientation takes the ion and releases it at the inner side of the vesicle. This procedure is reversible and driven by the concentration gradient until reaching equilibrium.

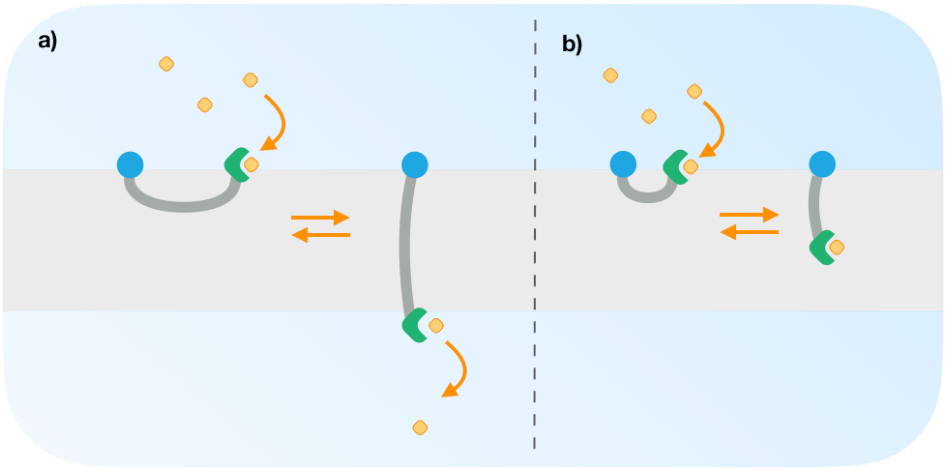

Figure 5.8 Illustration of ion transport mechanism in the lipid bilayer mediated by a) long transducers can span the membrane, and b) short transducer that cannot span or cross the lipid bilayer. The blue head group (for example a galactose unit) is hydrophilic and therefore is locked at the outer leaflet of the lipid bilayer. The green catalytic head group is amphiphilic and can partition between aqueous-membrane interface and hydrocarbon environment. When there is a concentration gradient of metal ion (orange) across the membrane, the catalytic head group binds the metal, brings it across the lipid bilayer, and releases it at the inner side of the membrane.

These findings are further pieces of evidence that transducer might be U-shaped in the lipid bilayer and have the ability to transport ions across the membranes, which help us better understand the transmembrane signalling experiment in the previous section.

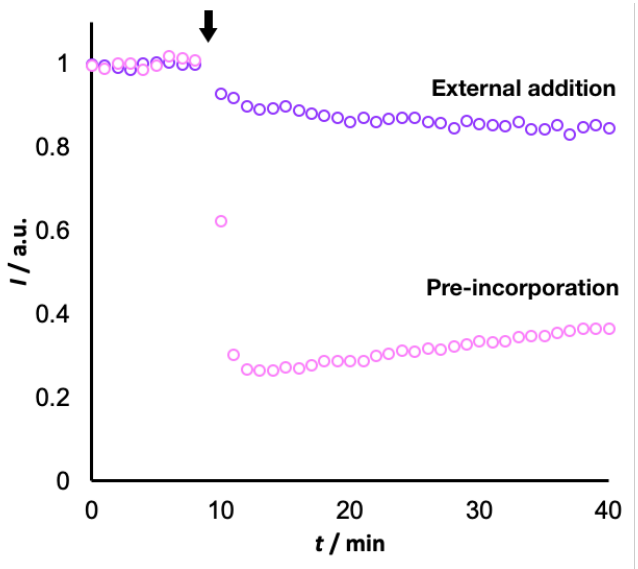

Figure 5.9 Copper transport assay of short galactose transducer **5-2** with different transducer loading techniques. Time dependence of the normalized fluorescence emission intensity at 510 nm (exciting at 415 nm) of 0.1 mM POPC 200 nm vesicles encapsulating 250 μM HPTS in 25 mM HEPES 150 NaCl buffer at pH

7. Pink data: 5 mol% transducer pre-incorporated in the membrane, 10 μM $CuCl_2$ externally at t = 10 min. Purple data: 10 μM $CuCl_2$ externally at t = 0 min. An aliquot of transducer (1 mM in DMSO) was added at t = 10 min (indicated by the arrow) to reach 5 μM bulk concentration (5 mol% loading relative to POPC lipids).

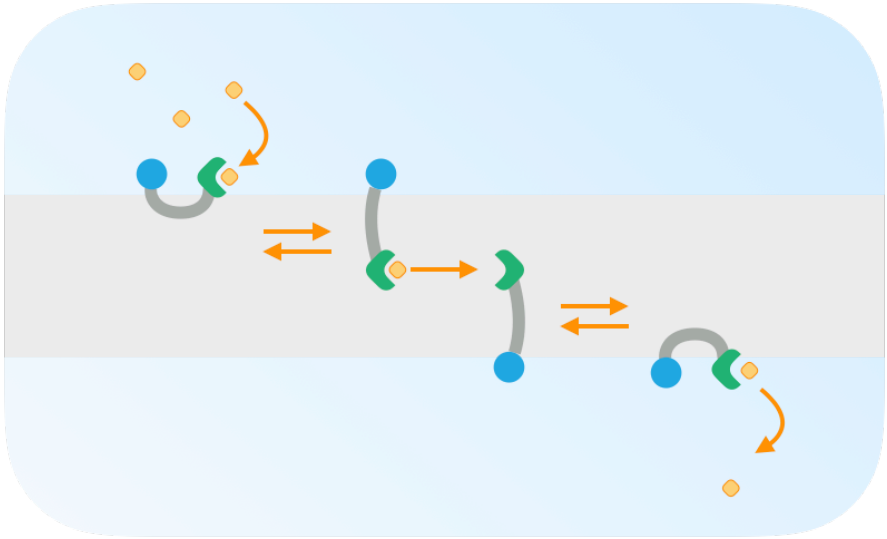

Figure 5.10 Illustration of a proposed ion transport mechanism in the lipid bilayer with pre-incorporated short transducers that cannot span the membrane. The blue head group (for example a monosaccharide unit) is lipophobic and therefore is locked at the outer leaflet of the lipid bilayer. The green catalytic head group is amphiphilic and can partition between aqueous-membrane interface and hydrocarbon environment. When there is a concentration gradient of metal ion (orange) across the membrane, the catalytic head group binds the metal, brings it into the membrane. Another transducer in the other side of the membrane with opposite orientation takes the ion and releases it at the inner side of the membrane.

5.2.4 Enzymatic Cleavage of Galactose Transducers

5.2.4.1 In POPC Vesicles.

We used UPLC to monitor the enzymatic cleavage of membrane-embedded short galactose transducer **5-2**, see Figure 5.11. β-Galactosidase (0.2% relative to the transducer) was added into POPC vesicle suspension with 1 mol% loading of transducer. After 15 h of incubation, no change was observed in the UPLC chromatogram, indicating that the enzyme cannot hydrolyse the galactosidic bond of the transducer in the POPC membrane.

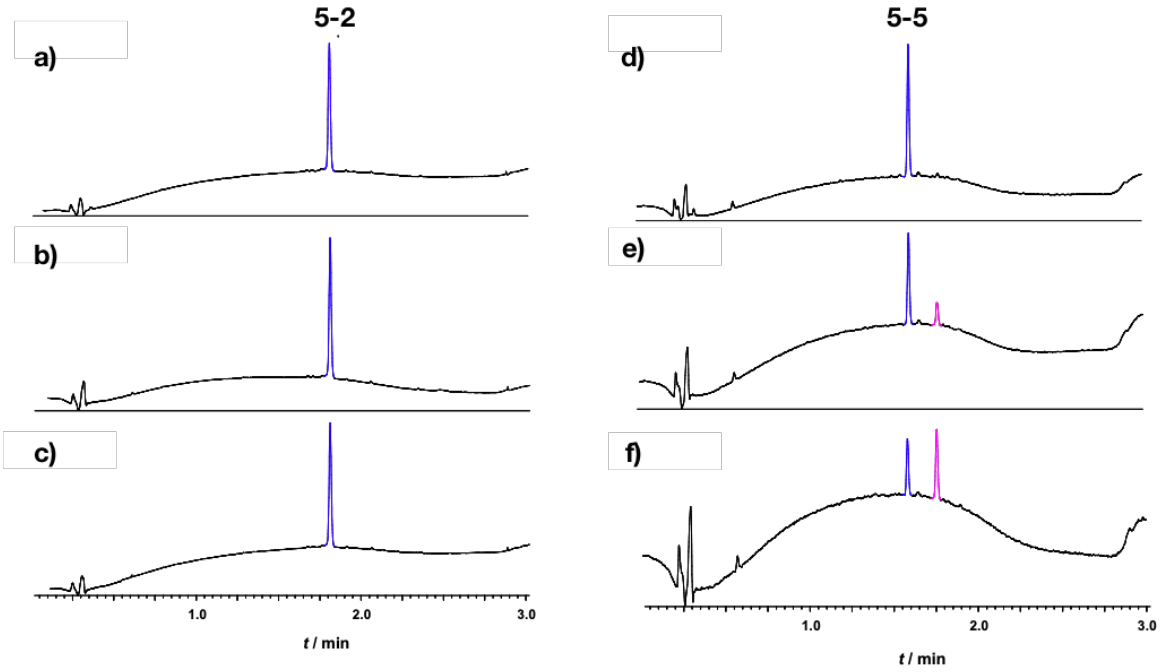

Figure 5.11 UPLC traces of attempted β-galactosidase enzymatic cleavage of short galactose transducer **5-2** (retention time: 1.81 min) and long galactose transducer **5-5** (retention time: 1.60 min). 1 mM 200 nm POPC vesicles with 1 mol% external loading of transducer (10 μM bulk concentration of the transducer). a), b), and c): 0 h, 5 h, and 15 h after addition of 1 mg/L (0.02 μM) of β-galactosidase to vesicles with transducer **5-2**. d), e), and f): 0 h, 5 h, and 20 h after addition of 1 mg/L (0.02 μM) of β-galactosidase to vesicles with transducer **5-5**. Column: ACQUITY UPLC® CSH C18, 2.1x 50 mm, 1.7 μm, 130 Å. Solvent A: 2 mM ammonium acetate in water/acetonitrile (95:5); Solvent B: acetonitrile. Gradient: 5-95% B over 1 min. Flow rate: 0.6 mL/min.

We then assembled vesicles with 1 mol% loading of long galactose transducer **5-5** in the membrane for the same experiment, see Figure 5.11b. Addition of 0.2% of β-galactosidase (relative to the transducer) to the vesicle suspension led to hydrolysis of glycosidic bond, as indicated by the decreased UV signal at t = 1.60 min in the chromatogram as well as the appearance of a new signal at t = 1.81 min. The new signal has a mass corresponding to long phenol transducer **5-6**. Considering the usual signalling experiments time scale is 10 h in our studies, the cleavage rate is relatively slow as only 12% of the transducer was cleaved by the enzyme in 5 h or 78% in 20 h. Nonetheless, these finding suggests that the addition of polyethylene glycol linker enables the galactose head group to be hydrolysed by β-galactosidase on the membrane surface.

5.2.4.2 In DNPC Vesicles.

The original design (Figure 5.1) of the transmembrane signalling system was to use β-galactosidase as an input signal to cleave the galactose unit of transducer and trigger translocation. However, as short galactose transducer **5-2** is inert to enzymatic cleavage when embedded in POPC vesicles and long galactose transducer can span the POPC lipid bilayer (achieving an ON state without input signal), we hypothesised that changing lipids to

dinervonoylphosphocholine (DNPC), a considerably longer phospholipid compared to POPC, would avoid the membrane-spanning but still enable the enzymatic cleavage, see Chemdraw model shown in Figure 5.14.

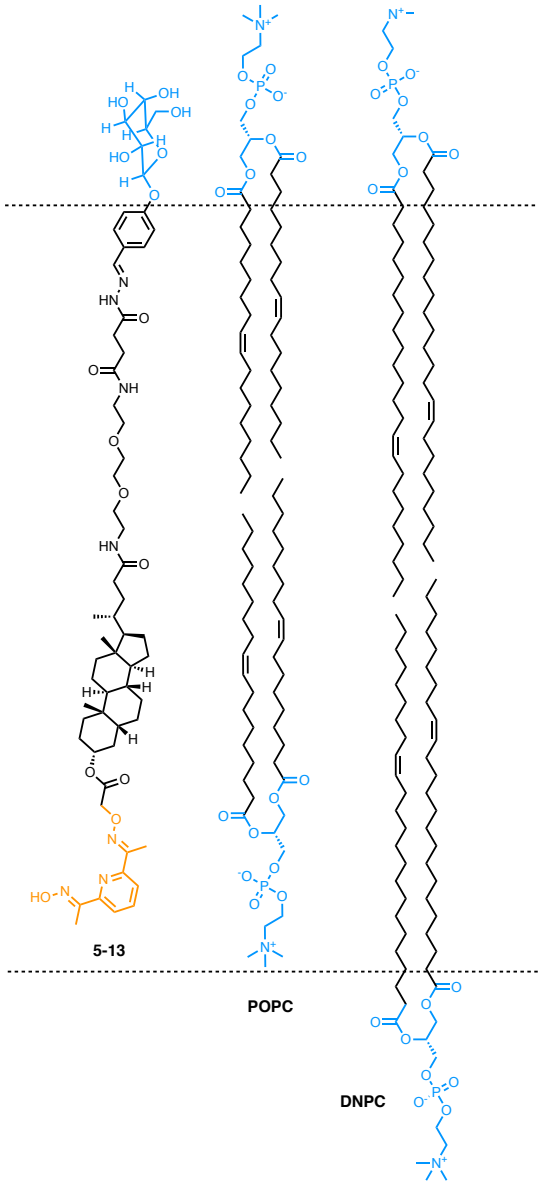

Figure 5.12 A Chemdraw model for length comparison. The hydrophilic region of POPC and DNPC is coloured blue. Catalytic region of long galactose transducer is coloured orange.

We first examined the enzymatic cleavage of long galactose transducer **5-5** in DNPC vesicles by UPLC, see Figure 5.15. β-Galactosidase is able to hydrolyse the glycosidic bond of the membrane-embedded transducer as expected. The observed hydrolysis rate from UPLC UV traces (68% conversion in 15 h) of the transducer at DNPC vesicles surface is slightly faster than that at POPC vesicles surface.

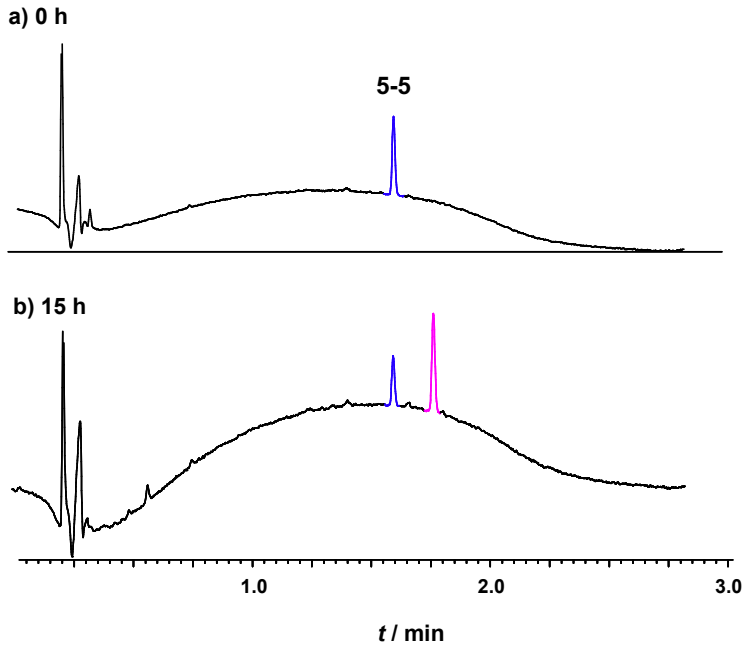

Figure 5.13 UPLC traces of β-galactosidase enzymatic cleavage of long galactose transducer **5-5** in DNPC vesicles. 0 h (a) and 15 h (b) after addition of 1 mg/L (0.02 μM) of β-galactosidase to 1 mM 200 nm DNPC vesicles with 1 mol% external loading of long galactose transducer **5-5** (10 μM bulk concentration of transducer, 500 eq. to β-galactosidase, retention time: 1.60 min, blue signal). Pink signal at retention time 1.80 min corresponds to long phenol (ON state galactose) transducer **5-6**. Column: ACQUITY UPLC® CSH C18, 2.1x 50 mm, 1.7 μm, 130 Å. Solvent A: 2 mM ammonium acetate in water/acetonitrile (95:5); Solvent B: acetonitrile. Gradient: 5-95% B over 1 min. Flow rate: 0.6 mL/min.

We then tested the transmembrane signalling ability of transducer **5-5** in DNPC vesicles. 0.1 mM 200 nM DNPC vesicles were prepared and suspended in HEPES buffer saline with $ZnCl_2$ on both sides at pH 7 and 5 mol% of transducer **5-5** were loaded externally. As DNPC has a phase transition temperature of 27°C (multilamellar vesicles) or 26°C (large unilamellar vesicles)[12], this experiment was conducted at 10°C above the transition temperature (36°C) to ensure that the lipid bilayer membrane remained fluid. The results are shown in Figure 5.15. As expected, the galactose transducer is in an OFF state (pink data) without the addition of β-galactosidase, indicating that the long transducer can no longer span the lipid bilayer. Although galactose transducer was cleaved in the membrane as confirmed by UPLC traces, the system cannot be switched ON with addition of β-galactosidase (blue data). The resulting phenol transducer appears to be membrane-impermeable in the DNPC lipid bilayer. A separate control experiment with external addition of long phenol transducer **5-6** (black data) also gave an OFF state. These results are consistent with previous experiments with POPC vesicles that phenol transducer cannot cross the bilayer membranes.

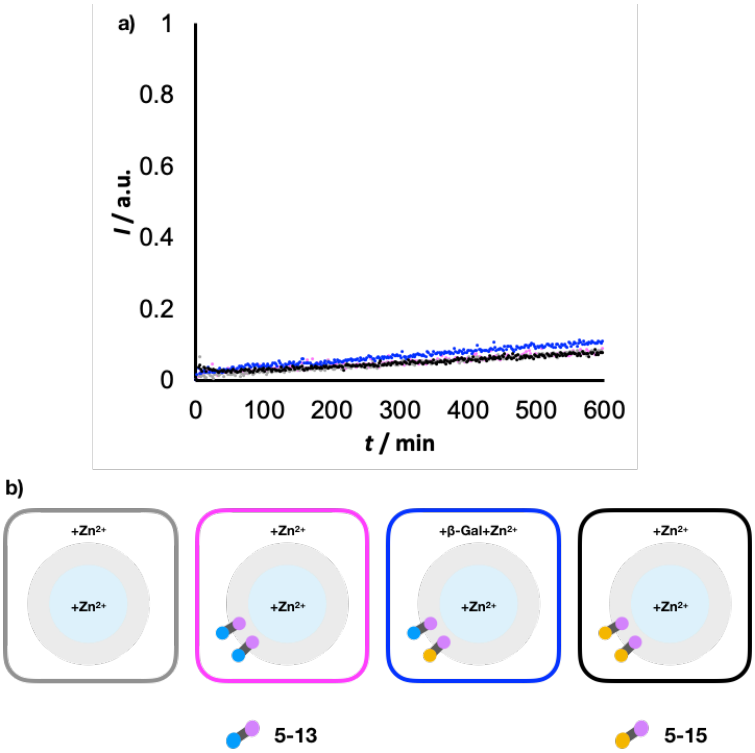

Figure 5.14 Signalling experiment of long galactose transducer **5-5**. Time dependence of the normalised fluorescence emission intensity at 510 nm (exciting at 415 nm) of 200 nm DNPC vesicles (0.1 mM final lipid concentration) containing 250 μM substrate **5-10** in 25 mM HEPES buffer 150 mM NaCl at pH 7 at 37°C. Grey data: background hydrolysis. Pink data: 5 mol% long galactose transducer **5-5** (in DMSO) and 250 μM $ZnCl_2$ added externally at t = 0 min to vesicles containing 250 μM $ZnCl_2$. Blue data: 5 mol% long galactose transducer **5-5** (in DMSO) and 250 μM $ZnCl_2$ added externally at t = 0 min, 10 ug/mL β-galactosidase added externally at t = 10 min. Black data: 5 mol% long phenol transducer **5-6** (in DMSO) and 250 μM $ZnCl_2$ added externally at t = 0 min to vesicles containing 250 μM $ZnCl_2$. b) Schematic illustration.

5.3 Conclusion

To conclude, we have synthesised transducers of different lengths with a hydrazide head group and used hydrazide-aldehyde chemistry to attach β-galactose unit as well as corresponding phenol moiety on them, obtaining four transducers (short and long). First, the catalytic activity and metal transport ability of each transducer were examined in an array of six signalling systems. The combined results of these signalling systems suggest that the short galactose transducer cannot cross the membrane but is able to transport metal ions when pre-incorporated in the lipid bilayer. We hypothesised that the pyridine oxime head group of a transducer could partition between membrane-water interface (U-shaped) and lipid hydrocarbon environment, enabling a possible metal-binding relay for transport mechanism. HPTS fluorescence quenching assay results are consistent with this hypothesis. Second, it is demonstrated that a polyethylene glycol linker is required for the glycosidic bond of the transducer to be cleaved by the enzyme at the membrane-water interface. However, the linker adds extra length to the transducers and allow them to span the POPC lipid bilayer. We then

assembled DNPC vesicles with long transducers. As expected, the transducer can no longer cross the membrane due to relatively short length compared to DNPC lipid. Unfortunately, the resulting hydrolysis product – a phenol transducer – did not cross the membrane. This is potentially due to the low pK_a value of the phenol group of the transducer, which could deprotonate at neutral pH environment. The deprotonated transducer is membrane-impermeable and therefore no ON state could be achieved. These findings revealed the metal transport ability of transducers and provided further understanding of the previously proposed translocation mechanism.

References

(1) Alberts, B.; Johnson, A.; Lewis, J.; Raff, M.; Roberts, K.; Walter, P. Signaling through Enzyme-Linked Cell-Surface Receptors. *Mol. Biol. Cell 4th Ed.* **2002**.

(2) Hurley, J. H. Structure, Mechanism, and Regulation of Mammalian Adenylyl Cyclase. *J. Biol. Chem.* **1999**, *274* (12), 7599–7602. https://doi.org/10.1074/jbc.274.12.7599.

(3) Craig, D. B.; Dovichi, N. J. Escherichia Coli β-Galactosidase Is Heterogeneous with Respect to the Activity of Individual Molecules. **1998**, *76*, 4.

(4) Juers, D. H.; Matthews, B. W.; Huber, R. E. LacZ β-Galactosidase: Structure and Function of an Enzyme of Historical and Molecular Biological Importance. *Protein Sci. Publ. Protein Soc.* **2012**, *21* (12), 1792–1807. https://doi.org/10.1002/pro.2165.

(5) Langton, M. J.; Keymeulen, F.; Ciaccia, M.; Williams, N. H.; Hunter, C. A. Controlled Membrane Translocation Provides a Mechanism for Signal Transduction and Amplification. *Nat. Chem.* **2017**, *9* (5), 426–430. https://doi.org/10.1038/nchem.2678.

(6) Langton, M. J.; Williams, N. H.; Hunter, C. A. Recognition-Controlled Membrane Translocation for Signal Transduction across Lipid Bilayers. *J. Am. Chem. Soc.* **2017**, *139* (18), 6461–6466. https://doi.org/10.1021/jacs.7b02345.

(7) Kölmel, D. K.; Kool, E. T. Oximes and Hydrazones in Bioconjugation: Mechanism and Catalysis. *Chem. Rev.* **2017**, *117* (15), 10358–10376. https://doi.org/10.1021/acs.chemrev.7b00090.

(8) Yatsimirsky, A. K.; Gómez-Tagle, P.; Escalante-Tovar, S.; Ruiz-Ramírez, L. Kinetics and Mechanism of Ester Hydrolysis by Metal Complexes of 2,6-Diacetylpyridine Dioxime. *Inorganica Chim. Acta* **1998**, *273* (1), 167–174. https://doi.org/10.1016/S0020-1693(97)05971-9.

(9) Hoff, E. A.; Abel, B. A.; Tretbar, C. A.; McCormick, C. L.; Patton, D. L. Aqueous RAFT at PH Zero: Enabling Controlled Polymerization of Unprotected Acyl Hydrazide Methacrylamides. *Polym. Chem.* **2017**, *8* (34), 4978–4982. https://doi.org/10.1039/C6PY01563H.

(10) Serjeant, E. P. *Ionisation Constants of Organic Acids in Aqueous Solution / by E.P. Serjeant and Boyd Dempsey.*; IUPAC chemical data series ; no.23; Pergamon: Oxford, 1979.

(11) McNally, B. A.; O'Neil, E. J.; Nguyen, A.; Smith, B. D. Membrane Transporters for Anions That Use a Relay Mechanism. *J. Am. Chem. Soc.* **2008**, *130* (51), 17274–17275. https://doi.org/10.1021/ja8082363.

(12) Metso, A. J.; Zhao, H.; Tuunainen, I.; Kinnunen, P. K. J. Observation of the Main Phase Transition of Dinervonoylphosphocholine Giant Liposomes by Fluorescence Microscopy. *Biochim. Biophys. Acta BBA - Biomembr.* **2005**, *1713* (2), 83–91. https://doi.org/10.1016/j.bbamem.2005.04.011.

5.4 Supporting Information

5.4.1 Synthetic Procedures and Characterisation

Materials and Methods

^{1}H NMR and ^{13}C NMR spectra were recorded on a 400-MHz Bruker® spectrometer. Chemical shifts are reported as δ values in ppm. Microwave reaction was carried out on a Biotage® Initiator+ microwave reactor. Flash chromatography was carried out on an automated system (Combiflash® Rf+ Lumen™) using pre-packed cartridges of silica (25 µm PuriFlash® Column) or neutral alumina (50 µm Redi*Sep*® Rf Column). SEC purification of the vesicles was carried out using GE Healthcare PD-10 desalting columns prepacked with Sephadex® G-25 medium. Ions exchange of the substrate was carried out using GE Healthcare disposable PD-10 gravity columns packed with CM Sephadex® C-25 medium. Fluorescence spectra were recorded using a Cary Eclipse fluorescence spectrophotometer (Agilent Technologies) in Hellma® Analytics Suprasil® quartz cuvettes. Measurements of pH were conducted using a Mettler-Toledo SevenCompact™ pH meter equipped with an InLab® Micro electrode. Vesicles were assembled in Eppendorf® polypropylene DNA LoBind® polypropylene microcentrifuge tube and extruded as described below using Avanti® Polar Lipids extruder kits, equipped with Avestin® LiposoFast Liposome Factory 200 nm polycarbonate membranes with GE Healthcare Whatman® 10 mm polyester filter support. Sonication was carried out using a Elma® Transsonic 420 sonicator. Vortexing was carried out on a Heidolph™ Reax Top Vortex Mixer. Solutions or vesicles suspensions were transferred using Eppendorf Multipette® Xstream Pippette with Combitips Advanced® or Hamilton Microliter™ syringes. All reagents and solvents were used without further purification. Lipids were purchased from Sigma-Aldrich® and used without further purification.

Synthesis and Characterisations

Synthesis of Short Hydrazide Transducer 5-1

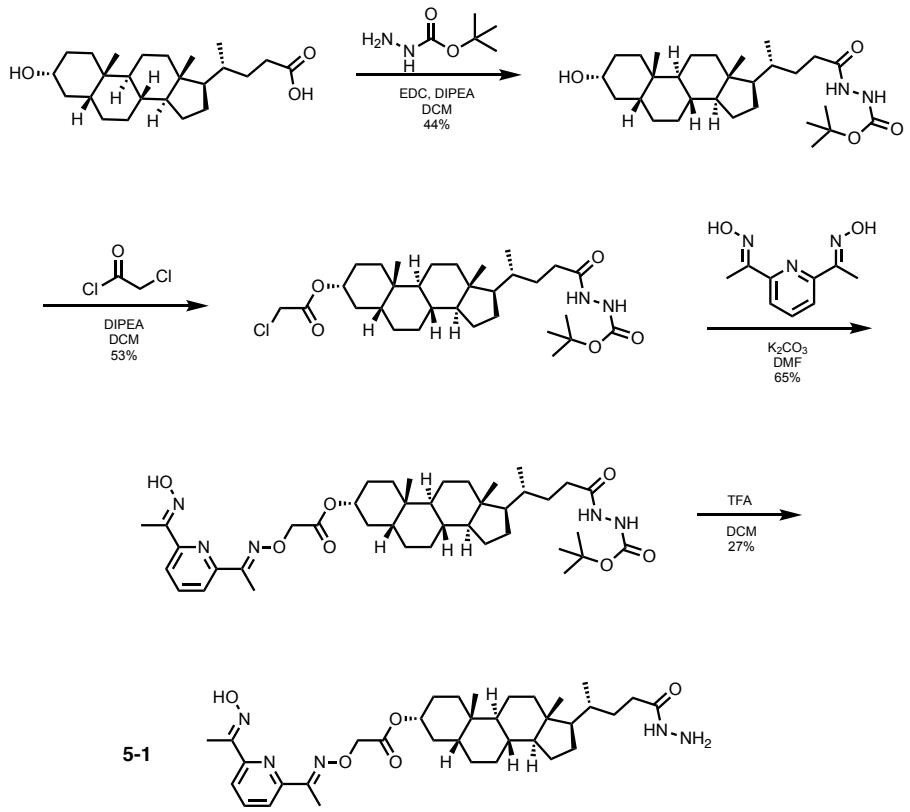

Scheme S5.1 Synthetic route for short hydrazide transducer **5-1**. (Synthesised and characterised by Dr Istvan Kocsis, used without further purification.)

Synthesis of Long Hydrazide Transducer 5-3

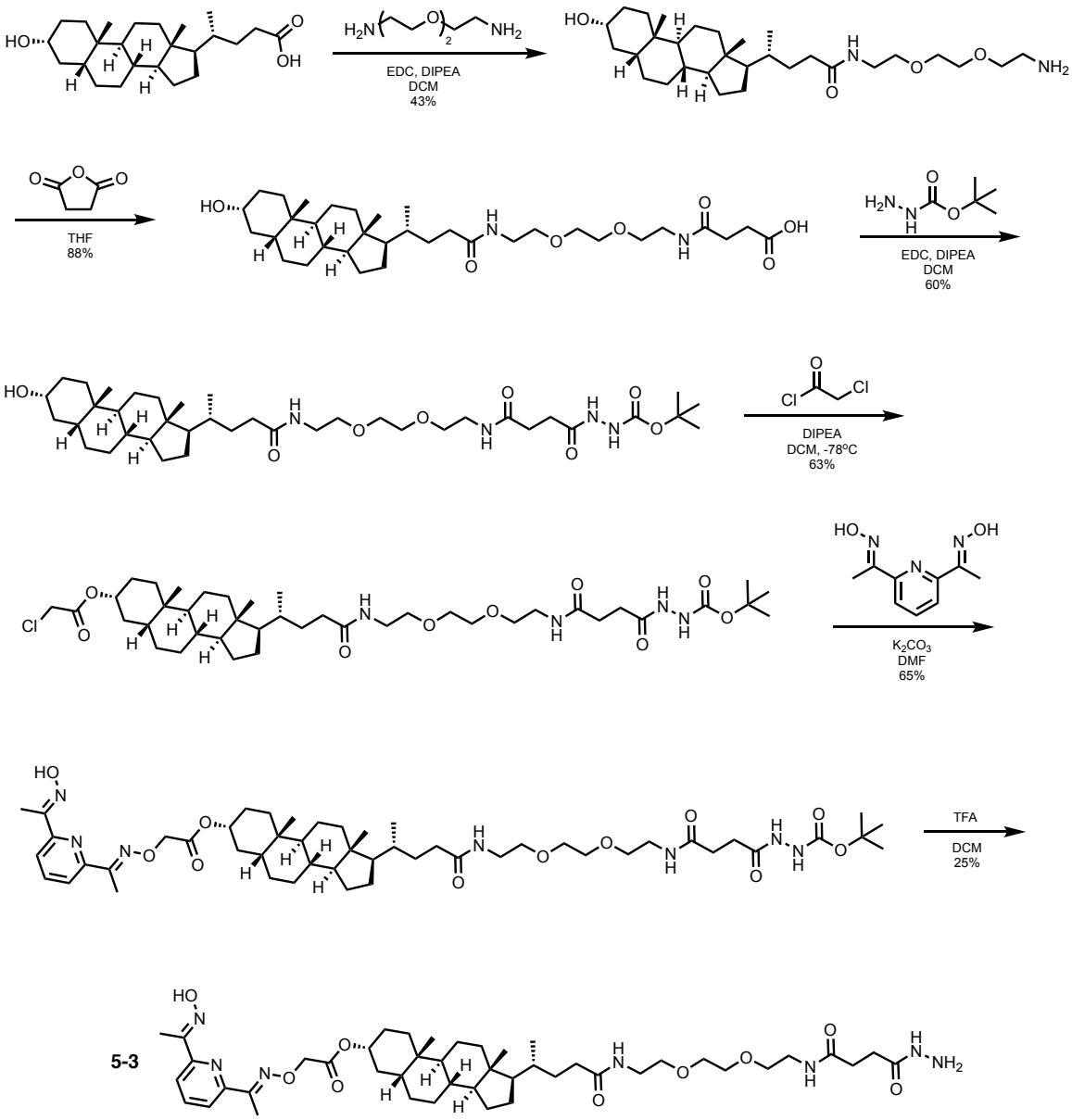

Scheme S5.2 Synthetic route for long hydrazide transducer **5-3**. (Synthesised and characterised by Dr Istvan Kocsis, used without further purification.)

Synthesis of Galactose Derivative 5-9

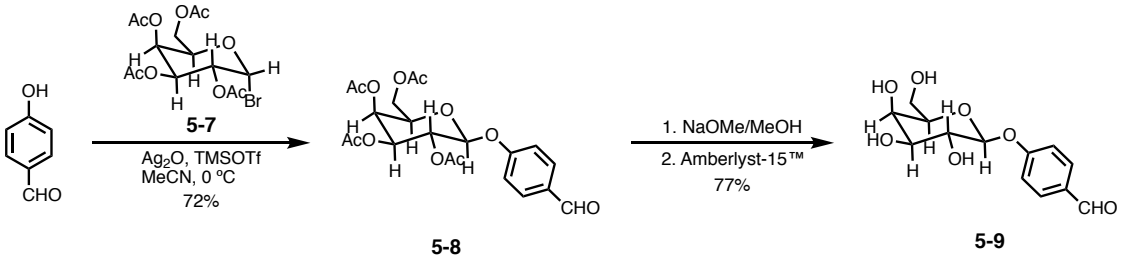

Scheme S5.3 Synthetic route for long hydrazide transducer **5-3**.

Compound 5-8

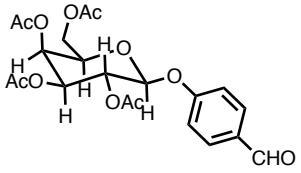

To a solution of acetobromo-α-D-galactose (400 mg, 0.972 mmol), 4-hydroxybenzaldehyde (118 mg, 0.972 mmol) in anhydrous chloroform (2 mL) was added silver oxide (224 mg, 1.94 mmol) with external cooling and the reaction mixture was stirred at room temperature overnight. The reaction mixture was diluted with ethyl acetate (20 mL), washed with hydrochloric acid (1 M), sodium bicarbonate (sat. aq.), brine, and dried over magnesium sulfate. The crude was purified by flash chromatography (silica, 0 – 40% ethyl acetate in petroleum ether) to yield the product as a colourless oil (396 mg, 72%).

^{1}H NMR (400 MHz, $CDCl_3$) δ (ppm): 9.93 (s, 1H), 7.87 – 7.84 (m, 2H), 7.12 -7.10 (m, 2H), 5.55 – 5.47 (m, 2H), 5.18 – 5.12 (m, 2H), 4.26 – 4.10 (m, 3H), 2.19 (s, 3H), 2.07 (s, 3H), 2.02 (s,3H).
^{13}C NMR (100 MHz, $CDCl_3$) δ (ppm): 190.6, 170.3, 170.1, 170.0, 169.3, 161.3, 131.8, 131.8, 116.7, 98.6, 71.3, 70.6, 68.4, 66.7, 61.3, 20.7, 20.6, 20.6, 20.6.
HR-MS (MS+): calcd. for $C_{21}H_{24}O_{11}$: 452.1319, found: 452.1313.
FT-IR (ATR): ν_{max} 1749, 1695, 1602, 1507, 1370, 1227, 1160, 1076 cm^{-1}.

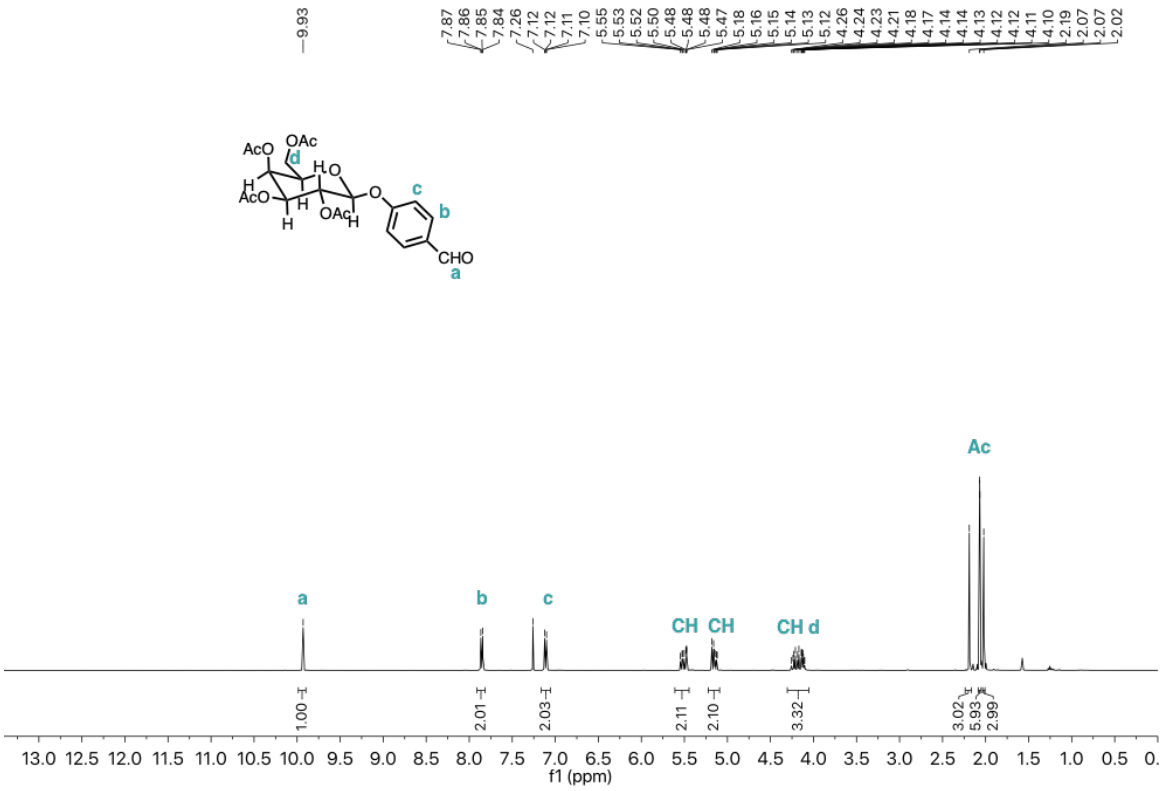

Figure S5.1 ^{1}H NMR spectra of compound **5-8**.

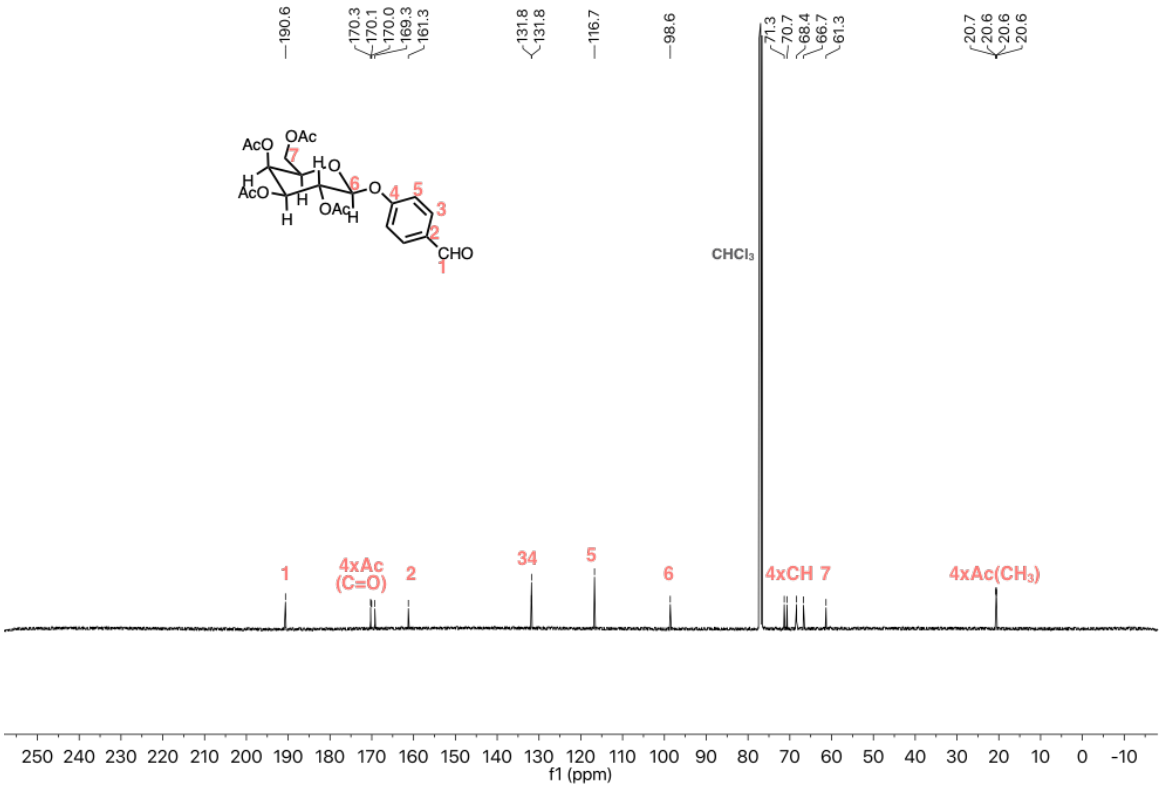

Figure S5.2 ^{13}C NMR spectra of compound **5-8**.

Compound 5-9

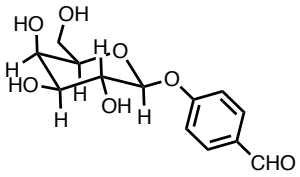

A solution of compound **5-8** (70 mg, 0.22 mmol) and sodium methoxide (12 mg, 0.22 mmol) in methanol (1 mL) was stirred at room temperature for 1.5 h. The reaction mixture was diluted with methanol (5 mL) and neutralized with Amberlyst-15 resin. The solution was poured into diethyl ether (50 mL), and the precipitate was filtered and dried to give the product as a white amorphous solid (34 mg, 77%).

^{1}H NMR (400 MHz, D_2O) δ (ppm): 9.83 (s, 1H), 7.97 (d, *J* = 8.6 Hz, 2H), δ 7.97 (d, *J* = 8.8 Hz, 1H), 7.29 (d, *J* = 8.8 Hz, 1H), 5.23 (d, *J* = 7.7 Hz, 1H), 4.04 (d, *J* = 3.3 Hz, 1H), 3.95 (t, *J* = 6.2 Hz, 1H), 3.89 – 3.86 (m, 1H), 3.82 (m, 1H).

^{13}C NMR (100 MHz, D_2O) δ (ppm): 195.0, 162.0, 132.6, 130.7, 116.5, 99.8, 75.6, 72.4, 70.3, 68.4, 60.6.

HR-MS (MS+): calcd. for $C_{13}H_{16}O_7$: 284.0896, found: 284.0897.

FT-IR (ATR): ν_{max} 3353, 1683, 1600, 1512, 1427, 1394, 1316, 1251, 1218, 1164, 1139, 1090, 1059, 1028 cm^{-1}.

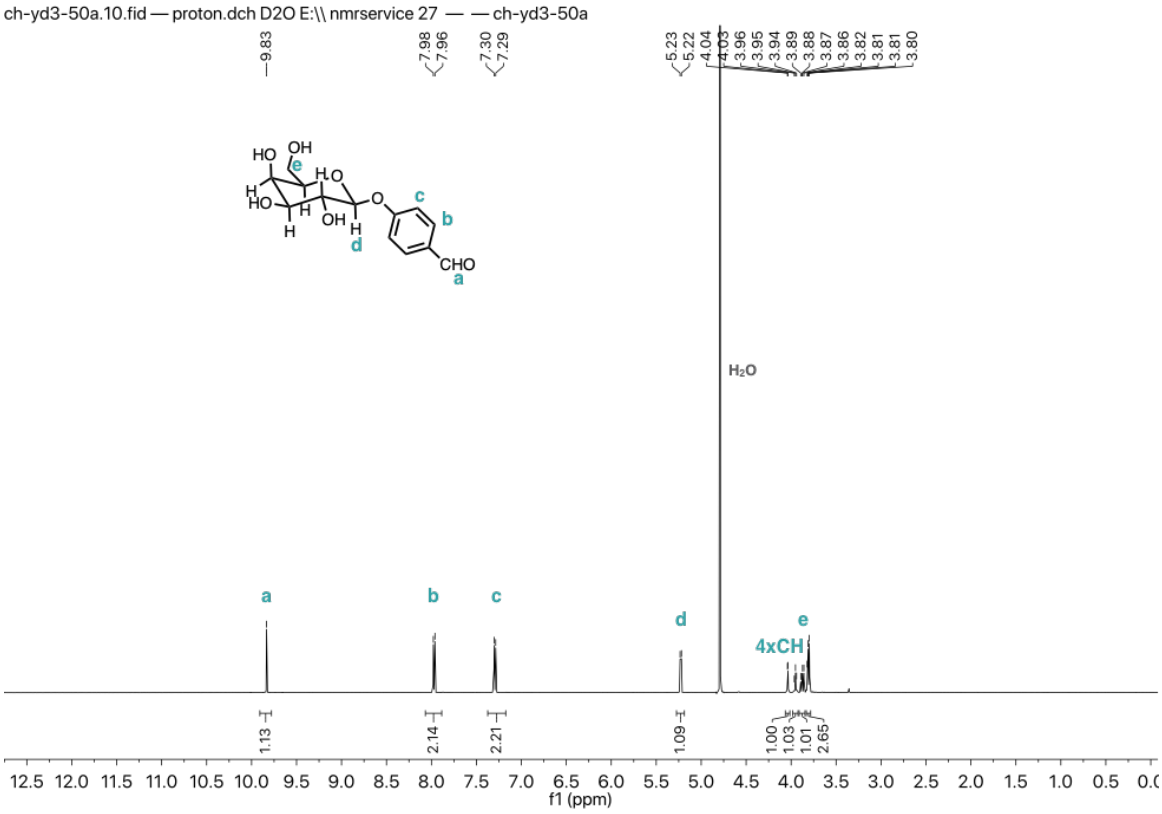

Figure S5.3 [1]H NMR spectra of compound **5-9**.

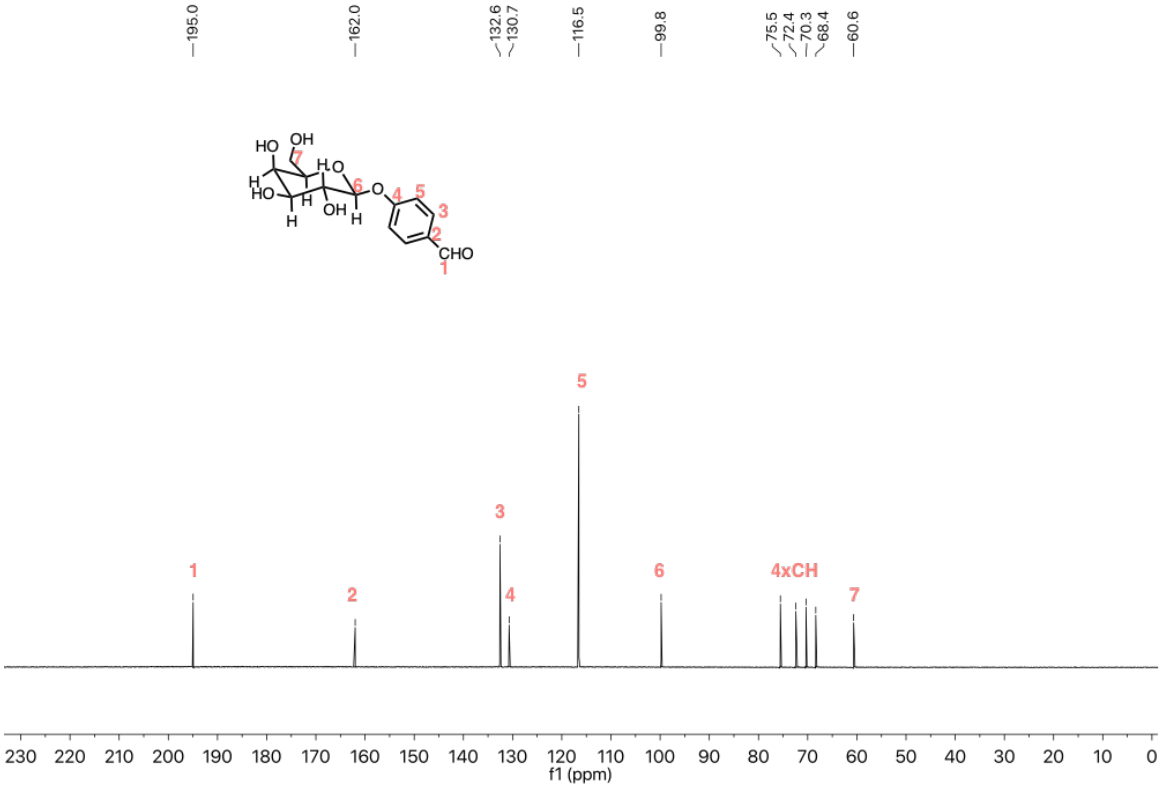

Figure S5.4 [13]C NMR spectra of compound **5-9**.

General protocol for hydrazide-aldehyde reaction

To a methanolic solution of 1 mM hydrazide transducer (1 eq.) and aldehyde (1.5 eq.) was added catalytic amount of acetic acid. The reaction was stirred at room temperature overnight and followed by LC-MS. Once the reaction was finished, the solvent was evaporated under a nitrogen beam for three times (re-dissolved in methanol). The product was used without further purification.

Compound 5-2 (short galactose transducer)

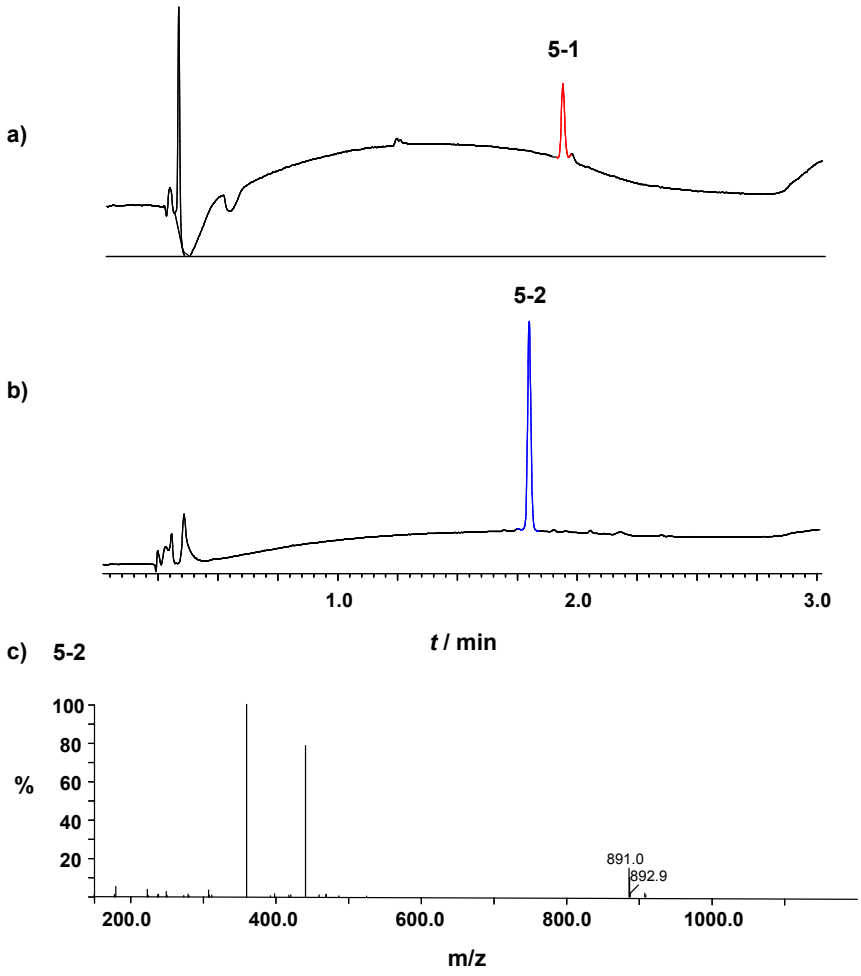

Figure S5.5 UPLC trace of a) starting material short hydrazide transducer **5-1** (retention time: 1.95 min) and b) a reaction mixture of compound **5-1** and compound **5-9**. c) The mass spectrum (ES+) of the single peak (retention time: 1.81 min) which corresponds to product short galactose transducer **5-2** (MW = 890.1; $[M+H^+]$).

Compound 5-5 (long galactose transducer)

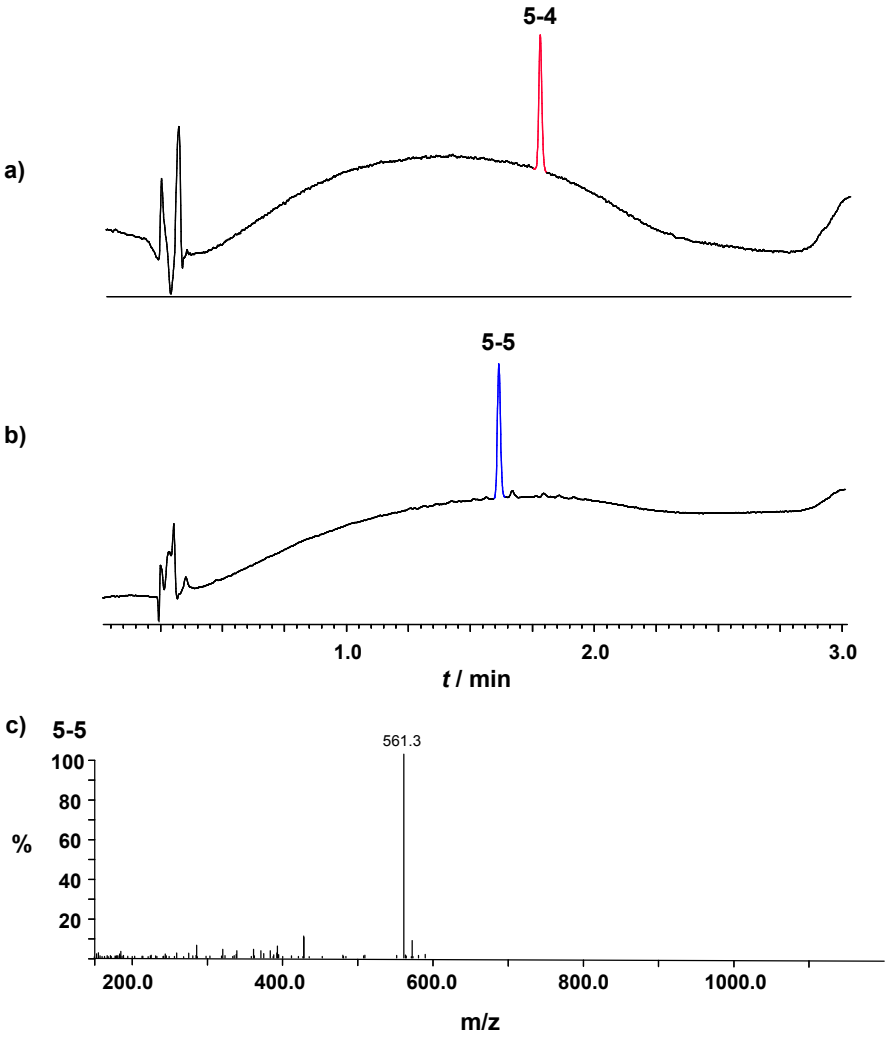

Figure S5.6 UPLC trace of a) starting material long hydrazide transducer **5-4** (red, retention time: 1.77 min) and b) a reaction mixture of compound **5-4** and compound **5-9.** c) The mass spectrum (ES+) of the single peak (blue, retention time: 1.62 min) which corresponds to product long galactose transducer **5-5** (MW = 1120.4; $[M+2H^+]$).

Compound 5-3 (short phenol transducer)

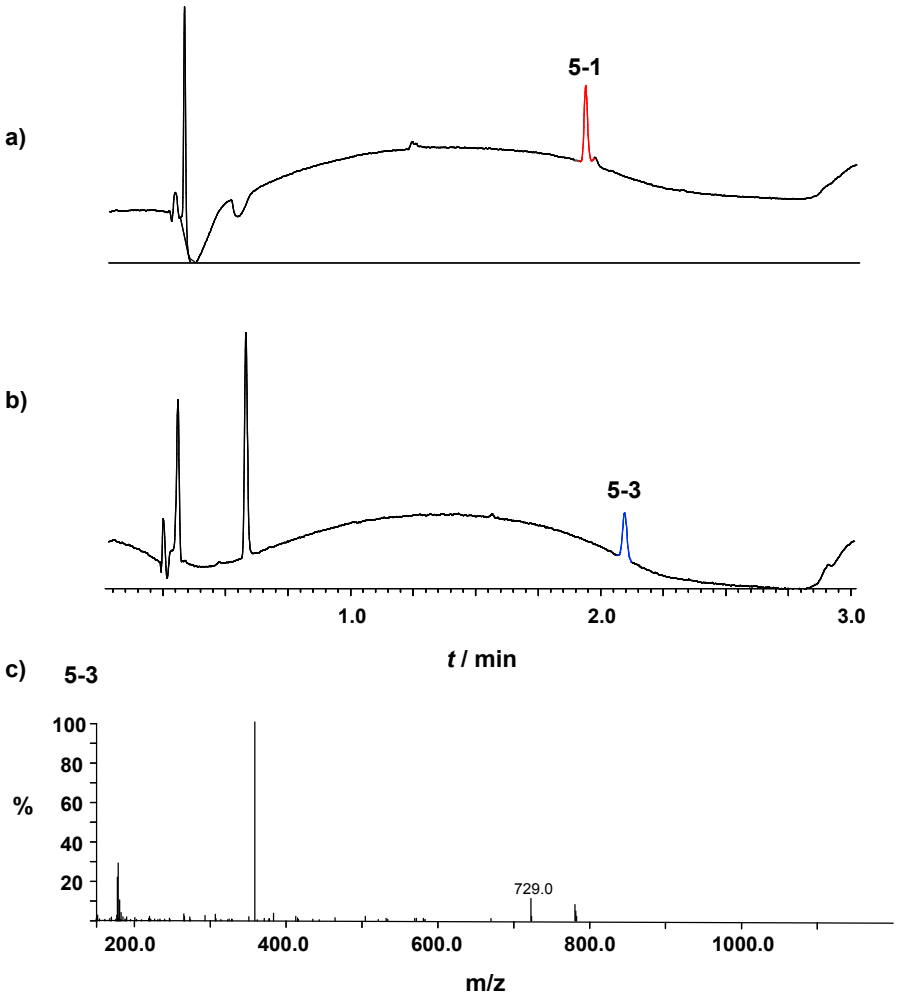

Figure S5.7 UPLC trace of a) starting material short hydrazide transducer **5-1** (red, retention time: 1.95 min) and b) a reaction mixture of compound **5-1** and 4-hydroxyl benzaldehyde (black, retention time: 0.59 min). c) The mass spectrum (ES+) of the peak (blue, retention time: 2.10 min) which corresponds to product short phenol transducer **5-3** (MW = 728.0; $[M+H^+]$).

Compound 5-6 (long phenol transducer)

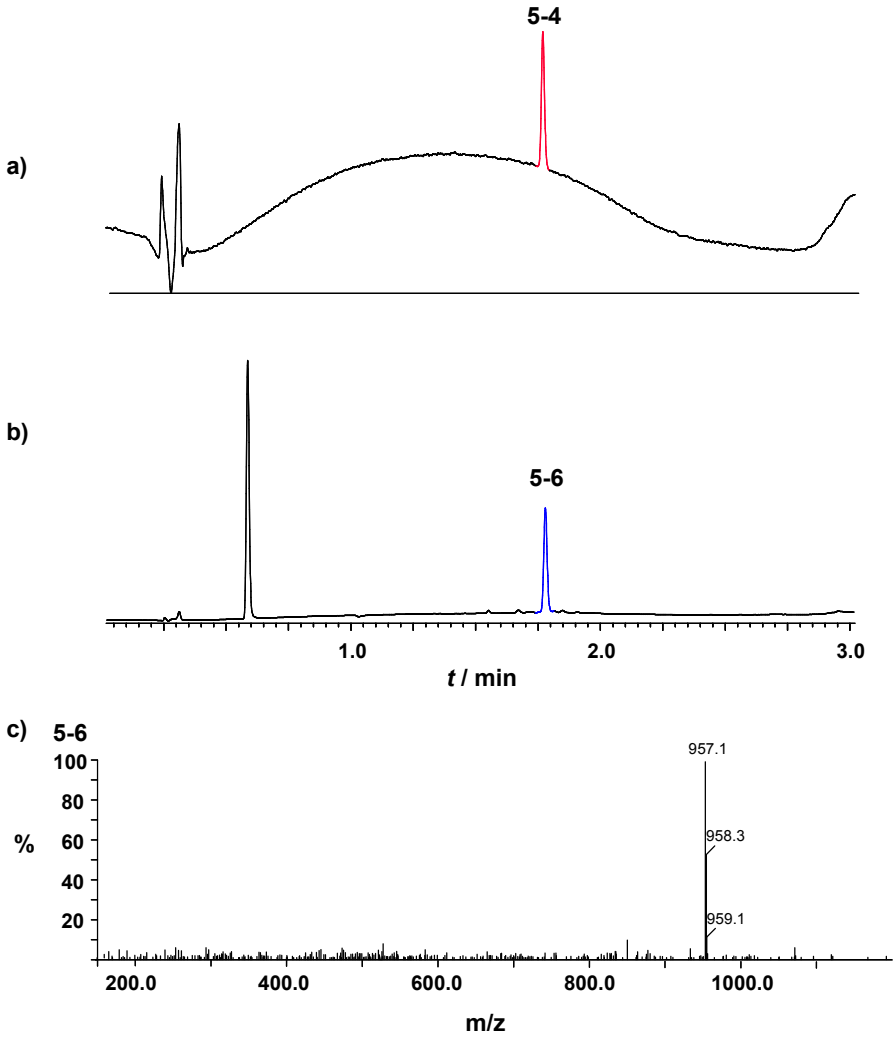

Figure S5.8 UPLC trace of a) starting material long hydrazide transducer **5-4** (red, retention time: 1.77 min) and b) a reaction mixture of compound **5-4** and 4-hydroxyl benzaldehyde (black, retention time: 0.59 min). c) The mass spectrum (ES-) of the peak (blue, retention time: 1.79 min) which corresponds to product long phenol transducer **5-6** (MW = 758.2; $[M\text{-}H^+]$).

5.4.2 Vesicle Experiments

General Protocol for Vesicle Preparation

To a 1.5 mL microcentrifuge tube was added a chloroform solution of lipids (POPC 100%) (and 5 mol% loading of transducer in System A, B, and C) in order to obtain a final lipid concentration of 1 mM in 3.5 mL (final elution volume). The solvent was evaporated using a dry nitrogen stream and dried under high vacuum for at least 2 h to yield a thin lipid film. To the microcentrifuge containing the lipids was added 25 mM HEPES 150 mM NaCl buffer (0.5 mL) at pH 7, as well as stock solutions of ester substrate (and zinc chloride in System A, C,

D, and F) as appropriate to reach final concentrations of 250 µM. After swelling for 1 min, the suspension was subjected to 5 cycles of freeze-thaw using liquid nitrogen and 35°C water bath. The suspension was extruded for 19 times through a 200 nm polycarbonate filter in an extruder apparatus, and then the vesicles were separated by a bulk solution using prepacked SEC columns eluting with the same HEPES buffer at pH 7. Vesicle suspensions can be further diluted using HEPES buffer to 0.1 mM lipid concentration. Finally, 250 µM zinc chloride is added externally in System B, C, E and F.

Fluorescence Measurements

Fluorescence excitation experiments were recorded using the following parameters: emission wavelength = 510 nm, excitation range 380–480 nm, recorded at 2-minute intervals. At the end of the experiment, 5% Triton X-100 (50 µL) and 1M NaOH (50 µL) was added to lyse the vesicles and hydrolyse all of the remaining substrate. The emission measured at this end point (I_{end}) and at the starting point (I_0) were used to normalize the data (see the equation below) taking into account of the dilution factor.

$$I_{norm} = \frac{I - I_0}{I_{end} - I_0}$$

Signalling Experiments

System A and D: To a 1 mL fluorescence cuvette was added 0.1 mM vesicle suspensions (800 µL) described above at *t* = 0 min; **System B, C, D, and E**: 250 µM zinc chloride was added to the 0.1 mM vesicle suspensions (800 µL) described above at *t* = 0 min.

Fluorescence Quenching Experiments

External addition method: 0.1 mM POPC 200 nm vesicles encapsulating 250 µM HPTS in 25 mM HEPES 150 mM NaCl were assembled at pH 7 by following the same protocol described above. 10 µM $CuCl_2$ was added to the vesicle suspensions at *t* = 0 min, followed by an addition of transducer (1 mM in DMSO) at *t* = 10 min; **Pre-incorporation method**: vesicles with 5 mol% loading of transducer were assembled by following the same protocol described above. 10 µM $CuCl_2$ was added to the vesicle suspensions at *t* = 10 min.

This page is intentionally left blank

Your identity is your most valuable possession. Protect it.

The Incredibles

6

^{19}F NMR Studies

6.1 Introduction

Membrane translocation is a recent artificial approach for transmembrane signal transduction developed in our group[1–3]. The key concept is based on the controlled translocation of a synthetic molecular transducer from the outside to the inside of a vesicle, which subsequently leads to catalytic hydrolysis of an encapsulated substrate. We rely exclusively on the fluorescent emission of the hydrolysed products in the vesicles to determine whether the system is ON or OFF: when the internal hydrolysis rate of substrate is low, we classify the system as OFF; when a relatively rapid increase in the product fluorescent emission is observed, the system is classified as ON. The proposed translocation mechanism is therefore inferred from collective observations of relative reaction rates of hundreds if not thousands of vesicle signalling experiments. However, apart from fluorescence measurements, there are few techniques that provide a more detailed understanding of how the transducers behave in the membrane as it is highly challenging to directly observe molecular movement within the lipid bilayer.

The transmembrane signalling as well as ion transport experiments in Chapter 5 suggest that the translocation mechanism may be much more complex than a simple translational movement. It is possible that the pyridine-oxime catalytic head group partitions between the membrane-aqueous interface and membrane hydrocarbon environment, and we hypothesised in Chapter 5 that the membrane-embedded transducer may be U-shaped so that both head groups can be exposed to the same aqueous phase.

^{19}F NMR spectroscopy is a powerful tool in the study of biological systems such as protein structure and dynamics.[4,5] ^{19}F nucleus is relatively easy to be incorporated in biomolecules through conventional protein-labelling techniques. Because of its small size, ^{19}F nucleus provides a rather non-perturbing probe compared to other probes such as fluorescent dyes which usually consist of large conjugated systems. More importantly, the chemical shift of ^{19}F has large dispersion and is sensitive to changes in the local environment, including Van der Waals interactions and local electrostatic fields.[6] ^{19}F chemical shift is determined primarily by the five 2p electrons of fluorine, which have a large paramagnetic term in the shielding formula. Therefore, water solvated and membrane-embedded fluorine-labelled molecules should have different chemical shifts, providing direct evidence on the local environment. In order to probe the positioning of the catalytic head group, we have designed and synthesised a series of fluorine labelled molecules that have the same pyridine-oxime catalytic head group as previously studied transducers, and used ^{19}F NMR spectroscopy to investigate the chemical environment in the lipid bilayer.

6.2 Results and discussion

6.2.1 Synthesis of ^{19}F-Labelled Molecules

Fluorine atom(s) should ideally be placed as close as possible to the catalytic centre so that they report directly on the position of the pyridine-oxime head group in the lipid bilayer. Two possible labelling positions are: 1) the alpha-position of the oxime, and 2) 3-, 4-, or 5-position of the pyridine ring. From the synthesis point of view, as the transducer is not symmetric, introducing a fluorine nucleus on the 3- or 5-position of pyridine dioxime precursor would result in a 50/50 mixture of two products, as shown in Scheme 6.1. This would complicate the synthesis as well as the interpretation of subsequent experiments. Therefore, 4-position of the pyridine would be the appropriate choice because a substitution on this position does not change the overall C_{2v} symmetry of pyridine dioxime. Trifluoromethyl group was selected as the signal is three times stronger than one single fluorine substitution, and as 4-trifluoromethyl pyridine, the corresponding starting material, is commercially available.

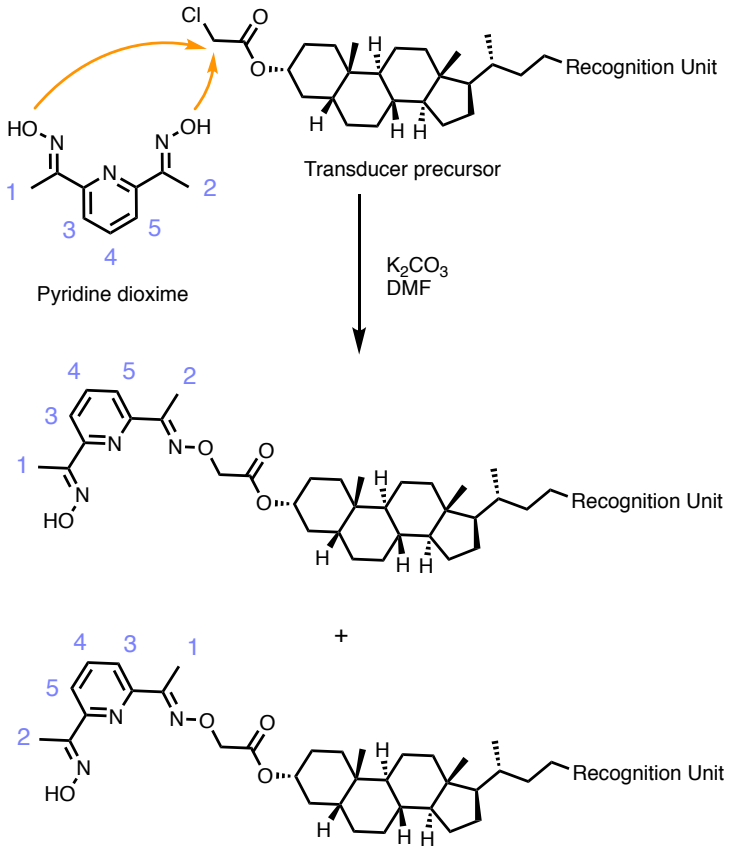

Scheme 6.1 Substitution of transducer precursor with pyridine-oxime *via* S_N2 mechanism

Figure 6.1 shows the structure of a series of ^{19}F-labelled molecules designed and studied in this chapter. **6-1** is the precursor of water soluble trifluoropyridine dioxime **6-2**. *O*-Monohexyl substituted pyridine dioxime **6-3** is a simplified version of an ON state transducer. The hexyl group represents the membrane anchor as well as the membrane-permeable recognition head group that would presumably allow pyridine unit to sit at the membrane-water interface. *O*,*O*-Dihexyl substituted pyridine dioxime **6-4** differs from the transducer mono-oxime structure. The two hexyl chains make the molecule highly hydrophobic and should allow the whole molecule to be embedded deep in the lipid bilayer. Compound **6-5** was designed as a closer mimic of the ON state transducer with another trifluoromethyl group attached to the other end of the lithocholic acid core. This trifluoromethyl group should always reside inside the membrane regardless of zinc(II) binding on the other end of the molecule. ^{19}F-labelled galactose transducer **6-6** was also synthesised as an example of an OFF state transducer.

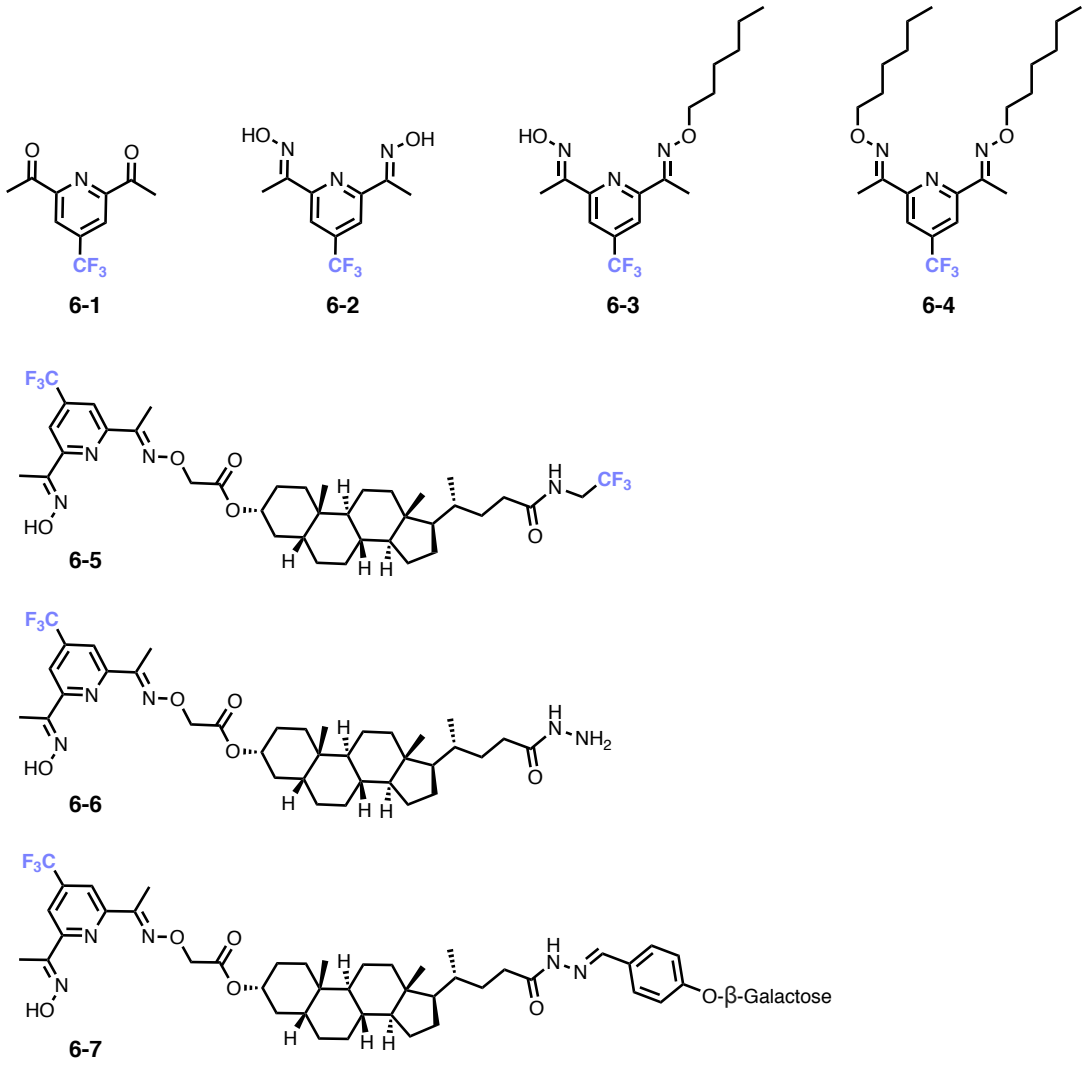

Figure 6.1 Structures of ^{19}F-labelled molecules.

The synthesis of each molecule is shown in Scheme 6.2 – 6.5. Compound **6-1** was synthesised from 4-trifluoropyridine with pyruvic acid by Minisci reaction.[7] Condensation of 2 equivalents of hydroxylamine with **6-1** gave pyridine dioxime **6-2**. *O*-Hexylhydroxylamine was synthesised in two steps from *N*-hydroxyphthalimide: substitution of 1-bromohexane under basic conditions followed by hydrolysis with hydrazine. Treating one equivalent of *O*-hexylhydroxylamine with compound **6-1** and subsequent condensation with hydroxylamine yielded *O*-monohexyl substituted pyridine dioxime **6-3**, whilst treating two equivalents of *O*-hexylhydroxylamine gave *O*,*O*-dihexyl substituted pyridine dioxime **6-4**.

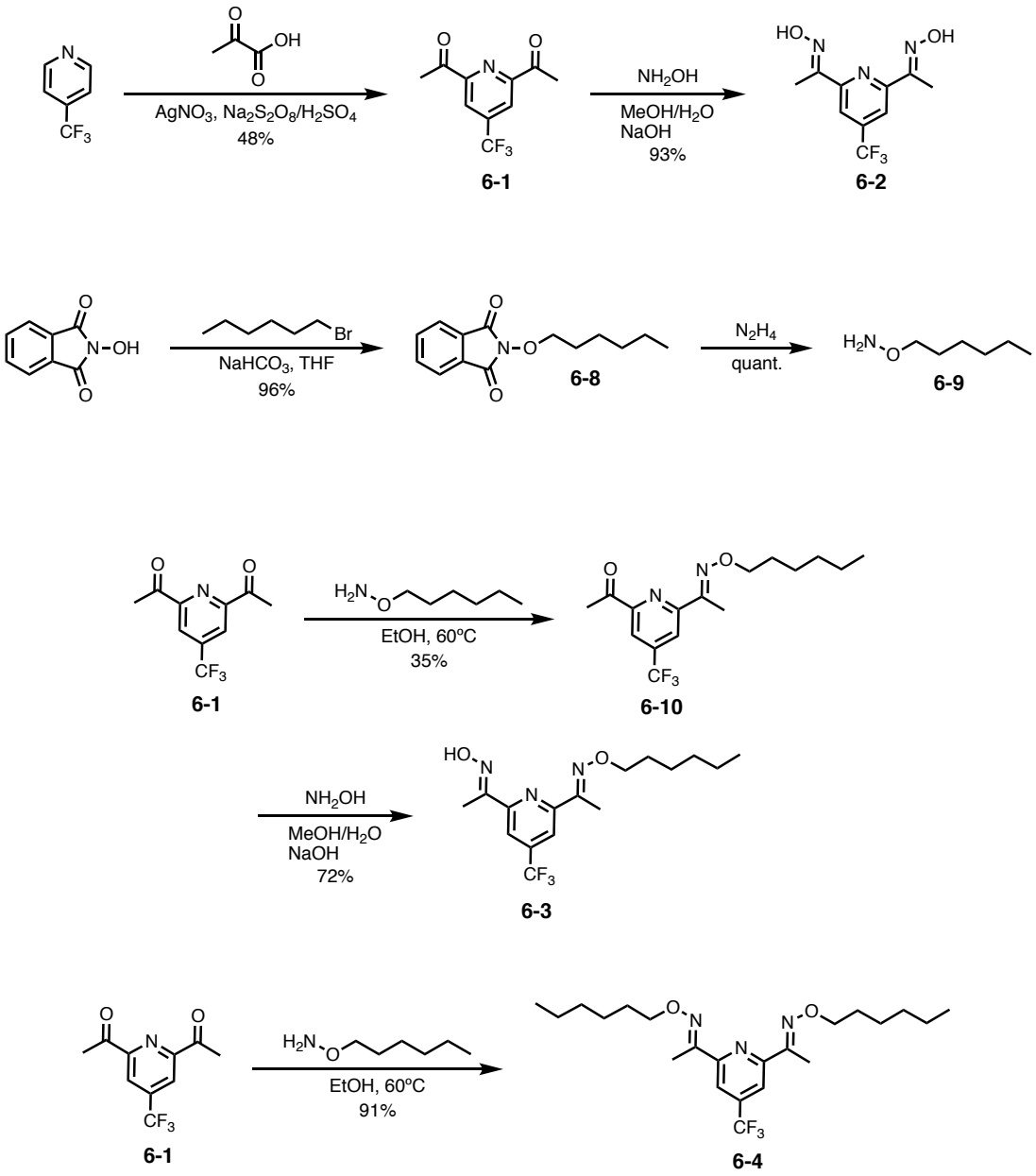

Scheme **6.2** Synthesis of compounds **6-1** - **6-4**.

Model transducer **6-5** was synthesised in four steps from lithocholic acid as shown in Scheme 6.3. EDC coupling of the carboxylic acid with 1,1,1-trifluoroethylamine gave intermediate amide **6-11**. Condensation of 1 equivalent of chloroacetyl chloride gave compound **6-12**. Subsequent functionalisation with 4-trifluoromethyl pyridine dioxime **6-2** ligand gave **6-5**.

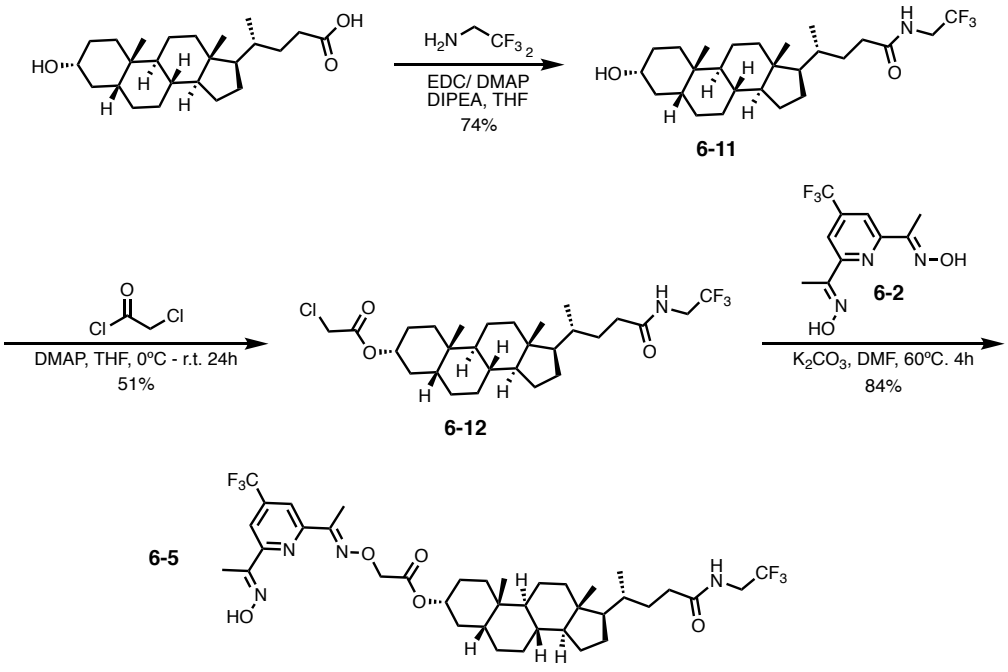

Scheme 6.3 Synthesis of **6-5**.

Synthesis of ^{19}F-labelled hydrazide transducer **6-6** and galactose transducer **6-7** is shown in Scheme 6.3. Starting material **6-13** was a generous gift from Dr Istvan Kocsis (unpublished results, for synthesis route see the Supporting Information). Functionalisation with 4-trifluoromethyl pyridine dioxime **6-2** ligand gave Boc-protected compound **6-14**. Deprotection using hydrochloric acid gave transducer **6-6**. Condensation of hydrazide **6-6** with 4-beta-galactose benzaldehyde **6-15** gave transducer **6-7**.

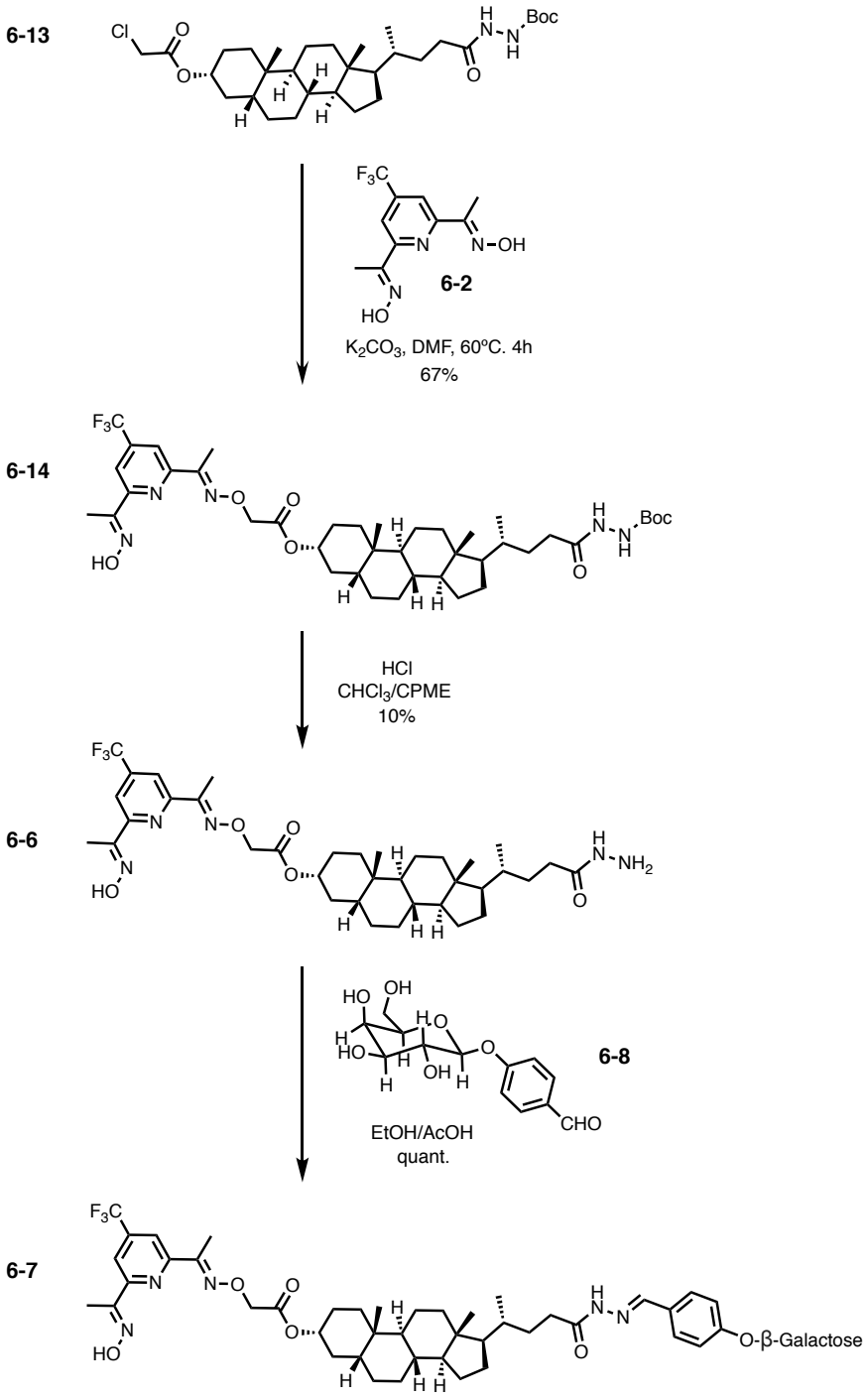

Scheme 6.4 Synthesis of ^{19}F-labelled transducer **6-6** and **6-7**.

6.2.2 ^{19}F NMR Studies in Chloroform

^{19}F NMR studies were conducted on a 400 MHz NMR spectrometer with Neo Prodigy BBO Cryoprobe. The results were highly reproducible with no or negligible batch-to-batch chemical shift differences of the same sample.[8]

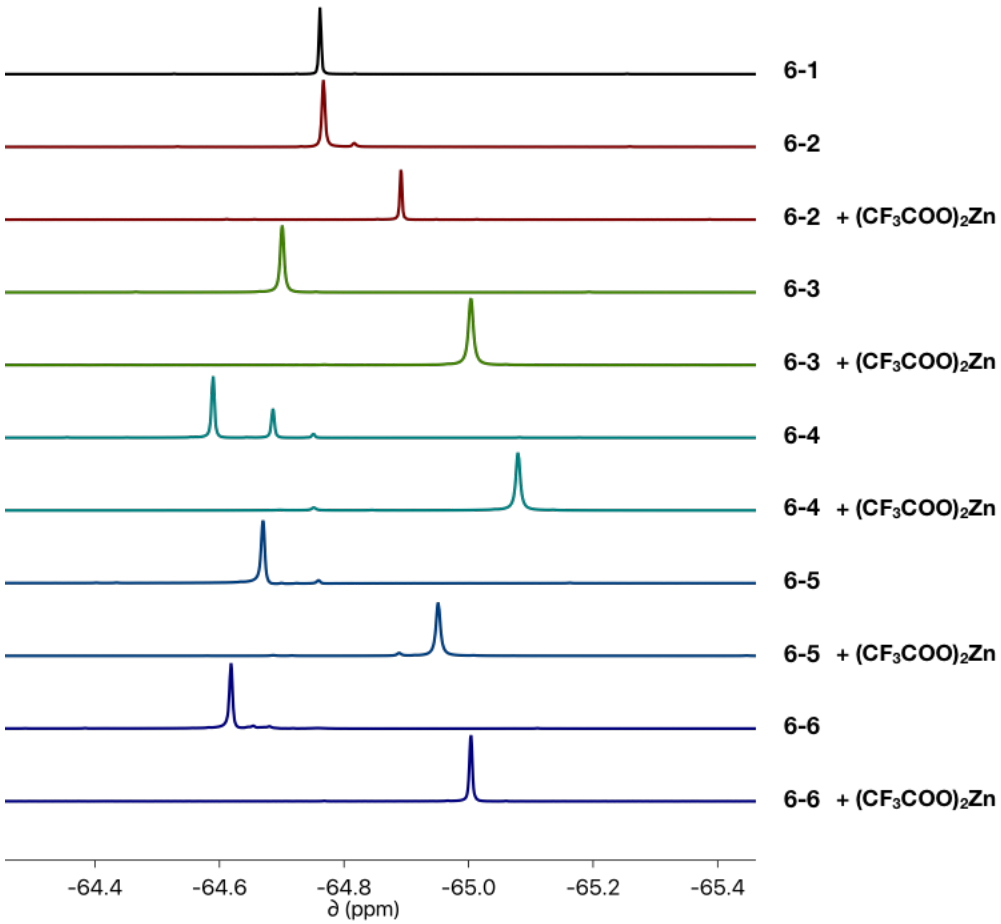

Figure 6.2 400 MHz ^{19}F NMR spectra of compound **6-1**— **6-6** (10 mM) and after addition of 20 mM of zinc trifluoroacetate in chloroform-d at room temperature.

The ^{19}F NMR spectra of all samples in deuterated chloroform are shown in Figure 6.2. In general, addition of zinc trifluoroacetate moves the fluorine signal upfield by 0.1 – 0.6 ppm. The chemical shift of the ^{19}F signal observed for the diketone **6-1**, the dioxime **6-2** and the mono-*O*-hexyl substituted pyridine dioxime **6-3** are very similar in chloroform. For *O,O*-dihexyl substituted pyridine dioxime **6-4**, two signals were observed in the ^{19}F NMR spectrum with a ratio of approximately 3:1. Two signals with close retention times were also observed in the UPLC trace and these two signals have the same molecular mass which corresponds to pyridine oxime **6-4**, see Supporting Information. This evidence suggests that pyridine dioxime **6-4** has two isomers in slow exchange on the NMR and LC-MS time scale. One possible explanation for the existence of isomers is that compared to **6-2** and **6-3**, **6-4** cannot form an intramolecular hydrogen bond (see Figure 6.3 and 6.4) which would favour the *E,Z*- isomer. Upon binding with zinc(II), the two signals observed for **6-4** changed to one signal at -65.08 ppm. This suggests that *E/Z* isomers of **6-4** were able to convert to *E,E*-isomer at room temperature as zinc complexation requires specific *E,E*- configuration (see Figure 6.4).

^{19}F chemical shifts observed for transducer **6-5** were -64.67 ppm (a singlet) -72.54 ppm (a triplet), corresponding to the trifluoromethyl group on the pyridine and the trifluoromethyl group on the amide. Zinc(II) complexation shifted the singlet upfield -0.36 ppm and the triplet remained unchanged as zinc binding has no effect on the amide bond at the other end of the molecule. ^{19}F chemical shift observed for hydrazide transducer **6-6** was -64.63 ppm. Binding with zinc(II) shifted the signal upfield 0.38 ppm to -65.01 ppm. The galactose transducer **6-7** had very poor solubility in chloroform and therefore the ^{19}F NMR spectrum could not be recorded.

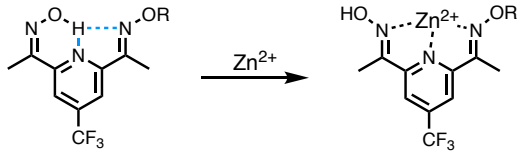

R = H **6-1**

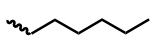

6-2

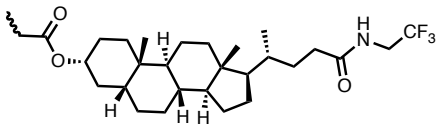

6-3

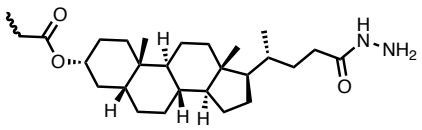

6-4

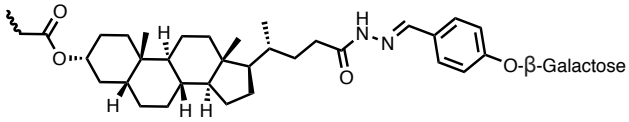

6-5

Figure 6.3 Proposed intramolecular hydrogen-bond in compound **6-1**, **6-2**, -**6-3**, **6-5**, **6-6** breaks upon zinc(II) binding.

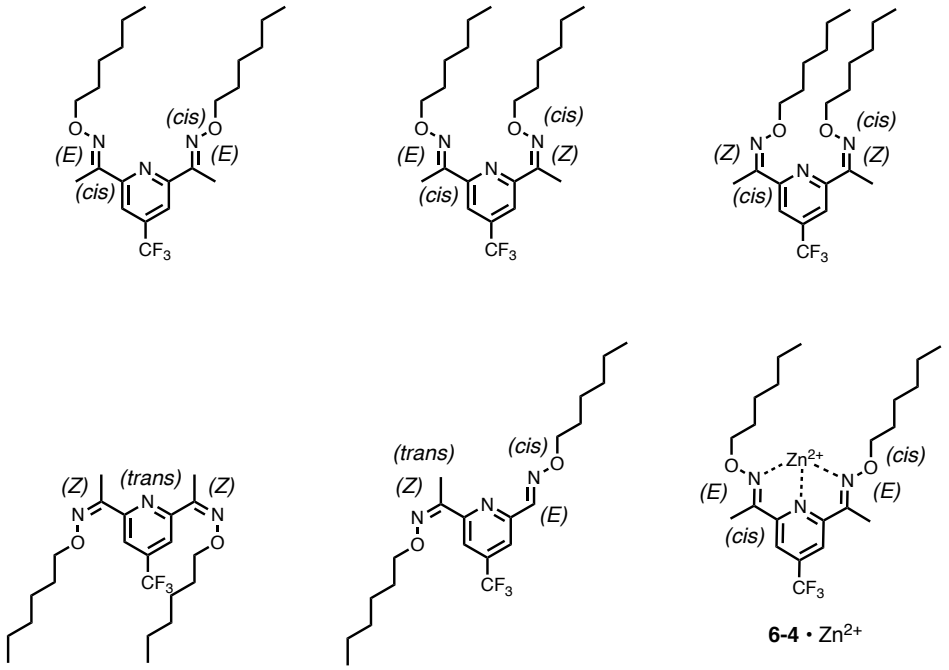

Figure 6.4 Possible E/Z and cis-/trans- isomers of *O,O*-dihexyl oxime **6-4** and zinc(II) complex **6-4**•Zn(II).

6.2.3 ^{19}F NMR Studies in Water and Lipid Bilayer Membrane

We then pre-incorporated the compounds into 20 mM 200 nm POPC vesicles to achieve a 5 mol% loading (relative to lipids) in HEPES buffer saline with 10 v/v% deuterated water at pH 7. This HEPES buffer solution with deuterated water was prepared in one batch for all NMR studies to avoid any solvent isotope effect.[9] The ^{19}F NMR spectra were recorded, and another set of data for each compound was recorded after addition of 25 mM $ZnCl_2$ in the buffer solution. The relative concentration of Zn^{2+} is similar to that used in the signalling experiments in the previous chapters and the published results. All spectra are shown in Figure 6.5. Compared to ^{19}F NMR spectra in chloroform, the spectra recorded in the POPC membrane are significantly broader. As T_2 relaxation is caused by transient magnetic fields and usually due to molecular tumbling, when movement is more restricted, for example in a lipid bilayer in this case, the molecular motion becomes slower, thus the elongated autocorrelation time τ_c drives T_2 relaxation faster and resulting in line broadening (T_2 is in inverse proportion to the signal width at half-height). Anisotropic molecular motion due to packing into lipid bilayer might contribute to further line broadening as well.

Compound **6-1** is not soluble in water. When incorporated into POPC membrane, the ^{19}F chemical shift observed for **6-1** is -64.57 ppm. Pyridine dioxime **6-2** is an amphiphile with good water solubility, for which ^{19}F chemical shift observed is -64.65 ppm in a HEPES buffer. Upon addition of $ZnCl_2$, the signal did not move. Incorporating pyridine dioxime **6-2** into POPC membranes results a 0.35 ppm chemical shift downfield to -64.30 ppm compared to the results in buffer without vesicles. Addition of $ZnCl_2$ moved the signal upfield to –64.72

ppm. These results suggested zinc(II) binds compound **6-2** in water and at the membrane surface.

O-Hexyl mono-oxime **6-3** is not water soluble, however, it can be dissolved in the lipid bilayer and the ^{19}F chemical shift observed is -64.46 ppm. Zinc(II) binding did not change either the shape or the chemical shift of the signal. Similar to the spectrum in deuterated chloroform, when incorporated into lipid bilayer membranes, there are two ^{19}F chemical shifts observed for *O*,*O*-dihexyl substituted pyridine dioxime **6-4**, which possibly correspond to *E*/*Z*-isomers. However, whilst the two signals did merge into one upon zinc binding in chloroform, adding zinc chloride to the system has no effect on the ^{19}F NMR spectrum when the compound is in the membrane environment.

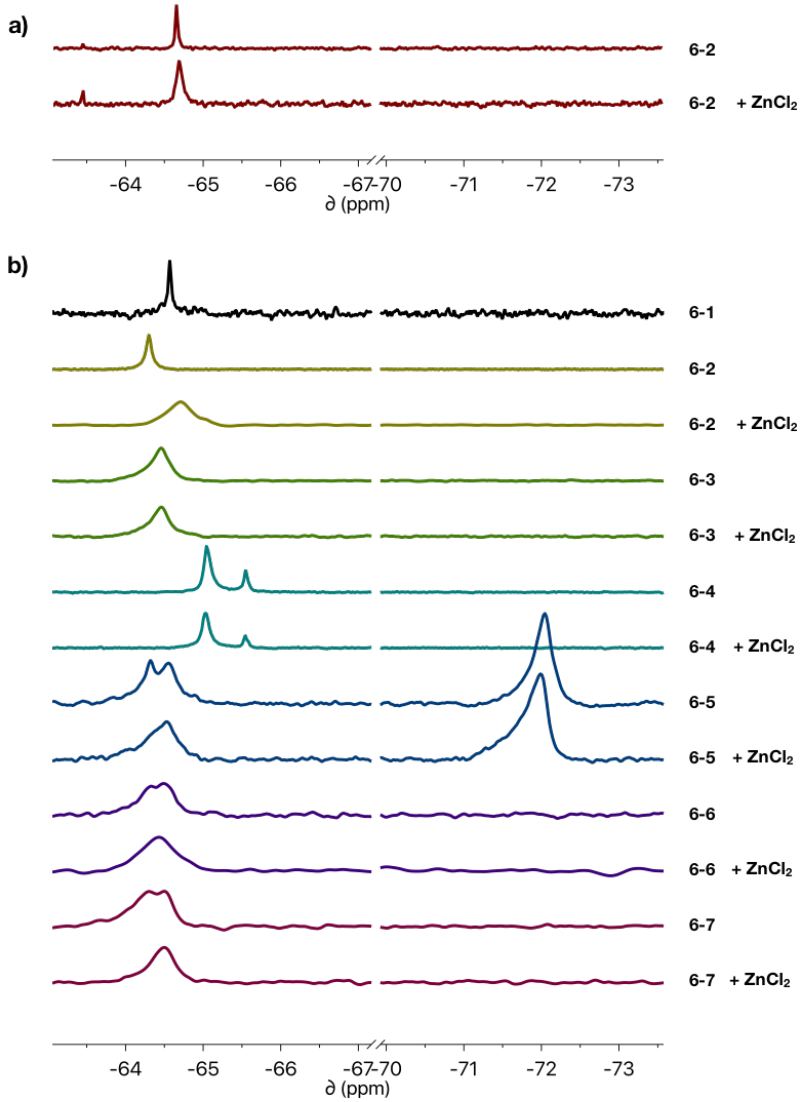

Figure 6.5 400 mM ^{19}F NMR spectra at room temperature of a) 1 mM pyridine dioxime **6-2** in 25 mM HEPES buffer 150 mM NaCl with and without 5 mM $ZnCl_2$; b) compound **6-1** — **6-7** embedded in 20 mM 200 nm POPC vesicles (5 mol% loading) in 25 mM HEPES 150 mM NaCl buffer at pH 7. Samples with $ZnCl_2$ were prepared with additional 5 mM $ZnCl_2$.

There are two possible ways to interpret these two observations: 1) Zn^{2+} does not bind to membrane embedded *O*-hexyl mono-oxime **6-3** and *O*,*O*-dihexyl-substituted pyridine dioxime **6-4**, or 2) binding Zn^{2+} does not change the chemical environment of trifluoromethyl pyridine in this particular experiment. However, without further experimental evidence we cannot draw a definite conclusion.

As expected, the trifluoromethyl group at the alpha position of amide bond of transducer **6-5** remains unchanged when zinc(II) is introduced into the system, because this part of the transducer is hydrophobic and therefore embedded inside the lipid bilayer. The fact that two ^{19}F signals were observed for **6-5**, **6-6**, and **6-7** when embedded into POPC membranes suggests that for each of the transducers, the pyridine-oxime head group is in two different chemical environments in slow exchange. These two signals could correspond to the pyridine unit of the transducer partitioning in between lipid bilayer and the membrane-water interface. Adding $ZnCl_2$ merged the two signals into one, indicating that all transducers were able to bind zinc(II) regardless of the attached recognition head group. For galactose transducer **6-7**, the saccharide head group is polar, therefore should preferably locate in the aqueous phase. In the presence of Zn^{2+}, the pyridine-oxime head group should also be at the membrane-water interface for a couple of reasons: First, this metal ion-ligand complex is charged, hydrophilic and therefore prefers aqueous environment over hydrocarbon chains; Second, this compound catalyzes the hydrolysis reaction in the presence of zinc (see Supporting Information). As the substrate is highly charged and not membrane-permeable, the catalytic head group can only participate in the reaction in the aqueous environment. These results suggest that transducers could be in equilibrium between the two states at the membrane-water interface, see Figure 6.8.

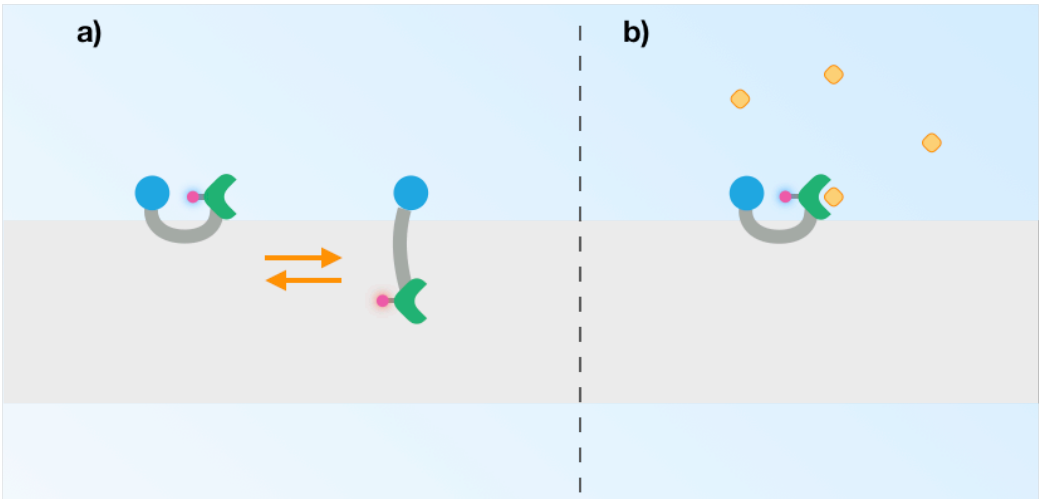

Figure 6.6 Schematic illustration of a) transducer in lipid bilayer membrane without the presence of Zn^{2+} (yellow), where the catalytic head group (green) partitions at membrane-water interface and membrane environment, and b) upon Zn^{2+} binding, the catalytic head group resides solely at the membrane-water interface. 19F label is shown in red.

6.3 Conclusion

To conclude, we have synthesised a series of model molecules and transducers with trifluoromethyl group at the 4-position on pyridine mono-oxime and used ^{19}F NMR to determine the positioning of the catalytic head group in the lipid bilayer membrane. Zinc(II)-binding is confirmed in chloroform-d for all molecules. These molecules can be incorporated into POPC lipid bilayers. There are two signals of fluorine signals observed for transducers without zinc(II) binding in the membrane, indicating the catalytic head group is at two different local chemical environments in slow exchange. Adding zinc chloride into the system merges two signals into one, which confirms zinc binding to transducers at membrane-water interface. Based on these observations, it is suggested that in the OFF state, transducers could be U-shaped as the catalytic head group may partition between membrane-water interface and membrane environment. This study provides further understanding of the previously proposed translocation mechanism. For the first time the system has been studied by using NMR spectroscopy techniques to examine the transducer movement on a molecular level, benefiting any further development of artificial transmembrane signalling systems in the group or beyond.

References

(1) Langton, M. J.; Keymeulen, F.; Ciaccia, M.; Williams, N. H.; Hunter, C. A. Controlled Membrane Translocation Provides a Mechanism for Signal Transduction and Amplification. *Nat. Chem.* **2017**, *9* (5), 426–430. https://doi.org/10.1038/nchem.2678.

(2) Langton, M. J.; Williams, N. H.; Hunter, C. A. Recognition-Controlled Membrane Translocation for Signal Transduction across Lipid Bilayers. *J. Am. Chem. Soc.* **2017**, *139* (18), 6461–6466. https://doi.org/10.1021/jacs.7b02345.

(3) Langton, M. J.; Scriven, L. M.; Williams, N. H.; Hunter, C. A. Triggered Release from Lipid Bilayer Vesicles by an Artificial Transmembrane Signal Transduction System. *J. Am. Chem. Soc.* **2017**, *139* (44), 15768–15773. https://doi.org/10.1021/jacs.7b07747.

(4) Chen, H.; Viel, S.; Ziarelli, F.; Peng, L. 19 F NMR: A Valuable Tool for Studying Biological Events. *Chem. Soc. Rev.* **2013**, *42* (20), 7971–7982. https://doi.org/10.1039/C3CS60129C.

(5) Marsh, E. N. G.; Suzuki, Y. Using 19F NMR to Probe Biological Interactions of Proteins and Peptides. *ACS Chem. Biol.* **2014**, *9* (6), 1242–1250. https://doi.org/10.1021/cb500111u.

(6) Sloop, J. C. 19-Fluorine nuclear magnetic resonance chemical shift variability in trifluoroacetyl species https://www.dovepress.com/19-fluorine-nuclear-magnetic-resonance-chemical-shift-variability-in-t-peer-reviewed-article-ROC (accessed Sep 29, 2019). https://doi.org/10.2147/ROC.S38495.

(7) Minisci, F.; Galli, R.; Cecere, M.; Malatesta, V.; Caronna, T. Nucleophilic Character of Alkyl Radicals: New Syntheses by Alkyl Radicals Generated in Redox Processes. *Tetrahedron Lett.* **1968**, *9* (54), 5609–5612. https://doi.org/10.1016/S0040-4039(00)70732-5.

(8) Rosenau, C. P.; Jelier, B. J.; Gossert, A. D.; Togni, A. Exposing the Origins of Irreproducibility in Fluorine NMR Spectroscopy. *Angew. Chem. Int. Ed.* **2018**, *57* (30), 9528–9533. https://doi.org/10.1002/anie.201802620.

(9) Solvent-Induced Deuterium Isotope Effects on 19F Chemical Shifts of Some Substituted Fluorobenzenes. Formation of Inclusion Complexes. *J. Magn. Reson. 1969* **1985**, *62* (3), 487–496. https://doi.org/10.1016/0022-2364(85)90217-3.

6.4 Supporting Information

6.4.1 Synthetic procedures and characterizations

Materials and methods

^{1}H NMR and ^{13}C NMR spectra were recorded on a 400-MHz Bruker® spectrometer. Chemical shifts are reported as δ values in ppm. Flash chromatography was carried out on an automated system (Combiflash® Rf+ Lumen™) using pre-packed cartridges of silica (25 µm PuriFlash® Column) or neutral alumina (50 µm RediSep® Rf Column). GPC purification of the vesicles was carried out using GE Healthcare PD-10 desalting columns prepacked with Sephadex® G-25 medium. Fluorescence spectra were recorded using a Cary Eclipse fluorescence spectrophotometer (Agilent Technologies) in Hellma® Analytics Suprasil® quartz cuvettes. Measurements of pH were conducted using a Mettler-Toledo SevenCompact™ pH meter equipped with an InLab® Micro electrode. Vesicles were assembled in Eppendorf® polypropylene Protein LoBind® polypropylene microcentrifuge tube and extruded as described below using Avanti® Polar Lipids extruder kits, equipped with Avestin® LiposoFast Liposome Factory 200 nm polycarbonate membranes with GE Healthcare Whatman® 10 mm polyester filter support. Solutions or vesicles suspensions were transferred using Eppendorf Multipette® Xstream Pippette with Combitips Advanced® or Hamilton Microliter™ syringes. All reagents and solvents were used without further purification. Chemicals were purchased from Sigma-Aldrich® and used without further purification.

Synthesis and Characterizations

Compound 6-1

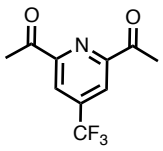

Synthesis of compound **6-1** has been previously reported.[1] Briefly, 4-(trifluoromethyl) pyridine (0.76 g, 6.8 mmol, 1 eq.) was dissolved in 0.5 M sulfuric acid (40 mL). Pyruvic acid (1.8 g, 20.4 mmol, 3.0 eq.) and silver nitrate (0.12 g, 0.68 mmol, 0.1 eq., 10 mol% dissolved in 1 mL of deionized water) were added. Finally, sodium persulfate (4.9 g, 20.4 mmol, 3 eq.) was added with vigorous stirring. The reaction mixture was stirred at 70°C overnight. The reaction was basified to pH 10 using concentrated sodium hydroxide. The reaction mixture was extracted with dichloromethane (3 x 20 mL) and the extracts were combined and filtered through a short silica pad. After evaporation of solvent, the crude was purified by flash chromatography to give the product as colorless needle-like crystals (750 mg, 48% yield).

^{1}H NMR (400 MHz, $CDCl_3$) δ (ppm): 8.43 (2H), 2.82 (6H).
^{13}C NMR (100 MHz, $CDCl_3$) δ (ppm): 197.8, 154.0, 141.0 (q, *J* = 35 Hz), 121.6 (q, *J* = 280 Hz), 120.5 (q, *J* = 12 Hz), 25.6.
^{19}F NMR (400 MHz, $CDCl_3$) δ (ppm): -64.76 (s, 3F).
HR-MS (ES+) calcd. for. $C_{10}H_9NO_2F_3$: 232.0585, found: 232.0589
All characterization data matched literature.[1]

Compound 6-2

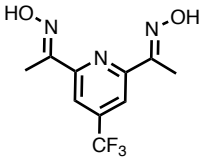

To a solution of compound **6-1** (200 mg, 0.86 mmol, 1 eq.) and hydroxylamine hydrochloride (180 mg, 2.60 mmol, 3 eq.) in 1:1 (v/v) chloroform and methanol mixture was added sodium hydroxide (72.4 mg, 1.81, 2.1 eq.). The reaction mixture was microwaved at 90 °C for 2 h. 10 mL of cooled and deionized water was added to the mixture. The precipitate was filtrated and air dried to result the product as white solid (210 mg, 93% yield).

^{1}H NMR (400 MHz, DMSO-d_6) δ (ppm): 11.94 (2H), 7.96 (2H), 2.24 (6H).

^{13}C NMR (100 MHz, DMSO-d_6) δ (ppm): 157.9, 156.2, 140.0 (q, J = 34 Hz), 125.5 (q, J = 220Hz), 122.2, 116.6, 12.7.

^{19}F NMR (400 MHz, DMSO-d_6) δ (ppm): -63.74 (s, 3F).

HR-MS (ES+) calcd. for. $C_{10}H_{11}N_3O_2F_3$: 262.0803, found: 262.0813.

FT-IR (ATR): ν_{max} 3241, 3081, 2929, 1569, 1411,1278, 1174, 1134, 1015 cm^{-1}.

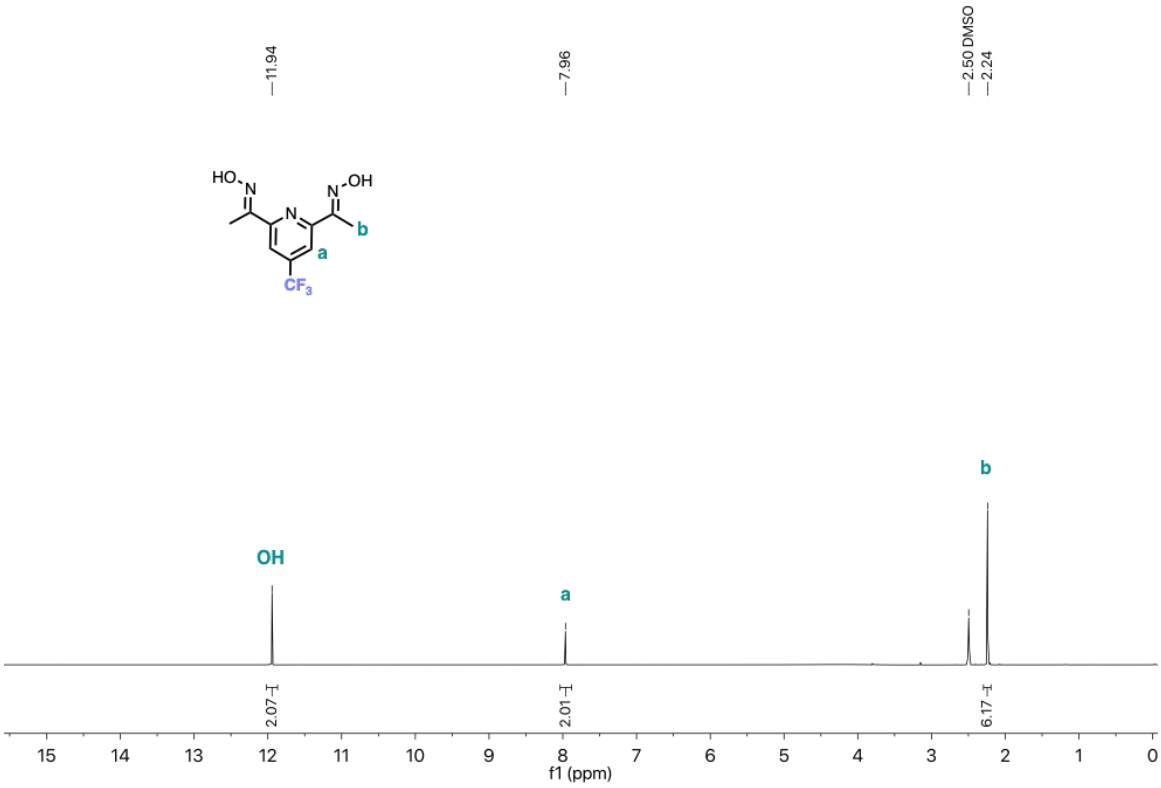

Figure S6.1 ^{1}H NMR spectrum of compound **6-2**.

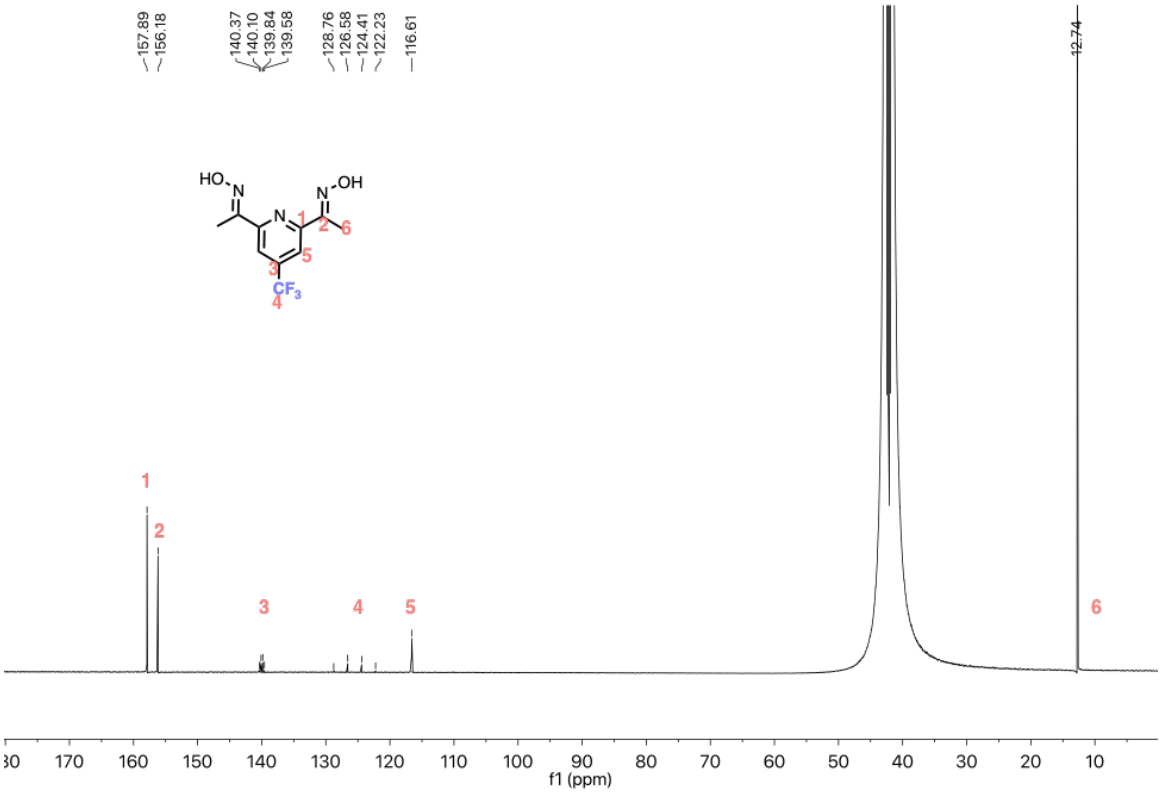

Figure S5.2 ^{13}C NMR spectrum of compound **6-2**.

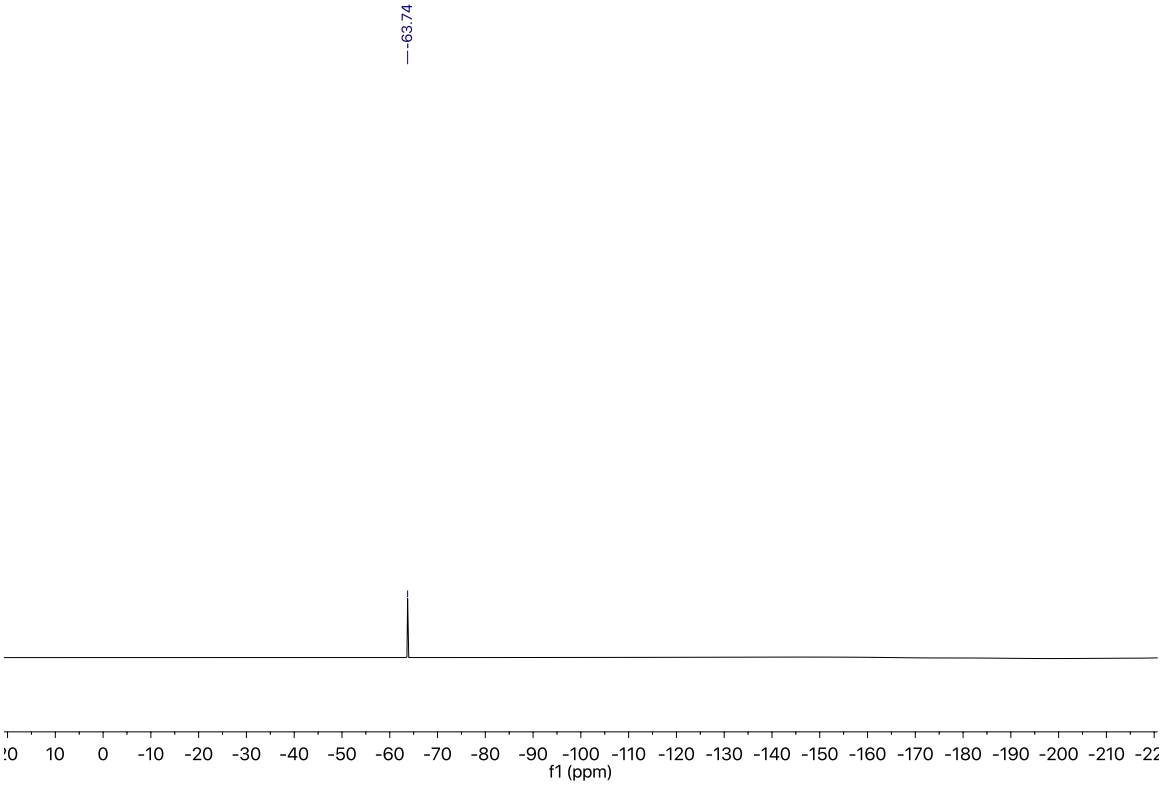

Figure S6.3 ^{19}F NMR spectrum of compound **6-2**.

Compound 6-8

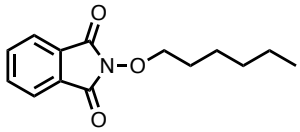

The synthesis of compound **6-8** was adapted from literature.[2] To a solution of *N*-hydroxyphtalimide (1 g, 6.1 mmol, 1 eq.), 1-bromohexane (2.2 g, 12.2 mmol, 2 eq.) in 8 mL of dimethylformamide was added *N,N*-diisopropylethylamine (0.95 g, 7.2 mmol, 1.2 eq.). The reaction mixture was stirred at 70 °C for 4 h. After the solvent was evaporated, the residue was re-dissolved in 20 mL of chloroform, washed with lithium chloride (5% aq.), sodium bicarbonate (sat. aq.), brine, and dried over anhydrous magnesium sulfate. The product was purified by flash chromatography on silica (petroleum ether/ethyl acetate:8/2) to yield the product as white solid (1.45 g, 96% yield).

^{1}H NMR (400 MHz, $CDCl_3$) δ (ppm): 7.86 – 7.81 (m, 2H), 7.76 – 7.72 (m, 2H), 4.20 (t, J = 6.8 Hz, 2H), 1.82 – 1.75 (m, 2H), 1.52 – 1.45 (m, 2H), 1.36 – 1.31 (m, 4H), 0.90 (m, 3H).
^{13}C NMR (100 MHz, $CDCl_3$) δ (ppm): 163.7, 134.4, 129.0, 123.4, 78.6, 31.5, 28.1, 25.2, 22.5, 14.0.
HR-MS (ES+) calcd. for $C_{14}H_{18}NO_3$: 248.1287, found: 248.1293.
All characterization data matched literature.[2]

Compound 6-10

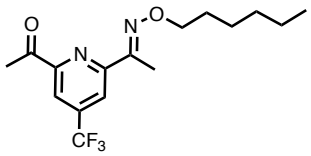

Compound **6-9** is prepared by mixing 2 eq. of hydrazine with compound **6-8**, followed by filtration and evaporation and use without further purification. To an ethanolic solution of compound **6-1** (60 mg, 0.26 mmol, 1 eq.) was added compound **6-9** (31 mg, 0.26 mmol, 1 eq.). The reaction mixture was microwaved at 60°C for 4 h. After evaporation of the solvent, the residue was purified by flash chromatography (silica, 1%-5% ethyl acetate in petroleum ether) to yield the product as a white solid (21 mg, 35% yield).

^{1}H NMR (400 MHz, $CDCl_3$) δ (ppm): 8.35 (s, 1H), 8.17 (s, 1H), 4.28 (t, *J* = 6.8 Hz, 2H), 2.77 (s, 3H), 2.38 (s, 3H), 1.79 – 1.72 (m, 2H), 1.46 – 1.28 (m, 7H), 0.92 – 0.87 (m, 3H).
^{13}C NMR (100 MHz, $CDCl_3$) δ (ppm): 198.7, 155.5, 153.8, 153.5, 139.6 (q, *J* = 35 Hz), 122.6 (q, *J* = 280 Hz), 119.3 (q, *J* = 4 Hz), 116.6 (q, *J* = 4 Hz), 75.3, 31.6, 29.2, 25.7, 25.6, 22.6, 14.0, 10.6.
^{19}F NMR (400 MHz, $CDCl_3$) δ (ppm): -64.72 (s, 3F).
HR-MS (ES+) calcd. for. $C_{16}H_{22}N_2O_2F_3$: 331.1633, found: 331.1632.
FT-IR (ATR): ν_{max} 3305, 2925, 2864, 1735, 1652, 1624, 1448, 1363, 1273, 1270, 1173, 1140, 1086, 1021 cm^{-1}.

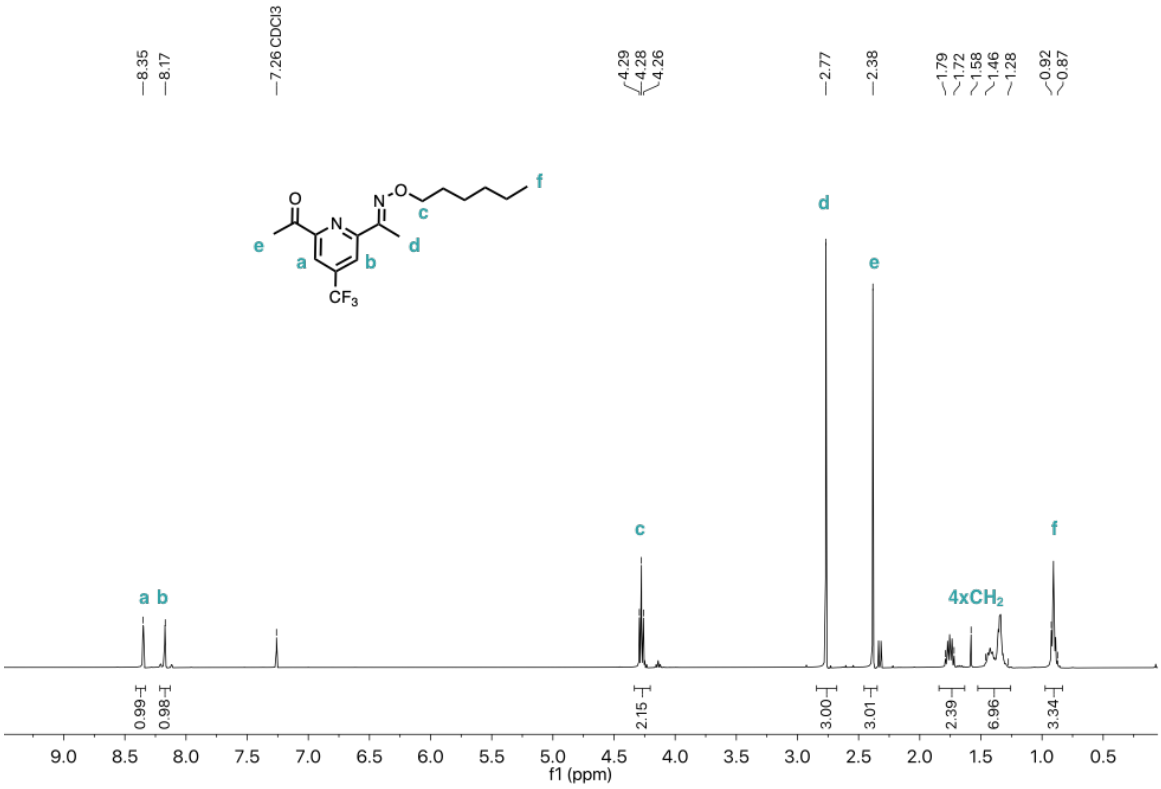

Figure S6.4 [1]H NMR spectrum of compound **6-10**.

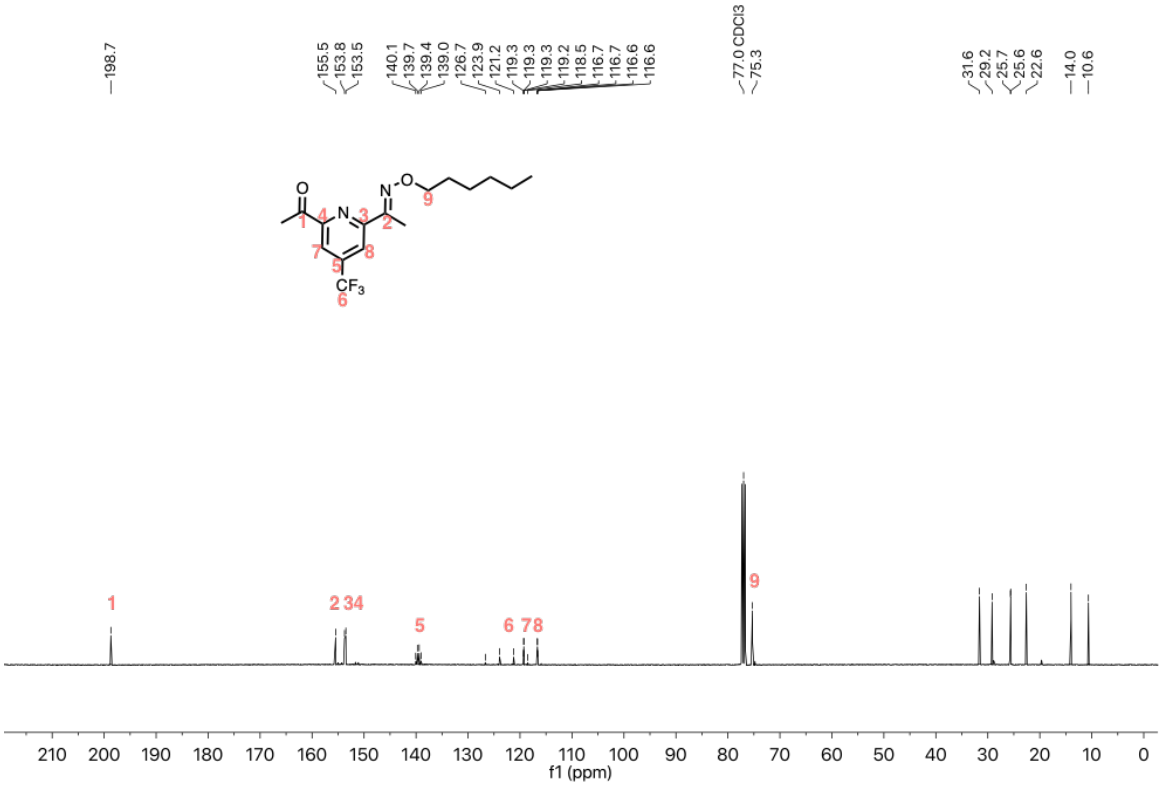

Figure S6.5 [13]C NMR spectrum of compound **6-10**.

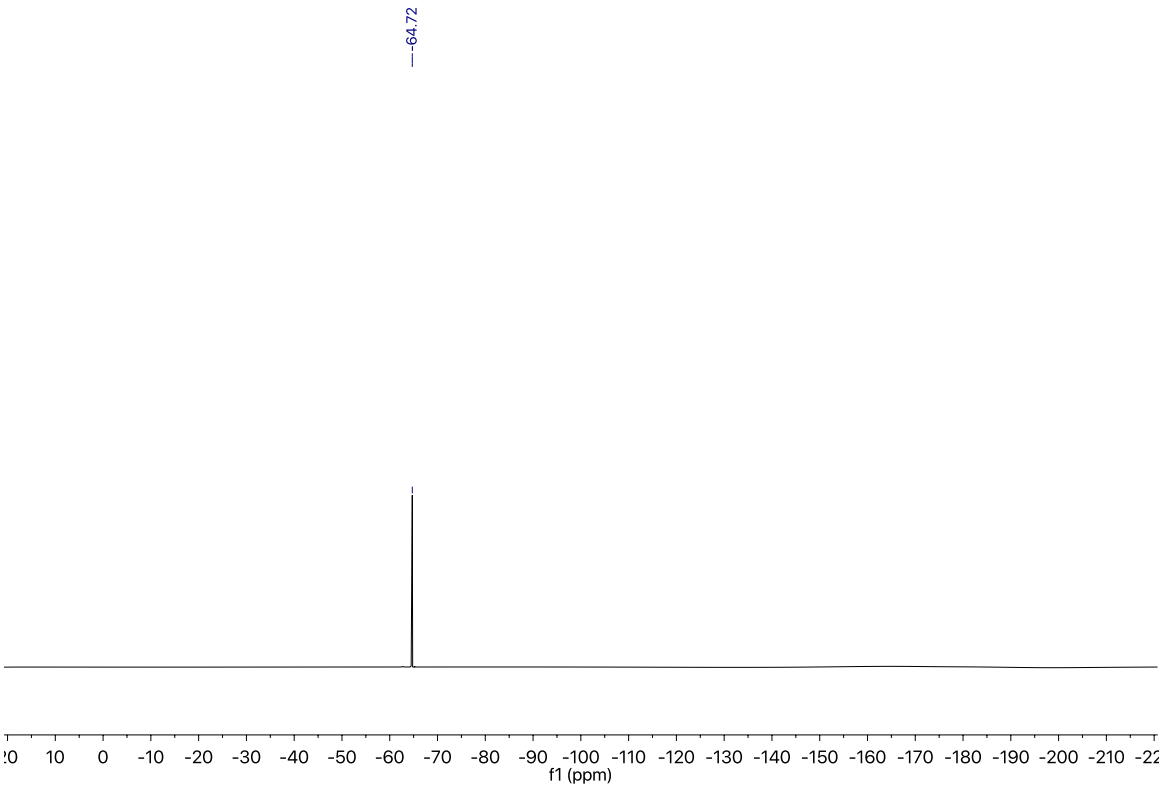

Figure S6.6 ^{19}F NMR spectrum of compound **6-10**.

Compound 6-3

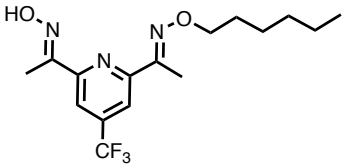

To a solution of compound **6-10** (20 mg, 0.06 mmol, 1 eq.), hydroxylamine hydrochloride (4.6 mg, 0.07 mmol, 1.2 eq.) in 3 mL of ethanol/water:9/1 mixture was added sodium hydroxide (2.7 mg, 0.07 mmol, 1.1 eq.). The reaction mixture was microwaved at 60°C for 5 h. After evaporation of the solvent, the residue was purified by flash chromatography (silica, 1%-5% ethyl acetate in petroleum ether) to yield the product as a white solid (15 mg, 72% yield).

^{1}H NMR (400 MHz, $CDCl_3$) δ (ppm): 8.12 (s, 1H), 8.02 (s, 1H), 4.26 (t, *J* = 6.8 Hz, 2H), 2.41 (s, 3H), 2.36 (s, 3H), 1.78 – 1.71 (m, 2H), 1.45 – 1.33 (m, 6H), 0.92 – 0.87 (m, 3H).
^{13}C NMR (100 MHz, $CDCl_3$) δ (ppm): 157.1, 155.4, 154.9, 154.8, 139.3 (q, *J* = 35 Hz), 123.3 (q, *J* = 280 Hz), 116.3 (q, *J* = 4 Hz), 115.9 (q, *J* = 4 Hz), 75.6, 32.1, 29.7, 26.1, 23.1, 14.5, 11.3, 10.8.
^{19}F NMR (400 MHz, $CDCl_3$) δ (ppm): -64.70 (s, 3F).
HR-MS (ES+) calcd. for $C_{16}H_{23}N_3O_2F_3$: 346.1742, found: 346.1737.
FT-IR (ATR): ν_{max} 3249, 2938, 2923, 2878, 2852, 1366, 1278, 1183, 1129, 1045, 1008 cm^{-1}.

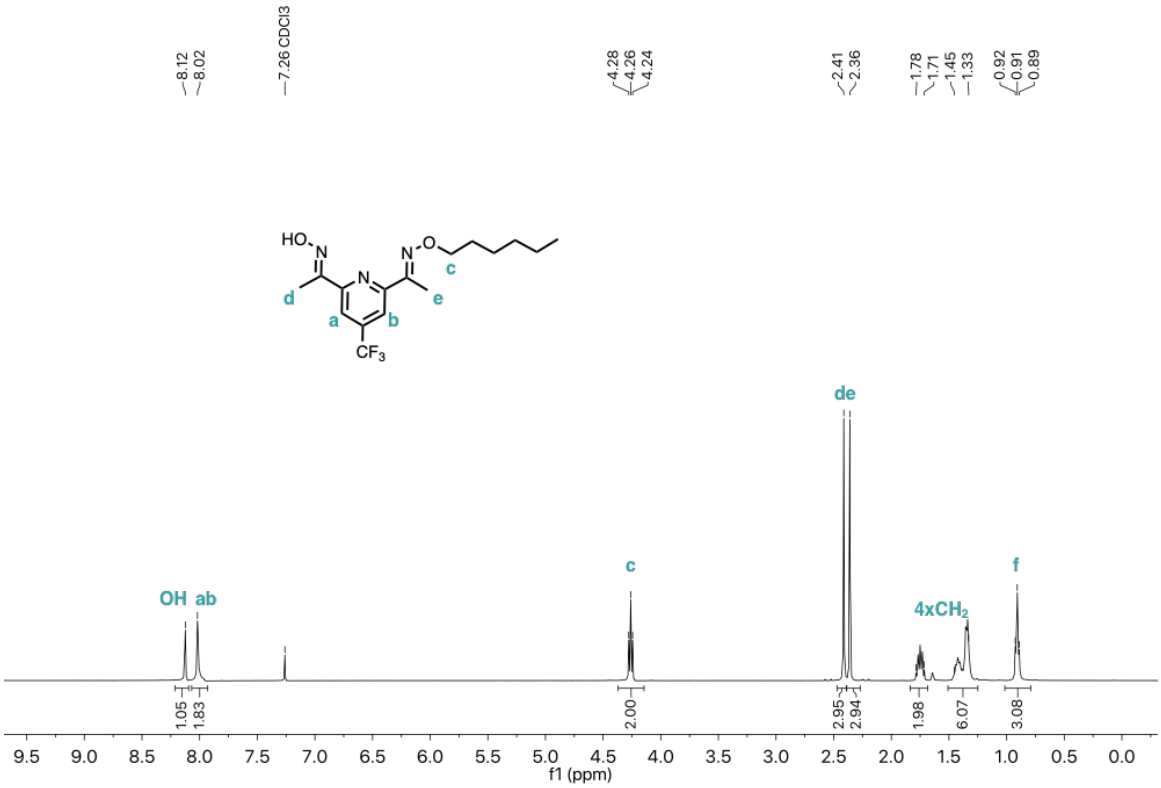

Figure S6.7 ^{1}H NMR spectrum of compound **6-3**.

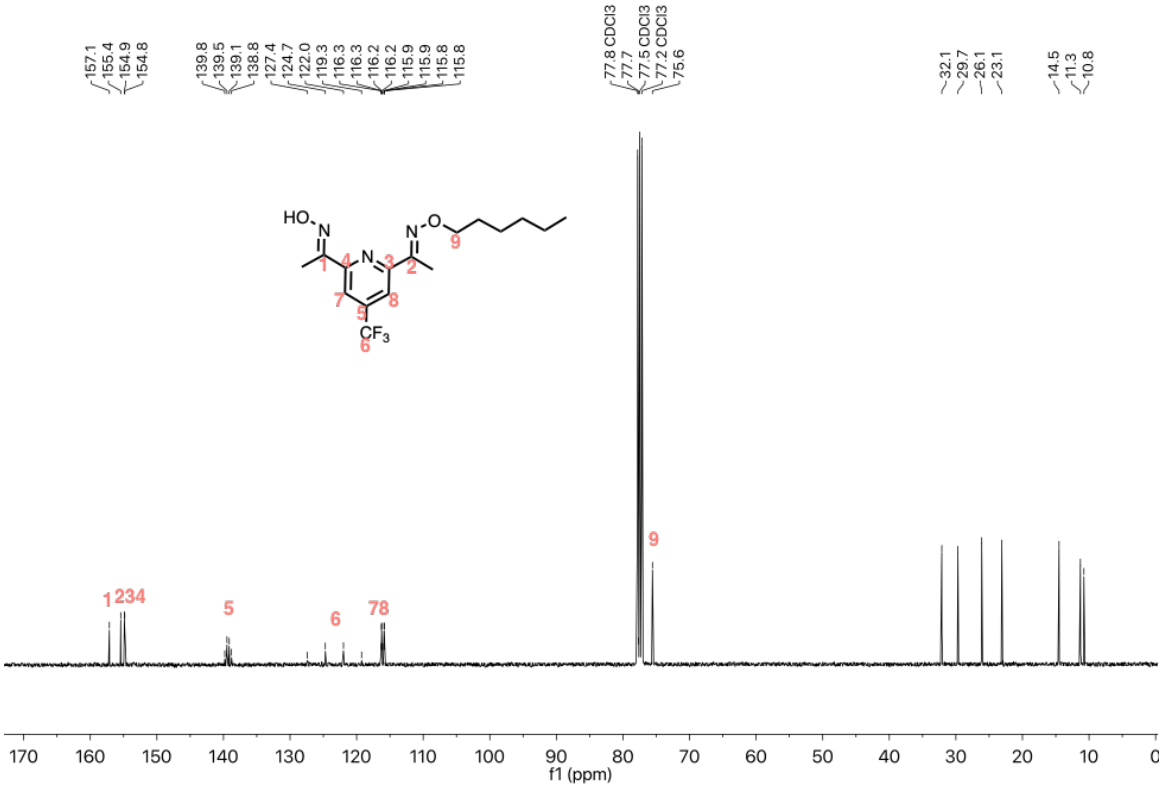

Figure S6.8 ^{13}C NMR spectrum of compound **6-3.**

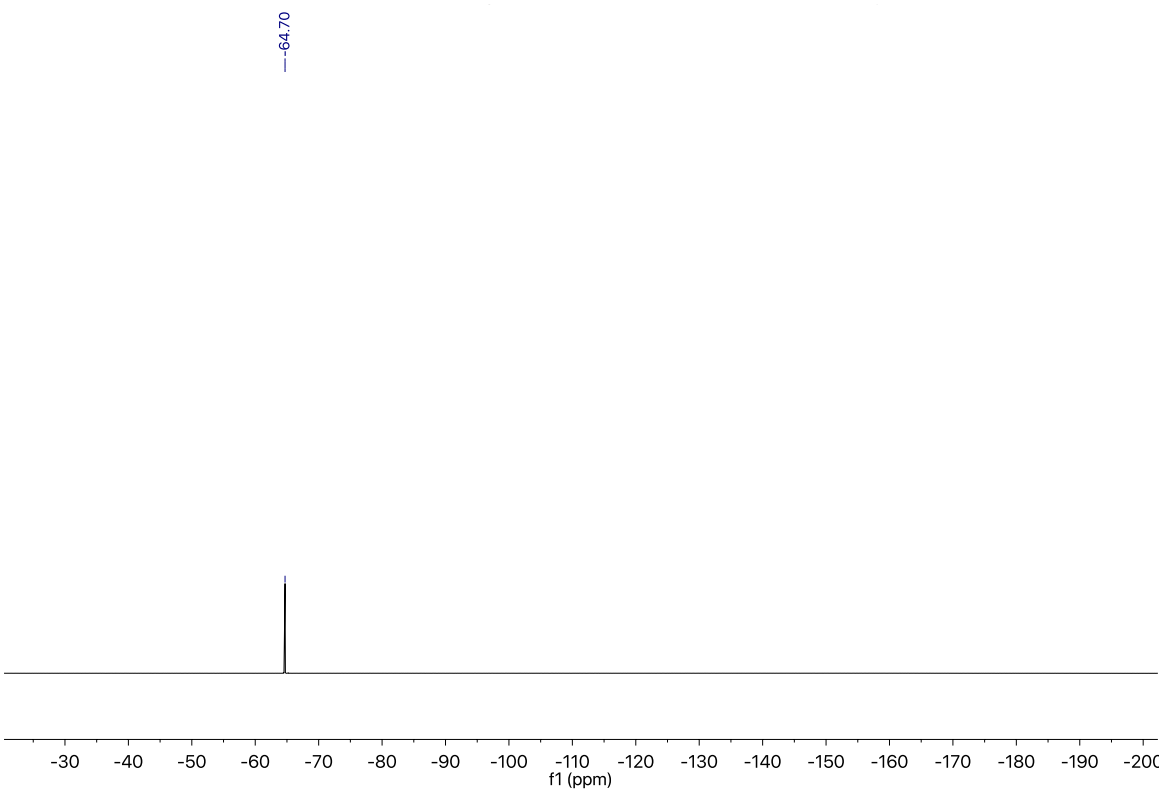

Figure S6.9 ^{19}F NMR spectrum of compound **6-3.**

Compound 6-4

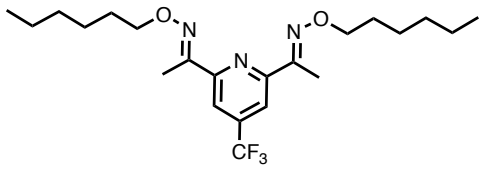

Compound **6-9** is prepared by mixing 2 eq. of hydrazine with compound **6-8**, followed by filtration and evaporation and used without further purification. To a methanolic solution of compound **6-1** (100 mg, 0.43 mmol, 1 eq.) was added compound **6-9** (390 mg, 1.08 mmol, 7 eq.). The reaction mixture was microwaved at 100°C for 20 h. After evaporation of the solvent, the residue was purified by flash chromatography on silica (1%-5% ethyl acetate in petroleum ether) to yield the product as a white solid (170 mg, 91% yield).

^{1}H NMR (400 MHz, $CDCl_3$) δ (ppm): 8.08 (s, 2H), 4.25 (t, *J* = 6.8 Hz, 4H) (E/Z isomer) , 2.35 (s, 6H), 1.78 – 1.71 (m, 4H), 1.44 – 1.34 (m, 12H), 0.92 – 0.87 (m, 6H).
^{13}C NMR (100 MHz, $CDCl_3$) δ (ppm): 154.9, 154.5, 138.8 (q, *J* = 35 Hz), 123.2 (q, *J* = 280 Hz), 115.5 (q, *J* = 4 Hz), 75.2, 31.8, 29.4, 25.8, 22.8, 14.2, 11.0.
^{19}F NMR (400 MHz, $CDCl_3$) δ (ppm): -64.60 (s), -64.70 (s) (*E/Z* isomers).
HR-MS (ES+) calcd. for $C_{22}H_{35}N_3O_2F_3$: 430.2681, found: 430.2678.
FT-IR (ATR): ν_{max} 2956, 2936, 2875, 2857, 1568, 1497, 1467, 1431, 1364, 1277, 1132, 1045 cm^{-1}.

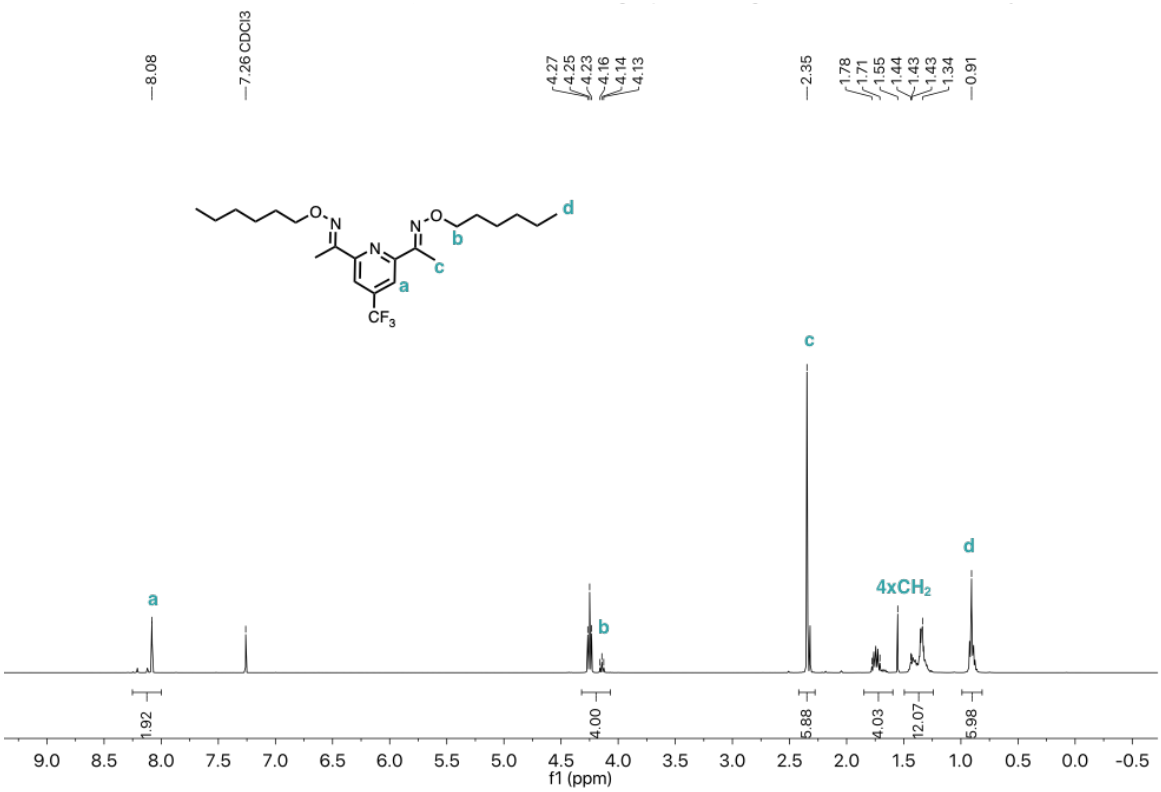

Figure S6.10 ^{1}H NMR spectrum of compound **6-4** (with E/Z isomer).

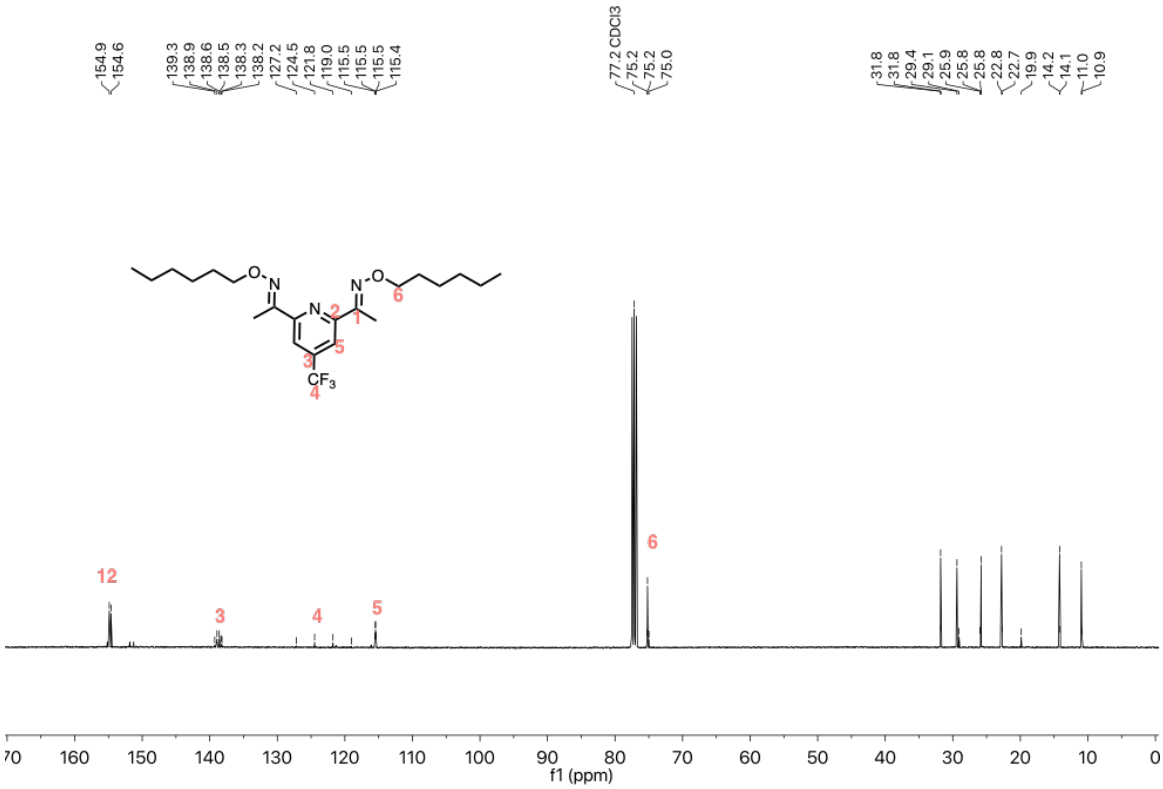

Figure S6.11 ^{13}C NMR spectrum of compound **6-4** (with *E*/*Z* isomer).

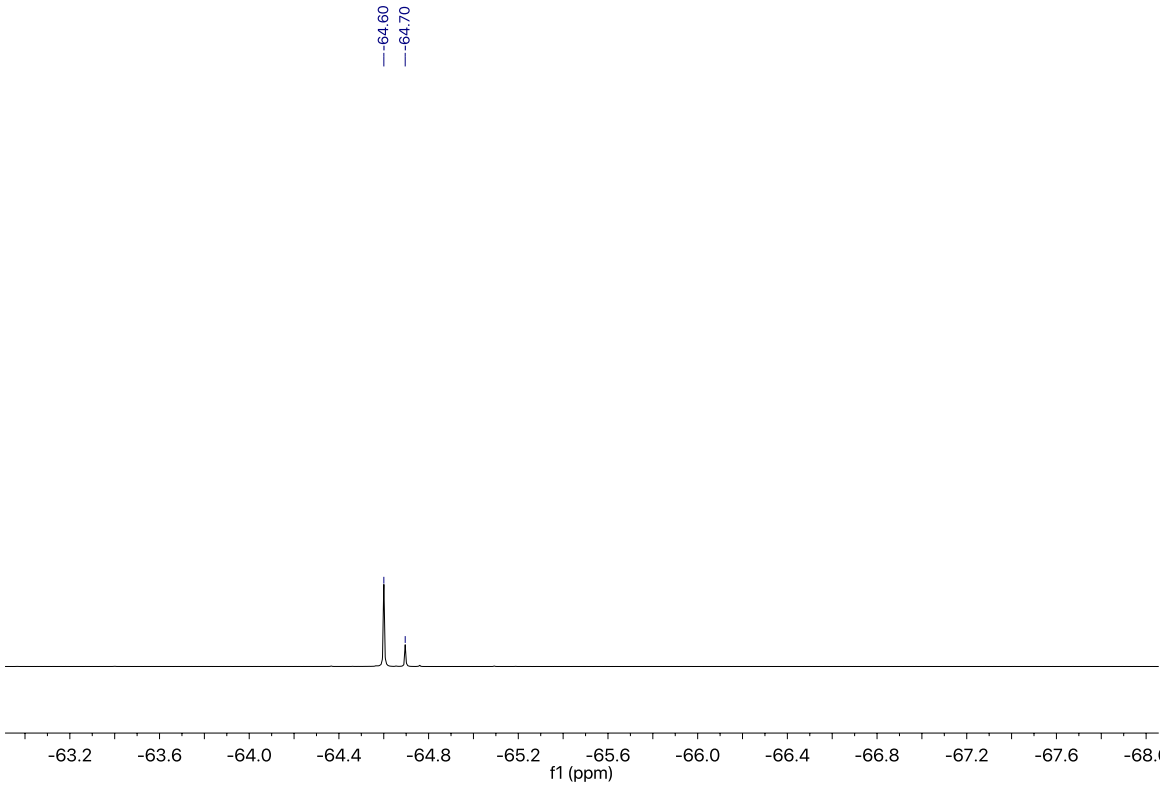

Figure S6.12 ^{19}F NMR spectrum of compound **6-4** (with *E*/*Z* isomer).

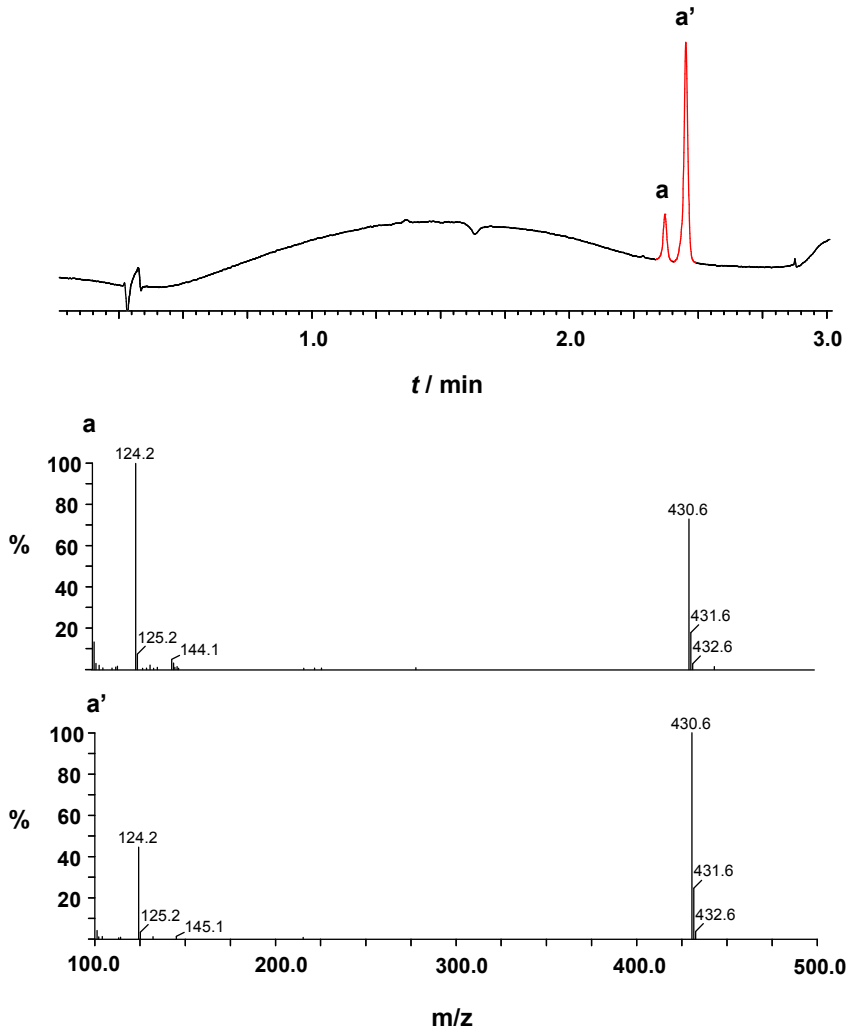

Figure S6.13 LC-MS traces of compound **6-4** isomers and the corresponding mass chromatograms (MW = 430.3; [M^+]).

Compound 6-11

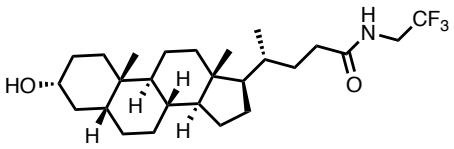

A solution of lithocholic acid (1 g, 2.66 mmol, 1 eq.), 2,2,2-trifluoroethylamine (525 mg, 5.3 mmol, 2 eq.), EDC•HCl (560 mg, 2.92 mmol, 1.1 eq.), DMAP (24 mg, 0.2 mmol, 0.1 eq.), and DIPEA (377 mg, 2.92 mmol, 1.1 eq.) in 20 mL of tetrahydrofuran was stirred at r.t. overnight. The reaction mixture was diluted with 50 mL of ethyl acetate, washed with hydrochloric acid (1 M, aq.), water, sodium bicarbonate (sat. aq.), brine, and dried over anhydrous magnesium sulfate. Evaporation of solvent gave the product as a white solid (888 mg, 74% yield).

^{1}H NMR (400 MHz, MeOD-d_4) δ (ppm): 3.89 (q, *J* = 9.4 Hz, 2H), 3.59 – 3.51 (m, 1H), 2.34 – 2.15 (m, 2H), 2.04 – 0.96 (m, 33H), 0.70 (m, 3H).
^{13}C NMR (100 MHz, $CDCl_3$) δ (ppm): 173.5, 121.6 (q, *J* = 220 Hz, 1C), 71.9, 56.5, 55.9, 42.7, 42.1, 40.4, 40.2, 36.4, 35.8, 35.3, 35.2 34.6, 33.3, 31.4, 30.5, 28.2, 27.2, 27.1, 26.4, 24.2, 23.4, 20.8, 18.3, 12.0.
^{19}F NMR (400 MHz, MeOD-d_4) δ (ppm): -74.02 (t, *J* = 85 Hz, 3F).
HR-MS (ES+) calcd. for $C_{26}H_{42}O_2N_1F_3{}^{23}Na$: 480.3060, found: 480.3046.
FT-IR (ATR): ν_{max} 3485, 3288, 2934, 2863, 1733, 1678, 1542, 1457, 1384, 1275, 1162 cm^{-1}.

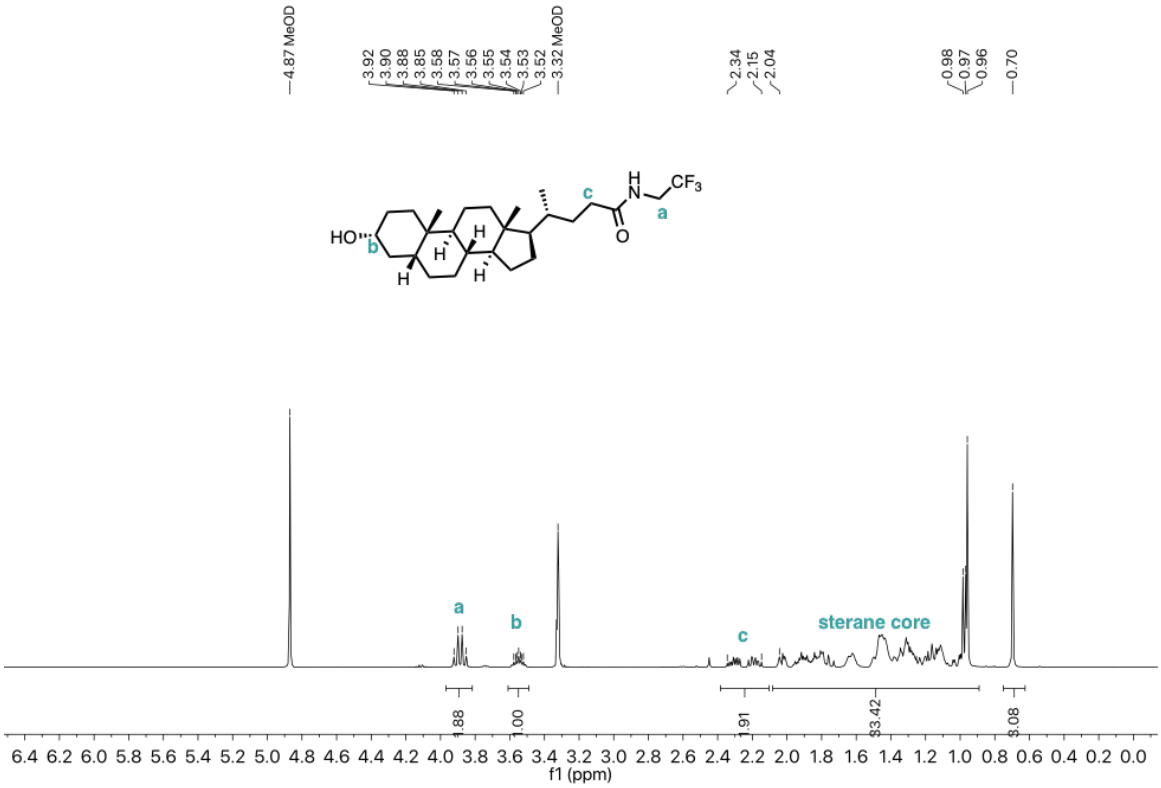

Figure S6.14 ^{1}H NMR spectrum of compound **6-11**.

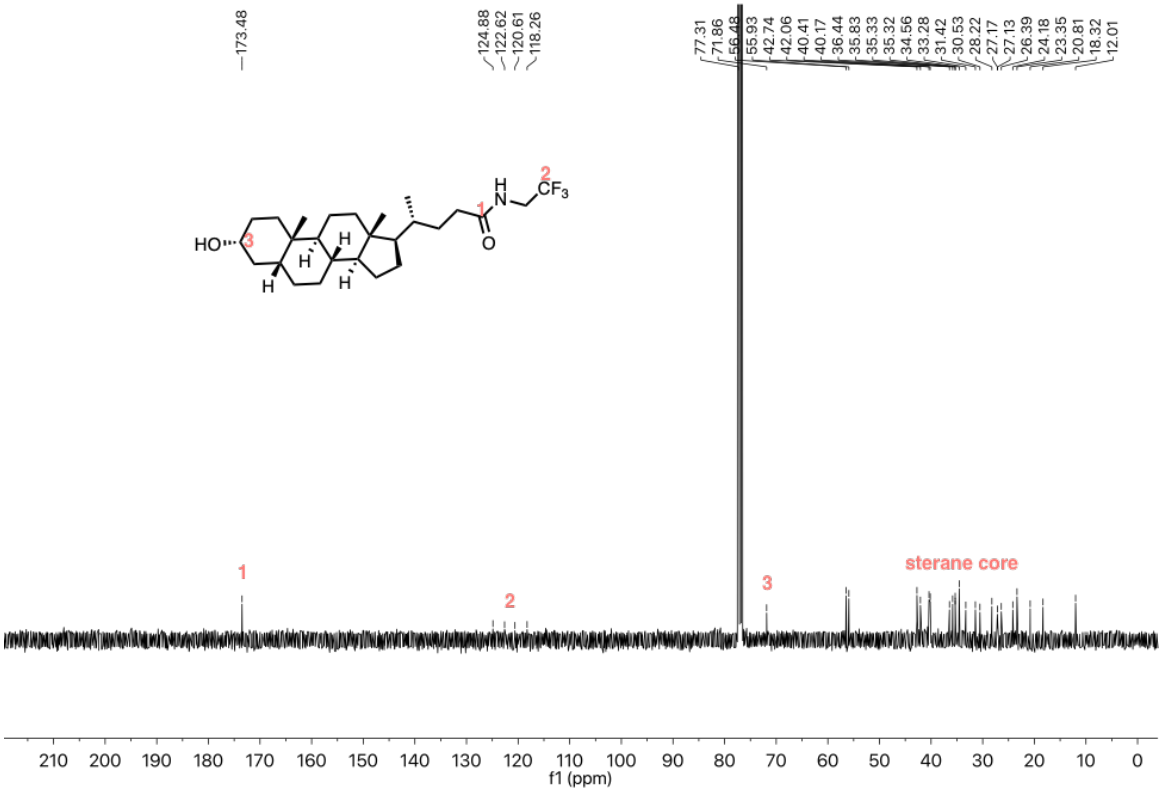

Figure S6.15 ^{13}C NMR spectrum of compound **6-11**.

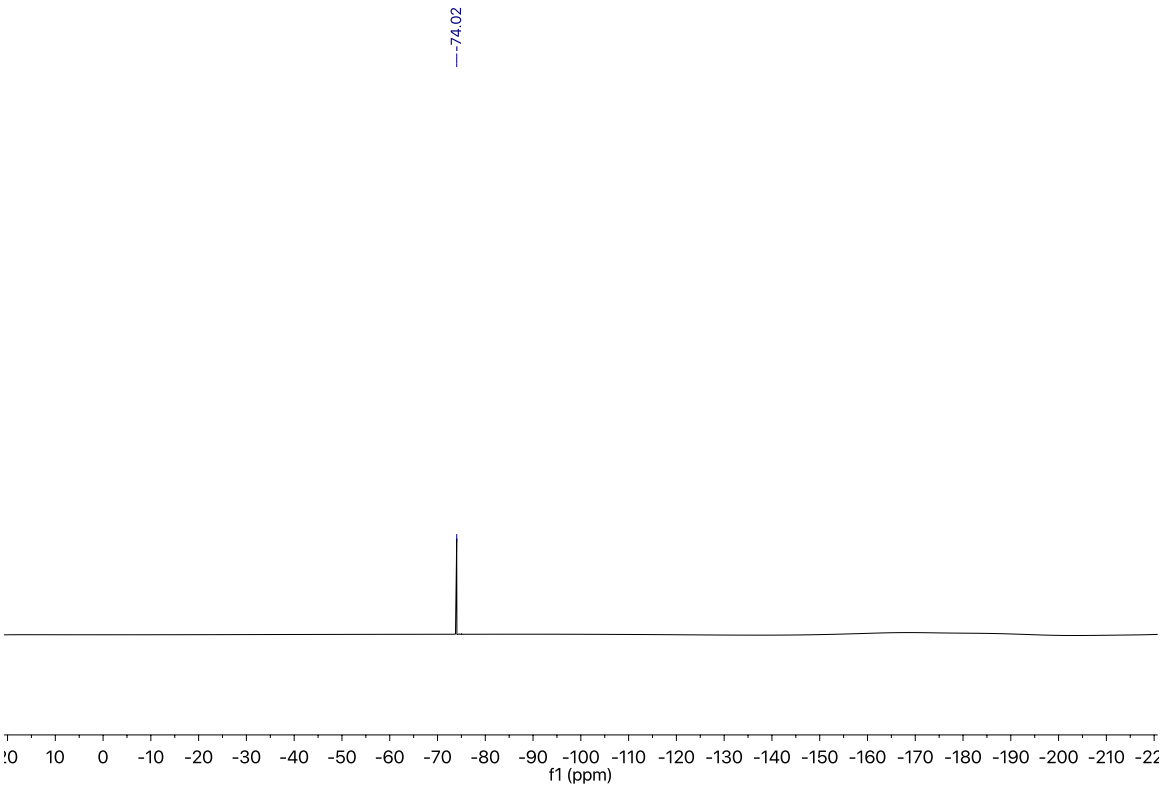

Figure S6.16 ^{19}F NMR spectrum of compound **6-11**.

Compound 6-12

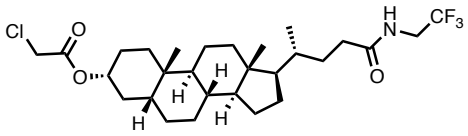

To a solution of compound **6-11** (200 mg, 0.44 mmol, 1 eq.), DMAP (5 mg, 0.04 mmol, 0.1 eq.), DIPEA (0.5 mL) in 5 mL of tetrahydrofuran was added chloroacetyl chloride (108 mg, 0.87 mmol, 2 eq.) with external cooling at -78 °C. The reaction mixture was stirred at r.t. overnight. The reaction was quenched with 2 mL of methanol and the solvent was evaporated. The residue was re-dissolved in 50 mL of ethyl acetate, washed with hydrochloric acid (1 M, aq.), water, sodium bicarbonate (sat. aq.), brine, and dried over anhydrous magnesium sulfate. After evaporation, the crude was purified by flash chromatography (silica, 0 – 10% methanol in dichloromethane) to give the product as white solid (100 mg, 41%).

^{1}H NMR (400 MHz, $CDCl_3$) δ (ppm): 5.64 (t, *J* = 5.6 Hz, 1H), 4.86 – 4.78 (m, 1H), 4.03 (s, 2H), 3.97 – 3.88 (m, 2H), 2.35 – 2.11 (m, 2H), 1.98 – 0.92 (m, 32H), 0.64 (m, 3H).
^{13}C NMR (100 MHz, $CDCl_3$) δ (ppm): 173.5, 166.8, 124.1 (q, *J* = 220 Hz, 1C), 76.8, 56.4, 56.0, 42.7, 41.9, 41.2, 40.5 (q, *J* = 30 Hz, 1C), 40.4, 40.1, 35.8, 35.4, 34.9, 34.6, 33.3, 32.0, 31.4, 28.2, 27.0, 26.4, 26.3, 24.2, 23.3, 20.8, 18.3, 12.0.
^{19}F NMR (400 MHz, $CDCl_3$) δ (ppm): -74.02 (t, *J* = 85 Hz, 3F).
HR-MS (ES+) calcd. for $C_{26}H_{42}O_2N_1F_3{}^{23}Na$: 480.3060, found: 480.3046.
FT-IR (ATR): ν_{max} 3288, 2938, 2868, 1748, 1666, 1540, 1448, 1422, 1323, 1283, 1160, 986 cm^{-1}.

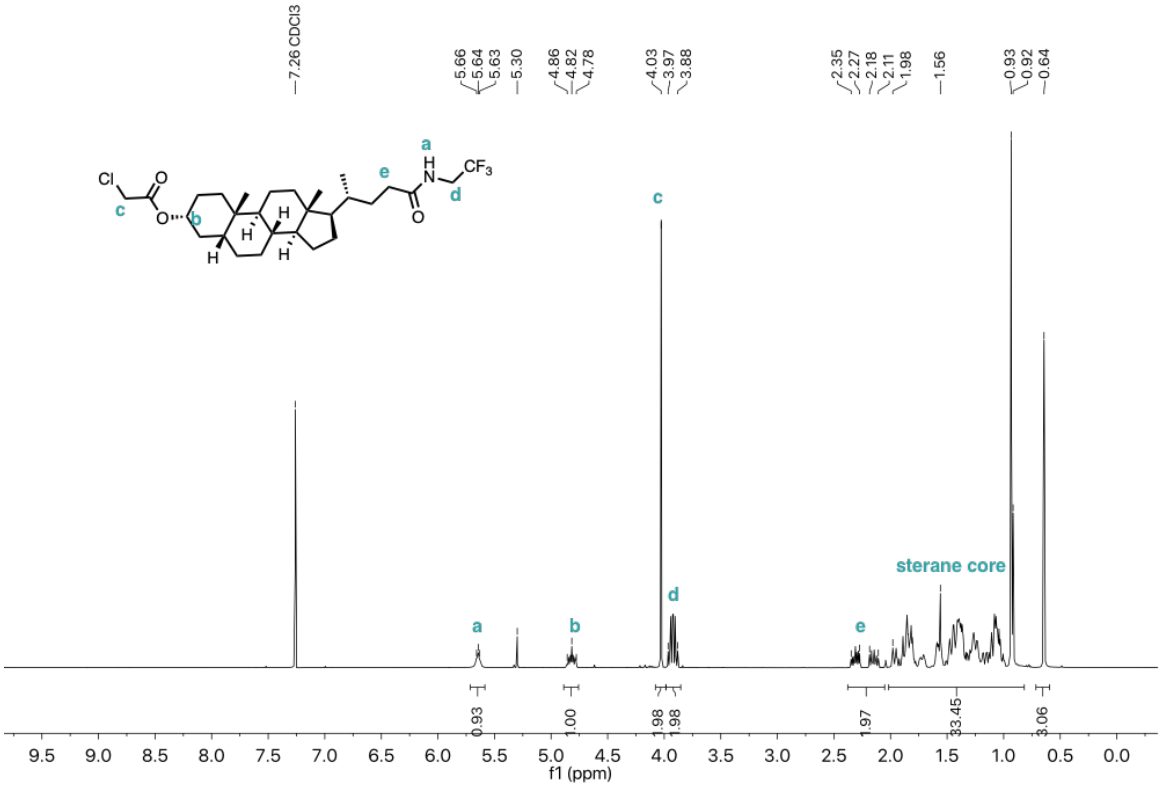

Figure S6.17 [1]H NMR spectrum of compound **6-12**.

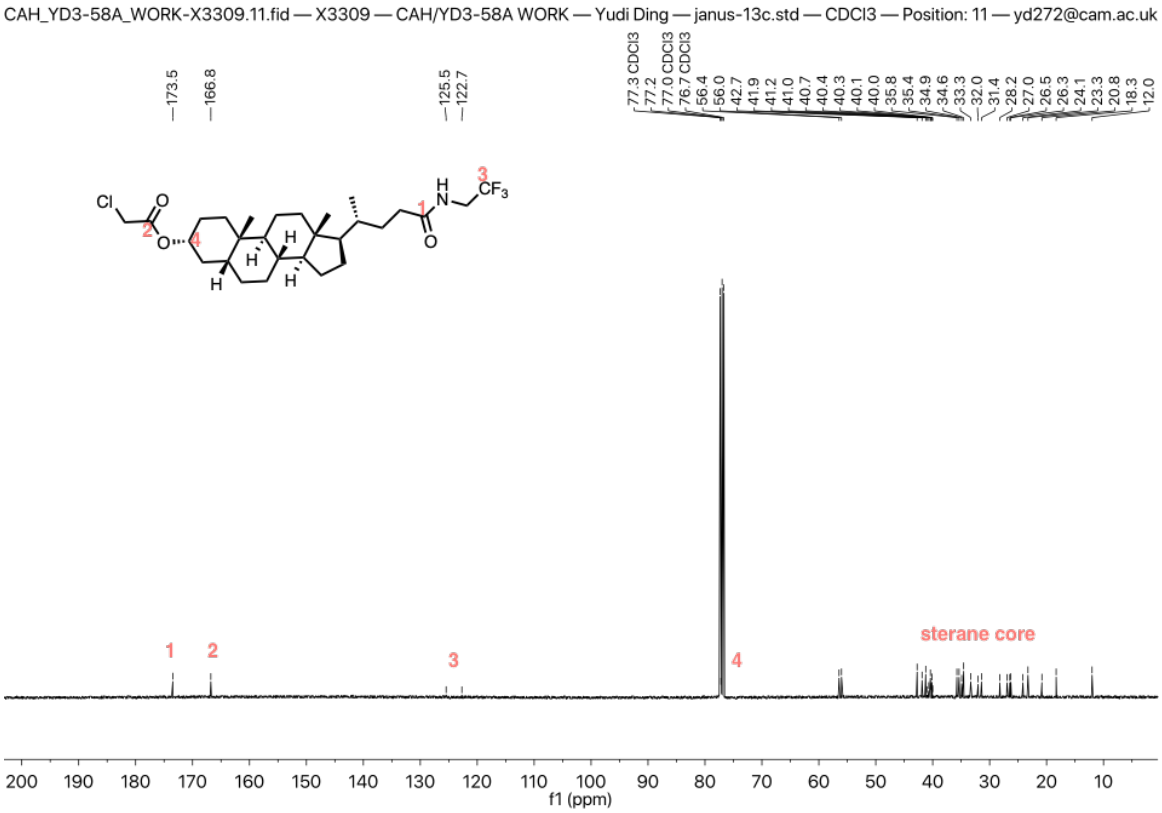

Figure S6.18 [13]C NMR spectrum of compound **6-12**.

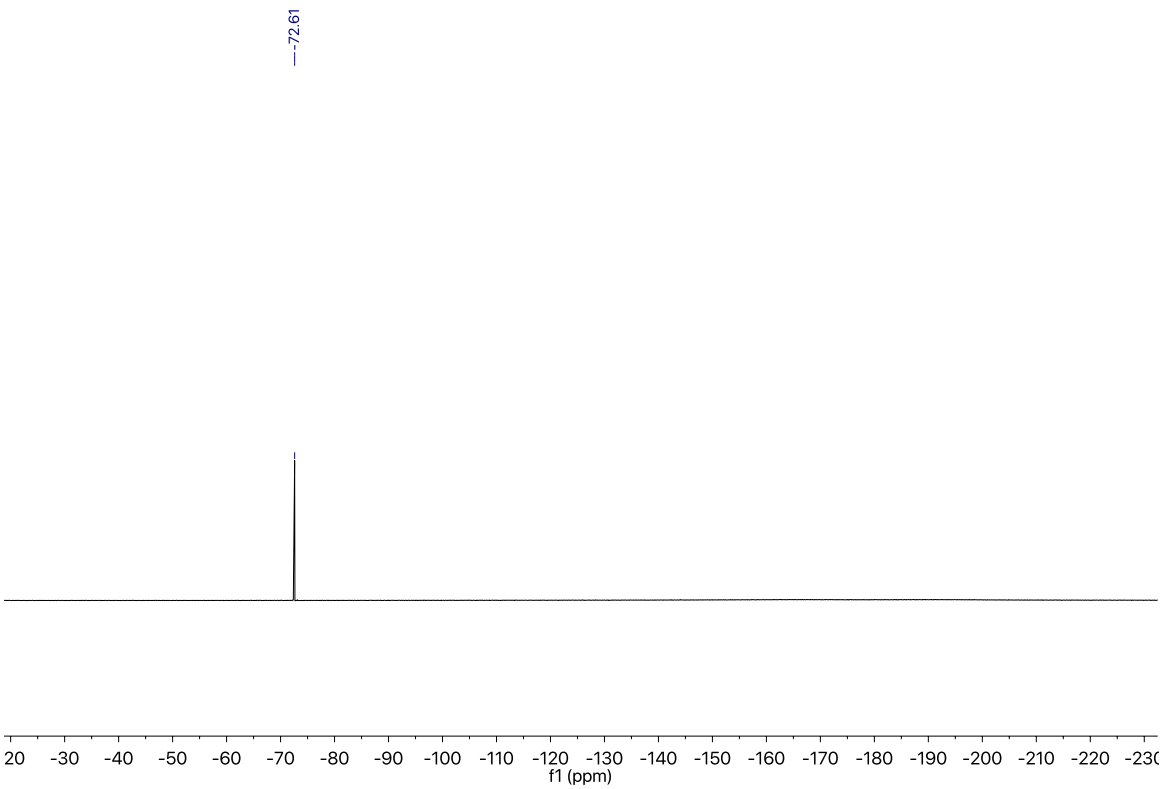

Figure S6.19 ^{19}F NMR spectrum of compound **6-12**.

Compound 6-5

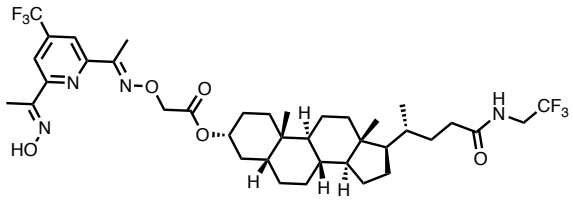

To a solution of compound **6-12** (50 mg, 0.094 mmol, 1 eq.) and compound **6-2** (74 mg, 0.28 mmol, 3 eq.) in DMF (1 mL) was added potassium carbonate (65 mg, 0.47 mmol, 5 eq.). The reaction mixture was stirred at 60 °C for 1 h and then diluted with ethyl acetate (10 mL). The organic phase was washed with lithium chloride (5%, aq.), hydrochloric acid (1 M, aq.), water, sodium bicarbonate (sat. aq.), brine, and dried over anhydrous magnesium sulfate. After the solvent was evaporated, the crude was purified by flash chromatography (silica, 10% - 40% ethyl acetate in petroleum ether) to give the product as white solid (60 mg ,84%).

^{1}H NMR (400 MHz, $CDCl_3$) δ (ppm): 8.73 (s, 1H), 8.08 (s, 1H), 8.09 (s, 1H), 5.73 (t, *J* = 6.5 Hz, 1H), 4.85 – 4.77 (m, 3H), 2.45 (s, 3H), 2,40 (s, 3H), 2.40 – 2.13 (m, 2H), 1.91 – 0.74 (m, 34H), 0.60 (m, 3H).

^{13}C NMR (100 MHz, $CDCl_3$) δ (ppm): 174.4, 169.5, 156.7, 155.9, 154.8, 154.0, 138.8 (q, *J* = 4 Hz, 1C) , 123.4 (q, *J* = 220 Hz, 1C), 120.4 (q, *J* = 220 Hz, 1C), 115.7(q, *J* = 4 Hz, 1C), 115.6(q, *J* = 4 Hz, 1C), 75.3, 71.4, 56.6, 55.8, 42.6, 41.7, 40.6 (q, *J* = 30 Hz, 1C), 40.4, 40.1, 35.6, 35.4, 34.8, 34.4, 33.1, 32.0, 31.4, 28.2, 26.9, 26.4, 26.2, 24.1, 23.2, 20.7, 18.1, 11.9, 11.1, 10.0.

^{19}F NMR (400 MHz, $CDCl_3$) δ (ppm): -64.67 (s, 3F), -74.02 (t, *J* = 85 Hz, 3F).

HR-MS (ES+) calcd. for $C_{38}H_{52}O_5N_4F_6{}^{23}Na$: 781.3734, found: 781.3720.

FT-IR (ATR): ν_{max} 3306, 3081, 2935, 2868, 1737, 1667, 1567, 1448, 1364, 1275 1224, 1088, 1024 cm^{-1}.

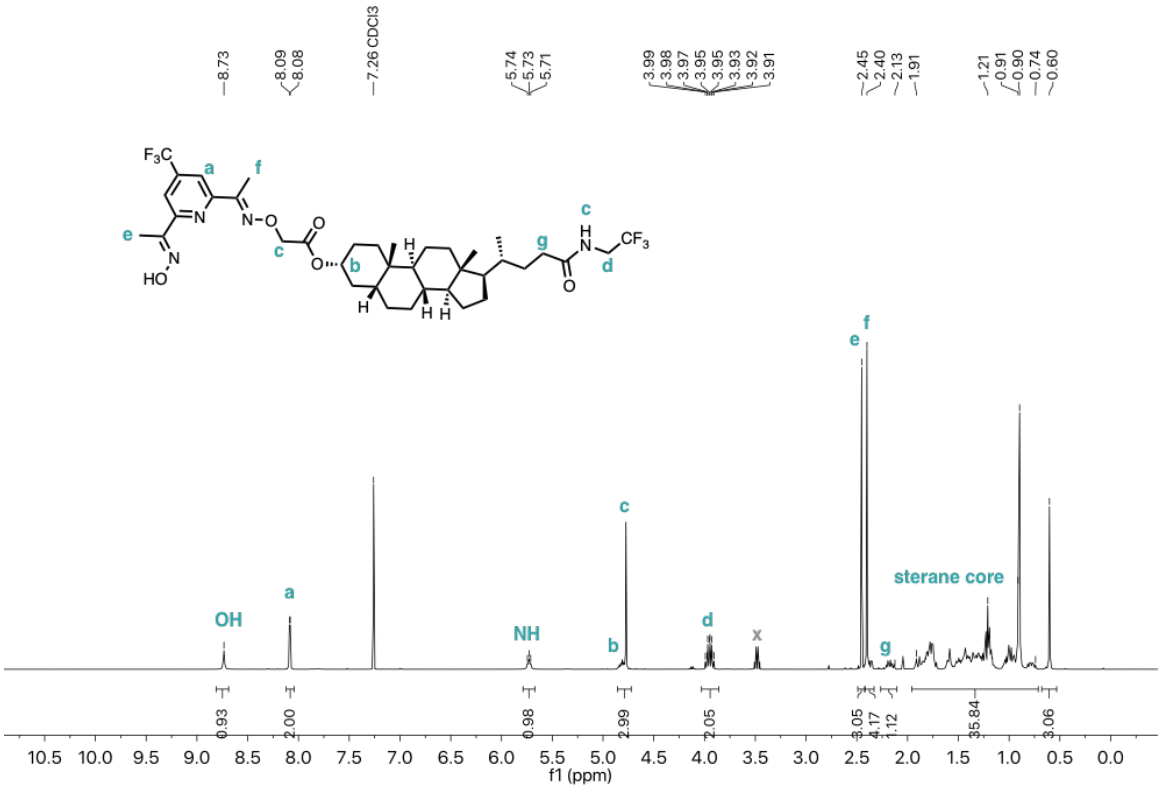

Figure S6.20 ^{1}H NMR spectrum of compound **6-5**.

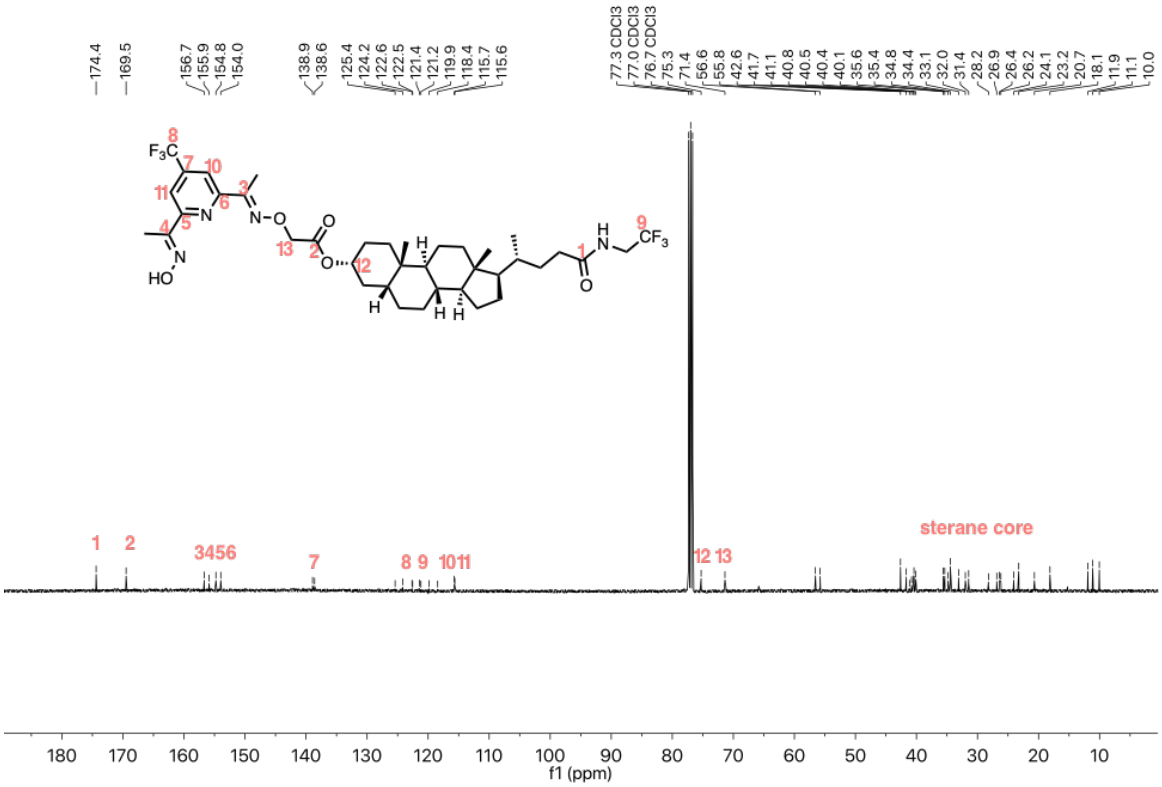

Figure S6.21 ^{13}C NMR spectrum of compound **6-5**.

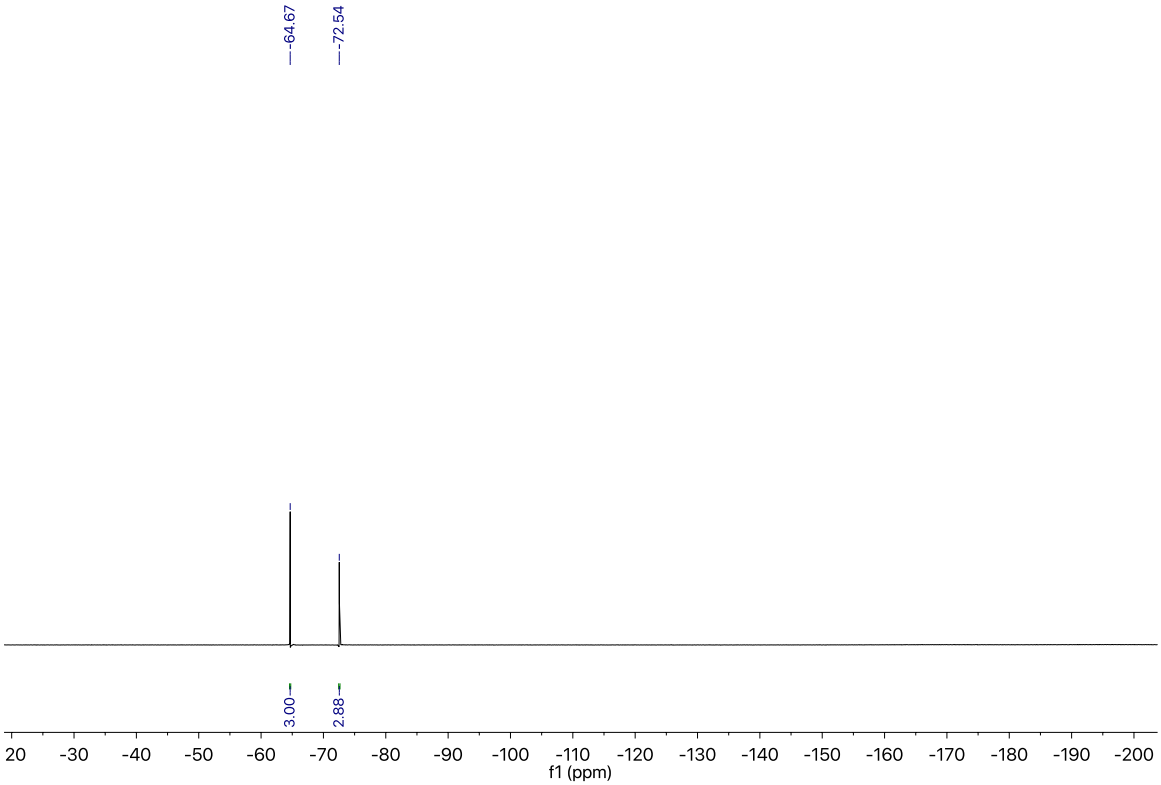

Figure S6.22 ^{19}F NMR spectrum of compound **6-5**.

Compound 6-15

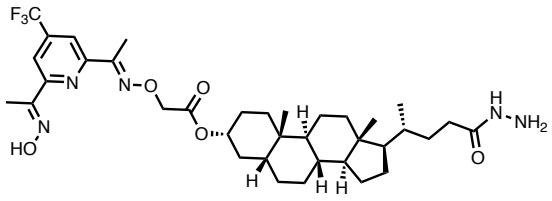

To a solution of compound **6-13** (30 mg, 0.053 mmol, 1 eq.) and compound **6-2** (21 mg, 0.079 mmol, 1.5 eq.) in 1 mL of DMF was added potassium carbonate (22 mg, 0.16 mmol, 3 eq.). The reaction mixture was stirred at 60 °C for 5 h and then diluted with 20 mL of ethyl acetate. The organic phase was washed with lithium chloride (5%, aq.), hydrochloride acid (1 M, aq.), water, sodium bicarbonate (sat. aq.), brine, and dried over anhydrous magnesium sulfate. After the solvent was evaporated, the crude was purified by flash chromatography on silica (10% - 40% ethyl acetate in petroleum ether) to give the product as white solid. Compound **6-2** coeluted with the product and the product was used in the next step without further purification.

To a solution of crude compound **6-14** (20 mg, 0.053 mmol, 1 eq.) in 1 mL dichloromethane was added 0.1 mL of trifluoroacetic acid and the reaction mixture was stirred at r.t. overnight. The solvent was evaporated under a nitrogen beam and the crude was purified by flash chromatography on silica (methanol in dichloromethane) to give the product as white solid (3 mg, 17% yield).

^{1}H NMR (400 MHz, $CDCl_3$) δ (ppm): 9.36 (br, 1H), 8.10 (s, 2H), 6.87 (br, 1H), 4.83 – 4.73 (m, 3H), 3.98 (br, 2H), 2.46 (s, 3H), 2.41 (s, 3H), 2.32 – 2.03 (m, 2H), 1.89 – 0.63 (m, 33H), 0.59 (s, 3H).
^{13}C NMR (100 MHz, $CDCl_3$) δ (ppm): 169.5, 156.5, 155.8, 154.9, 154.0, 138.8 (q, *J* = 34 Hz, 1C) 122.8 (q, *J* = 220 Hz, 1C), 115.6 (q, *J* = 4 Hz, 1C), 115.40 (q, *J* = 4 Hz, 1C), 75.2, 71.4, 56.7, 55.5, 50.9, 42.5, 41.6, 40.5, 40.1, 35.5, 35.3, 34.8, 34.4, 31.9, 31.3, 30.8, 29.7, 28.2, 26.8, 26.3, 26.1, 24.0, 23.2, 20.6, 18.0, 11.9, 11.1, 10.1.
^{19}F NMR (400 MHz, $CDCl_3$) δ (ppm): -64.62 (s, 3F)
HR-MS (ES+) calcd. for $C_{36}H_{53}N_5O_5F_3$: 692.3987, found: 692.3999.
FT-IR (ATR): ν_{max} 3305, 2925, 2864, 1735, 1652, 1624, 1448, 1363, 1273, 1207, 1173, 1140, 1086, 1021 cm^{-1}.

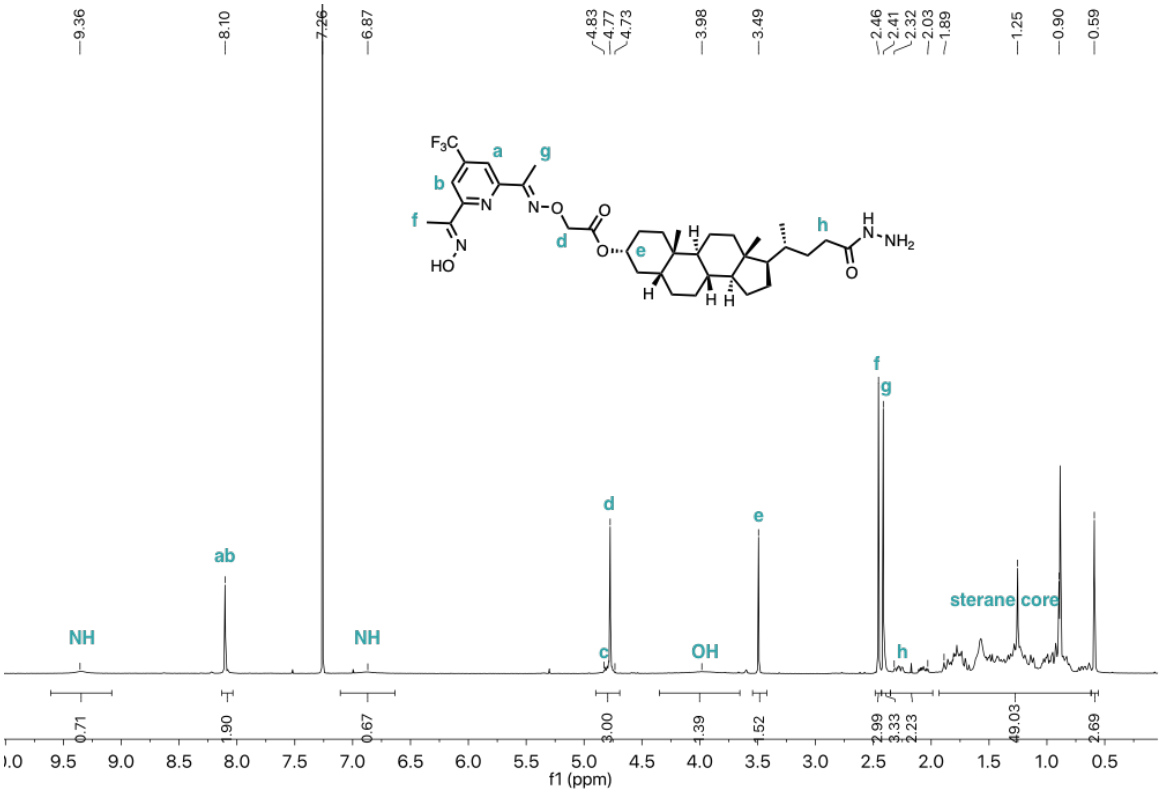

Figure S6.23 ^{1}H NMR spectrum of compound **6-15.**

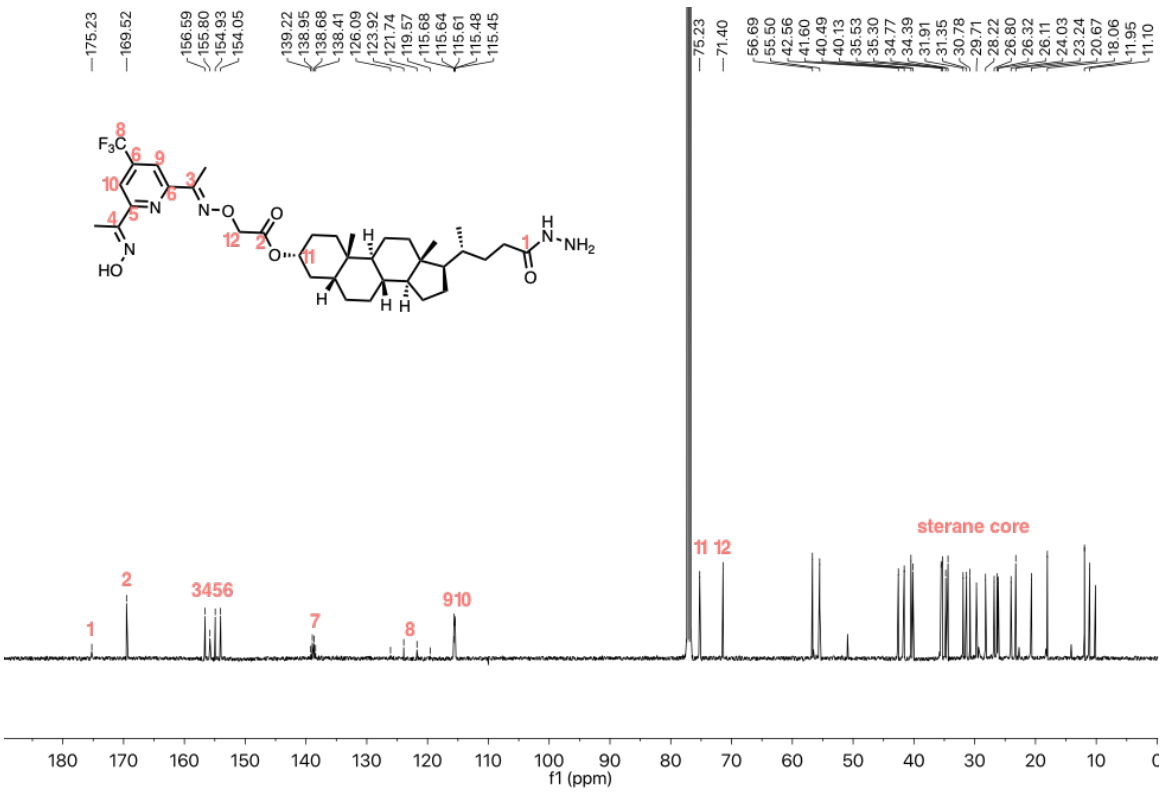

Figure S6.24 ^{13}C NMR spectrum of compound **6-15.**

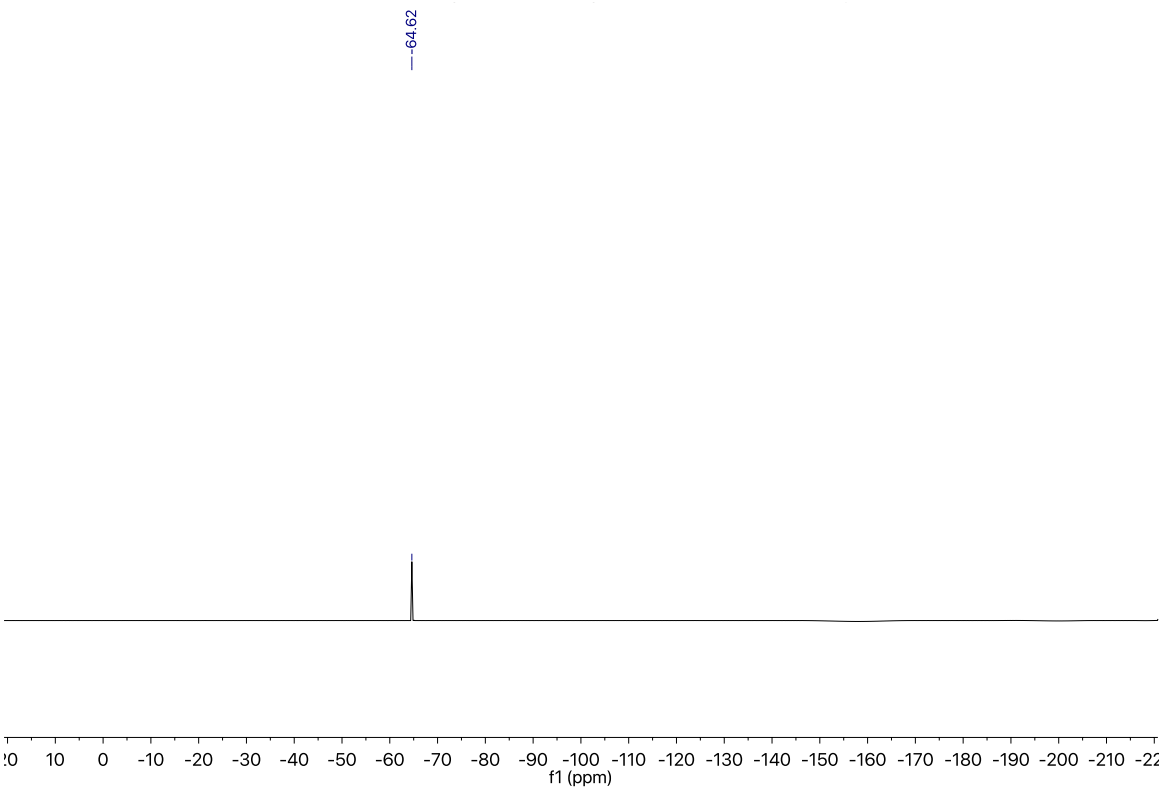

Figure S6.25 ^{19}F NMR spectrum of compound **6-15.**

Synthetic route of compound 6-13

Compound **6-13** was synthesized and characterized by Dr Istvan Kocsis from lithocholic acid in two steps: EDC coupling with Boc-protected hydrazine followed by condensation with chloroacetyl chloride. The compound was used as received without further purification.

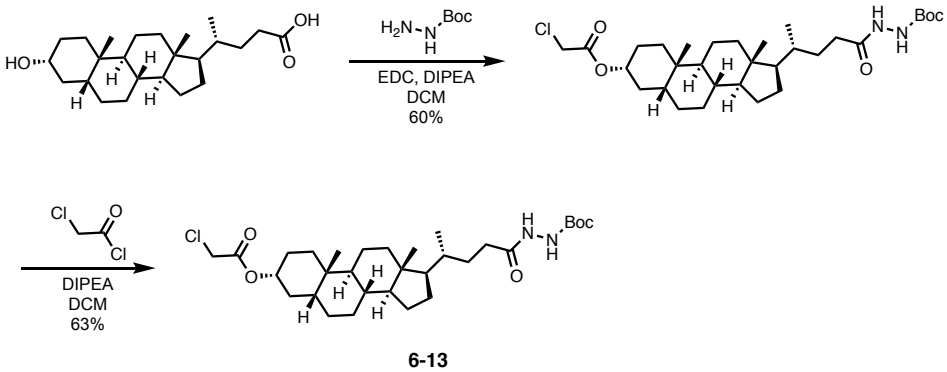

Scheme S6.1 Synthetic route of compound **6-13** (by Dr Istvan Kocsis).

General protocol for hydrazide-aldehyde reaction

To a methanolic solution of 1 mM hydrazide transducer (1 eq.) and aldehyde (1.5 eq.) was added catalytic amount of acetic acid. The reaction was stirred at room temperature overnight and followed by LC-MS. Once the reaction was finished, the solvent was evaporated under a nitrogen beam for three times (re-dissolved in methanol). The product was used without further purification.

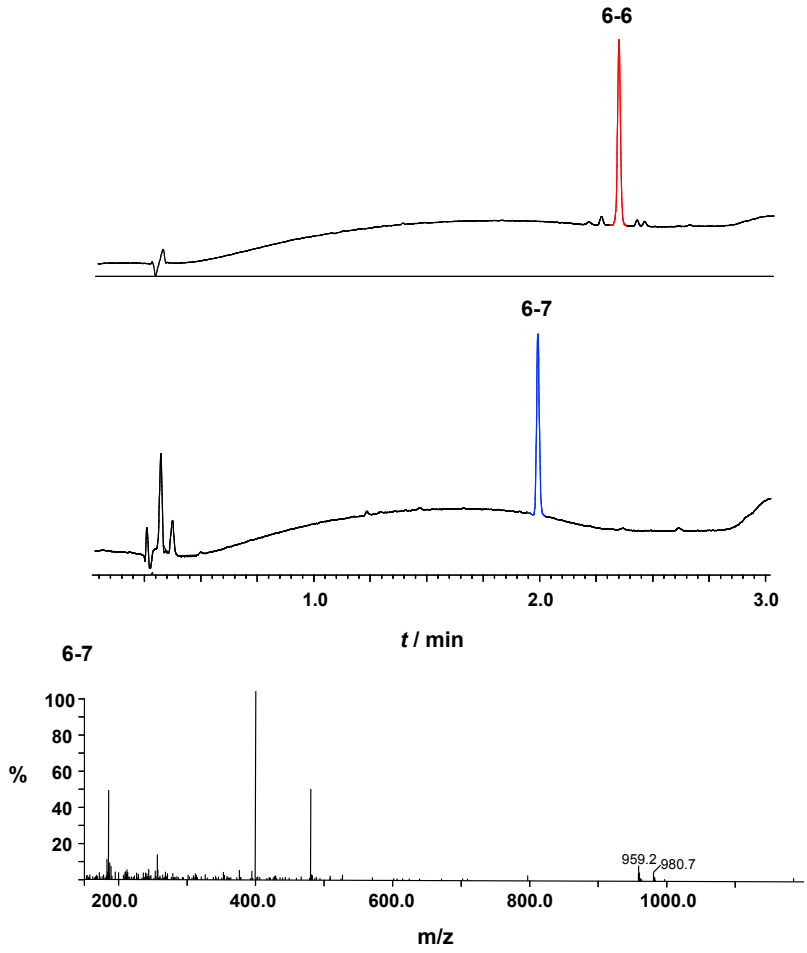

Figure S6.26 UPLC trace of a) starting material hydrazide transducer **6-6** (retention time: 2.34 min) and b) a reaction mixture of compound **6-6** and compound **6-15**. c) The mass spectrum of the single peak (retention time: 1.99 min) which corresponds to product galactose transducer **6-7**.

Compound **6-7**: HR-MS (ES+) calcd. for $C_{49}H_{67}N_5O_{11}F_3$: 958.4784, found: 958.4779.

6.4.2 Vesicle Experiments

General protocol for vesicle preparation

To a 1.5 mL microcentrifuge tube was added a chloroform solution of POPC and transducer or other molecules (5 mol% loading) in order to obtain a final lipid concentration of 20 mM in 1 mL (final elution volume). The solvent was evaporated using a dry nitrogen stream and dried under high vacuum for at least 2 h to yield a thin lipid film. To the microcentrifuge containing the lipids was added 25 mM HEPES 150 mM NaCl buffer (0.5 mL) at pH 7 (for measurements with zinc(II), a stock solutions of zinc chloride as appropriate was also added to reach final concentrations of 5 mM). After swelling for 1 min, the suspension was subjected to 5 cycles of freeze-thaw using liquid nitrogen and 35 °C water bath. The suspension was extruded for 19 times through a 200 nm polycarbonate filter in an extruder apparatus, and then the vesicles were separated by a bulk solution using prepacked SEC columns eluting with the same HEPES buffer at pH 7.

6.4.3 Catalytic Activity of Compound 6-2

4-Trifluoropyridine dioxime **6-2** catalytically hydrolyses substrate **6-9** in aqueous solution with the presence of Zn^{2+}. This suggests that the trifluoromethyl group does not affect the catalytic activity of the pyridine oxime head group.

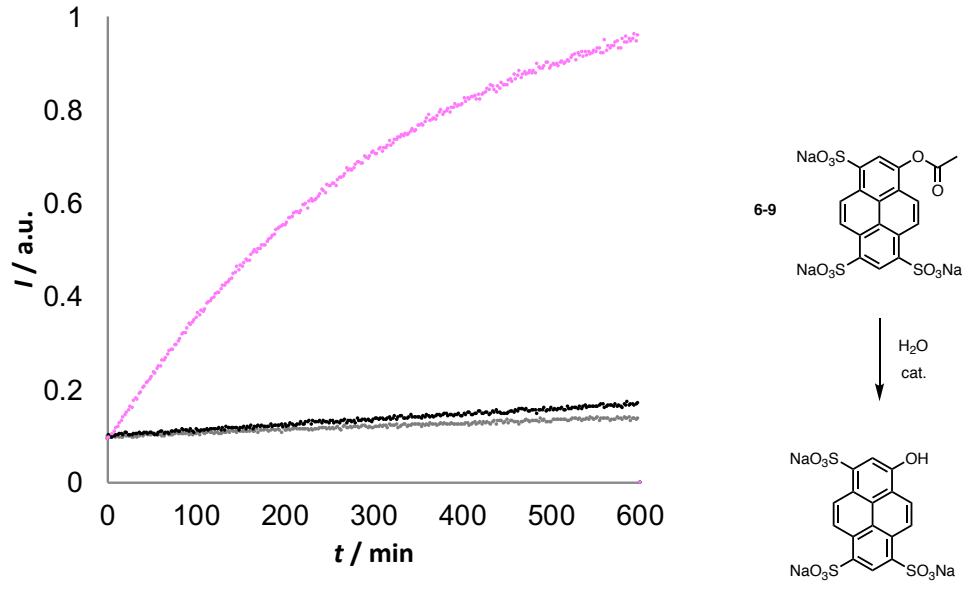

Figure S6.27 Time dependence of fluorescence emission of normalized fluorescence emission intensity at 510 nm (exciting at 415 nm). The catalytic hydrolysis (pink) was obtained by adding 1 uM pyridine dioxime **6-2** to a solution of 25 uM substrate **6-9**, 250 μM zinc chloride, and 25 mM HEPES buffer 150 mM NaCl at pH 7. Control experiment without zinc chloride (black) and background hydrolysis of substrate in buffer (grey) are also shown in comparison.

References

(1) Gygi, D.; Hwang, S. J.; Nocera, D. G. Scalable Syntheses of 4-Substituted Pyridine–Diimines. *J. Org. Chem.* **2017**, *82* (23), 12933–12938. https://doi.org/10.1021/acs.joc.7b02571.

(2) Zhu, D.; Zhu, Q.; Gu, C.; Ouyang, D.; Qiu, M.; Bao, X.; Yang, R. Alkoxyl Side Chain Substituted Thieno[3,4-c]Pyrrole-4,6-Dione To Enhance Photovoltaic Performance with Low Steric Hindrance and High Dipole Moment. *Macromolecules* **2016**, *49* (16), 5788–5795. https://doi.org/10.1021/acs.macromol.6b00927.

Appendix – Comparison of Substrates

Introduction

We studied three substrates for the translocation signalling system: substrate 7-**1**, 7-**2**, and 7-**3**, structures are shown in Figure 7.1. Substrate 7-**3** was synthesised in one step from HPTS by condensation with benzoyl chloride (Scheme 7.1). Vesicle experiments are monitored by following the fluorescent emission of the hydrolysed product (HPTS) in vesicles. These three substrates have different background hydrolysis and ON state hydrolysis rate. Besides, the corresponding hydrolysis products (acetic acid, 2-naphthoic acid, and benzoic acid for 7-**1**, the 7-**2**, and 7-**3**, respectively) may cause different effects on the bilayer membrane. For example, 7-**2** could be used to trigger controlled release of the vesicle cargo as 2-naphtoic acid is a known surfactant that can disrupt the membrane integrity.[1] The membrane permeability ($P_{membrane/water}$) of benzoic acid is approximately 10 times lower than 2-naphthoic acid[2], which suggests that benzoic acid should be less disruptive for the lipid bilayer than 2-naphthoic acid.

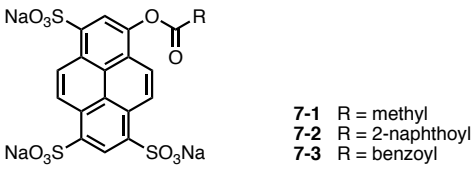

Figure 7.1 Molecular structures of substrates **7-1** – **7-3**.

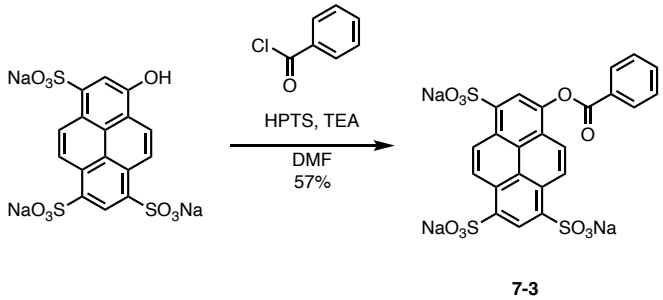

Scheme 7.1 Synthesis of substrate **7-3**.

Hydrolysis Rate

To benchmark the hydrolysis rate of three substrates, we assembled vesicles with 2.5 mol% morpholine transducer 7-4[3] (synthesised and reported by Dr Langton) in DOPC/DOPE vesicles with substrate encapsulated at neutral pH. The system was turned ON by raising external pH from 7 to 9, results are shown in Figure 7.2. The background hydrolysis rate of the substrate 7-**2** and 7-**3** are both significantly slower than that of 7-**1** (~ 12 h timescale).

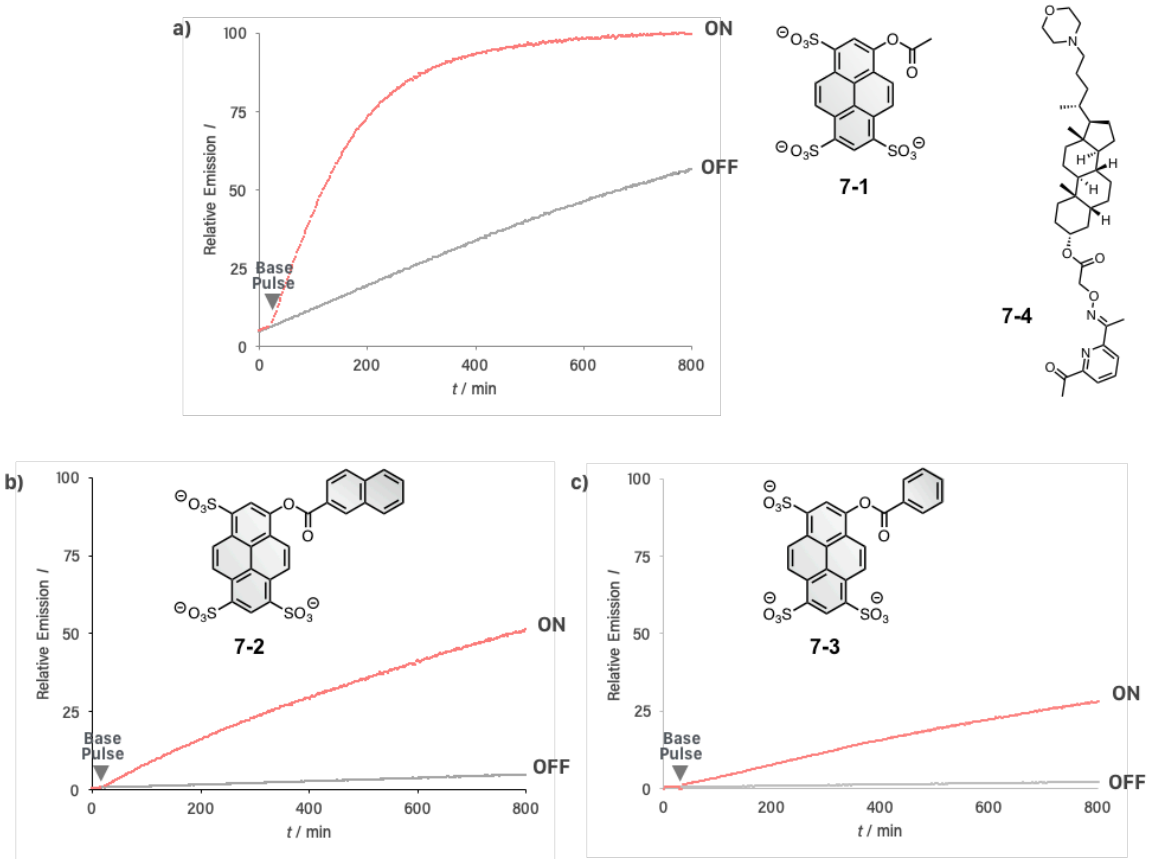

Figure 7.2 Hydrolysis rate comparison of substrates. Time dependence of the normalized fluorescence emission intensity at 510 nm (exciting at 415 nm) of vesicles composed of lipids with 2.5 mol% **7-4** encapsulating (a) 250 μM **7-1**, (b) 250 μM **7-2** and (c) 250 μM **7-3**. Grey data: vesicles incubated at pH 7. Red data: vesicles incubated at pH 7 initially, then raised to external pH of 9 after 20 min (indicated by an arrow). All experiments were conducted in 200 nm DOPC/DOPE vesicles (3/2 molar ratio, 2 mM lipid concentration) containing 250 μM ZnCl2 and 250 mM HEPES buffer and suspended in 250 mM NaCl at pH 7. Data shown in b) was conducted by Dr M. J. Langton and L. M. Scriven.

Calcein Release Assay

Calcein is a water soluble fluorescent dye that self-quenches at concentrations above 70 mM. It is commonly used as an indicator of vesicle leakage. To examine whether the substrates can cause vesicle membranes to become permeable, a calcein release assay was conducted (Figure 2.3). DOPC/DOPE vesicles with 2.5 mol% loading of transducer 7-4 containing calcein

solution (70 mM) and substrate (25 μM) were prepared at pH 7. Raising the external pH to 9 initiated the transduction and turned on the catalytic hydrolysis reaction of the substrate encapsulated in the vesicles. Release of calcein molecules from the vesicles results in a significant fluorophore dilution which increases the fluorescence emission. Total release of calcein was achieved by lysis of the vesicles upon adding excess detergent (Triton X-100). The results using substrates 7-**2** and 7-**3** are shown in Figure 2.12.

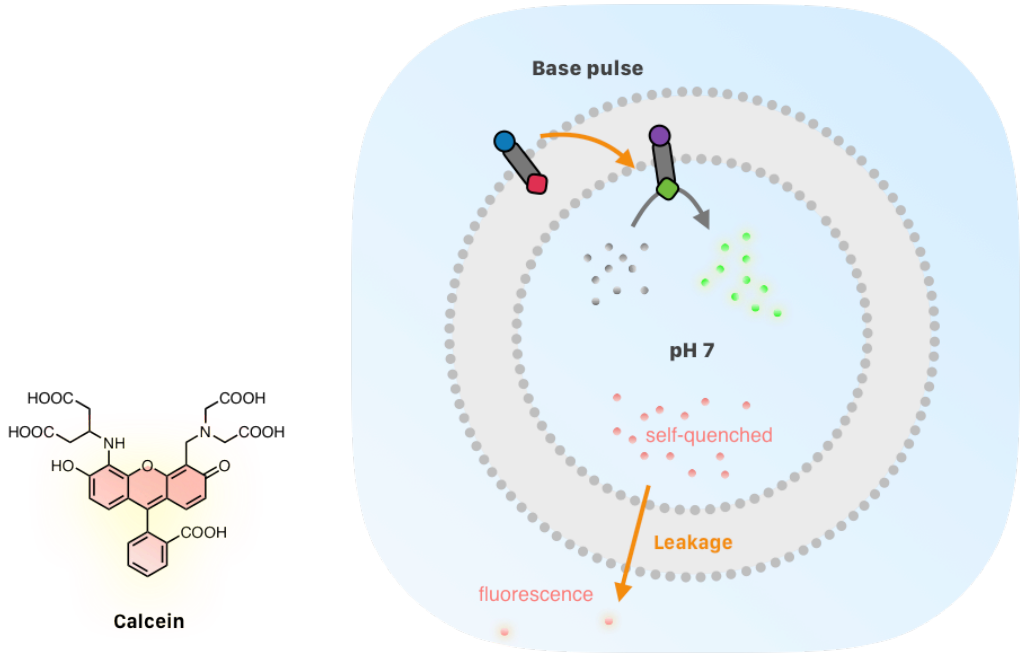

Figure 7.3 Schematic representation of calcein release assay. 200 nm DOPC/DOPE vesicles containing 70 mM calcein, 25 μM substrate **7-2** or **7-3**, 250 μM $ZnCl_2$ and 250 mM HEPES buffer at pH 7. An external input signal (base pulse) initiates the translocation of the transducer from the outer to the inner leaflet of a lipid bilayer membrane and catalyses the turnover of substrate to generate its corresponding products. If the product is dissolved in the lipids, it will enhance the membrane permeability and facilitate the calcein cargo release. At high concentration, fluorescence emission of calcein is self-quenched. Releasing from internal vesicle solution to the extracellular solution will significantly reduce the calcein concentration, which activates the fluorescence emission.

The results suggest that raising the external pH to 9 has no effect on DOPC/DOPE membrane permeability to calcein over a period of 10 hours. Similarly, vesicles containing substrates 7-**2** or 7-**3** in the OFF state did not release their contents (Figure 7.4, red data), demonstrating that the substrates do not affect the permeability of the bilayer. For vesicles containing substrate 7-**2**, raising the external pH to 9 initiates the translocation and generates 2-naphthoic acid inside the vesicles. This leads to a rapid release of calcein (Figure 7.4, ON state). On the contrary, using 7-**3** as substrate has little effect on calcein release in this signalling experiment. Less than 5% of calcein leaked out during a period of 10 hours, which indicates that benzoic acid does not interfere with membrane permeability.

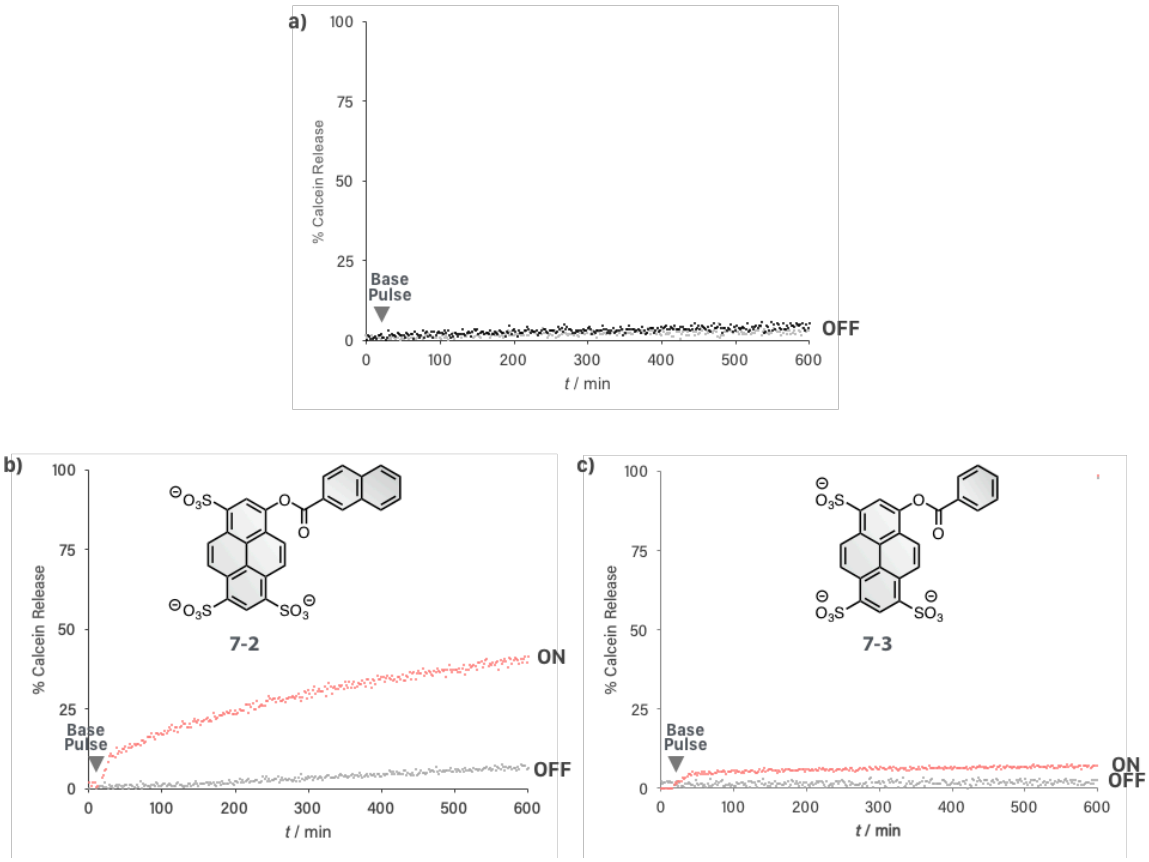

Figure 7.4 Time dependence of calcein release initiated by signal transduction. 200 nm DOPC/DOPE vesicles (lipid concentration 0.5 mM) with 2.5 mol% transducer **7-4** containing 70 mM calcein, 250 μM $ZnCl_2$, 250 mM HEPES at pH 7 suspended in 400 mM NaCl. a) Without substrate encapsulation. b) With 25 μM substrate **7-2**, c) with 25 μM substrate **7-3**. Addition of NaOH to raise the external pH to 9 (black or red data, addition indicated by an arrow). Grey data: control experiments at pH 7 (without addition of NaOH). Calcein emission at 540 nm (exciting at 470 nm) was calibrated to 100% release by lysis with Triton X-100. Data shown in b) was conducted by Dr M. J. Langton and L. M. Scriven, graphics have been re-illustrated.

To further confirm that leakage of the cargo is the effect of 2-naphthoic acid, external addition of 2-naphthoic acid and benzoic acid to calcein-containing (70 mM) vesicles was investigated. Addition of 2-naphthoic acid in methanol (<0.5% v/v, concentration of 2-naphthoic acid at 50 μM) lead to a rapid release of calcein from the vesicles (Figure 2.13a, red data). In the absence of benzoic acid (Figure 7.5a, grey data) or upon addition of an aliquot of the same volume of neat methanol, the calcein remains encapsulated and the vesicles over the course of the experiment. When benzoic acid was added, minimal release of calcein (less than 3%) was observed (Figure 7.5b). These results are in line with the calcein release assay initiated by the transmembrane signal transduction experiments.

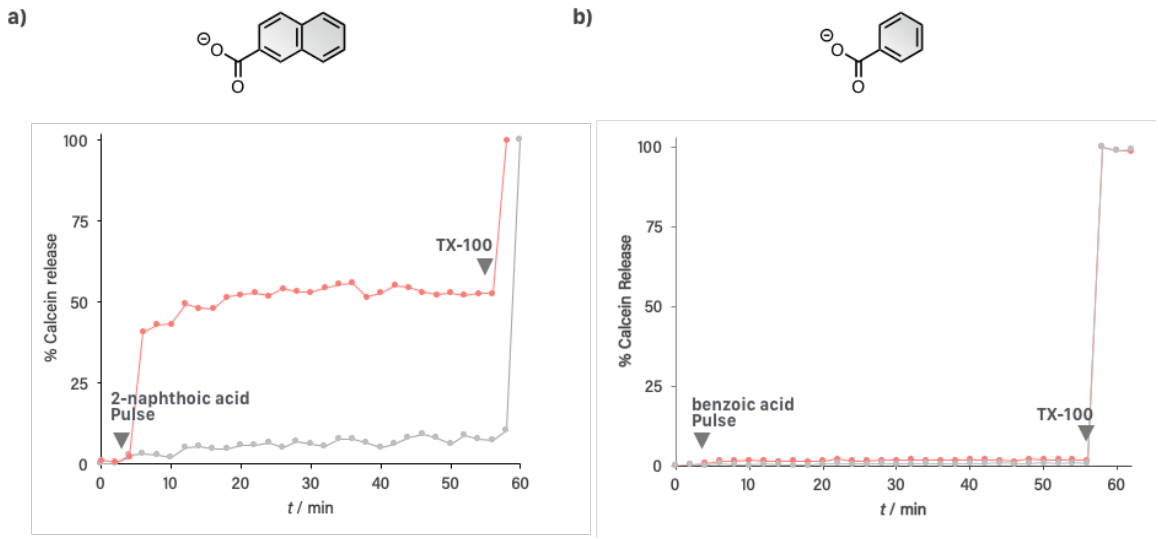

Figure 7.5 Calcein release assay initiated by external addition of P3 and P5. 200 nm DOPC/DOPE vesicles (lipid concentration 0.5 mM) containing 70 mM calcein and 250 mM HEPES at pH 7 suspended in 400 mM NaCl. Grey data: background release. Red data: release triggered by addition of (a) 2-naphthoic acid in methanol or (b) benzoic acid in water (50 μM). Calcein emission at (a) 540 nm (exciting at 470 nm) or (b) 534 nm (exciting at 470 nm) was calibrated to 100% release by lysis with Triton X-100. Data shown in a) was conducted by Dr M. J. Langton and L. M. Scriven.

Conclusion

Substrate 7-**2** and substrate 7-**3** were synthesised and the signalling experiments show that both substrates have significantly slower background rates compared to substrate 7-**1**. Due to the difference of membrane partition coefficient between 2-naphthic acid and benzoic acid, using substrate 7-**2** in the vesicle experiments lead to controlled release of the content in the vesicles by disrupting the lipid bilayer, whilst substrate 7-**3** does not cause such effect.

Reference

(1) Langton, M. J.; Scriven, L. M.; Williams, N. H.; Hunter, C. A. Triggered Release from Lipid Bilayer Vesicles by an Artificial Transmembrane Signal Transduction System. *J. Am. Chem. Soc.* **2017**, *139* (44), 15768–15773. https://doi.org/10.1021/jacs.7b07747.

(2) Xiang, T.-X.; Anderson, B. D. The Relationship between Permeant Size and Permeability in Lipid Bilayer Membranes. *J. Membr. Biol.* **1994**, *140* (2), 111–122. https://doi.org/10.1007/BF00232899.

(3) Langton, M. J.; Keymeulen, F.; Ciaccia, M.; Williams, N. H.; Hunter, C. A. Controlled Membrane Translocation Provides a Mechanism for Signal Transduction and Amplification. *Nat. Chem.* **2017**, *9* (5), 426–430. https://doi.org/10.1038/nchem.2678.

Synthetic Procedures and Characterisations

Substrate 7-3

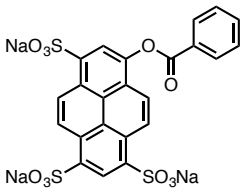

To a solution of pyranine (200 mg, 0.381 mmol) in anhydrous *N,N'*-dimethylformamide (10 mL) was slowly added the solution of benzoyl chloride (267 mg, 1.90 mmol) using same solvent at 0 °C. The reaction was stirred at r.t. for 48 h. The reaction mixture was then poured in a mixture of acetone (300 mL) and diethyl ether (100 mL). The precipitate was washed with cold acetone (3 x 10 mL) and diethyl ether (10 mL). The resulting solid was redissolved in water and purified by passing through an ion exchange column (Sephadex C-25, sodium form). The solvent was removed to yield the product as an orange solid (137 mg, 57%).

^{1}H NMR (400 MHz, D_2O) δ (ppm): 9.25-9.12 (m, 4H), 8.71 (s, 1H), 8.49 (d, *J* = 9.6 Hz, 1H), 7.40 (d, J = 7.6 Hz, 2H), 6.91 (t, J = 7.6 Hz, 1H), 6.62 (d, J = 7.6 Hz, 1H).
^{13}C NMR (100 MHz, D_2O) δ (ppm): 166.22, 144.12, 138.08, 136.03, 136.01, 133.34, 129.48, 128.88, 128.70, 127.39, 126.97, 126.39, 126.19, 125.32, 125.30, 125.07, 124.51, 124.41, 123.22, 120.00.
HR-MS (ES+): calcd. for $C_{23}H_{11}O_{11}Na_4S_3$: 650.9049, found: 650.9045.
FT-IR (ATR): ν_{max} 3423, 1723, 1643, 1632, 1601 cm^{-1}.

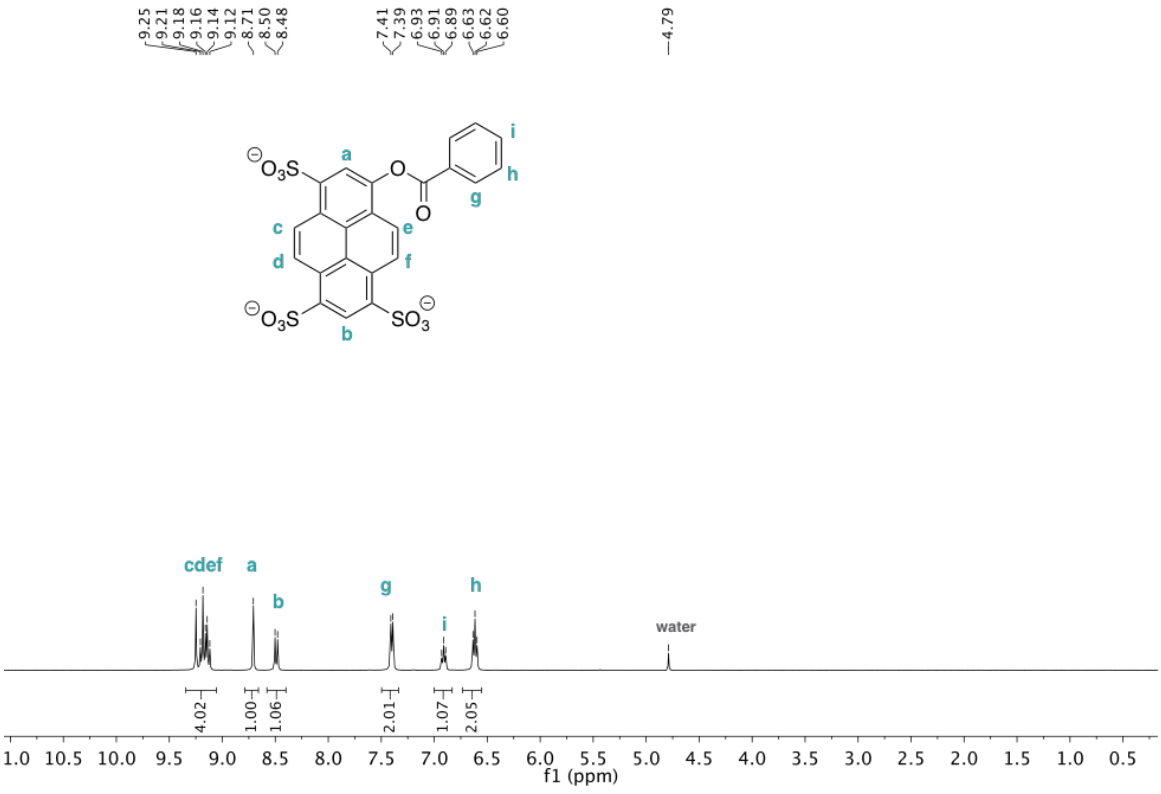

Figure 7.6 ^{1}H NMR spectrum of compound **7-3**.

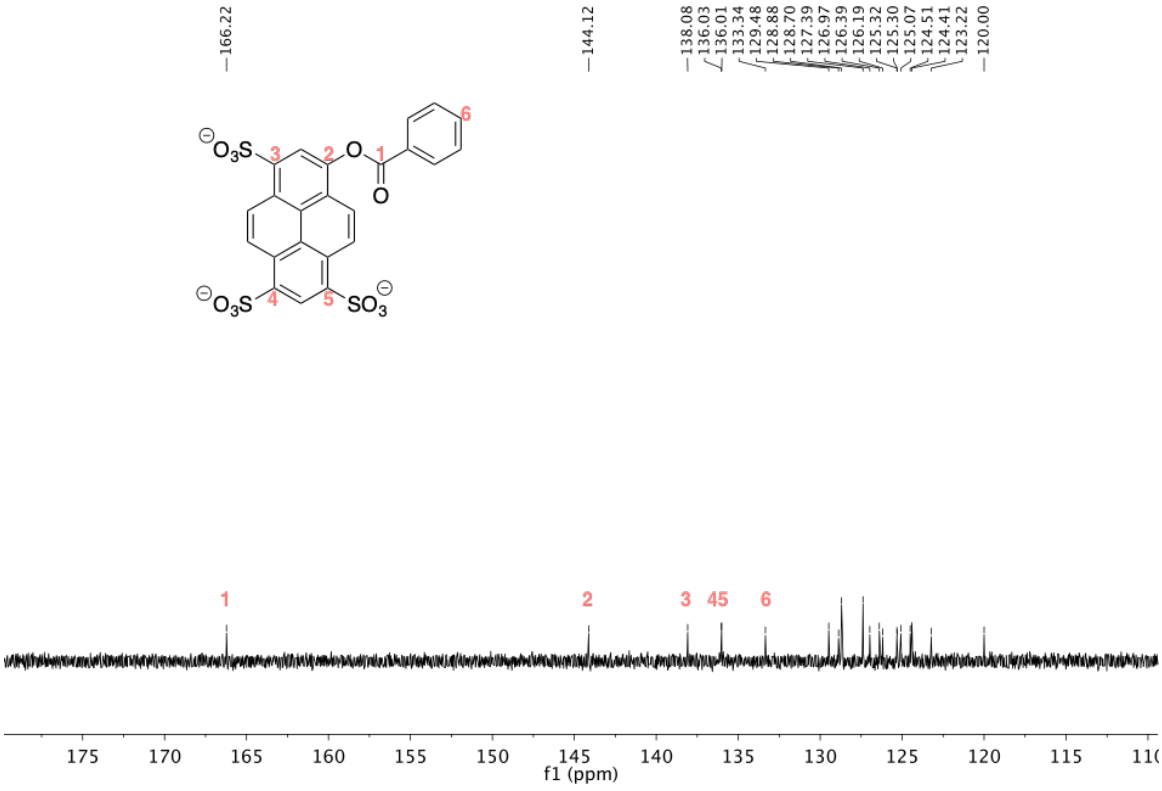

Figure 7.7 ^{13}C NMR spectrum of compound **7-3**.

This page is intentionally left blank

List of Publications (2016 – 2019)

1 Henkel, S.; Misuraca, M. C.; **Ding, Y.;** Guitet, M.; Hunter, C. A. Enhanced Chelate Cooperativity in Polar Solvents. *J. Am. Chem. Soc.* **2017**, *139* (19), 6675–6681. https://doi.org/10.1021/jacs.7b01765.

2 Frantz, M.-C.; Dropsit-Montovert, S.; Pic, F.; Prévot-Guéguiniat, A.; Aracil, C.; **Ding, Y.**; Lima, M.; Alvarez, F.; Ramos, S.; Mao, L.; Lu, L.; Xu, J.; Marat, X.; Dalko-Csiba, M. Divergent Entry to C-Glycosides from Unprotected Sugars. *Org. Lett.* **2019**, *21* (8), 2684–2687. https://doi.org/10.1021/acs.orglett.9b00666.

3 **Ding, Y.**; Williams, H. N.; Hunter, C. A. A Synthetic Vesicle-to-Vesicle Communication System. *J. Am. Chem. Soc.* **2019**, *141* (44), 17847-17853. https://doi.org/10.1021/jacs.9b09102.

This page is intentionally left blank

Acknowledgement

Karl Marx describes that the capitalist society consists of two parts: the *base* (means and relations of production, including capital) and *superstructure* (everything ideology-related), and that the base determines superstructure. Therefore, first and foremost, I thank the UK Engineering and Physical Sciences Research Council (EPSRC), Trinity College Cambridge, Queens' College Cambridge, and the Department of Chemistry for the scholarships and financial support, without which my life in Cambridge would certainly not have been as enjoyable.

Thanks again to Prof. Christopher A. Hunter for his trust in me and provided an invaluable opportunity of learning at this world-renowned institute. Thanks again to Dr Matthew J. Langton and Dr Istvan Kocsis who directly supported this work. To Prof. Nicolas H. Williams for the detailed discussions and feedback, it was always a pleasant journey to go to Sheffield and catch up with the Output Team. Thanks again to Prof. Steven V. Ley for being my mentor, and I look forward to hearing more about the start-up development stories. To Prof. Jeremy K. M. Sanders for having never fallen asleep during my presentations and for making useful suggestions in the group meetings. To Prof. Jonathan R. Nitschke, my probational year examiner as well as my internal examiner of the *viva voce*, who oversaw how this project has evolved over the years and provided constructive feedback on the project. Special thanks to Dr Simon J. Webb, my external examiner, who went through this dissertation in absolute detail and provided extra scrutiny to the work. I wish we have had met and discussed earlier so I could avoid many of my frustrations in the lab.

I am fortunate to be surrounded by the incredible members of the Hunter group, and thanks a million for the amazing *viva* celebration video! To Dr Giulia Iadevaia for being the No.1 film director, for being an early adopter of my visual identity guidelines, and for being a top Instagram influencer. To Dr M. Cristina Misuraca for allowing me to peak into Chris' calendar and help me catch him whenever I wanted to. To Dr Mark Williamson for being the most British person I have ever known and explain the British culture to me with great patience. To Dr Pavle Trošelj for being the one who always listens to me, comforts me, understands me and supports me. I look forward to little Maro's growing up and becoming fluent in Mandarin. To Dr Stefan Henkel for not only providing a list of movies like everyone else does that I need to catch up with but also arrange and spend time watching them with me. I enjoyed *The Matrix* (1999), *Kill Bill* (2003) and a zombie movie that I cannot remember the name. To Dr Judith Weber my favourite German girl, for her positiveness towards life and her big lovely smile, for our Waltz dance and Klimt's kiss. To Petr Motloch for being an awkwardly straightforward but truly caring friend, and for willing to become one of the FFFs (friend, family, and fools) investor of my silly start-up (and I will let him decide which "F" he is). To Dr Jorge Gomez Magenti for his mouth-watering Valencian paella, for his big hugs and big heart, for the chicken soup delivery when I was sick. To Dr Lucas Carreras Vinent for bringing so much fun and laughter to my life, and for valuing our friendship over anything else. To Dr Elena Sanna Martinez for being unconditionally supportive and for the amazing Spanish coca (not pizza!). To Gloria Tobajas Curiel for being more excited than myself

for my own life, and for all the celebrations you encouraged me to have. To Lucia Trevisan for sharing all the joy and frustrations with me, and for being extra cautious and disciplined in the lab (I am thinking of the aqua regia I stole from you). To our legendary Dr Ana Belenguer for being the most energetic and cheerful person of the group, and for all the encouragements and compliments I received from her that boosted a little bit of ego in myself. To Dr Luca Gabrielli for being the most adorable person in this world. This man outperformed me in ordering Chinese take-ways and I hereby award him, on behalf of Ting from the Golden House, the Yudi's Best Dinner Companion Award. To Mark Driver the President who encouraged me to contester the committee role in the QMCR. To Filip Szczypiński for being tolerant to my messy fume cupboard (at the cost of listening to all his wine comments in lab), for the fancy dinners and balls, and for the excessive use of the rainbow emoji [🌈]. To Dr Sarah J. Pike for always correcting my poor English grammar, for practicing French with me whenever possible, and for the lovely Sunday roast she cooked. To bravissimo Dr Francesco Fasano for his Italian accent, humour, and the ultimate love and need to ask for no spicy for the Malay Kong Pao Chicken. To Peter Bolgar for his passion towards the Chemistry Olympiad and the bravery to teach in Saudi Arabia. To Maria Chiara Storer for the love of learning Chinese and the Chinese culture. To Diego Núñez Villanueva for being my supervisor during my Master's project and for always being incredibly kind and helpful. To Dr Carlo Bravin for the love of classical music and the great saxophone performance. To Karine Hakobyan for appreciating my limerick which took me a whole weekend to write up. To Dr Jonathan A. Swain for having intrigued me into rowing, which I immediately abandoned. To Dr Marion Donnier-Maréchal for perfecting my French and for always bringing a delicious Gallete des Rois during the feast of the Epiphany. To Dr Michael A. Jinks for training me to understand the strongest Birmingham accents. After I can manage to understand him, I have full confidence to talk to any British person in the UK. To Dr Alexander E. Stross and Dr Maria Ciaccia for the best craftmanship regarding the little man displaying male potency that built out of a champagne cork wire. To Dr Nicola De Mitri for the being the one that feels my pain and joy of being a graphic designer, and for his impressive 3D rendering work series that are super fun to watch. To Flore Keymeulen for not being embarrassed for singing *La Vie en Rose* with me when we were both stupidly drunk at the liqueur tasting. To Mohit Dhiman and Tim Chisholm for starring in the *viva* video. I hope you had fun for the shooting, and I am sure there will be much more fun in your PhD journeys ahead. Special thanks to Maxime P. F. Couturier for being an honorary member of the Hunter Group (a reference to my rotavap named "Bring A Friend"), and for being my most handy French dictionary and grammar book of all time. To Ennio Lavagnini but I will not say anymore in the risk of going beyond category 18 in the British Board of Film Classification (BBFC) standards.

To all the help and support I received from the Department of Chemistry. Many thanks to Rachel MacDonald who has been of great help over the years, and to Gaby Bocchetti who saved my arse in printing posters and dissertations multiple times before the deadlines.

Many thanks to my college tutor Dr Laurence Tiley for many of the mid-table dinners that I have been invited to, for the support of funding applications for either learning language or academic travel, and for being incredibly supportive for the MCR and student welfare. To Prof. Elizabeth A. Hall for encouraging me and pushing through my rebranding initiative of the college. To the President Lord Eatwell for writing me the congratulation letter and for introducing me to the Bohemian Club prior to my trip to San Francisco. I certainly enjoyed the personal gift that he left for me at the Plodge, which generated an extra round of compliments from the porters.

To Dr Rebecca Myers for bringing me onto the entrepreneurship journey at the Judge Business School, as well as to the twenty STAR people of the first EnterpriseTECH STAR cohort, for the learning journey we shared, the awkward team building activities we went through, and the fantastic show we

performed at the Fitzwilliam Museum. I cannot emphasise about more how this journey has changed my perspective of this world. During the programme, I have travelled half of the globe, talked to some of the most ambitious CEOs of start-ups, investors, industry leaders, and academics, and I was pleased to discover that people trust in what I am doing and what I can achieve. It helped me find strength in myself, and more importantly, believe in myself that I am able to use the experience and knowledge that I gained throughout my education to challenge the status quo in this world. A big thank you to Susannah E. Evans, my brilliant co-founder of our virgin start-up, for the pitch videos we made, for the sun we enjoyed in California, for the vegan Chinese food we shared, for the designers' studios we bluntly showed up to, for the mushrooms we experimented in Amsterdam, for referring to me as a "robot" (which I take as a compliment), for being supportive and encouraging during the last (and worst) month before I submitted this dissertation, and for being open and sharing from business due diligence to the boys of our lives. I cannot wait to have more surprises and amazing adventures with this evilly beautiful strong independent cis-gendered heterosexual bi-curious woman (don't we all hate labels?). Sometimes I wonder how two persons who are fundamentally different like us could possibly become best partners in crime. "It's *yin* and *yang*", she said.

Thank you to my beloved parents for still spoiling me when I am 27 years old - my European friends are very jealous. Thank you to my brother Qi He, you are the one who gives me strength even when you have left us. I miss you.

27 Nov 2019 eve in Bermondsey, London


UNIVERSITY OF
CAMBRIDGE